UNIVERSIDAD DE MURCIA

FACULTAD DE MEDICINA

Study of the Therapeutic Effect of Human Wharton's Jelly Mesenchymal Stem Cells in an Experimental Murine Model of Wound Healing.

Estudio del Efecto Terapéutico de las Células Mesenquimales de la Gelatina de Wharton del Cordón Umbilical Humano en un Modelo Murino de Cicatrización de Heridas.

D. José Eduardo Millán Rivero

2015

A mi hijo Pablo

AGRADECIMIENTOS

Desde muy joven sentí que la investigación sería lo que daría plenitud a mi vida académica y profesional. Aún recuerdo lo placentero que resultaba "jugar" con microscopios y tubos de ensayo en los laboratorios de biología y química de mi colegio. Afortunadamente tuve profesores que con sus enseñanzas sembraron en mí el deseo de ser científico y de dar los primeros pasos en el fascinante mundo de las ciencias.

Mi segunda gran escuela fué la Facultad de Medicina (UCLA-Venezuela) donde además de aprender los oficios propios del médico descubría que la medicina sentaba sus bases sobre el trabajo de miles de científicos.

Con la intención de ahondar en mi formación académica tomé la decisión de dirigír mis pasos hacia España y comenzar un doctorado en la Facultad de Medicina de la Universidad de Murcia. Agradezco a Joaquín y a Noemí por abrirme las puertas del Departamento de Fisilogía Humana y darme la oportunidad de formar parte de su grupo de investigación.

Durante todo este tiempo me han acompañado personas muy valiosas, entre ellas quiero hacer una mención especial a mi querida amiga Paola. Quiero que sepas que has sido mi guía y mi maestra. Quiero darte las gracias por todo el tiempo y esfuerzo que has dedicado para la realización de esta tesis. Eres ejemplo de sencillez, perseverancia, lealtad y trabajo.

No puedo dejar de mencionar a Moisés. Gracias amigo por hacerme sentir que cuento contigo.

Gracias también a todos mis compañeros y amigos del LAIB por animarme en cada momento y compartir conmigo la pasión por la investigación.

Hago una mención de honor al Dr José María Moraleda por su invaluable apoyo.

A continuación quiero agradecer a David y Carlos por todo el conocimiento, interés, esfuerzo y dedicación que han aportado durante la dirección de esta tesis. Gracias a ustedes este trabajo ha sido posible. Cada opinión o comentario ha tenido un gran valor para mí.

Asímismo agradezco a Salvador Aznar y José Luis Cenis por creer en este proyecto y apotar los recursos necesarios para su consecución. Gracias por su generosidad.

Este trabajo tuvo sus inicios durante una estancia en el Centro Médico Universitario de Leiden (LUMC. Holanda) bajo la tutoría del Dr Willem Fibbe y Dr Jaap Jan Zwaginga, a quienes debo gran parte de mis conocimientos y habilidades. Determinante también fué el aprendizaje junto a mi compañero Mark vand der Garde, quien se tomó el tiempo y la dedicación necesaria para juntos desarrollar gran parte de los protocolos incluidos en esta tesis.

En Holanda tuve la fortuna de conocer a mis amigos y hermanos Stefano y Francesco. A ti Stefano, te doy gracias por animarme en todo momento y sobretodo cuando más lo necesitaba. Gracias por compartir la fé y la esperanza en aquel en quién creemos. A ti Panchittino, muchas gracias por toda la paciencia que tuviste mientras resolvíamos los problemas técnicos de redacción de este manuscrito. Eres además ejemplo de humildad y sabiduría.

Muchas gracias a todos mis amigos de Holanda por todos los momentos llenos de alegría, bailes y camaradería que me hicieron sentir como en casa. De todos he aprendido el valor de la amistad.

A mis amados padres José y Pastora a quienes agradezco el don de la vida y cada uno de los esfuerzos que han hecho para hacer de mí lo que soy. Gracias por su ejemplo y amor incondicional.

A mis hermanas María y Rosmary por todo el amor que me han dado y porque sé que cuento con ustedes en todo momento.

A mi esposa Haydée por toda la paciencia, amor y apoyo demostrados a lo largo de todos estos años.

A mi hijo "arcoiris" Pablo, a quién amo infinitamente y dedico esta tesis. Gracias por venir a nuestras vidas y llenarlas de alegría.

Hace años descrubí que la ciencia y la fé no están reñidas, por eso agradezco con toda mi alma al autor de mi vida por darme la oportunidad de venir a este mundo a saborear sus alegría y tristezas y permitirme disfrutar de esta meta que ahora concluyo.

Y finalmente, gracias a las monjas Carmelitas descalzas de Barquisimeto (Venezuela) por sus oraciones.

Nomenclature

1-MT	1-methyl-tryptophan
7-AAD	7-Amino-Actinomycin
α-SMA	Alpha-smooth muscle actin
ALP	Alkaline phosphatase
AMSCs	Adult Mesenchymal Stem Cells
APCs	Antigen presenting cells
AT-MSCs	Adipose tissue mesenchymal stem cells
BCIP	5-Bromo-4-chloro-3-indolyl phosphate
bFGF	Basic fibroblast growth factor
BM-MNCs	Bone marrow-derived mononuclear cells
BM-MSCs	Bone marrow mesenchymal stem cells
BMPs	Bone Morphogenic Proteins
cAMP	Adenosine 3',5'-cyclic monophosphate
CB-MSCs	Cord blood mesenchymal stem cells
CFU-GM	Granulocyte macrophage colony-forming unit
cGMP	Guanosine 3',5'-cyclic monophosphate
CLI	Critical limb ischemia
ConA	Concanavalin A
COX	Cyclooxygenase enzyme
DCs	Dendritic cells
DMEM	Dulbecco's Modified Eagle's medium
DMSO	Dimethyl sulfoxide
ECM	Extracellular matrix
EDTA	Ethylenediaminetetraacetic acid
EGF	Epidermal growth factor
ELISA	Enzyme-linked immunoabsorbent assay
EMSCs	Embryonic mesenchymal stem cells
FBS	Fetal bovine serum
FGFRs	Fibroblast growth factor receptors
FMSCs	Fetal mesenchymal stem cells
GDFs	Growth differentiation factors
GDNFs	Glial-derived neurotrophic factors
GM-CSF	Granulocyte-macrophage colony-stimulating factor
GPCRs	G-protein-coupled receptors
GVHD	Graft versus host disease
HB-EGF	Heparin-binding epidermal growth factor
IBMX	3-isobutyl-1-methylxanthine
ICAM-1	Intercellular adhesion molecule-1
iDCs	Immature myeloid dendritic cells
IDO	Indoleamine 2,3-dioxygenase
IGF-1	Insulin-like growth factor-1
IL	Interleukin
IP-10	Interferon gamma-induced protein 10
KGF	Keratinocyte growth factor
LPS	Lipopolysaccharide
MAPK	Mitogen-activated protein kinase
MCP-1	Monocyte chemoattractant protein 1
mDCs	Mature myeloid dendritic cells
MHC	Major histocompatibility complex
MIG	Monokine induced by gamma interferon
MIS	Mülllerian inhibitory substance
MLC	Mixed lymphocyte cultures
MMPs	Matrix metalloproteinase
MNCs	Mononuclear cells
MSCs	Mesenchymal stem cells
NBT	Nitro blue tetrazolium chloride
NK	Natural killer
NO	Nitric oxide
PBS	Phosphate-buffered saline
PD	Population doubling level
PDEs	Phosphodiesterases
PDGF	Platelet-derived growth factor
PDT	Population doubling time
PE	Phycoerythrin
PGE2	Prostaglandin E2
PHA	Phytohemagglutinin
Pl-MSCs	Placenta mesenchymal stem cells
PlGF	Placental growth factor
PMN	Polymorphonuclear neutrophils
Prdx6	Peroxiredoxin 6
ROS	Reactive oxygen species
SEM	Scanning electron microscopy
SF	Silk fibroin
SLPI	Secretory leukocyte protease inhibitor

TB	Toluidine blue
TGF	Transforming growth factor
TLRs	Toll-like receptors
Tregs	Regulatory T cells
UC-MSCs	Umbilical cord mesenchymal stem cells
USSCs	Unrestricted somatic stromal cells
VCAM-1	Vascular cell adhesion molecule-1
VEGF	Vascular endothelial growth factor
Wj-MSCs	Wharton's jelly mesenchymal stem cells

Contents

Chapter 1

INTRODUCTION

1.1 Skin

The skin is the largest organ in the human body, covering the entire external surface and forming about 8% of the total body mass. The skin forms a self-renewing and self-repairing interface between the body and the environment. At the body's surface, the main function of the skin is to act as a barrier to prevent the loss of essential body fluids and invasion of microbes and irritants. Loss of the integrity of large portions of the skin as a result of injury or illness may lead to major disability or even death [1].

The adult skin consists of two tissue layers: a keratinized stratified epidermis and the dermis, an underlying thick layer of collagen-rich dermal connective tissue providing support and nourishment. Appendage such as hairs and glands are derived from and linked to the epidermis but project deep into the dermal layer [2] (see Figure 1.1).

The epidermis consists mainly of keratinocytes and contains few Langerhans cells, a specialized form of dendritic cells, some pigment-producing melanocytes, and Merkel cells. Keratinocytes express several types of cytokeratins, cytoplasmatic proteins which are expressed only by epithelial cells and form intermediate filaments through assembly into bundles and generate the toughness properties of the epidermal surface. [3].

The dermal layer is organized by loose and dense irregular connective tissue, which is composed predominantly of an extracellular matrix (ECM) made of collagen fibers bundles in a basket wave arrangement, all embedded within proteoglycans. Fibroblasts, the major cell type of the dermis, produce and maintain most of the ECM components. Several types of immune cell can be found in the dermis, such as macrophages, T cells, and mast cells. Also, endothelial cells line the blood vessels

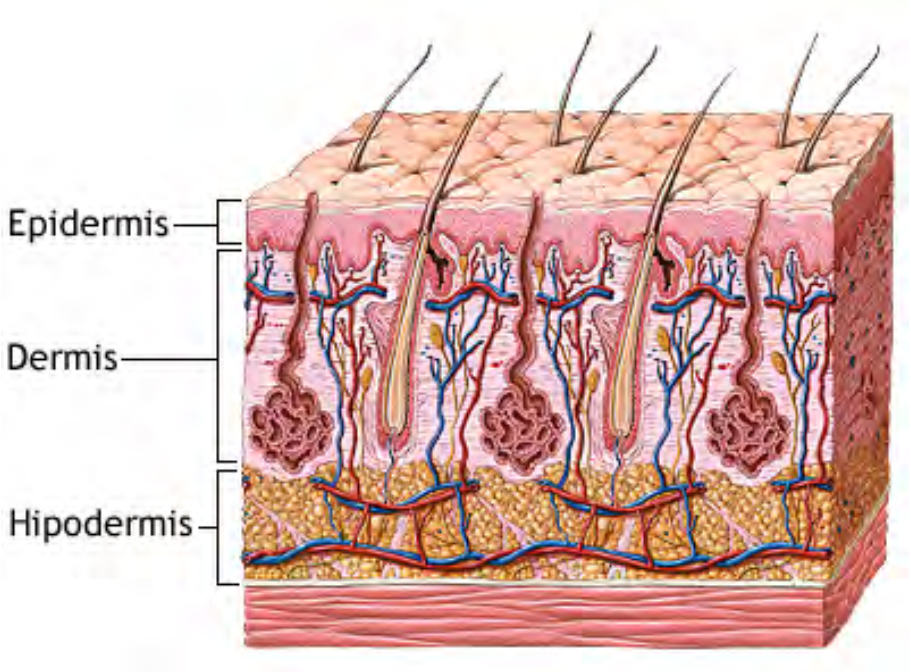

Figure 1.1: **Structure of Human Skin.** Source: Health Illustrated Encyclopedia, A.D.A.M.

and play a critical role in the skin's immune response by controlling the extravasation of leukocytes. In addition, a network of nerve fibers extends throughout the dermis, serving a sensory role in the skin. These nerve fibers also secrete neuropeptides, which influence immune and inflammatory responses in the skin through their effect on endothelial cells, leukocytes and keratinocytes [4].

In contrast to the dermis, the epidermis is a constantly renewing tissue. The proliferation of keratinocytes is restricted to the basal cell layer, where stem cells are located. During an apoptosis-like process of terminal differentiation, keratinocytes change their expression profile and properties and migrate to the outer surface of the epidermis. This generates several densely-packed layers of keratinocytes with dead, flat and keratin-filled corneocytes at the surface, which form a protective envelope [5].

Cutaneous wounds are the result of disrupted skin integrity. Wound healing is a dynamic, interactive biological process involving soluble mediators, blood cells, extracellular matrix proteins, and parenchymal cells. The purpose of wound healing is to repair the skin to prevent infection and to restore the tissue integrity and function. Wound healing consists of three distinct and overlapping phases: inflammation, cell proliferation (neoangiogenesis, granulation, and re-epithelialization), and a remodeling phase (extracellular matrix remodeling).

Healing of most of the injuries ends in the formation of a scar; that is a tissue

mainly composed of dense regular connective tissue. Scar tissue lacks a range of physiological epidermal appendages, such as follicles or sweat glands. As a result, healing by fibrosis generates life-long disability with huge spending on public health, whereas the response to injury through the process of regeneration can completely restore the original tissue architecture what would considerably improve human health [6].

1.2 Wound Healing

1.2.1 Phases of wound Healing

1.2.1.1 Inflammation (Figure 1.2 (a))

Tissue injury causes the disruption of blood vessels and extravasation of blood components. Haemostasis occurs immediately after injury and involves the constriction of blood vessels and the formation of a platelet plug, followed by a fibrin matrix, which becomes the scaffold for infiltrating cells [8]. Platelets not only facilitate the formation of a hemostatic plug but also degranulate by releasing a wide range of growth factors (i.e., epidermal growth factor (EGF), platelet-derived growth factor (PDGF), and transforming growth factor-beta (TGF-β)) from the alpha granules. These and other growth factors provide chemotactic signals for recruiting inflammatory cells to the wound site, initiate the process of re-epithelialization and connective tissue contraction, and stimulate the wound angiogenic response [2].

The inflammatory process begins with the recruitment of neutrophils, macrophages, and lymphocytes. Leukocytes are slowed down and pulled from the rapid bloodstream due to the expression of adhesion molecules of the selectin family on the surface of endothelial cells lining capillaries at the wound site. Then, tighter binding and arrest of the rolling leukocytes, mediated by adhesion molecules of the integrin family, lead to transendothelial migration or diapedesis, allowing to the leukocytes cross the endothelial lining of the blood vessel and enter the extravascular space [9].

Several leukocyte lineages infiltrate the wound site at different time points during the inflammatory response to tissue damage. Neutrophils are the first leukocytes to be recruited into the wound. They mainly clean the wounded area of foreign particles and bacteria, but they also serve as a source of pro-inflammatory cytokines that activate local fibroblasts and keratinocytes. If the wound is not highly infected, the neutrophil infiltration ceases after a few days and then expended neutrophils and other cells and extracellular matrix debris at the wound site are

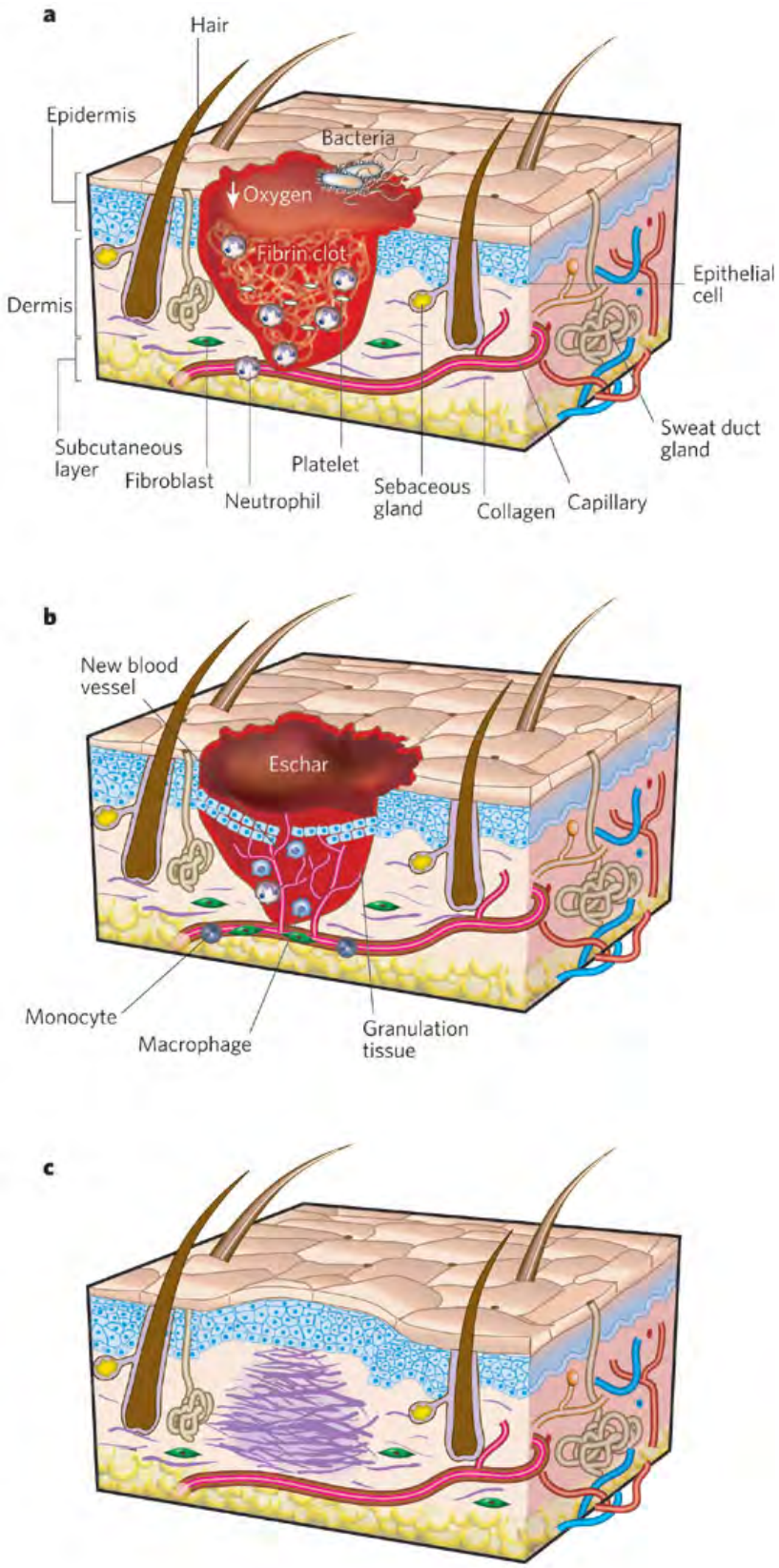

Figure 1.2: **Phases of wound healing**: inflammation (a), re-epithelialization (b) and remodeling (c) [7].

cleared away by tissue macrophages. In response to specific chemoattractants, such as fragments of extracellular-matrix protein, TGF-β, and monocyte chemoattractant protein 1 (MCP-1), monocytes also appear in the wound, where differentiate into macrophages. Macrophages are the major producers of cytokines (e.g. IL-1 and IL-6), chemokines and growth factors (fibroblast growth factor (FGF), epidermal growth factor (EGF), transforming growth factor beta (TGF-β), and platelet-derived growth factor (PDGF)) that direct ulterior cell migration in response to injury [1, 10].

Thus, the inflammatory response after any tissue damage protects the wound from microbial infection and produces bioactive molecules that act at the wound site. Therefore, wound closure is a greatly regulated process in terms of time-dependent expression of cytokines, chemokines and growth factors, as well as in their actions on cellular receptors. These factors are crucial not only for enhancing inflammation but also for setting well-defined stop signals to block the inflammatory cascade when appropriate since a prolonged inflammatory reaction is the main reason for impaired wound healing [11].

1.2.1.2 Re- epithelialization (Figure 1.2 (b))

The second stage of wound repair occurs 2-10 days after injury and is characterized by cellular migration and proliferation of different cell types. The first event is the **migration of keratinocytes** over the injured dermis. An epidermal layer is reconstituted from the edges of the wound and the hair follicles remnants. The migrating epidermal cells permeate the wound, separating eschar tissue from the provisional matrix and healthy dermis. Cells surrounding hair follicles contribute importantly to re-epithelialization. These cells act as normal cut epidermal wound edges and spread out like growing islands from the follicle stump. Finally, the epidermal cells at the wound margin begin to proliferate behind the actively migrating cells what provides a supply of extra cells to replace those lost during injury [2]. Extracellular matrix proteins, including collagen, fibronectin, and vitronectin, provide support for cell movement, vehicles for changing cell behavior, and structures that restore function and integrity to the tissue [12]. Once the epithelial defect has been repaired, and epidermal migration has ceased, basement membrane proteins reappear in a very coordinated sequence from the margin of the wound inward. Finally, epidermal cells return to their normal phenotype, over again tightly attaching to the reestablished basement membrane and underlying connective tissue [1].

The migration and proliferation of epidermal cells during re-epithelialization is due in part to the local release of growth factors (i.e., epidermal growth factor

(EGF), transforming growth factor-alpha (TGF-α), and keratinocyte growth factor (KGF)), and increased expression of growth factor receptors.

The formation of new blood vessels through **angiogenesis** and the sprouts of capillaries associated with fibroblasts and macrophages replace the fibrin matrix with new stroma or granulation tissue. Macrophages release growth factors that stimulate fibroplasia and angiogenesis; fibroblasts produce the new extracellular matrix needed to support cell ingrowth, and blood vessels carry oxygen and nutrients necessary to maintain cell metabolism. Several growth factors released at the wound site, e.g., vascular endothelial growth factor (VEGF) and basic fibroblast growth factor (bFGF or FGF2) promote the proliferation of endothelial cells.

Upon injury, resident dermal **fibroblasts** surrounding the wound **begin to proliferate**, and after 3-4 days following damage they migrate into the provisional matrix of the wound clot where they lay down their own collagen-rich matrix. The fibroblasts are responsible for the synthesis, deposition, and remodeling of the extracellular matrix. Several growth factors at the wound site, e.g., FGF, TGF-β, and PDGF serve either as mitogens or as chemotactic factors for wound fibroblasts. TGF-β and PDGF also cause phenotypic changes in these cells transforming fibroblasts into myofibroblasts, which express α-smooth muscle actin (α-SMA) and resemble smooth muscle cells in their capacity to generate a strong contractile force, enabling wound closure [13].

1.2.1.3 Remodeling (Figure 1.2 (c))

The last stage of wound repair begins 2-3 weeks after injury and last for even more than a year. Every process initiated upon injury decrease and end during the remodeling. Cells in the wound site, i.e., endothelial cells, macrophages, and myofibroblasts undergo apoptosis or get out of the wound, leaving a relative acellular mass that is made primarily of collagen and other extracellular matrix proteins. Matrix metalloproteinases (MMPs) and other enzymes, e.g., tissue plasminogen activator and urokinase plasminogen activator are important components of the wound that facilitate cell movement and the expected remodeling of ECM. MMPs are responsible for transforming an acellular matrix composed mainly of type III collagen to one predominantly made of type I collagen [7]. Integrins are also important since these transmembrane receptors represent the bridges for cell-cell and cell-extracellular matrix interactions. Thus, integrins have two main functions: the attachment of the cell to the ECM, and the signal transduction from the ECM to the cell (outside-in signaling) [12].

The final result is a scar, which keep approximately 70% of the tensile strength

of the normal skin [1].

1.2.2 Growth factors and cytokines involved in wound healing

The success of the wound healing process depends on growth factors, cytokines, and chemokines involved in a complex integration of signals that coordinate cellular processes. These agents are biologically active polypeptides that act to alter the growth, differentiation and metabolism of a target cell [13].

1.2.2.1 Epidermal Growth Factor family

Members of the EGF family are the most important growth factors involved in epithelialization during cutaneous wound healing. The main members involved in wound healing include: EGF, transforming growth factor-alpha (TGF-α) and heparin-binding EGF (HB-EGF). These ligands bind to and activate the EGF receptor (EGFR) that plays an important role in re-epithelialization by increasing keratinocyte proliferation and cell migration in acute wounds.

EGF is secreted by platelets, macrophages, and fibroblasts and acts in a paracrine fashion on keratinocytes, significantly accelerating re-epithelialization and increasing tensile strength in wounds after acute injury. One *in vivo* study has shown that topical application of human biosynthetic EGF accelerates epidermal regeneration in split-thickness wounds and partial-thickness burns [14]. The significant enhancement of epidermal regeneration suggested the potential clinical use of EGF for accelerating healing of burns, wounds from trauma, diabetic ulcers, skin graft donor sites, and others. Thus, EGF may be useful for treating patients with chronic wounds if delivered by gene therapy, polymers, or electrospun nanofibers that keep a constant growth factor concentration, maintaining its presence in the wound and avoiding its rapid degradation.

TGF-α is secreted by platelets, keratinocytes, macrophages, fibroblasts, and lymphocytes and function in an autocrine fashion on keratinocytes. Li et al. proved that TGF-α promotes *in vitro* human keratinocyte migration and proliferation [15]. *In vivo* studies found that TGF-α is required for early stimulation and maintenance of wound epithelialization when granulation tissue is not present (i.e., partial thickness wounds). Moreover, wound epithelialization occurs normally in full-thickness wounds in the absence of TGF-α, probably due to some compensation for the other growth factors in the EGF-family [16].

HB-EGF is produced and secreted by human keratinocytes and acts as an

autocrine growth factor after binding to the EGFR subtypes HER1 and HER4. Given that HB–EGF is a potent mitogen for fibroblasts and keratinocytes as well as being an inducer of cell migration, it was suggested that HB–EGF might be involved in the induction of granulation tissue and re-epithelialization [17]. Studies of wound healing revealed that wound closure was markedly impaired in keratinocyte-specific HB-EGF-deficient mice. Shirakata et al. demonstrated that endogenous HB-EGF is the predominant growth factor involved in the epithelialization of skin wound healing *in vivo* and that it functions by up-regulating keratinocyte migration, rather than proliferation [18].

1.2.2.2 Fibroblast Growth Factor family

FGFs comprise a structurally related family of at least 22 members, of which FGF-1 (acidic FGF), FGF-2 (basic FGF), FGF-7 (keratinocyte growth factor (KGF-1)) and FGF-10 (KGF-2) have been shown to be the most important for keratinocyte migration. FGFs are expressed in specific spatial and temporal patterns and are involved in angiogenesis, wound healing, embryonic development and various endocrine signaling pathways. FGFs are produced by fibroblasts, endothelial cells, smooth muscle cells, chondrocytes and mast cells. In vertebrates, FGFs may have an intracrine, paracrine or endocrine functions. Paracrine and endocrine FGFs act via cell-surface FGF receptors (FGFRs), while, intracrine FGFs act independent of FGFRs [19].

FGF-2, FGF-7, and FGF-10 are the most important members involved in cutaneous wound healing. **FGF-2** (basic FGF) stimulates the proliferation, differentiation and migration of regenerated keratinocytes. It favors angiogenesis in granulation tissue by stimulating the infiltration and proliferation of capillary endothelial cells and, as well as promoting migration of fibroblasts; it also stimulates them to produce collagen. Due to its early release by inflammatory cells in wound healing, FGF-2 is involved in initiating granulation tissue formation, although it continues to be important during subsequent tissue remodeling [20].

FGF-7, or keratinocyte growth factor-1 (KGF-1), and its homolog **FGF-10**, or KGF-2, are important members of the FGF family and are both highly expressed during the early stages of wound healing. These growth factors accelerate the repair of injured skin and mucosal tissues by stimulating the proliferation, migration and differentiation of epithelial cells, and they have direct chemotactic effects during the tissue remodeling process [21]. Also, FGF-7 and FGF-10 reduce reactive oxygen species (ROS)-induced apoptosis of keratinocytes in the wound bed by increasing the transcription of several factors involved in the detoxification of ROS, that is

good for preserving these cells for re-epithelialization.

Finally, FGF-7 is a paracrine and epithelium-specific growth factor produced by cells of mesenchymal origin in response to pro-inflammatory cytokines and steroid hormones. A number of studies showed that pro-inflammatory cytokines such as tumor necrosis factor-α (TNF-α), interleukin-6 (IL-6), and especially IL-1 are potent inducers of KGF expression, suggesting that infiltrating inflammatory cells such as monocytes and neutrophils produce inflammatory cytokines, which induce KGF/FGF-7 expression from local mesenchymal cells to promote epithelial proliferation [22].

1.2.2.3 Transforming growth factor β family

The TGF-β family consists of a number of closely related proteins designated TGF-β1-3, as well as a number of distantly related proteins that include the Inhibins and Activins, Mülllerian Inhibitory Substance (MIS), the Bone Morphogenic Proteins (BMPs), Growth Differentiation Factors (GDFs), and the Glial-derived Neurotrophic Factors (GDNFs) family.

TGF-β1, **TGF-β2,** and **TGF-β3** are the main forms found in mammals, but TGF-β1 predominates. TGF-β is produced by activated macrophages, fibroblasts, keratinocytes, lymphocytes and platelets. TGF-β is a particularly pleiotropic growth factor family, having effects on cell proliferation, adhesion, and differentiation. It is known to be the most potent growth factor involved in wound healing throughout the body.

TGF-β1 is released by degranulating platelets at the site of injury where plays an important role in the phases of inflammation, angiogenesis, re-epithelialization, ECM deposition, and remodeling. Several studies suggest that TGF-β1 is a potent chemoattractant for fibroblasts and cellular mediators of inflammation, including neutrophils and monocytes [23].

Montesano and Orti investigated the influence of TGF-β, PDGF, FGF and EGF on the ability of fibroblasts to contract a collagen matrix in an *in vitro* system. TGF-β, but not the other growth factors tested, markedly enhanced the efficiency of human fibroblasts to contract collagen gels that is likely due to mechanisms such as increased synthesis of actin, fibronectin, and matrix receptors. Thus, TGF-β released from platelets and inflammatory cells at sites of tissue injury stimulates wound healing not only by recruiting fibroblasts for stimulating them to produce collagen (particularly type I and III) and other matrix constituents but also by promoting the contraction of the provisional wound matrix [24, 25].

Angiogenesis is a complex and multistage process, which is controlled by a variety

of factors and whose stimulation may be responsible for an increased healing capacity. VEGF is a potent direct angiogenic factor that stimulates *in vitro* endothelial cell migration and activation, and *in vivo* angiogenesis. Riedel et al. demonstrated a decreased expression of angiogenic VEGF in tissue samples of chronic wounds compared to normal skin. Furthermore, the treatment of human keratinocytes with TGF-β antisense oligonucleotides *in vitro* upregulated VEGF secretion and angiogenic activity. The angiogenic activation of endothelial cells probably plays a role in promoting and regulating other biological events, such as inflammation, fibroblast proliferation, ECM synthesis, and epithelialization in wound healing. It was suggested that antisense TGF-β oligonucleotides might have a potential therapeutic role in the treatment of chronic wounds due to their pro-angiogenic effect [26].

TGF-β regulates expression of several matrix metalloproteinases, enzymes that degrade the extracellular matrix. Some investigators have documented the inhibitory effect of TGF-β on several MMPs, e.g. MMP-1, MMP-3 and MMP-9. MMP-9 degrades the type IV collagen in the basement membrane, MMP-3 (stromelysin 1) degrades a broad range of matrix proteins, and MMP-1 (collagenase-1) specifically degrades the interstitial collagens, types I, II and III. Because of its ability to break down collagen and its expression by many different cell types, MMP-1 has a major role in modeling and remodeling the extracellular matrix. Since TGF-β1 can suppress transcription of the MMP-1 gene, this growth factor has an important role in modulating matrix metabolism [27, 28]. Finally, TGF-β may also be of importance in its ability to inhibit B and T-lymphocyte function and proliferation.

1.2.2.4 Platelet-derived growth factor (PDGF)

PDGF comprises a family of homo or heterodimeric growth factors including **PDGF-AA**, **PDGF-AB**, **PDGF-BB**, **PDGF-CC**, and **PDGF-DD**. PDGFs bind to and activate two structurally related protein tyrosine kinase receptors, PDGF receptor-α and PDGF receptor-β. This growth factor is produced by platelets, macrophages, vascular endothelium, fibroblasts, and keratinocytes. Thus, the principal cells involved in early wound healing all synthesize and secrete PDGF, although platelets are the earliest and largest source [29].

PDGF plays a role in every phase of wound healing. Following injury PDGF, is released from platelet granules and is present in wound fluid. Afterward, this growth factor stimulates mitogenicity and chemotaxis into the wound first of monocytes and then for fibroblasts, smooth muscle cells, and endothelial cells. PDGF acts synergistically with TGF-β and EGF and besides stimulates the production of

fibronectin and hyaluronic acid. PDGF is, therefore, involved in cell recruitment at all stages of wound healing: the stimulation of epithelial and endothelial cells, matrix formation and modulation of other growth factor activities [20].

Uutela et al. have shown that PDGF-D recruits macrophages to sites of its expression and causes significant increase in interstitial fluid pressure in the dermis of PDGF-D–overexpressing mice during the wound healing process. Also, combined expression of PDGF-D with VEGF-E can induce a strong angiogenic response and promote stabilization of the newly generated enlarged and leaky vessels induced by VEGF-E alone [29]. Lindahl et al. demonstrated that PDGF-B-deficient mouse embryos were found to lack microvascular pericytes in capillaries formed through angiogenesis. These mice developed numerous capillary microaneurysms that caused hemorrhages and edema after the rupture at late gestation when blood pressure increased. Thus, PDGF is important for proliferation and migration of pericytes to the capillaries and consequently increase the structural integrity of these vessels [30].

1.2.2.5 Vascular endothelial growth factor (VEGF)

Vascular endothelial growth factor is a homodimeric glycoprotein that exists in five isoforms referred to as **VEGF-A**, **VEGF-B**, **VEGF-C**, **VEGF-D**, and placental growth factor (**PlGF**). VEGF is produced by many cells types that participate in wound healing: endothelial cells, fibroblasts, smooth muscle cells, platelets, neutrophils, and macrophages. In humans, VEGF binds to receptors Flt-1 (VEGFR-1) and KDR (VEGFR-2), both high-affinity receptors that are localized to the endothelial surface of developing and mature blood vessels.

An essential feature of normal wound repair is the formation of granulation tissue, i.e. fibrovascular tissue containing fibroblasts, collagen and blood vessels, which is the hallmark of an established healing response. The vascular component depends upon angiogenesis, in which new vessels appear as early as day three after wounding [31].

VEGF is a highly specific mitogen for endothelial cells *in vitro*, and it has angiogenic properties *in vivo*. Moreover, it enhances the permeability of local blood vessels. Since angiogenesis and increased vascular permeability are characteristic features of wound healing, VEGF may play an important role in tissue repair. VEGF is released by activated platelets following an injury. Monocytes have both a direct and indirect role in the angiogenic phase of wound healing. Monocytes express the VEGF receptor Flt-1 and respond chemo tactically to VEGF. Once recruited to the tissue, macrophages induce angiogenesis by releasing VEGF, but also in part by

producing TNF-α, which may in turn induce VEGF expression in keratinocytes and fibroblasts. Other cytokines and growth factors that act as paracrine factors enhancing VEGF expression include TGF-β1, EGF, TGF-α, KGF (from keratinocytes and arterial smooth muscle cells), bFGF, PDGF-BB, and IL-1β [32].

Stimulation of angiogenesis is one of the most important roles of VEGF in wound healing. Wound healing angiogenesis involves multiple steps including vasodilation, basement membrane degradation, endothelial cell migration, and proliferation. Subsequently, capillary tube formation occurs, followed by anastomosis of parallel capillary sprouts (loop formation), and finally new basement membrane formation.

VEGF induces endothelial cell migration in wound healing through two primary mechanisms, chemotaxis and by increasing vascular permeability mediated by nitric oxide and prostacyclin. In the initial phase of angiogenesis, endothelial cells migrate before mitotic division. VEGF induces endothelial cells growth on the surface of a collagen matrix to invade the underlying matrix and stimulates their proliferative response.

VEGF is also upregulated by hypoxia due to metabolic derangements of the wound environment. The resulting angiogenesis restores tissue perfusion, reestablishes microcirculation, and increases oxygen tension at the wound site. Specifically, hypoxia enhances VEGF expression in monocytes and other cell types such as fibroblasts, keratinocytes, myocytes, and endothelial cells [33]. Similarly, hypoxia stimulates the expression of Flt-1 on cultured endothelial cells. As a result, there is a gradient of VEGF expression that parallels the hypoxic gradient, and endothelial cells afterward migrate towards the most hypoxic areas [34].

In summary, direct and indirect evidence implicates VEGF as a significant factor in wound healing immediately after an injury. Induced by inflammatory cells and local wound conditions, VEGF potentially alleviates tissue hypoxia and metabolic deficiencies by promoting early events in angiogenesis, as well as endothelial cell function. Maximal activity occurs during a "window" period approximately three to seven days after injury. Once the wound is granulated, angiogenesis ceases, and blood vessels decline as endothelial cells undergo apoptosis. The reduction in VEGF and the loss of apoptosis may contribute to this transition from hypercellular granulation tissue to a hypocellular scar [35].

1.2.2.6 Granulocyte-macrophage colony-stimulating factor (GM-CSF)

GM-CSF is a highly pleiotropic cytokine with many effects on granulocytes/macrophages, including chemotaxis and cellular adhesion, also priming the production of pro-inflammatory cytokines. *In vivo* studies have shown that GM-CSF

enhances wound healing by promoting re-epithelialization, recruitment of leukocytes, increased angiogenesis and upregulation of pro-inflammatory mediators (e.g., IL-6 and MCP-1). Promotion of re-epithelialization following GM-CSF treatment of diabetic mice also lead to a parallel reduction in collagen deposition in diabetic wounds [36].

GM-CSF can promote the growth and maturation of myeloid cells, in particular, the proliferation and differentiation of neutrophil progenitors both *in vitro* and *in vivo*. It also stimulates the function of mature neutrophils. Thus, it may be suggested that GM-CSF may have a crucial role in the neutrophil response to infection. Yönem et al. investigated the effects of systemic human recombinant GM-CSF treatment in diabetic patients with foot infections. They found that GM-CSF treatment caused significant improvement in the absolute number and phagocytic activity and the respiratory burst of neutrophils in patients with a diabetic foot infection. Nevertheless, the amelioration of neutrophil function was not associated with shortening of either duration of antibiotic administration or duration of hospitalization [37].

Finally, *in vivo* studies have demonstrated that GM-CSF influence the migration and proliferation of human endothelial cells suggesting that this growth factor may act as a regulatory signal outside the hematopoietic system by promoting angiogenesis [38].

1.2.2.7 Pro-inflammatory Cytokines

Some pro-inflammatory cytokines such as interleukin-1 (IL-1), interleukin-6 (IL-6), and TNF-α are up-regulated during the inflammatory phase of wound healing [1]. IL-1β and IL-6 have mitogenic and proliferative effects on keratinocytes and contribute to the process of wound healing.

IL-1 is strongly expressed by monocytes, tissue macrophages, and dendritic cells, but is also produced by B lymphocytes, NK cells, and epithelial cells. IL-1 is an essential pro-inflammatory cytokine which possesses multiple properties and affects almost all cell types. It is a mediator of the acute phase of inflammation by induction of local and systemic responses. IL-1 can increase the expression of adhesion molecules such as intercellular adhesion molecule-1 (ICAM-1) and vascular cell adhesion molecule−1 (VCAM-1) on mesenchymal and endothelial cells, which together with the induction of chemokines, promote the infiltration of inflammatory and immunocompetent cells from the circulation into the extravascular space. IL-1β is also an angiogenic factor and plays a role in tumor metastasis and blood vessel formation [39].

Thomay et al. investigated the role of IL-1 signaling in the constitution of the

inflammatory cellular infiltrate and the healing response that follows cutaneous and deep tissue wounds in mice. The most important findings of the study were the reductions in inflammatory cell infiltration, epidermal hyperplasia, and fibrosis found in incisional wounds in IL-1 receptor type I (IL-1R) knockout mice. In addition, these mice had a marked decrease in fibrosis in deep tissue wounds. These findings suggested that pharmacological interference with IL-1 signaling could have therapeutic value in the prevention of hypertrophic scarring and the treatment of fibrotic diseases [40].

IL-6 is a pleiotropic cytokine produced by macrophages, T cells, fibroblasts, keratinocytes, and endothelial cells. It exhibits various activities on a wide range of cells including lymphocytes, hepatocytes, and neurons.

Several studies suggested that IL-6 has crucial roles in inflammation, particularly during the early phase. Zi-Qing et al. evaluated the pathophysiological role of IL-6 in wound healing processes of IL-6-deficient BALB/c knockout (KO) mice compared to wild-type (WT) control mice. In WT mice, skin excisions upregulated IL-6 gene expression by keratinocytes, neutrophils, macrophages, and myofibroblasts at the wound sites. There was no significant difference in T-cell recruitment between WT and IL-6 KO mice. However, reduced neutrophil and macrophage infiltration in IL-6 KO mice was observed along with lowered expression of some adhesion molecules and cytokines such as ICAM-1, VCAM-1, IL-1, MIP-1, MIP-2, KC, and TGF-β. IL-6 can upregulate the IL-1 expression and consequently the expression of some adhesion molecules (i.e., ICAM-1 and VCAM-1) what affect both leukocyte extravasation and chemokines gene expression. TGF-β and VEGF gene expression was also significantly attenuated in IL-6 KO mice that could be responsible for reduced collagen accumulation and angiogenesis. These observations suggested that IL-6 had crucial roles in wound healing, probably by regulating leukocyte infiltration, angiogenesis, and collagen accumulation [41].

On the other hand, **TNF-α** is produced by activated macrophages, although it can be produced by many other cell types such as $CD4^+$ lymphocytes, NK cells, neutrophils, mast cells, eosinophils, and neurons. TNF-α has a beneficial role in host defense against pathogens, but in excess, it is associated with damaging effects.

TNF-α can exert several functions depending on the concentration and duration of the exposure to this cytokine. Low levels of TNF-α can promote wound healing by indirectly stimulating inflammation and enhancing macrophage-produced growth factors. However, TNF-α has a detrimental effect on healing when present at higher levels and prolonged periods of time. In addition, TNF-α suppresses synthesis of

ECM proteins and TIMPs while increasing synthesis of MMPs (MMP-1, MMP-2, MMP-3, MMP-9, MMP-13, and MT1-MMP) in impaired acute wound healing and chronic wound healing states what finally affect cell migration and collagen deposition [13].

Ashcroft et al. described an animal model of severely impaired wound healing (i.e., Secretory Leukocyte Protease Inhibitor (SLPI) null mouse model), comparable to chronic wound healing in elderly humans, which have in common augmented leukocyte infiltration and protease activity during initial stages of injury and tissue destruction. They have reported that TNF-α levels, both systemically and in acute wounds, were significantly increased in humans predisposed to impaired healing and that elevated local tissue levels declined in parallel with healing. They have shown that TNF-α inhibition reverses the impaired healing phenotype and dampened excessive inflammation in the SLPI null animals and significantly accelerated the rate of wound healing [42].

IL-1β and TNF-α can promote the induction of keratinocyte growth factor, FGF-7, which can in turn promote re-epithelialization at the wound site. Thus, these pro-inflammatory cytokines are directly and/or indirectly involved in the wound healing process, and their upregulation is required for optimal skin wound healing [19].

1.2.2.8 Chemokines

Chemokines constitute a family of chemoattractant cytokines that selectively recruit monocytes, neutrophils, and lymphocytes, inducing chemotaxis through the binding to G-protein-coupled receptors (GPCRs). Chemokines could act as secondary pro-inflammatory mediators, i.e., they are typically induced by primary pro-inflammatory mediators such as IL-1 and or TNF-α. By recruitment of leukocytes, chemokine activity leads to activation of host defense mechanisms and stimulates the early events of wound healing [43].

Chemokines can be classified into four subfamilies on the basis of the number and location of the cysteine residues at the N-terminus of the molecule, and are named CXC, CC, CX3C, and C, in agreement with the systematic nomenclature. Chemokines are also grouped into two main functional subfamilies: inflammatory and homeostatic chemokines. Inflammatory chemokines control the recruitment of leukocytes in inflammation and tissue injury, whereas homeostatic chemokines fulfill housekeeping functions such as homing leukocytes to and within secondary lymphoid organs as well as in the bone marrow and the thymus during hematopoiesis [44].

Monocyte chemoattractant protein-1 (MCP-1 or CCL2) is a member of the CC chemokine family and a potent chemotactic factor for monocytes. CCL2 is

produced by many cell types, including endothelial, fibroblasts, epithelial, smooth muscle, mesangial, astrocytic, monocytic, and microglial cells. However, monocyte/macrophages are found to be the major source of CCL2. CCL2 regulates the migration and infiltration of monocytes, memory T-lymphocytes, and natural killer (NK) cells.

CCL2 mediates its effects through its receptor CCR2, and, unlike CCL2, CCR2 expression is relatively restricted to certain types of cells. It is important to note that CCR2 has dual roles and has both pro-inflammatory and anti-inflammatory actions. The pro-inflammatory role of CCR2 is dependent on antigen-presenting cells (APCs) and T cells, whereas the anti-inflammatory role of CCR2 is dependent on CCR2 expression in regulatory T cells [44].

Wetzler et al. observed a large induction and sustained expression of the inflammatory cytokines IL-1β and TNF-α mRNA during the late phase of repair in diabetic mice, indicating a prolonged inflammatory response at the wound site. MCP-1 was also strongly increased at the mRNA and protein level in keratinocytes what brought about a prolonged presence of neutrophils and macrophages in the chronic wound. In addition, macrophages can also express MCP-1 in a regulatory feedback mechanism that triggers attraction of additional macrophages into the wound. Finally, MCP-1 represents an attracting signal also for wound keratinocytes and endothelial cells during repair *in vivo* [45]. Thus, delayed wound-re-epithelialization, angiogenesis, and collagen synthesis is also present within the wounds of MCP-1 KO mice [46].

Engelhardt et al. found by using incisional adult skin wounds that changes in sets of chemokines actively regulate the migration and accumulation of the major leukocyte subtypes in wounds (i.e., neutrophils, monocytes/macrophages, and lymphocytes). Firstly, migration of neutrophils to the denuded wound surface at day 1 correlates temporally and spatially with IL-8 and GRO-α mRNA expression, whereas the enhanced expression of MCP-1 is responsible for the migration of macrophages from day 2 onward. Then, lymphocyte migration is initially paralleled by MCP-1 expression and then after four days by IP-10 expression [47].

IL-8 and GRO-α stimulate re-epithelialization, i.e., by increasing keratinocyte migration and proliferation, but also augment neoangiogenesis as evidenced by an increase in the number of vessels within the wound area. The chemokines MCP-1, MIG, and IP-10, are both T-cell attractant and highly expressed at sites of lymphocyte accumulation. Mig and IP-10 can also inhibit endothelial cell chemotaxis and angiogenesis induced by IL-8 or bFGF; thus these chemokines may exert an angiostatic effect that prevent from possible unlimited vessel growth produced by

the continuous presence of factors such as bFGF and PDGF without blocking other repair processes involved in wound healing. Because MCP-1, IL-8, and GRO-α are inducible by TNF-α and IL-1 whereas synthesis of MIG and IP-10 is stimulated mainly by IFN-δ, the differential chemokine expression profiles may reflect a high expression of TNF-α and IL-1 in the early phase and a delayed expression of IFN-δ in the late phase of wound healing [47].

Persistent production of pro-inflammatory cytokines and reduced release of pro-angiogenic and pro-healing factors are associated with persistent inflammation, reduced angiogenesis and granulation tissue formation, and impaired closure seen during impaired healing. Cytokines can modulate the activity of keratinocytes, fibroblasts, endothelial cells and inflammatory cells by acting both autocrine and paracrine fashion to achieve efficient healing.

Mirza and Koh determined the relative contributions of different cell subsets to the production of cytokines and growth factors during normal and impaired wound healing. They found that the monocytes/macrophages subset was the dominant producer of pro-inflammatory cytokines IL-1β, TNF-α and IL-6 in both non-diabetic and diabetic mice and was a significant producer of VEGF-A, IGF-1, and TGF-β1. The neutrophils/T cells/B cells subset was also a significant producer of TNF-α and IL-10 whereas the keratinocyte/fibroblast/endothelial cells subset contributed significant amounts of VEGF, IGF-1, and TGF-β1. Sustained production of pro-inflammatory cytokines and impaired production of healing associated factors were evident in each subset in diabetic mice [48].

The skin is frequently exposed to aggressive molecules (e.g., ultraviolet irradiation, toxic chemicals) which induce the formation of reactive oxygen species (ROS). In skin wounds, ROS are produced largely by inflammatory cells as a defense against bacterial infection. Nonetheless, these molecules can damage the inflammatory cells themselves and other cells at the wound site. For this reason, cells produce low molecular weight antioxidant proteins and increase the expression of ROS-detoxifying enzymes as a mechanism to protect inflammatory and resident cells from ROS toxicity. Genes encoding the ROS-detoxifying enzymes are under the control of the Nrf2 transcription factor. The Nrf2 gene is a target of keratinocyte growth factor (KGF), a cytoprotective growth factor for epithelial cells that is highly expressed in skin wounds [49]. Nrf2 mRNA was significantly up-regulated in keratinocytes and macrophages in a murine full-thickness excisional wound model, thus regulating inflammation but not re-epithelialization in skin wounds [50].

One of the wound-regulated genes encodes peroxiredoxin 6 (Prdx6). Peroxiredoxins consist of a family of six enzymes that catalyze the reduction of hydrogen

peroxide and a wide range of organic peroxides through redox-active cysteines. Some studies revealed that overexpression of Prdx6 in different cell types protected from ROS-induced cytotoxicity, whereas antisense-mediated knockdown of this enzyme enhanced the sensitivity to oxidative stress. Kumin et al. shown that peroxiredoxin-6 deficient mice had a severe hemorrhage in the granulation tissue following skin injury, which correlates with the extent of oxidative stress and counteract proper wound healing. At the ultrastructural level, endothelial cells appeared highly damaged, and their rate of apoptosis was enhanced. Furthermore, knocking down Prdx6 in cultured endothelial cells increased their susceptibility to oxidative stress [51]. The wound microenvironment attracts MSCs, and local inflammation and oxidative stress influences the behavior of these cells by creating a low-oxygen environment. Hypoxia induces MSCs to proliferate at a faster rate and promote wound healing through increased epithelialization, accelerated wound closure, and angiogenesis [52].

1.3 Abnormal Wound Healing. Chronic Wounds

Chronic wounds are defined as wounds that do not heal within three months. Besides, these wounds do not follow the gradual process of physiologic healing, thus being unable to restore anatomic and functional integrity in an appropriate period. Chronic wounds are often associated with diabetes or obesity. It has been estimated that 1-2% of people in developed countries will suffer from chronic wounds in their lifetime. With an aging population and increasing rates of obesity and diabetes, it is clear that this problem is set to rise [6].

Multiple local and systemic factors can lead to impaired wound healing by adversely affecting one or more phases of this process. The factors that influence repair include oxygenation, infection, age and sex hormones, stress, diabetes, obesity, medications, alcoholism, smoking, and nutrition. Many of these factors are related, and the systemic factors act through the local effects affecting wound healing [53]. In contrast, the wound healing process can sometimes result in excessive dermal fibrosis that can induce the formation of keloids and hypertrophic scars in predisposed individuals [54].

Standard treatment of chronic wounds is commonly addressed to modify controllable causative factors such as antibiotic treatment of infected wounds, pressure relief of decubitus areas, revascularization of ischemic limbs, and compression garments for venous insufficiency. Surgical debridement and negative pressure wound therapy are frequently used techniques, even when they are not an optimal treatment because of the lengthy healing time required for this method. The use of skin

substitutes has been proved to be a useful tool for treating this difficult condition, but so far no ideal therapy is available to treat troublesome chronic wounds. Thus, new therapies in this area are required to optimize outcomes for the patients [55].

Mesenchymal stem cells are emerging as a promising candidate for cell-based therapy for the treatment of chronic wounds because of their enormous potential for enhancing tissue repair and regeneration following injury. MSCs can be isolated from a variety of adult and fetal tissues, including dental pulp, adipose tissue, skin, cord blood, liver, synovium, pancreas, lung, placenta, amniotic fluid, and peripheral blood. Bone marrow MSCs are usually considered as a gold standard and the most investigated cell type. However, the use of MSCs obtained from bone marrow exposes the donor to a painful and invasive procedure, leading to the use of non-invasive and ethically non-problematic sources. Thus, MSCs obtained from ethically approved sources that otherwise would be discarded in hospitals, i.e., MSCs from placenta (Pl-MSCs), umbilical cord (UC-MSCs), Wharton's jelly (Wj-MSCs), and adipose tissue (AT-MSCs), are also used in studies, considering their multiple properties [56].

1.4 Mesenchymal Stem Cells

1.4.1 Definition

Mesenchymal stem cells (MSCs) are undifferentiated cells that can self-renew and differentiate into multiple cell types. Friedenstein et al. first isolated and recognized the multilineage differentiation capacity of the mesenchymal stromal cell [57]. Their plasticity or potency is hierarchical ranging from totipotent (differentiating into all cell types including placenta), pluripotent (differentiating into cells of the three germ layers, ectoderm, mesoderm and endoderm, but not trophoblastic cells), multipotent (differentiating into cells of more than one type but not necessarily into all the cells of a given germ layer) to unipotent (differentiating into one type of cell only, e.g. muscle or neuron) [58].

The International Society for Cellular Therapy (ISCT) proposed three minimal criteria to define human MSCs [59]:

- MSC must be plastic-adherent when maintained in standard culture conditions using tissue culture flasks.
- More than 95% of the MSC population must express CD105 (endoglin), CD73 (ecto-5'-nucleotidase) and CD90 (Thy 1), as measured by flow cytometry.

Besides, these cells must lack expression ($\leq$ 2% positive) of CD45 (pan-leukocyte marker), CD34 (primitive hematopoietic progenitors and endothelial cells marker), CD14 or CD11b (expressed on monocytes and macrophages), CD79α or CD19 (markers of B cells) and HLA class II (not expressed on MSC unless stimulated, e.g. by IFN-γ). Only one of the macrophage and B cell markers needs to be tested.

- The cells must be able to differentiate into osteoblasts, adipocytes and chondroblasts under the standard *in vitro* tissue culture-differentiating conditions.

1.4.2 Classification

Stem cells can be classified into embryonic, fetal, and adult stem cells based on their time of isolation during ontogenesis.

1.4.2.1 Embryonic Mesenchymal Stem Cells (EMSCs)

EMSCs are derived from the inner cell mass (ICM) of the blastocyst which is an early stage pre-implantation embryo. EMSCs divide indefinitely (self-renewal) in culture while maintaining their capacity for extensive *in vitro* and *in vivo* differentiation (pluripotency) [60]. Use of EMSCs for tissue regeneration application is limited because the differentiation of these cells is difficult to control, and the ability to form all tissue types brings about the risk of *in vivo* tumorigenicity and teratoma formation. Moreover, chromosomal stability is difficult to preserve when EMSCs are kept in culture over multiple passages. Embryonic stem cell (ESC) research also has ethical problems since isolation of EMSCs implicates destruction of the embryo while the cells are extracted, a process that has provoked objection from political, religious, and social groups. Therefore, the use of EMSCs in clinical practice remains largely theoretical, and ESC research is mainly directed toward studying disease states and biological processes [52].

1.4.2.2 Adult Mesenchymal Stem Cells (AMSCs)

AMSCs are the most commonly used MSCs and they have been extensively characterized for their therapeutic potential. AMSCs can be isolated from many tissue types including brain, dental pulp, skeletal muscle, bone marrow, skin, fat, and pancreas. However, these cells are difficult to extract in sufficient numbers for therapeutic applications and have restricted plasticity and limited proliferative capacity compared with EMSCs [58]. Finally, use of AMSCs in cell-based therapy could avoid

many of the ethical limitations associated with other stem cell types, especially embryonic stem cells. Among the wide range of adult stem cells, bone-marrow-derived mesenchymal stem cells (BM-MSCs) and adipose-derived- stem cells are of particular relevance to tissue engineering in the setting of chronic wounds. Stem cells proffer great potential for enhancing tissue repair and regeneration upon injury. Continuous advances in stem cells biology and skin tissue engineering have generated translational opportunities for the development of novel stem cell-based wound healing therapies, which manifest promising results in preclinical and clinical trials for the treatment of chronic wounds [55].

1.4.2.3 Fetal Mesenchymal Stem Cells (FMSCs)

FMSCs can be isolated from two distinct sources, the fetus proper and the supportive extra-embryonic structures (amniotic fluid, Wharton's jelly, placenta, and amnion). Extra-embryonic tissues as stem cell source offer many advantages over both embryonic and adult stem cell sources. Extra-embryonic tissues are routinely discarded at birth, so little ethical concerns attend the harvest of the resident stem cell populations. The extracorporeal nature of fetal stem cell sources facilitates isolation, eliminating invasive procedures for patients; that implies adult stem cell isolation. Most significantly, the comparatively high volume of extra-embryonic tissues and ease of physical manipulation augment the number of stem cells that can be isolated. In this sense, Wj-MSCs have shown to exhibit high proliferation capacity compared to adult BM-MSCs, and thus can be scaled up easily for regenerative medical applications [60, 61].

General functions of MSCs include supporting of the *ex vivo* expansion of hematopoietic stem cells, act as immune modulators, release cytokines and growth factors, and home to sites of pathology.

1.4.3 Human Umbilical Cord

1.4.3.1 Wharton's Jelly Mesenchymal Stem Cells

In 1656, Thomas Wharton first described the umbilical cord as the connective tissue that links fetus and the human placenta. The umbilical cord contains two umbilical arteries and one umbilical vein, which are protected by a gelatinous matrix rich in proteoglycans and mucopolysaccharides named Wharton's jelly. McElreavey et al. in 1991 first isolated the mesenchymal stromal cells from Wharton's jelly portion of the human umbilical cord (Wj-MSCs) [62].

The umbilical cord is normally thrown away after either normal vaginal delivery

or cesarean section, and then it can be easily obtained with no risk for collection and ethical concerns. The umbilical cord MSCs have more primitive properties than other adult MSCs obtained later in life, which might make them a useful source of MSCs for clinical applications. Furthermore, Wj-MSCs are more similar to fetal MSCs regarding their *in vitro* expansion potential, and lengthy passaging of them is not related to any aberrant cell cycle profile and acquired tumor formation capabilities [61].

Wj-MSCs have been used for broad range of applications such us Parkinson's disease [63, 64, 65], neurological disorders [66], neural damage associated with cardiac arrest/resuscitation [67], kidney injury [68], lung injury [69], orthopedic injury [70], cancer therapy [71], retinal disease [72], and cerebral global ischemia [73].

1.4.4 Immunomodulatory Properties of Mesenchymal Stem Cells

The immunomodulatory effects of MSCs are not only apparent in T lymphocytes but also in B lymphocytes, dendritic cells (DC), or NK cells. MSCs can inhibit immune cell proliferation, reduce immune cell cytokine secretion, and alter immune cell subtypes [74].

Mesenchymal stem cells have immune avoidance mechanisms that reduce immunogenicity that is necessary to avoid the acute rejection response by the host following xenogeneic transplantation. Hypoimmunogenicity of MSCs confers a critical advantage in their use for cell therapy. In humans, these cells express low surface levels of major histocompatibility complex (MHC) class I molecules and express neither MHC class II molecules nor costimulatory molecules, such as CD40, CD40L, CD80, or CD86. The expression of MHC class I, although weak, protects MSCs from NK cell-mediated killing; also, the lack of MHC class II expression confers to these cells the ability to escape immune recognition by $CD4^+$ T cells [56].

Two different general mechanisms, one cell contact-dependent and one - independent, have been proposed to explain the immunosuppressive capability of mesenchymal stem cells.

Nicola et al. conducted a key study aimed to analyze the mechanisms underlying BM-MSC-mediated suppression of T-lymphocyte proliferation in both mixed lymphocyte culture and the presence of polyclonal activators. BM-MSCs significantly inhibited both $CD4^+$ and $CD8^+$ T cell proliferation even when using transwell system, suggesting that soluble factors were also involved in this process besides the cell-cell contact [75]. Regarding the direct effect of MSC on T cells, it was demonstrated that MSCs express adhesion molecules on their surface such as integrins,

intercellular adhesion molecules (ICAM-1, ICAM-2), vascular cell adhesion protein (VCAM)-1, CD72, and CD58, that bind to T lymphocytes with high affinity [76].

Recent studies have shown that MSCs have the capacity to sense their microenvironment and migrate in response to signals produced by inflamed tissues (e.g., growth factors, cytokines, or chemokines). These cues may have a role in determining the function of MSCs, either promotion of pathogen clearance or suppression of inflammation.

MSC immunomodulation takes place over a multistage process involving (1) MSC responsiveness to inflammation and possible migration to the site of tissue injury, (2) licensing or activation of MSCs, (3) promotion of pathogen clearance if required and (4) modulation of inflammation [77].

Following the migration of MSCs to the site of inflammation, they need to be activated to exert their immunosuppressive effects. In particular, the immunosuppressive function of MSCs is elicited by IFNγ and the concomitant presence of any of three other pro-inflammatory cytokines, TNF-α, IL-1α, or IL-1β [78, 79, 80]. Importantly, regulation of several MSC immunomodulatory molecules (including indoleamine 2,3-dioxygenase (IDO), prostaglandin E2 (PGE2), TGF-β, TSG-6 and nitric oxide (NO) by pro-inflammatory cytokines has been observed [80]. In addition to pro-inflammatory cytokines, toll-like receptors (TLRs) signaling may differentially license MSCs; with TLR4 priming inducing a pro-inflammatory phenotype (MSC1) and secretion of IL-6, IL-8, and TGF-β, and TLR3 priming inducing anti-inflammatory MSCs (MSC2) (producing IDO, PGE2, IL-4, and IL-1RA) [81]. Other study showed that, in the presence of INF-γ, either TNF-α or IL-1α induces the expression of adhesion molecules ICAM-1 and VCAM-1, which are also essential for MSC-mediated immunosuppression [82].

The effect of INF-γ in MSCs licensing has been studied *in vivo*, in an experimental murine model of Graft versus Host Disease (GVHD). MSC, pre-treated with IFN-γ, became immediately active and could suppress GVHD more efficiently than a fivefold greater number of MSC that were not activated. Furthermore, when administered at the time of bone marrow transplantation, INF-γ-treated MSCs could prevent GVHD mortality [79].

1.4.4.1 MSCs Re-educate Monocytes/Macrophages in the Context of Tissue Repair

In response to activating signals, macrophages become polarized into either a classical M1 phenotype (pro-inflammatory, stimulated by TLR engagement or IFN-γ) or an alternative M2 phenotype (anti-inflammatory, stimulated by IL-4/IL-13). M1

macrophages are characterized by their high-level production of pro-inflammatory cytokines including TNF-α and IL-1β whereas M2 are commonly associated with secretion of IL-10 [83].

It has been described that MSCs may interact with macrophages at sites of inflammation and influence their polarization. Several studies have demonstrated that production of IDO and PGE2 are involved in MSC modulation of macrophage function. Ylöstalo et al. shown that human MSCs cultured as 3D spheroids produced PGE2 that changed stimulated macrophages from a primarily pro-inflammatory M1 phenotype to a more anti-inflammatory M2 phenotype [84].

1.4.4.2 MSCs Produce Immunosuppressive Soluble Factors

Many of the mechanisms by which the MSCs modulate the immune responses implies the production of immunosuppressive factors, most of which are produced once the MSCs have been activated. More than thirty soluble factors have been associated with the immunomodulation capacity on T-lymphocyte activation and proliferation by MSCs, such as hepatic growth factor (HGF), TGF-β, IDO, PGE2, NO, IL-6, IL-10, semaphorin-3A, galectin (Gal)-1, and Gal-9. Nonetheless, some relevant differences are well acknowledged between species and should be considered for the interpretation of results obtained by the use of MSCs from mice [56].

Indoleamine 2,3-dioxygenase (IDO) is an enzyme that catabolizes tryptophan (an essential amino acid required for T-cell proliferation) into kynurenine metabolites that regulate T-cell proliferation. Expression of IDO on MSCs is induced by stimulation with IFN-γ or through stimulation with TLR3 and TLR4 ligands [78, 85]. MSC-derived IDO has been associated with the re-education of immune cells including macrophage polarization to the anti-inflammatory M2 phenotype, induction of tolerogenic dendritic cells (DCs) and T regulatory cells *in vivo* as well as promoting a Th1–Th2 switch [86].

IDO is also known to have a role in microbial defense; thus it may be possible that MSC-derived IDO could enhance microbial clearance as well as inhibition of immune responses [77].

Tumor necrosis factor-inducible gene 6 protein (TSG-6) is an IL-1/TNF-inducible protein with anti-inflammatory properties. TNF-α stimulation of MSCs leads to the production of significant amounts of TSG-6.

MSC-derived TSG-6 has been shown to mediate protective effects in murine models of myocardial infarction [87], corneal injury [88], allogeneic corneal transplant as well as zymosan-induced peritonitis [89]. In all models, TSG-6 inhibited the early inflammatory response, and specifically neutrophil infiltration and pro-inflammatory

cytokines.

Prostaglandin E2 (PGE2) Prostaglandins are small lipid molecules that regulate numerous processes in the body, including kidney function, platelet aggregation, neurotransmitter release and modulation of immune function. The production of prostaglandins begins with the liberation of arachidonic acid from membrane phospholipids by phospholipase A_2 in response to inflammatory stimuli. After, arachidonic acid is converted to PGH_2 by the cyclooxygenase enzymes COX-1 and COX-2 (known formally as prostaglandin endoperoxide H synthases). Then, cell-specific prostaglandin synthases convert PGH_2 into a series of prostaglandins [90]. MSCs constitutively express COX-2 and produce PGE2 that is enhanced by stimulation with IFN-γ and TNF-α as well as by TLR3 but not TRL4 ligands [81].

Several studies support the role of MSC-derived PGE2 in the suppression of T-cell activation and proliferation both *in vitro* and *in vivo*, MSC reprogramming of macrophages and DCs, and inhibition of mast cell function.

MSCs alter the Helper T-Cell Balance Efficient host defense against invading pathogenic microorganisms is achieved through coordination of complex signaling networks that link the innate and adaptive immune systems. Upon interaction with cognate antigen presented by antigen-presenting cells such as dendritic cells (DCs), $CD4^+$ T cells can differentiate into a variety of effector subsets (i.e., classical Th1 cells and Th2 cells, Th17 cells, follicular helper T (Tfh) cells, and induced regulatory T (iTreg) cells) and produce distinct patterns of cytokines [91].

MSCs have the capacity to modulate T-cell proliferation and function through shifting the balance from a pro-inflammatory Th1 phenotype (secreting IFN-γ and TNF-α) to a more anti-inflammatory Th2 profile (secreting increased levels of IL-4, IL-5, IL-10, IL-13 and the Th2 chemokine CCL1), and vice versa for Th2-driven pathologies. MSCs also modulate Th17 differentiation in favor of IL-4-producing Th2 cells or the generation of Treg [92].

MSCs induce tolerogenic DCs MSCs can interfere with the development of both myeloid and plasmacytoid DCs but also with the key features of DC function; i.e., migration, maturation and antigen presentation. Several mechanisms have been implicated in these effects including both soluble factors and contact-dependent signals [93]. MSCs can also re-programme conventional lymphocyte stimulatory DCs into anti-inflammatory DCs with a tolerogenic phenotype. These DCs may produce higher levels of anti-inflammatory cytokines including IL-10 and lower levels of the pro-inflammatory cytokines IL-12 and TNF-α. The exposure to MSCs also results in enhanced phagocytic activity typical of tolerogenic DCs [94].

MSC induction of Treg and immune tolerance Regulatory T cells (Tregs) are a subpopulation of T lymphocytes characterized by surface expression of CD4, IL-2 receptor (CD25) and the transcription factor forkhead box P3 (FoxP3). These cells possess the capacity to suppress other immune cells (including T cells) and can be produced both in the thymus, as a functionally mature subpopulation of T cells, or induced from naive T cells in the periphery. Di Ianni et al. suggest that MSCs provide a homeostatic niche for Tregs, since they recruit, regulate, and maintain T regulatory phenotype and function over time [95].

Tregs have an important role in controlling not only allo- and autoreactive T cell responses but also inducing and maintaining tolerance to self and non-self antigens. MSC expansion or induction of Tregs has been associated with protection from some of alloreactive, autoimmune and allergic diseases including organ transplantation, allergic airway disease, type-1 diabetes and inflammatory bowel disease [77].

PGE2, TGF-β, and IL-10 are the major soluble factors involved in MSC promotion of Tregs *in vivo*, although the mechanisms that lead to the generation of Tregs and subsequent induction of tolerance are varied and dependent on the microenvironment (i.e., allergic, alloreactive, autoreactive) [96, 97].

Regarding organ transplantation, MSCs may enhance allograft survival and in some cases, induce tolerance by the promotion of Tregs [98]. Ge et al. performed a study to address whether MSCs induce kidney allograft tolerance. They found that MSCs inhibited T cell proliferation and promoted a Th2-dominant response, while inducing tolerogenic DCs with attenuated allostimulatory capacity and decreasing anti-donor antibodies. These anti-inflammatory effects and the induction of tolerance maintaining Tregs were mediated by MSC-derived IDO, as evidenced by the inability of IDO-knockout MSCs to achieve allograft tolerance [86].

1.5 Stem Cell Therapy and Tissue Regeneration

1.5.1 Mesenchymal Stem Cells for Cutaneous Wound Healing

The rapidly developing fields of stem cell biology and skin tissue engineering have created translational opportunities for the development of novel stem cell-based wound healing therapies that show promising results in preclinical and clinical trials for the treatment of chronic wounds. Cell therapy is most appropriately defined as a set of strategies to use living cells as regenerative therapy to repair, replace, or restore biological function [6].

The prognosis of extensive and deep burns is not entirely satisfactory because of scar formation and the loss of normal function and skin appendages, which severely

affects the quality of life after survival. Therefore, reducing the formation of scars and reestablishing the normal anatomy and function of the skin and its appendages have become the aim of regenerative medicine research. Fortunately, with research focused on a better understanding of stem cell biology, several experiments have shown that adult stem cells can participate in tissue and organ regeneration in almost all lesions. Mansilla et al. performed a full-thickness skin defect on the dorsum of mice and used human BM-MSCs obtained from a healthy young donor to accelerate the wound healing. The cells were injected intravenously or applied to the wound in a fibrin polymer implant. There was no immune rejection, and all skin defects healed without scar or retraction at a median time of 14 days after wounding [99].

Recently, Isakson et al. have extensively reviewed the role of adult MSCs in cutaneous wound healing. They demonstrated accelerated wound closure and enhanced histological parameters in wounds treated with MSC therapies, irrespective of cell isolation or delivery method [55].

Badiavas et al. were the first to treat chronic wounds with MSCs. Three patients having chronic cutaneous ulcerations with more than 1-year duration received treatment with both fresh autologous bone marrow aspirate and cultured bone marrow cells derived from those aspirates. All patients showed clinical improvement in their wounds within days following administration of bone marrow aspirate or cultured bone marrow cells. Wounds showed a steady overall decrease in wound size and increase in the vascularity of the dermis and the dermal thickness of the wound bed [100].

Another of the earlier studies investigating the effects of human BM-MSCs on skin repair was performed by Mansilla et al. BM-MSCs were either injected systematically or applied in a polymer implant onto full-thickness skin defect in mice, which resulted in accelerated wound healing without scar or retraction in comparison to control group. Besides, there was not an immune rejection of the transplanted cells thus confirming that human MSCs are not immunologically reactive, trespassing species defense barriers either when locally implanted or systemically administered [99].

Falanga et al. used autologous BM-MSCs from patients with acute wounds from skin cancer surgery and patients with chronic, long-standing, nonhealing lower extremity wounds. The MSCs were delivered using a fibrin polymer spray system, and the cells were found to promote the generation of new elastic fibers within the wound with strong direct correlation between the number of cells applied and the subsequent decrease in wound size [101].

Dash et al. again used autologous BM-derived MSCs to treat chronic nonhealing ulcers (diabetic foot ulcers and Buerger disease) of the lower extremities. Treatment with MSCs led to a significant reduction in ulcer size and increased pain-free walking distance in the implant group as compared to the control group. Biopsy micro-sections of implanted tissues showed the development of dermal cells (mainly fibroblasts), including mature and immature, inflammatory cells. This study indicated that autologous implantation of BM-derived MSCs in nonhealing ulcers accelerates the healing process and improves clinical parameters significantly [102].

Clinical benefit of systemic administration of MSCs has also been observed by Lu et al., who made a comparison of BM-MSCs with BM-derived mononuclear cells (BM-MNCs) for the treatment of diabetic critical limb ischemia (CLI) and foot ulcers. Under ordinary treatment, the limbs of 41 type 2 diabetic patients with bilateral CLI and foot ulcers were injected intramuscularly with BM-MSCs, BM-MNCs, or normal saline. The ulcer healing rate of the BM-MSCs group was significantly higher than that of BM-MNCs at six weeks after injection and reached 100% four weeks earlier than BM-MNCs group. After 24 weeks of follow-up, the improvements in limb perfusion induced by the BM-MSCs transplantation were more significant than those by BM-MNCs regarding painless walking time, ankle-brachial index, transcutaneous oxygen pressure, and magnetic resonance angiography analysis. Thus, BM-MSCs therapy turned out to be better tolerated and more efficient than BM-MNCs for increasing lower limb perfusion and promoting foot ulcer healing in diabetic patients with CLI [103].

All these clinical results suggest that MCSs provide clinical benefits and should be used in a range of wound types to increase the rate of healing as well as reduce scarring. However, there are still many issues to be addressed including the effect of the source of the MSCs, the benefits of MSCs alone or within a matrix, the timing and frequency of MSC administration, and the number of cells administered.

1.5.2 Mesenchymal Stem Cells Delivery

Both topical and systemic MSCs delivery methods have been shown to be effective for wound healing. While systemic delivery of MSCs has been shown to deposit cells at the injury site, cell engraftment and survival, have been limited. This has led to the majority of studies looking at novel cell delivery systems to enhance wound healing [55].

Yoshikawa et al. cultured human BM-MSCs and placed them in artificial dermis made of collagen sponge that was later implanted subcutaneously into the dorsal wound of a nude mouse. Furthermore, BM-MSCs suspension was injected sub-

cutaneously around the wound without the artificial dermis. Concerning histologic findings, only the artificial dermis containing the cultured cells showed any improvement in repair with increased vascularity, fat, and matrix deposition compared to the other groups. The next step following the study in mice was to treat 20 patients with chronic wounds using cultured autologous BM-MSCs/artificial dermis composite grafts. The wounds mostly healed in 18 of the 20 patients; the remaining two patients died of causes unrelated to transplantation. Thus, autologous BM-MSCs transplantation was shown to be therapeutically effective in all patients [104]. This study was the first to suggest that the use of scaffold for administering the MSCs to the wound may be more beneficial than just injecting the cells around the wound site. Hence, the delivery of cells is an important and often neglected aspect of any therapeutic approach. Recent studies have used new and innovative cell delivery systems that maximize the efficacy of MSC therapy for non-healing cutaneous wounds.

Recent advances suggest that Wj-MSCs reinforced with microparticles [105] and scaffolds [106] can be effectively used for a variety of clinical applications. Vojtassák et al. described a technique for treatment of chronic non-healing wound (diabetic ulcers) using autologous biograft composed of autologous skin fibroblasts on biodegradable collagen/hyaluronan membrane (Coladerm) in combination with autologous MSCs derived from the patient's bone marrow. The bone marrow aspirate was applied directly to the wound and injected into the edges of the wound, finally covered with prepared autologous biograft. The patient received two additional treatments with cultured MSCs on day 7 and 17. The wound showed a steady overall decrease in wound size and increase in the vascularity of the dermis and the dermal thickness of the wound bed after 29 days of combined treatment [107].

More recently, Sabapathy et al. have proved that combined therapy of Wj-MSCs and decellularized amniotic membrane has better wound healing capabilities when compared to injection of BM-MSCs alone. The histological analysis of regenerated wound tissue revealed reduced scar formation with hair growth, and better development and organization of the glandular tissues in membrane grafted tissues compared to control, or plain Wj-MSCs injected animal model [61].

1.6 Electrospun Silk Scaffold for Regenerative Medicine

1.6.1 Silk Fibroin

Silk is a biomaterial composed of fibrous proteins synthesized in specialized glandular epithelial cells of organisms members of the class Arachnida, and several worms of the order Lepidoptera, i.e. mites, butterflies, and moths. Among silk variants, particular interest is given to the silkworm silk of *Bombyx mori* specially in the textile industry and medical sutures [108].

Native *Bombyx mori* silk is composed of silk fibroin (SF) protein coated with sericin, a group of hydrophilic glycoproteins (20-310 kDa) produced in the middle silk gland of *B. mori*, that act with glue-like functions. The silk fibroin fibers are about 10-25 μm in diameter, and consists of a light (∼26 kDa) chain (L-chain) and a heavy (∼390 kDa) chain (H-chain), which are present in a 1:1 ratio and linked by a single disulfide bridge (Figure 1.3, A) [109]. Glycoprotein P25 (25 kDa) is also associated with these chains, primarily by non-covalent interactions, providing the integrity of the complex [110]. H-fibroin, L-fibroin, and P25 are assembled in the ratio of 6:6:1 in mulberry silk [111].

The amino acid composition of silk fibroin consists mainly of 43% glycine (Gly), 30% alanine (Ala), and 12% serine (Ser). Heavy chain SF is characterized by a series of alternating hydrophobic and hydrophilic domains rendering the molecule amphiphilic [112]. The heavy chain consists of 12 domains that form the crystalline regions (β-sheet structures) in silk fibers. These regions are composed of Gly-X repeats, where X is Ala, Ser, Threonine (Thr), and Valine (Val). Each domain is comprised of sub-domain hexapeptides that are rich in Gly, Ala, Ser and tyrosine (Tyr). The less crystalline forming regions of the fibroin heavy chain or linkers, are between 42-44 amino acid residues in length and have an identical 25 amino acid residue not found in the repetitive domains [113]. The result is a hydrophobic protein that self-assembles to form strong and resilient materials. The prevalence of β-sheet-forming regions within the fibroin structure confers the protein-based materials with high mechanical strength and toughness (Figure 1.3, B) [114].

The concentration of silk protein augments during the succession from synthesis to spinning in the glands, with changes in chemistry and physical characteristics, along with mechanical alignment in shear flow. Chain alignment is involved in later processing stages, and the internal drawdown of fibers plays a significant role in the critical final steps that lead to fiber formation. Silks are not “squeezed out” of the

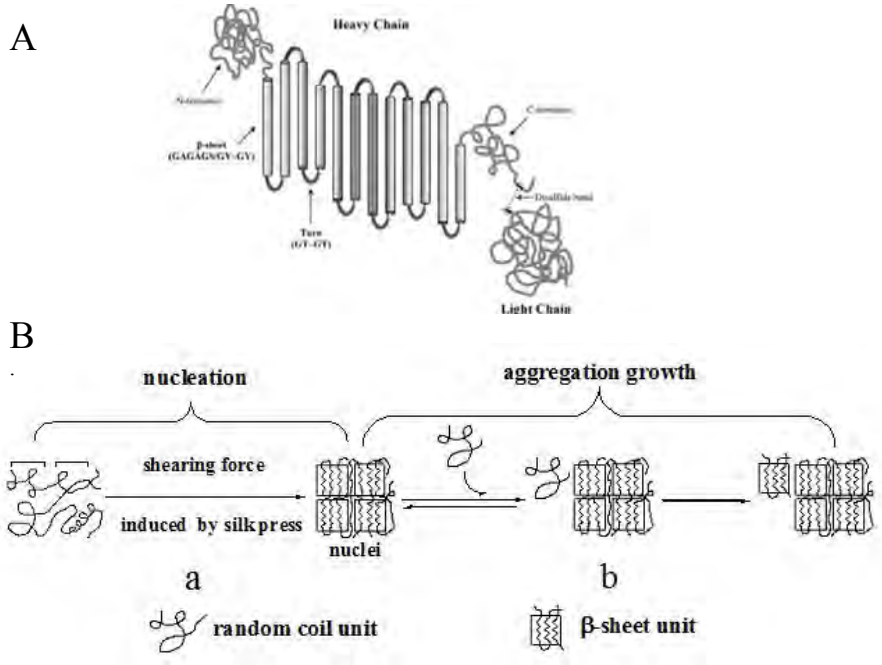

Figure 1.3: **Silk chemical structure [116]**.

glands but are mostly pulled out by the "figure eight" movement of the head of the silkworm while spinning [115].

Silk fibroin biomaterial in various formats has shown good biocompatibility, slow and controllable degradability, and minimal inflammatory response. Furthermore, the excellent mechanical properties of silk fibroin make it a unique natural polymer. Silk fibroin matrices in the form of electrospun nanofibers have demonstrated potential in various tissue regeneration/repair applications [117].

1.6.2 Electrospinning of Silk Fibroin Fibers

Electrospinning process was first introduced in the early 1930s and has been used for many years in the textile industry for manufacturing non-woven fiber fabrics. In recent years, this technology has gained much interest, especially in the production of ultra-fine polymer fibers for tissue engineering. The electrospun nanofibrous structure is a nonwoven, three-dimensional, porous and nano-scale fiber-based matrix produced by an electrospinning process [118]. Electrospun fibers can be produced in a broad range of diameters, ranging from a few nanometers to a few microns, depending on the mode of processing. The fibers can be made to form a porous structure that is ideal for drug and/or cell delivery [119].

In the method of electrospinning, many factors can be manipulated to create scaffolds of different geometries and with various structural properties. These ele-

ments include electrospinning parameters, e.g., the electrical force, the distance of the electric field, the length and radius of the spinneret, and the solution flow rate. Likewise, solution parameters, such as concentration, viscosity, ionic strength and conductivity [120].

Electrospun silk fibroin scaffolds have two distinctive characteristics that make them very appropriate for tissue engineering. First, the morphology and architecture of the electrospun structure is similar to those of some natural ECM in the skin, that are composed of randomly oriented collagens of nanometer-scale diameters. Second, the scaffold structure changes dynamically over time, as the polymer nanofibers degrade allowing the seeded cells to proliferate and produce their own ECM. The mechanical property of a scaffold is another important aspect of its design since it must maintain the structural integrity and stability at the defect site of the host. Also, the structure at the implant site must provide sufficient biomechanical support during the process of tissue regeneration and structure degradation after surgery [118, 121].

Porosity is thought to be an essential parameter for tissue engineering scaffolds used for the skin reconstitution. Such nanofibrous scaffolds should mainly be made porous to benefit cellular infiltration and proliferation. The better porosity of scaffolds used for cellular penetration should normally be within the range of 60-90%. It is not easy to make well-defined pore sizes through the electrospinning technique because of the randomly deposited fibers. Thus, the overall network architecture structure created best mimics the natural ECM, and this provides an advantage in its application as tissue engineering scaffolds [122].

1.6.3 Characteristics of Silk Fibroin as Biomaterial

Biomaterial design is an important element of tissue engineering, incorporating physical, chemical, and biological cues to guide cells into functional tissues via cell migration, adhesion, and differentiation. Many biomaterials need to degrade at a rate commensurate with new tissue formation to allow cells to deposit new ECM and regenerate functional tissue. In addition, biomaterials may need to include provisions for mechanical support appropriate to the level of functional tissue development [108].

There are several general characteristics necessary for scaffold design. The first requirement is that the material should be biocompatible, able to support appropriate cellular activity to optimize tissue regeneration without eliciting undesirable local or systemic responses, such as rejection, inflammation or immune activation, in the host. Because of its non-mammalian origin, use of silk proteins could be associ-

ated with some adverse immunological response to a foreign body. Sericin has been linked to immunogenic reactions of silk whereas silk fibroins have not, albeit it can be easily separated from SF by extraction in alkaline solutions. Toxicological evaluations of SF have been encouraging, placing foreign body reactions following the implantation of SF films comparable to those observed with type I collagen films and less than what was observed for films made from polylactide-co-glycolide (PLGA) synthetic polymer, which is a slowly degrading polymer used in the pharmaceutical market for controlled drug delivery [112].

Secondly, the scaffold should have a porous architecture with high surface area to allow for maximum cell loading and cell-matrix interactions, as well as to improve transport into and out of the matrix for nutrients and oxygen. Moreover, this structure is desirable for locally sequestering and delivering bioactive molecules, and providing space for tissue in-growth. Furthermore, the large surface area of electrospun nanofibers allow the adsorption of liquids and protects the wound from bacterial penetration and dehydration [123].

On the other hand, most tissue engineering applications and tissue regeneration approaches require scaffolds that are fully biodegradable or absorbable. Biodegradability implies the disintegration of solid polymeric devices by biological elements, giving fragments that can disperse, but not eliminate from the body. While biosorption reflects the total elimination of the initial foreign material through natural pathways, i.e. through filtration or metabolization of the degraded bio-products [124]. Furthermore, it is useful if the degradation rate of the scaffold matches the rate of tissue regeneration to optimize the transfer of functions from the artificial matrices to native ECM on a time-dependent basis during tissue regeneration. Faster rates of degradation of the scaffold may lead to a loss of tissue integrity and function while a degradation rate that is too slow can result in barriers to transport or mechanical mismatches such as stress shielding, resulting in long-term failure of the system [117].

Scaffolds should also be mechanically matched to the target tissue, sterilizable without compromising structural or other related properties and for clinical success the production of the scaffold must be reproducible, economical and scalable. Collectively, these general rules for scaffold design are focused more at the macroscopic level. In order to realize the active role of artificial scaffolds in regulating the behavior of cells, the interface between the biomaterial and the cells must be examined [117].

Silkworm silk is an excellent polymer for biomedical application due to the higher strength when compared to commonly used polymeric degradable biomaterials, e.g.

collagen and polylactic acid (PLA). Besides the excellent mechanical properties, silk fibroin has other significant advantages such as biocompatibility, water based processing, biodegradability and the presence of easy accessible chemical groups for functional modifications [125]. Finally, the degradation rate can be adapted from months to years after implanting *in vivo*, based on processing procedures employed during material formation [126].

1.7 Silk Fibroin Biomaterial for Tissue Regeneration

The main aim of engineered tissue regeneration is the construction of a biocompatible scaffold that, in combination with living cells and/or bioactive molecules, replaces, regenerates, or repairs damaged tissues [123]. Tissue engineering basically involves the process of harvesting relevant cells from a patient or donor, expanding or manipulating the cells *in vitro*, seeding these cells into a three-dimensional (3D) scaffold and inducing them to proliferate, differentiate and eventually develop into the desired tissue for implantation. In this regard, at least three key factors should be considered for successful tissue regeneration: (i) the cells that will form the tissue, (ii) the scaffold that provides structural and anchoring support to the cells, and (iii) cell-matrix (scaffold) interactions that direct tissue growth [127].

The scaffold serves as a mimic for the native ECM and plays a pivotal role in tissue regeneration by providing temporary support for the cells during the formation of a more natural ECM by the cells. The scaffold also plays a critical role in providing the appropriate chemical, morphological and structural cues to direct the cells towards a targeted functional outcome. Therefore, scaffold design has become one of the central themes in regenerative medicine, and many efforts are spent on designing suitable scaffold systems to optimize cell and tissue outcomes [117].

Silk fibroin biomaterial in various formats has shown good biocompatibility, slow and controllable degradability, and minimal inflammatory response. Furthermore, the excellent mechanical properties of silk fibroin make it a unique natural polymer. Silk fibroin matrices in the form of electrospun nanofibers have demonstrated potential in various tissue regeneration/repair applications [117].

1.7.1 Skin Tissue

Min et al. have carried out a series of studies to investigate the potential of silk electrospun matrices for accelerating early stages wound healing. They studied the

cell attachment and spreading of normal human keratinocytes and fibroblasts seeded on methanol-treated silk fibroin nanofibers alone or coated with ECM proteins (i.e., type I collagen, fibronectin, and laminin). In the cell activity assessment, the electrospun SF nanofibers coated with collagen-I were found to promote the adhesion and spread of keratinocytes, but not for fibroblasts. Laminin coating stimulated cell spreading, but not cell attachment. Importantly, cell adhesion and spreading on fibronectin-coated silk matrices was found comparable to that on BSA controls [128].

In another study Min et al. prepared three types of SF matrices, including a matrix woven from SF microfibers, a nonwoven matrix of SF nanofibers, and a matrix of SF film. Then, they examined the effect of the three types of SF matrix on the cell adhesion and spreading of normal human epithelial cells. The results indicated that the SF nanofiber matrix may be preferable than SF film or SF microfiber matrices for biomedical applications since nanofibrous matrices promoted human keratinocyte adhesion and spreading, especially when a type I collagen coating was included. The authors attributed the results to the higher level of surface area for cells to attach to due to its three-dimensional features (high porosity and high surface area-to-volume ratio) and less brittle structure provided by SF nanofibers. Since the final goal of the scaffold design is the production of an ideal structure that can replace the natural ECM proteins until host cells can repopulate and resynthesize a new natural matrix, SF nanofibers may be a good candidate for the biomedical applications, such as wound dressing and scaffolds for tissue engineering [129].

1.8 Mouse Excisional Wound Splinting Model

The mouse excisional wound healing model has been broadly used to study wound healing, cutaneous regeneration, stem cell and tissue transplantation, and immune rejection [130, 131]. Nevertheless, this model has some limitations because of the differences in the characteristics of wound healing between rodents and humans. In rodents, whose skin is mobile, the primary mechanism of wound closure is contraction; while, in humans, where the skin is tethered to the subcutaneous tissue, wounds are heal by re-epithelialization and granulation tissue formation [132]. In mice, full-thickness incisional and excisional wounds on the dorsum that are allowed to heal by second intention show marked contraction due to the activity of the *panniculus carnosus*. Such wound contraction occurs very early during wound healing and can account for up to 90% of wound closure, a situation very different from that in man [133].

The aim of animal wound healing models is to reproduce human physiology and predict therapeutic outcomes. There are several types of animal wound models described in the literature. In an excisional wound model, healing occurs from the wound margins. This kind of model allows the broadest assessment of the mechanisms involved in wound healing. The wounds are easily harvested and can be analyzed by immunohistochemistry and molecular methods. In addition, this technique allows drugs and bioactive factors to be applied directly to the wound bed or injected into the tissue around the wound, providing an evaluation of new pharmacologic treatment and predicting potential clinical outcomes in humans [134].

The excisional wound splinting model differs from the excisional wound model in that a splinting ring firmly adheres to the skin around the wound. Consequently, wound closure caused by skin contraction is avoided, and wounds heal through a process similar to human [135].

The mouse excisional splinting model provides an appropriate method for assessing the effect of stem cells in cutaneous regeneration. Wu et al. have used this model to study the effects of MSCs and cytokines on cutaneous repair and regeneration in wild-type and genetically modified mice [130, 131, 136].

HYPOTHESIS Nowadays, non-healing or chronic wounds represent an increasingly prevalent and costly public health problem. As a consequence of longer lifespans in the current population, the number of patients who suffer diabetes, and other chronic aging-related diseases is growing significantly. Importantly, there is a link with aging-associated diseases and wound healing impairment [137]. On the other hand, other wound healing challenges also arise at any age because of accidents, burns, and other traumatic injuries. However, despite the significant therapeutic advances, many patients fail to respond to the available treatments, being necessary the finding of more effective alternative therapies.

MSCs based-therapies present some advantages over pharmaceuticals, or protein/growth factors treatments, and progenitor cells, as MSCs can interact with the surrounding cell types and biochemical environment to express in a regulated manner the appropriate trophic factors for enhanced dermal wound healing. Thus, a paracrine signaling, such as the release of factors that promote angiogenesis, immunomodulation and recruitment of endogenous tissue stem cells, as well as differentiation, have been described as possible mechanisms underlying the positive wound healing effects of MSCs [138, 139]. Therefore, MSCs have emerged as important therapy to reduce the formation of fibrotic tissue and the appearance of scars following a cutaneous injury [140].

From the different available sources of MSCs, the umbilical cord represents a cost-effective, productive, feasible, accepted, and non-invasive method to isolate MSCs, and is considered advantageous compared with bone marrow and adipose-derived MSCs for some researchers [141].

However, one limitation of MSC therapy is the method of delivering the cells. Although systemic delivery is an attractive possibility, the engraftment efficiency can be difficult to predict without improved methods to ensure that the cells will home to the site of injury. Therefore, local administration of the MSCs may require an appropriate carrier and/or scaffold to ensure that the cells remain viable and can efficiently migrate into the wound bed [142]. Recently, several different biosynthetic scaffolds have been used alone or in combination with cells to treat wounds [143, 144]. Among the various scaffolds employed, silk fibroin cellularized with MSCs from different sources has been shown to be effective in repairing experimental wounds of the skin [145, 146].

Given their mesenchymal phenotype and easy isolation, we hypothesized that human Wj-MSCs may constitute an alternative source of cells for dermal wound healing as they avoid the inherent sourcing limitations displayed by human BM-MSCs. In this study, we pretended to investigate the behavior of Wj-MSCs both *in vitro* and *in vivo* when cultivated on electrospun silk fibroin scaffolds and implanted in immunocompetent mice. Thus, the purpose of the present study was to determine whether Wj-MSCs delivered in silk fibroin scaffolds into skin defects in SKH1 mice would contribute to dermal wound healing.

Chapter 2

OBJECTIVES

2.1 General

1. Standardize the protocol for the isolation and characterization of human Wharton's jelly mesenchymal stem cells.

2. Investigate the therapeutic effect of transplanted human Wharton's jelly mesenchymal stem cells on cutaneous wound healing process in mice.

2.2 Specific

1. To standardize the explant method for the isolation of mesenchymal stem cells from the Wharton's jelly of the human umbilical cord.

2. To study the ability of the Wharton's jelly mesenchymal stem cells to differentiate into adipocytes, osteoblasts, and chondroblasts and compare to that displayed by bone marrow-derived mesenchymal stem cells.

3. To analyze the expression of mesenchymal stem cell markers by flow cytometry when cultured on plastic and after seeding in a silk fibroin scaffold.

4. To analyze the proliferation kinetics of bone marrow and Wharton's jelly-derived mesenchymal stem cells.

5. To study the mechanisms involved in the immunosuppressive properties of the Wharton's jelly mesenchymal stem cells.

6. To test the ability of a three-dimensional nanofibrous scaffold fabricated by electrospinning of silk fibroin to support the growing and spreading of human Wharton's jelly MSCs and its use in wound healing.

7. To assess the effect of Wharton's jelly mesenchymal stem cells in cutaneous regeneration by using the excisional wound splinting model in SKH1 mice.

8. To perform an histological and immunohistochemical study of the wound healing process in the transplanted mice, regarding inflammation, re-epithelialization, granulation tissue formation, angiogenesis and remodeling of the wound.

9. To test the safety and biodistribution of the locally implanted human Wj-MSCs in the murine model of wound healing.

Chapter 3

MATERIALS AND METHODS

3.1 Collection of Human Umbilical Cord Samples

Human umbilical cords were collected after obtaining informed consent from patients undergoing full-term pregnancy elective caesarean section either at hospitals in the Netherlands (according to Netcord–FACT standards) or, at the Virgen de la Arrixaca Clinical University Hospital (HCUVA) in Murcia, Spain. Ethical permission from the Medical Ethical Board of the Leiden University Medical Center (LUMC), Leiden, The Netherlands, and from the Research Ethics Committee (CEIC) of the HCUVA was fulfilled.

The informed consent outlined the project and was signed by the donor and witnessed (see Annexes). Cords were excluded from individuals with stillbirth, preeclampsia, infectious disease, sexually transmitted disease, or hepatitis-positive mother.

A sheet containing the information about the collection of the umbilical cord was fulfilled after the delivery and before processing the cord. Time of delivery, time of explant procedure, cord weight and general appearance of the umbilical cord (i.e., thickness, length and proportion of Wharton's jelly) were registered in the registration form (see Annexes).

3.2 Wharton's jelly Mesenchymal Stem Cells Isolation

Protocols for isolation and characterization of the Wharton's jelly mesenchymal stem cells (Wj-MSCs) were first carried out in the Jon J van Rood Center for Clinical Transfusion Medicine Research (Sanquin Blood Supply Foundation, Leiden, the

Netherlands) and Leiden University Medical Center (LUMC, Leiden, the Netherlands). The initial project was partially supported by the Department of Immunohematology and Blood Transfusion (LUMC) and the Hematopoietic Transplant and Cellular Therapy Unit, Hematology Department (HCUVA, Spain).

Some of the steps used to isolate mesenchymal stem cells (MSCs) from the Wharton's jelly of the umbilical cord were adapted from the method previously described by Seshareddy et al. and DeBruyn et al. [147, 148].

Mesenchymal stem cells from the Umbilical Cord were compared to the Bone Marrow-derived mesenchymal stem cells (BM-MSCs) regarding the differentiation capability and T-cell proliferation inhibition potential.

Bone marrow (BM) was collected from patients undergoing knee or hip replacement surgery at the LUMC with the informed consent of the donor. First, mononuclear cells (MNCs) were isolated from the BM aspirates using a Ficoll-Paque density gradient centrifugation (1.077 g/ml, GE Healthcare Life Sciences, Little Chalfont, United Kingdom). Then, the MNCs were seeded into culture flasks, containing Dulbecco's Modified Eagle's medium (DMEM) with 10% fetal bovine serum (FBS), and 1% Penicillin-Streptomycin (all from Life Technologies, Carlsbad, CA, USA), at a density of $1.5x10^5$ cells/cm^2. After overnight culture in a humidified incubator at 37 $^\circ$C and 5% CO_2, non-adhering cells were washed from the flask with phosphate-buffered saline (PBS) (BioWest, Nuaillé, France). Adherent cells were grown to confluence and passaged. After three passages, cells were cryopreserved in FBS with 10% dimethyl sulfoxide (DMSO) (Sigma-Aldrich, St. Louis, MO, USA). The MSCs that were used throughout this study were between passage 3 and 6.

3.2.1 Explant Method for the Isolation of Wharton's jelly Mesenchymal Stem Cells

After the labor, the umbilical cord was clamped at both ends and then was cut using a scalpel to separate it from the placenta and the newborn. Then, the umbilical cord was collected and stored in a sterile specimen cup, containing PBS with 1% antibiotic/antimycotic mix (Life Technologies, Woerden, The Netherlands), at 4^{o}C until processing. The cord was processed within 12 hours after birth and, it was handled in an aseptic fashion, and treated in a type II Biological Safety Flow Cabinet (see Figure 3.1).

First, the surface of the cord was rinsed with sterile PBS to remove as much blood as possible. It was manipulated in a sterile 150 mmØ petri dish (Soria Genlab, Spain). Subsequently, the cord was placed in a sterile cup containing a povidone-iodine antiseptic solution (Betadine®) for three min and then was deposited into

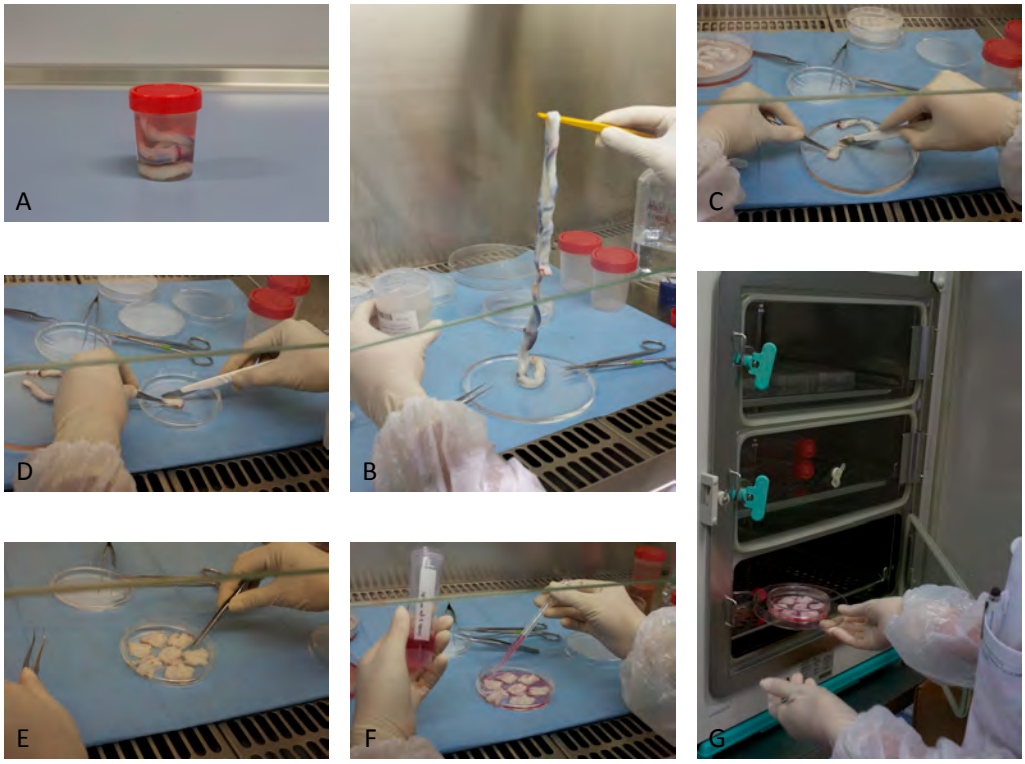

Figure 3.1: **Explant method for the isolation of Wj-MSCs.** (A-B) Human umbilical cord was collected from a full-term pregnancy elective caesarean section, (C) umbilical cord was cut into 3–5-cm long pieces using a sterile scalpel, (D) amnion was incised lengthwise, and blood vessels with clots inside were removed, (E) cord pieces were placed with the inside faced to the bottom of a sterile 10-cm petri dish, (F) 10 ml of complete culture medium were added carefully, (G) the culture plates were placed in a humidified incubator at 37 ° C and 5% CO_2.

another cup containing 70% ethanol for few seconds. Afterward, the cord was rapidly transferred to another container with PBS to remove the alcohol and to finish the process of washing and sterilization.

The cord was cut into 3-5-cm long pieces using a sterile scalpel. After, the tissue sample was washed with PBS thoroughly and then was cut along the horizontal axis. Also, blood vessels with blood clots inside were removed. Cord pieces were placed with the inside faced to the bottom of a sterile 10-cm petri dish (Greiner, Alphen a/d Rijn, the Netherlands). Then, the explants were left to attach to the plate, and next 10 ml of complete culture medium were added carefully. The culture plates were placed in a humidified incubator at 37 ° C and 5% CO_2. The medium was refreshed every three days, and after ten days of culturing, the segments were removed. Finally, the MSCs adhering to the plate were grown to confluence and submitted to serial diluted passages.

3.3 Protocols for *in vitro* Culture, Storage and Recovery of Wharton's jelly Mesenchymal Stem Cells

Umbilical cord-derived mesenchymal stem cells are easily cultured and expandable *in vitro*, and may be cryogenically stored, thawed, and later recovered. The collection process is described below.

3.3.1 Passaging the cells

Wj-MSCs must be passaged when they are 80-90% confluent by following the next steps:

1. The medium is aspirated off, and the cells are rinsed twice with sterile PBS (Ca^{2+} free).

2. Certain amount of pre-warmed, trypsin-EDTA (0.05%) solution is added to the plate and/or flask to cover the culture surface, i.e., for T-25 flask- ≈1 ml, for T-75 flask or 10 cm petri dish- ≈2 ml, and for T-175 flask add ≈5 ml of the enzymatic solution.

   (a) The plate and/or the flask is allowed to sit at 37^{o}C for 1-2 min. Then, the detachment of the cells is observed under a microscope and facilitated by repeatedly tapping the plate and/or the flask gently on a hard surface.

   (b) It is important to avoid contact with trypsin-EDTA for more than 5 min because the cells are sensitive to enzymatic treatment. Thus, if the cells do not lift, gently scrape the bottom of the flask, with a cell scraper, side to side for several min until the entire surface has been scraped free of cells.

3. The trypsinization reaction is neutralized by adding the same volume of medium containing 10% FBS. Afterward, the solution containing the cells is transferred to 50 ml sterile tube, and centrifuged at 1200 rpm 5 min at room temperature. Then, the supernatant is discarded, and the cells are re-suspended gently in 1 ml of culture medium.

4. Next, the cells are counted by trypan blue exclusion using an automated cell counter and then transferred to a new flask at a concentration of 3-5x10^3 cells/cm^2 in fresh complete medium. Afterward, the plates and/or flasks are labeled and incubated at 37^{o}C and 5% CO_2.

5. The cells are fed every three days by aspirating off the medium and replacing it with fresh complete medium. The amount of medium in a plate or flask is as follows: for 10 cm petri dish- ≈10 ml; for T-25 flask- ≈7 ml; for T-75 flask- ≈10 ml; and for T-175 flask correspond ≈20 ml of culture medium.

3.3.2 Cryopreservation

The cells collected for freezing should be in the growth phase. This procedure is made as follows:

1. Previously, the cells are detached by trypsinization as described in 3.3.1 section.

2. After, calculate the amount of vials that are pretended to freeze. Usually, one million cells are frozen per vial in a final volume of 1 ml.

3. Prepare 2X freezing medium (FBS + 20% DMSO)

4. Then, add FBS to the cell suspension to the appropriate volume that correspond to half of the total volume (e.g., to freeze four vials, add FBS until the volume is 2 ml). Cool the cell suspension to 4^{o}C in the fridge.

5. Slowly add 2X freezing medium to the cell suspension until the final volume is reached (e.g., for four vials, add 2 ml of 2X freezing medium).

6. The cells in the freezing medium are transferred into cryovials at 4^{o}C. Immediately, the cryovials are transferred to a controlled rate cooler and placed in a -80^{o}C freezer. Finally, after 1 or 2 days, the cryovials are transferred to a liquid nitrogen tank.

3.3.3 Thawing the mesenchymal stem cells

For thawing the Wj-MSCs:

Remove the vials from the liquid nitrogen tank and plunge into 37^{o}C water bath with gently swirling.

1. Before the last ice crystal has melted, the vials are wiped down twice with 70% ethanol and moved to the biosafety cabinet. It is important not vortex cells at any time.

2. After, the contents of the vials are added slowly with gentle swirling to 10 ml of fresh complete medium in a 50 ml tube.

3. Next, the cells are centrifuged at 1200 rpm 5 min at room temperature. Afterward, the supernatant is discarded, and then the pellet is resuspended in 1 ml of medium. It is recommended to make a live/dead counting of cells by trypan blue exclusion, to check the cell viability.

4. Finally, the mesenchymal stem cells are seeded at a density of 1x10^4 cells/cm^2 for the first passage following the thaw. After 24 hours of seeding, remove non-adherent cells and add fresh complete medium. If cells do not attach to the bottom of the flask after 24 hours of being thawed and do not start growing, discard and try a second vial.

3.4 Characterization of Human Wharton's jelly Mesenchymal Stem Cells

3.4.1 *In vitro* Multilineage Differentiation Capacity

Differentiation analysis was carried out to demonstrate that Wj-MSCs possess mesodermal plasticity under *in vitro* conditions. Protocols for MSCs differentiation were followed as previously described [149, 150]. Differentiation capacity of MSCs from the umbilical cord was compared to that from adult's bone marrow-derived MSCs. Mesenchymal stem cells from both cell sources at passage four were used in these assays. An arbitrary scoring system was used for assessing the degree of cell differentiation. Cultures showing no differentiated cells were scored as 0, a few differentiated cells as 1, moderate differentiation as 2, and robust differentiation as 3 (Figure 4.5).

3.4.1.1 Osteogenic and Adipogenic Differentiation

For osteogenesis and adipogenesis, hWj-MSCs and BM-MSCs were plated at a density of 5x10^4 cells/cm^2 in 24-well culture plates. Half of the wells were grown in osteogenesis-inducing medium and the other half in osteogenesis/adipogenesis-inducing medium. Cells kept in standard culture medium (DMEM (4.5 g/l glucose) supplemented with 10% FBS, 50U/ml penicillin/streptomycin, and 2 mM L-glutamine) were used as negative control. After three weeks, the cultures were tested by histochemical staining for the presence of alkaline phosphatase activity, calcium deposits, and lipid droplets.

Osteogenic induction was accomplished using a standard culture medium supplemented with 50 μg/ml ascorbic acid, 10 mM β-glycerol phosphate, and 100 nM dexamethasone. Ascorbic acid facilitates osteogenic differentiation by increasing col-

lagen type 1 secretion into the extracellular matrix while β-glycerol phosphate serves as a phosphate source for hydroxylapatite, also inducing osteogenic gene expression. Dexamethasone is a glucocorticoid that modulates muscle, fat, cartilage and bone differentiation from multipotential progenitors by inducing Runx2 expression by FHL2/β-catenin-mediated transcriptional activation [151, 152].

Under the influence of the differentiation medium, the mesenchymal stem cells form aggregates or nodules and increase their expression of alkaline phosphatase (ALP). Alkaline phosphatase is a hydrolase enzyme responsible for dephosphorylating molecules such as nucleotides, proteins, and alkaloids under alkaline conditions. ALP is present in all tissues but is particularly concentrated in bone, in which it plays a role in mineralization. 5-Bromo-4-chloro-3-indolyl phosphate (BCIP) is a chromogenic substrate often used in combination with nitro blue tetrazolium chloride (NBT) for the colorimetric detection of alkaline phosphatase activity. The BCIP/NBT substrate system, when reacted with intracellular alkaline phosphatase, produces an insoluble dark blue-purple precipitate that is easily observable. On the other hand, Alizarin red S is a commonly used stain to identify calcium deposits into the extracellular matrix (i.e., nodules of mineralization) in the differentiated culture of mesenchymal stem cells. Calcium forms an Alizarin Red S-calcium complex in a chelation process, and the end product is an orange-red birefringent precipitate.

Adipogenesis was induced using a standard culture medium supplemented with 0.5 mM 3-isobutyl-1-methylxanthine (IBMX), 100 μM indomethacin, 5 μg/ml insulin, and 1 μM dexamethasone. Insulin is a hormone that is known to prompt the proliferation and differentiation of preadipocyte by mimicking the role of insulin-like growth factor-1 (IGF-1) and activating mitogen-activated protein kinase (MAPK) pathways [153].

IBMX is a widely-used non-specific inhibitor of adenosine 3',5'-cyclic monophosphate (cAMP) and guanosine 3',5'-cyclic monophosphate (cGMP) phosphodiesterases (PDEs). By inhibiting PDEs, IBMX increases cellular cAMP and cGMP levels, activating cyclic nucleotide-regulated protein kinases. Elks et als. showed that physiological concentrations of corticosteroids (e.g., dexamethasone) are required to produce optimal differentiation of 3T3-Ll adipocytes, as observed by increased expression of α-glycerophosphate dehydrogenase, a key enzyme in lipogenesis and neutral lipid accumulation. IBMX, while not as important as dexamethasone in inducing differentiation, clearly augmented α-glycerophosphate dehydrogenase activity and the accumulation of neutral fat, and enhanced the rate at which insulin and dexamethasone promote differentiation [154].

Indomethacin is a non-selective inhibitor of cyclooxygenase (COX) 1 and 2, en-

zymes that participate in prostaglandin synthesis from arachidonic acid. Styner et al. have shown that indomethacin has a unique role in promoting early adipogenesis in MSCs, that is independent of its effects on COX2 or prostaglandins generated from COX2. Thus, indomethacin may serve as ligands for PPARγ2, enhancing transcription of critical gene targets important for the fat formation [155].

The adipogenic differentiation was manifest by the accumulation of lipid-rich vacuoles within the cells and confirmed using Oil Red O staining. Oil Red O is a lysochrome (fat-soluble dye) diazo dye used for staining of neutral triglycerides and lipids on frozen sections, and some lipoproteins on paraffin sections.

Control cultures were maintained without osteogenic and adipogenic supplements, respectively. All cells were maintained for 21 days in a humidified incubator at 37^{o}C and 5% CO_2 with medium change once a week.

3.4.1.2 Chondrogenic Differentiation

For chondrogenic differentiation studies, nearly confluent Wj-MSCs and BM-MSCs at passage four on T-75 tissue culture flasks were detached by 0,25% trypsin-EDTA solution, and consequently 2x10^5 MSCs were seeded in a 96-well plate. After that, the culture plate was centrifuged at 120g for 10 min. Following the removal of the supernatant, culture media was gently added to wells without disturbing the cell pellets, and then allowed to settle down at 37^{o}C in 5% CO_2 in a humidified incubator. Upon observing the detachment of cell cluster in few days, the medium was carefully replaced with serum-free standard culture medium in the control group, whereas in the others, it was replaced with the same culture medium containing 50 μg/ml ascorbate-2-phosphate, 40 μg/ml L-proline, and 100 μg/ml sodium pyruvate, supplemented with 1% insulin-transferrin-sodium selenite media supplement (ITS), 10 ng/ml transforming growth factor-β3 (TGF-β3) and 100 nM dexamethasone.

Ascorbate-2-phosphate has been known to modulate chondrocyte growth and differentiation by stimulating proliferation in monolayer, and by increasing collagen type II mRNA expression in short-term cultures. The TGF-β superfamily of cytokines has been long known to regulate chondrogenic events during development. Dexamethasone and TGF-β3 have been shown to upregulate type II collagen, aggrecan, and anionic proteoglycans genes expression in micromass pellets of human mesenchymal stem cells. Nonetheless, the presence of culture supplements, such as ITS, is necessary to regulate the balance between cell growth (proliferation) and tissue growth (extracellular matrix synthesis), that may be critical to functional differentiation and tissue growth [156]. The presence of amino acid L-proline in the medium for chondrogenic differentiation contributes to collagen formation since its

ring structure helps to stabilize the collagen α-helice conformation.

The cell pellet was treated with chondrocyte differentiation medium for 21 days with medium changes every 3-4 days. After, the cell spheres were fixed with 10% neutral buffered formalin for 24 hours at room temperature, and then paraffin-embedded and sectioned (5 μm thick) to be finally stained with Toluidine blue dye. Toluidine blue (TB) is a basic thiazine metachromatic dye that selectively stains acidic tissue components (e.g., sulfates, carboxylates, and phosphate radicals). TB stains tissues based on the principle of metachromasia, i.e., the dye reacts with the tissues to produce a color different from that of the original dye and the rest of the tissue. It is used to stain proteoglycans and glycosaminoglycans in tissues such as cartilage. The strongly acidic macromolecular carbohydrates of cartilage are colored red or dark pink by the blue dye [157].

3.4.2 Proliferation Kinetics of Bone Marrow and Wharton's jelly-derived Mesenchymal Stem Cells

3.4.2.1 Growth characteristics of bone marrow and Wharton's jelly-derived MSCs

One of the most important parameters of clinical cell culture is the population doubling level (PD). Because the growth of cells varies significantly between donors and between preparations, the estimation of population doubling levels is a more precise way to measure cell growth kinetics compared to just consider the passage number of the cells. The passage number simply refers to the number of times the cells in the culture have been subcultured, often without consideration of the seeding densities or recoveries involved. The population doubling level refers to the total number of times the cells in the population have doubled since their primary isolation *in vitro*. PD level is synonymous with cumulative population doublings and its number directly correlates with replicative senescence (which is linked to loss of potency), and also with genomic instability.

On the other hand, the population doubling time (PDT) means the interval, calculated during the logarithmic phase of growth, during which the population has doubled.

Bone marrow and Wharton's jelly-derived MSCs of the primary cultures were subcultured under standard conditions. Briefly, freshly isolated MSCs were seeded in triplicate at a density of $3x10^3$ cells/cm^2 into T-25 flasks containing standard culture medium. When reaching 80-90% of confluence, around five days of culture, cells were trypsinized, and viable cells were counted and replated at the identical density into

new T-25 culture flasks. Ten passages were performed for each sample from both sources of mesenchymal stem cells. After each passage, the total number of viable cells was counted, and the population doubling time was calculated according to the following formula: (*No*: number of viable cells at seeding, *Nt*: number of viable cells at harvest, *t:* time)

$$PDT = t \cdot \left[\frac{\log_{10} 2}{(\log_{10} Nt - \log_{10} No)} \right]$$

Cumulative population doubling levels at each passage were calculated from the cell count by using the formula:

$$PD = \left(\frac{1}{\log_{10} 2} \right) \cdot \log_{10} \left(\frac{Nt}{No} \right)$$

The population doubling for each passage was calculated, and then added to the population doubling levels of the previous passages to yield the cumulated doubling level.

Five independent experiments were performed for the diverse umbilical cord donors and bone marrow samples.

3.4.2.2 MTT assay

The MTT assay was used to determine the metabolic activity of mesenchymal stem cells. The principle of the MTT assay lies in that for most viable cells mitochondrial activity is constant, and thereby increase or decrease in the number of viable cells is linearly related to the mitochondrial activity. Then, metabolically active cells react with the tetrazolium salt in MTT reagent to produce formazan crystals, which can be solubilized for homogenous measurement [158].

BM-MSCs and Wj-MSCs were cultured in T-75 flasks, and when confluence reached around 80-90%, the cells were detached by adding 0,25% trypsin-EDTA solution. The enzymatic activity of trypsin was neutralized by adding complete culture medium, and subsequently the cell suspension was centrifuged at 1200 rpm for 5 min. Next, the supernatant was removed, the pellet was resuspended in complete culture medium, and lastly the cell number was determined in the cell suspension by using an automated cell counter (TC20^{TM}. BIO-RAD).

Several amounts of cells, i.e., 5.0x10^2, 1.0x10^3, 2.5x10^3, 5.0x10^3, and 7.5x10^3 were plated in triplicates in 96-well plates and maintained in an incubator with 5% CO_2 at 37^{o}C. The outer wells were not used for the experiments due to evaporation

and were filled with PBS, to avoid the evaporation of the plate. Additional three wells were used as blanks, using culture medium only.

The colorimetric MTT assay was performed at several time points, i.e., 1, 2, 3, 4 and 7 days as follows:

After the appropriate incubation time, the culture medium was aspirated and replaced with DMEM high glucose without glutamine and phenol red (Gibco-Invitrogen, Paisley, Scotland).

Next, MTT solution (Thiazolyl Blue Tetrazolium Bromide) (Sigma-Aldrich) (5 mg/ml), was added to each well, and then the plate was kept in an incubator at 37 ^{o}C for 3.5 hours.

Once the incubation time was over, and the formazan crystals had been formed, MTT reagent was removed, and the DMSO solution was added to dissolve the crystals. The 96-well plate was then placed on a spectrophotometric plate reader (Infinite® 200 PRO, Tecan, Mänendorf, Switzerland), and the optical density (OD) of each well was measured at 565 nm (measure wavelength), and 690 nm (reference wavelength) in order to get a more exact measurement by correcting the background noise. Thus, any increase or decrease in viable cell number can be detected by measuring the OD; that is related to the formazan concentration.

3.4.3 Immunological Properties of Wharton's jelly Mesenchymal Stem Cells

3.4.3.1 Immune inhibition of adult peripheral blood mononuclear cells by Wj-MSC using allogeneic mature dendritic cells as stimulator

Dendritic cells (DCs) can be generated after culture of peripheral blood isolated monocytes in the presence of granulocyte-macrophage-colony-stimulating factor (GM-CSF) and interleukin-4 (IL-4). Dendritic cells are derived from CD34+ progenitors in the bone marrow. Human peripheral blood DCs are closely related to monocytes, being considered as a link between the innate and adaptative immune responses. Their common precursor is derived from the common granulocyte macrophage colony-forming unit (CFU-GM). DCs circulate in the blood in very low numbers and migrate into various tissues as a part of steady-state traffic. After contact with antigen, DCs migrate to draining lymph nodes, where they undergo functional maturation to become specialized antigen presenting cells (APCs). DCs are capable of activating naive T cells in the initiation of immune responses, and therefore, are desirable APCs for clinical adoptive immunotherapy [159].

Mixed lymphocyte culture experiments were used to evaluate whether Wharton's jelly-derived MSCs were able to suppress T-lymphocyte proliferation after stimulation with allogeneic mature DCs.

Isolation of Human Peripheral Blood Monocytes Monocytes were isolated from blood samples from healthy volunteers using the Human Monocyte Enrichment Cocktail (StemCell Technologies, Grenoble, France) following manufacture's protocol. All the protocols used to obtain and process the human samples were approved by the Clinical University Hospital Virgen de la Arrixaca Ethics Committee, and the patient's informed consent was previously signed.

Procedure:

1. Blood was drawn from an antecubital vein by using 21 gauge butterfly cannula system, and collected in 3 ml tubes (K3EDTA) (Venosafe^{TM}, Terumo, Tokyo, Japan). EDTA was added to the heparinized blood samples to a final concentration of 1 mM, i.e., 40 µl of a 250 mM EDTA solution for 10 ml of whole blood. Subsequently, RosetteSep^{TM} Human Monocyte Enrichment Cocktail was added at 50 µl/ml of whole blood, i.e., 500 µl of cocktail for 10 ml of blood. It was mixed well and then incubated in an orbital shaker for 20 min at room temperature.

2. After, the sample was diluted with an equal volume of PBS + 2% FBS and 1 mM EDTA, and then mixed gently.

3. The diluted sample was carefully layered on top of the Ficoll- Paque^{TM} solution to minimize mixing of density medium and sample. Volumes and tube sizes were used according to the manufacture's recommendations, e.g., for 10 ml of whole blood add 10 ml of PBS + 2% FBS and 15 ml of Ficoll-Paque solution in a 50 ml tube. Afterward, the tube was centrifuged for 20 min at 1200g at room temperature with the brake off.

4. The enriched monocytes were recovered from the interface between the plasma and the Ficoll-Paque layer and washed twice with PBS + 2% FBS. After centrifuging the sample at 700g for 7 min, the supernatant was removed, and the cells were resuspended in DMEM Low Glucose supplemented with 15% FBS, penicillin/streptomycin and L-glutamine. The final suspension of monocytes was counted and evenly distributed in a 6-well flat-bottom plate at a concentration of 1x10^6 cells/ml.

Immature myeloid dendritic cells (iDCs) differentiation For iDCs differentiation, 50 ng/ml GM-CSF (Sigma-Aldrich) and 25 ng/ml IL-4 (Invitrogen, Waltham, MA, USA) were added to the culture medium. The plate was maintained in an incubator at 37ºC and 5% CO2, with successive addition of the cytokines every three days for seven days. By day seven, more than 95% of the cells were $CD14^-$ $CD11c^+$ $CD1a^+$ $BDCA\text{-}1^+$.

Mature myeloid dendritic cells (mDCs) were obtained from iDCs, cultivated for 6 days as described above, by stimulation with 200 ng/ml lipopolysaccharide (LPS) (Sigma-Aldrich) for additional 24 hours as reported [160].

Mixed lymphocyte cultures and analysis of cytokine secretion Peripheral blood mononuclear cells were obtained by Ficoll-Paque centrifugation from fresh anticoagulated blood (no older than 8 hours) samples from healthy donors provided from the Department of Hematology, Clinical University Hospital Virgen de la Arrixaca. The mixed lymphocyte cultures (MLC) were performed by incubating responders MNCs and allogeneic stimulator mDCs at a 5:1 ratio, in 96-well round bottom plates (Sarstedt, Nümbrecht, Germany) maintained at 37ºC and 5% CO_2 for 5 days. Wj-MSCs were previously seeded in the wells at several ratios, i.e., 1:100, 1:25, 1:10, 1:5, and 1:1 (MSCs:MNCs) in triplicates, in order to study the dose-response suppressive effect of the Wj-MSCs on the proliferation capacity of MNCs. Wj-MSCs and mDCs were irradiated with 30 Gy after being seeded onto the plates, to prevent their proliferation.

Cellular proliferation was determined using an enzyme-linked immunoabsorbent assay (ELISA) BrdU colorimetric kit (Roche Diagnostic, Mannheim, Germany), based on the measurement of BrdU incorporation during DNA synthesis in proliferating cells. Briefly, BrdU labeling reagent was added to the wells 16 hours before determination. Then, the cells were fixed, DNA denatured and incubated with an anti-BrdU-POD antibody. After washing and substrate addition, OD at 450 nm was measured, also determining OD at 650 nm as reference wavelength. All experiments were performed in triplicate.

To quantify released cytokines, supernatants of MLCs were harvested on day five before the addition of BrdU and frozen at -80ºC until analysis. Human TGF-β (eBioscience, Hatfield, United Kingdom), PGE_2 (R&D Systems, Minneapolis, MN, USA), Indoleamine 2,3-dioxygenase (IDO) (Cusabio Biotech, BioNova Cientifica, Madrid, Spain), and INF-γ (Diaclone, BioNova Cientifica, Madrid, Spain) levels were measured by ELISA kits according to the manufacturer's protocols.

Inhibition assays Furthermore, several inhibitors were added from the beginning of the MLC, i.e., Indomethacin [50 uM]$_f$, 1-Methyl-tryptophan [1 mM]$_f$, and SB-431542 [10 uM]$_f$, to investigate if PGE_2, IDO, and TGF-β inhibition respectively had any effect on T-cell proliferation.

Indomethacin is a non-selective inhibitor of both COX-1 and COX-2, enzymes that participate in prostaglandin synthesis from arachidonic acid. 1-methyl-tryptophan (1-MT) is a competitive inhibitor of IDO, which is a rate-limiting enzyme in the catabolism of tryptophan. SB-431542 is a potent and specific inhibitor of the transforming growth factor-beta superfamily type I activin receptor-like kinase (ALK) receptors, specifically ALK4, ALK5, and ALK7 [161].

3.4.3.2 Immune inhibition of adult peripheral blood MNCs by Wj-MSCs and BM-MSCs using anti-CD3/CD28-coated beads

Dynabeads® Human T-Activator CD3/CD28 (Thermofisher Scientific, Waltham, MA, USA) is a simple method for activation and expansion of T lymphocytes using magnetic beads coated with anti-CD3 and anti-CD28 that does not require APCs stimulation. It provides a more physiologically related mechanism of activating T cells in comparison to the traditionally used mitogens such as phytohemagglutinin (PHA) and concanavalin A (ConA), by mimicking the binding of APCs to T cells [162].

The BM-derived MSCs served as positive controls and were isolated from bone marrow (BM) aspirates taken from patients undergoing knee or hip replacement surgery at the LUMC after informed consent of the donor. The MSC that were used throughout the study were between passage 3 and 6.

To analyze the effect of MSCs on the proliferation of peripheral blood MNCs, $1x10^5$ responders MNCs were cultured for 5 days in 24 well plates with αCD3αCD28 beads alone or in combination with different ratios of BM -or WJ-derived MSCs in a fully humidified incubator at 37°C and 5% CO2. On day 5, cultures were pulsed with [3H]thymidine ([3H]TdR; Amersham, Buckinghamshire, United Kingdom) 18 hours before harvest. Cells were harvested onto glass fiber filters, and radionuclide uptake was measured using a micro β-liquid scintillation counter. All experiments were performed in triplicate.

3.5 Elaboration and Characterization of Electrospun Silk Fibroin Scaffolds

3.5.1 Elaboration of Electrospun Silk Fibroin Scaffolds

3.5.1.1 Preparation of Fibroin

Preparation of fibroin is the starting point to obtain any of the scaffold formats it can be transformed (e.g., sponges, films, fibers and gels). Cocoons were obtained from silkworms reared in the sericulture facilities of the Instituto Murciano de Investigación y Desarrollo Agrario y Alimentario (IMIDA, Murcia, Spain). Silk fibroin scaffolds were made in the Department of Biotechnology (IMIDA) by following the protocol previously described by Aznar-Cervantes et al. [163].

Cocoons of *Bombyx mori* were chopped into 4 or 5 pieces and boiled in 0.02 M sodium carbonate ($Na_2CO_{3)}$ solution for 30 min, to remove the glue-like sericin proteins (Fig. 3.2 (A-B)). Then, the raw SF was rinsed thoroughly with water and dried at room temperature for three days (Fig. 3.2 (C)). The extracted SF was dissolved in 9.3 M lithium bromide (LiBr) (Acros Organics) for 3 h at 60ºC (Fig. 3.2, (D)), to generate a 20% solution that was dialyzed against distilled water for three days (Snakeskin Dialysis Tubing 3.5 KDa MWCO, Thermo Scientific) with eight total water changes (Fig. 3.2, (E)). The resultant 5-6% regenerated silk fibroin (RSF) solution was recovered and concentrated by dialysis against 30% polyethylene glycol (PEG) (10 kDa) for 24 h at 10ºC (Fig. 3.2, (F)), to obtain 19-20% RSF solutions that were used for the electrospinning experiments. The RSF solutions were kept in sealed Falcon tubes and refrigerated at 4ºC (Fig. 3.2, G)). This aqueous solution of pure silk fibroin could be processed into multiple material formats for use in biomaterials for biomedical applications.

3.5.1.2 Electrospinning and post-treatment of the SF Scaffold

The electrospinning system used in these experiments followed the design described in detail by Jose et al. [118]. It consisted of an insulated cabinet which housed an electrically-charged spinneret protruding through a focal plate, a syringe pump, and a grounded circular metallic collector. The collector surface (200 cm^2) was covered with aluminum foil. The electrospinning conditions were adjusted so that the Taylor cone was stable. A voltage of 19-21 kV was applied to the capillary tube, the distance between the tip of the tube and the collector was adjusted to 44 cm, and the selected injection rate of the polymer solution was 1ml/h. In all cases, 2.5 ml of 19% RSF solution were electrospun onto the same surface. The environmental conditions were

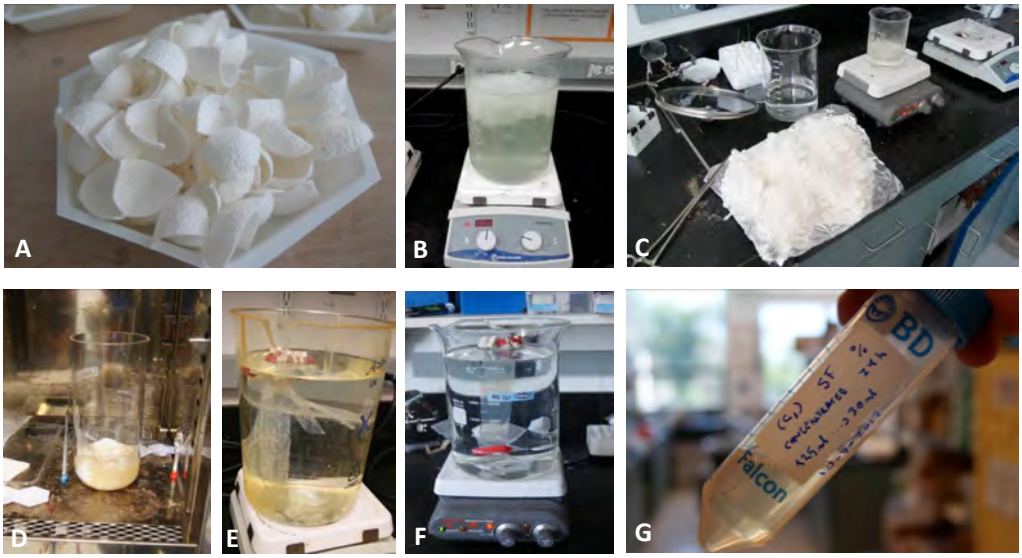

Figure 3.2: **Preparation of Fibroin**. Cocoons of *Bombyx mori* were chopped into 4 or 5 pieces and boiled in 0.02 M Na_2CO3 to remove the glue-like sericin proteins (A-B). Then, the raw silk fibroin was rinsed thoroughly with water and dried at room temperature for three days (C). The extracted SF was dissolved in 9.3 M LiBr for 3 h at 60^{o}C (D), to generate a 20% solution that was dialyzed against distilled water for three days (E). The resultant 5-6% RSF solution was recovered and concentrated by dialysis against 30% PEG for 24 h at 10^{o}C (F), to obtain 19-20% RSF solutions that were used for the electrospinning experiments (G).

recorded during the experiments, the average temperature and humidity ranging from 25-27^{o}C and 40-50%, respectively. After fabrication, the electrospun meshes were annealed by immersion in a bath of absolute methanol for 45 min, to induce a structural transition from an amorphous (random coil) to a β-sheet conformation. The electrospun meshes were placed between two pieces of filter paper, to facilitate drying for 24 h. This technique was employed to prevent the mats from curling or folding.

3.5.1.3 Sterilization of silk fibroin scaffolds

1. The silk fibroin meshes were cut by hand with an Iris Scissor curved sideways into 10 mm diameter disks.

2. SF patches were placed in a 48-well flat bottom plate (well diameter, bottom-11 mm) and next disinfected with 70% aqueous ethanol solution for 10 min. After that, ethanol was aspirated carefully and slowly to avoid sucking the scaffold, and then patches were left to dry in a sterile cell culture flow cabinet for one hour.

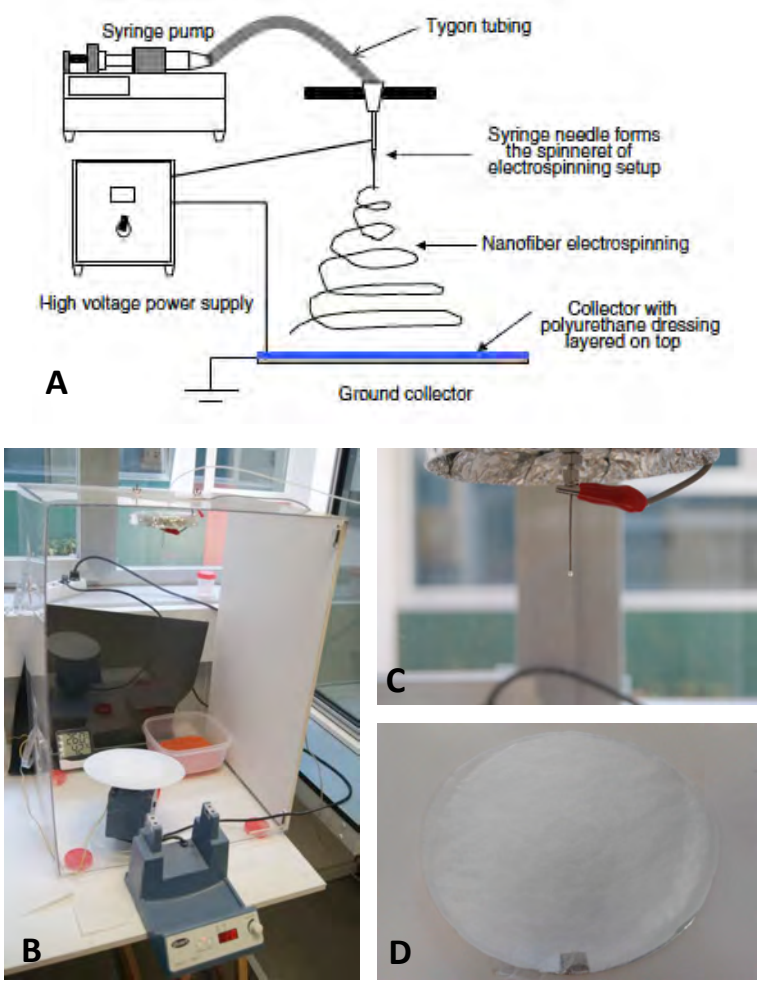

Figure 3.3: **(A) Schematic diagram of electrospinning apparatus.** Schematic diagram of electrospinning apparatus. Electrospinning involves the use of high voltage applied to a needle of a syringe, filled with an entangled polymer solution. The solution is pumped through a syringe at a constant rate, forming a droplet at the end of the needle. When the surface tension is overcome by electrostatic repulsion of charges within the solution, the jet is ejected, moving then toward metallic collector that is usually grounded. The solvent evaporates during jet traveling while the jet is elongated at very high strain rates (Polymer Physics Laboratory. Institute of Fundamental Technological Research. Poland). **(B) Electrospinning apparatus**. **(C) Taylor cone**. **(D) Silk fibroin scaffold**.

3. Two consecutive washes were made with sterile PBS for 15 min, and after pipetting out the liquid, the scaffolds were air-dried once again to ensure that all traces of alcohol had been cleared.

   (a) It was important to keep the plate uncovered for faster drying of the scaffolds after disinfection or washes steps.

   (b) Plates with scaffolds inside were left under the UV-C germicidal lamp in the cabinet for a couple of hours to ensure sterilization of the patches.

   The fibers did not suffer any change in morphology during sterilization. Thus, there was no apparent disruption of the architecture of the SF patches, as assessed by scanning electron microscopy analysis; in particular, the random arrangement typical of the SF fiber was kept.

3.5.2 Characterization of Physical and Mechanical Properties of Electrospun Silk Fibroin Scaffolds

3.5.2.1 Scanning Electron Microscopy

Conformational and structural analysis of electrospun silk fibroin scaffolds before and after seeding with mesenchymal stem cells was performed by Scanning Electron Microscopy (SEM) in the Experimental Science Support Service (SACE) at the University of Murcia.

The silk fibroin patches were fixed with 3% glutaraldehyde in 0.1M cacodylate buffer for 1.5 h at 4°C, and then they were rinsed and post-fixed in osmium tetroxide for 1 h. Subsequently, they were dehydrated by washing with solutions of increasing concentrations of ethanol, i.e. 30, 50, 70 and 90%, with a final dehydration in absolute ethanol. Finally, the samples were placed on metal stubs, dried by the Critical Point Method and gold coated. The meshes were visualized using a Jeol T-6100 scanning electronic microscope (SEAL Labs, El Segundo, CA, USA) at 15 kV, after being sputter-coated with gold. The pictures obtained were used to determine the maximum transverse size of the electrospun fibers, by means of ImageJ software; 60 fibers were measured as representative of each mesh, using at least three images per mesh (randomly-selected portions).

3.5.2.2 Mechanical Properties

Tensile tests were performed using a universal test frame machine (Qtest. MTS Systems, MN, USA). The mechanical properties of specimens (10 mm x 30 mm)

were recorded with a crosshead speed of 0.1 mm/s and a load cell of 5 N, under ambient conditions. The thickness of each piece of SF scaffold was determined with a Mitutoyo Digimatic Micrometer (Mitutoyo America Corporation, IL, USA) 0-25mm, with a resolution of 0.001mm and an accuracy of ±2 μm. Young's modulus (MPa), ultimate strength (MPa), and elongation at rupture (%) were determined using the stress–strain curves. Young´s modulus was calculated in the linear elastic portion of stress-strain curves generated. Each test was performed at least four times per scaffold.

3.6 Electrospun Silk Fibroin Scaffolds and Wharton's jelly Mesenchymal Stem Cells

Electrospun silk fibroin patches were used as scaffolds for culturing Wj-MSCs before transplantation. Initially, Wj-MSCs were grown in complete culture medium and maintained in a humidified incubator at 37ºC with 5% CO_2. Once Wj-MSCs reached 80-90% confluence, they were trypsinized as previously described, and passaged consecutively till passage four (see 3.3.1).

Four days before transplantation, MSCs were trypsinized, the number of cells was counted with a hemocytometer, and cells in suspension were then seeded onto the silk fibroin scaffolds as follows:

- Silk fibroin scaffolds were pretreated with FBS in order to facilitate initial adhesion of the mesenchymal stem cells. Thus, 100 μL of FBS were added over the mesh and incubated at 37ºC for a couple of hours.
- Afterward, the MSCs were seeded at different densities, i.e., $3x10^4$, $4x10^4$, $5x10^4$, and $6x10^4$cells/cm^2 onto the scaffold once the serum was removed from wells.
  - The different amount of cells were seeded onto the scaffolds in a volume of 200 μL and immediately incubated for half an hour at 37ºC. Finally, 500 μL of medium were added to each well and then the plate was kept in an incubator for four days until surgery or *in vitro* experiments.

SEM micrographs were taken when Wj-MSCs at different densities attached and proliferated on the silk fibroin scaffold four days after seeding (described in 3.5.2.1). Therefore, Scanning Electron Microscopy was used to evaluate cell adhesion, spreading and proliferation of human Wj-MSCs on the surface of the silk fibroin scaffolds.

3.6.1 Analysis of Expression of Mesenchymal Stem Cell Surface Markers by Flow Cytometry

To analyze possible phenotypic changes in the expression of mesenchymal markers on Wj-MSCs seeded on silk fibroin scaffolds, cells were seeded at a density of 5×10^4 cells/cm^2 in 48-well plates covered or not with silk fibroin scaffolds, and maintained in culture medium at 37°C for four days. Then, the Wj-MSCs were detached using a 0,25% trypsin-EDTA solution and afterward washed with PBS. Subsequently, the cells were incubated with fluorescence-conjugated specific monoclonal antibodies for CD73, CD90, CD105, CD14, CD20, CD34, CD45, CD80, CD86, and HLA-DR (Miltenyi Biotec, Bergisch Gladbach, Germany) for 30 min at 4ºC in the dark. This set temperature diminishes the possible nonspecific staining caused by temperature, whereas fluorescent attenuation is avoided by maintaining the sample in the dark during incubation. Unlabeled cells were used as control, and specific isotype monoclonal antibodies were used to exclude non-specific staining. The determination of these markers is recommended by the International Society for Cellular Therapy (ISCT) as essential to confirm the mesenchymal phenotype of the cells [59, 164].

After labeling and washing, cells were acquired using a BD FACS Canto flow cytometer (BD Biosciences, San Diego, CA) and analyzed with Kaluza analysis software (Beckman Coulter, Inc., Brea, California, USA).

3.6.2 Cell Viability Analysis

Apoptosis is a normal physiologic process that occurs during embryonic development besides in the maintenance of tissue homeostasis. The apoptotic program is characterized by certain morphologic features, including chromatin condensation, a reduction in cell volume, and internucleosomal cleavage of DNA. Apoptosis is also accompanied by a loss of plasma membrane asymmetry and attachment, resulting in the exposure of the membrane phospholipid phosphatidylserine (PS) at the surface of the cell. Annexin-V is a 36 kDa Ca^{2+} dependent phospholipid-binding protein that has a high affinity for PS, which is exposed on the surface of apoptotic cells but not on viable cells [165, 166].

Annexin-V conjugated to fluorochromes, e.g., phycoerythrin (PE), have been developed as a sensitive probe for flow cytometry analysis of apoptotic cells. Staining with Annexin-V is typically used in conjunction with a vital dye such as 7-Amino-Actinomycin (7-AAD) to identify live (Annexin-V$^-$/ 7-AAD$^-$), early apoptotic (Annexin$^+$/ 7-AAD$^-$) or late apoptotic and necrotic cells (Annexin-V$^-$ / 7-AAD$^+$ and Annexin-V$^+$ / 7-AAD$^+$).

In this study, apoptosis analysis by using Annexin-V Apoptosis Detection Kit (BD Bioscience, CA, USA) was carried out to discard possible cytotoxic effects of silk fibroin scaffolds on Wj-MSCs. At first, mesenchymal stem cells were seeded at a density of 1.5×10^4 cells/cm^2 on the silk fibroin scaffolds or the plastic bottom (as controls) in 48-well plates. They were maintained in complete culture medium for 1, 3, 5, 7, and 10 days in an incubator at 37 °C and 5% CO_2. Finally, cells were detached using a 0.25% trypsin-EDTA solution, washed with PBS and stained with PE-conjugated Annexin-V and 7-AAD (BD Biosciences) in Annexin-V-binding buffer for 15 min at room temperature according to the manufacturer's instructions.

The percentage of live, early apoptotic or late apoptotic and necrotic cells was analyzed on a FACS Canto flow cytometer. Lastly, percentages of each population were calculated and analyzed with Kaluza analysis software. All determinations were performed in triplicate.

3.7 Mouse excisional wound splinting model

3.7.1 Animals

Eight- to twelve-week-old hairless SKH1 male mice were used in the model of wound healing. Five animals were housed per cage and kept in a temperature-controlled animal facility with a 12-hour light/dark cycle before surgery. Mice were given *ad libitum* access to food and water. All techniques, protocols and animal proceedings employed were performed according to the Animal Ethics Committee of Murcia University following the Spanish and European governmental regulations on the use of animals for scientific research (Directive 86/609/EC (RD223/1998, RD1201/2005, LAW 32/2007) and Directive 2010/63/EU (RD53/2013, LAW 6/2013, Commission Recommendation 2007/526/EC)).

Hairless mice (SKH1 mice) are excellent for wound healing studies, as hair removal and associated inflammation are avoided, and hair regrowth does not obscure the wound healing response. Additionally, the lack of hair and skin pigmentation in hairless mice makes them ideal subjects for the application of new techniques of *in vivo* imaging, particularly light-based techniques such as luciferase-catalyzed luciferin light emission [167].

The mouse excisional wound splinting model was carried out as previously described by Galiano et al. and Wang et al. with some modifications (see Figure 3.4) [134, 135]. This model is readily reproducible, and the success rate for maintenance of the splint was 100%.

3.7.1.1 Anesthesia and creation of excisional wound

On the day of the surgery, the mice were individually anesthetized with 3% sevoflurane mixed with oxygen by using a vaporizer, and given preoperative analgesia with buprenorphine (0.1 mg/kg subcutaneously) 30 min before surgery, and then every 12 hours for three post-operative days. The anesthetic gas provides rapid induction and recovery and smooth adjustment of depth and duration of anesthesia (Fig. 3.4 (A)).

Each mouse then was prepared for aseptic surgery. The skin surface on the back of the mice was disinfected with povidone-iodine, followed by a rinse with 70% ethanol. Subsequently, two donut-shaped Silicone Wound Splints, 14 mm outer diameter (OD) X 10 mm inner diameter (ID) X 5 mm thick (Grace Bio-Labs, Bend, OR, USA), were fixed to the skin on each side of the dorsal surface midline. To ensure position interrupted 4-0 nylon sutures (Ethicon, Inc., Somerville, NJ, USA) were passed through the wound splint's suture sites (Fig. 3.4 (B)).

Next, a 10-mm diameter full-thickness wound, extending through the *panniculus carnosus*, was made aseptically within the splint using an Iris Scissor curved sideways. The inside edge of the splint exactly matched the edge of the wound, and thus the splinted hole area represented the original wound size (Fig. 3.4 (C)).

Photographs of individual wounds in each animal were taken with a digital camera (Nikon 1 J1, Tokyo, Japan) at different time points, i.e. on the day of surgery (day 0) and time of sacrifice (days 2, 7, 14, 21 and 28). At this point, stems cells can be employed according to the experimental protocol, i.e., injected into the edge of the wound or applied by silk fibroin patches cellularized with the Wj-MSCs.

In all cases, an occlusive sterile adhesive membrane (Oper film, IHT, Barcelona, Spain) was used to cover the wounds and splints completely (Fig. 3.4 (F)). Also, a self-adherent elastic wrap (Coban™, 3M Health Care, Loughborough, United Kingdom) dressed the wounds to prevent mice of removing the rings from the back. It is important to trim the wound dressing and adjust the tightness of the bandage so as not to restrict the breathing and movement of the mice.

The animals were placed in individual cages under a warming lamp and allowed to recover fully from anesthesia. Afterward, they were housed individually in a clean facility to avoid chewing of wounds and bandages by other mice. The animals were checked daily to ensure that the bandage was on, and to monitor manifestations of pain and weight loss. It is important to remark that the splints must be maintained positioned throughout the experiment, as removal of them will lead to rapid wound contraction and differ from the pattern of wound healing observed in humans. Antibiotic therapy was not administered since they can modify or alter some of the

phases of the wound healing process.

3.7.1.2 Removing bandages, photographing and harvesting wound tissue

After uncovering bandages, wounds can be photographed, and percentages of wound closure can easily be calculated. However, the presence of the scaffold along with the inflammatory exudate that occurs in response to surgery prevented from displaying the edges and then evaluate the resolution in time of the wound. Nevertheless, serial photographs can be used to estimate the clinical evolution of the wound regarding final appearance and scarring.

The Tegaderm® transparent dressings, sutures, and splints were carefully removed to collect wound tissue samples. Thus, the entire wound along with the 5-mm surrounding skin tissue was thoroughly excised and bisected by using an Iris Scissor.

Each wound sample was dissected across the center into two equal pieces;

- The outer half was left in RNAlater solution (Thermo Fisher Scientific) and stored at -80 ºC for further molecular analysis.
- The middle piece was carefully placed on a piece of sponge and secured with four stitches, one at each corner. Next, it was fixed in freshly prepared cold 4% paraformaldehyde in PBS at room temperature overnight for immunohistopathologic analysis.

3.7.2 Experimentation Groups and Stem Cell Transplantation

Two groups of seventy-five mice each group were experimentally related to two different human umbilical cord donors. Both groups were divided into five different subgroups (n=15), based on the type of treatment applied. Every subgroup underwent the sacrifice of three mice at different times, i.e., 48 hours, 7 days, 14 days, 21, and 28 days. There were made two wounds per mice with the same treatment applied to it, thus allowing replicate the number of experiments per animal and then diminishing the final number of mice. It was preferred not to use one wound as an internal control since the treated wound could have a local or systemic effect on the healing of the contralateral wound.

- Group 1: Wounds covered by Linitul® (Bama-Geve SLU, Barcelona, Spain), a gauze impregnated with Peru balsam and castor oil typically used to treat

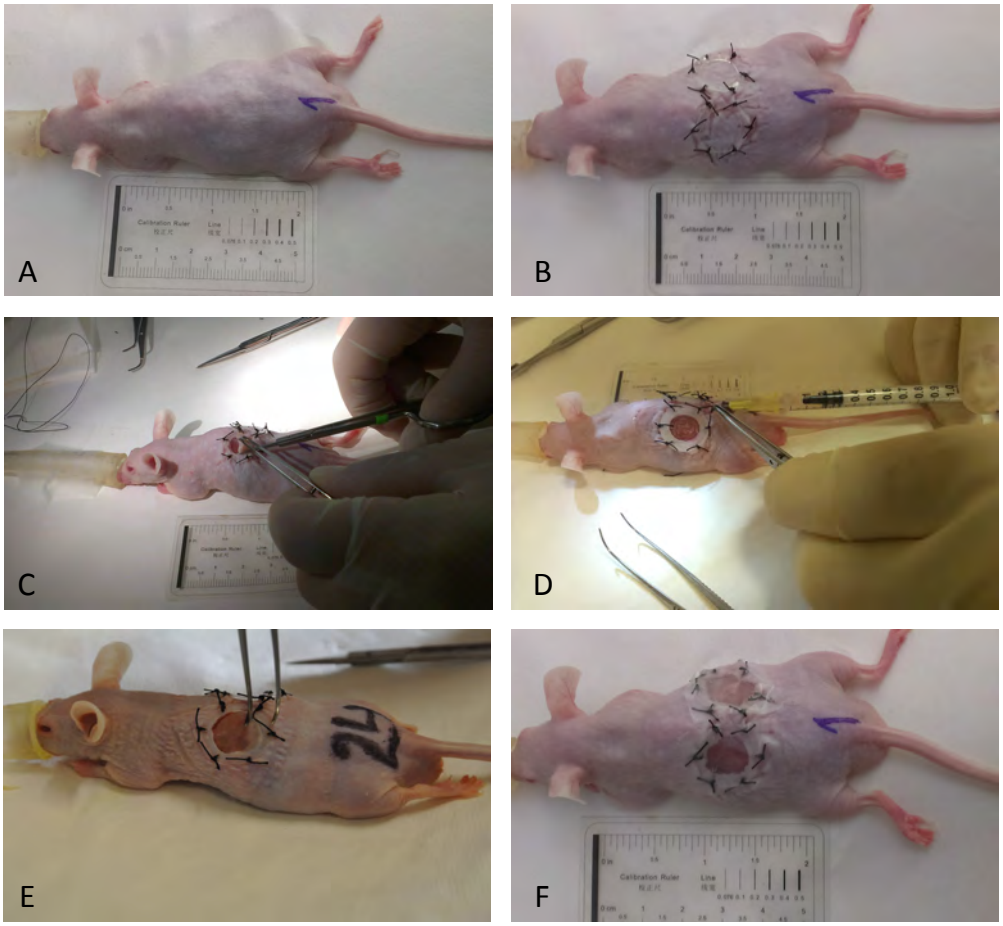

Figure 3.4: **Mouse excisional wound splinting model and stem cell transplantation.** (A) Following anesthesia, (B) silicone wound splints (14 mm OD X 10 mm ID X 5 mm thick) are fixed with interrupted sutures to the skin on each side of the dorsal surface midline. After, (C) two equal-sized 10-mm full-thickness cutaneous wounds are created on the dorsal skin so that the wound is centered within the splint. Subsequently treatment is applied, i.e., (D) stem cells are injected into the dermis around the wound edge or (E) cellularized silk fibroin scaffolds are placed onto the wound bed. Finally, (F) the wounds are dressed with Tegaderm® and self-adhering elastic bandages.

wounds, served as control group. In this group, neither cell transplantation nor scaffold grafting was carried out.

- Group 2: Wounds covered by silk fibroin scaffolds.
  - Sterile silk fibroin patches 10-mm diameter were placed on the wound bed. A hydrogel made from silk fibroin 0.7 % was dropped over the scaffold to keep it damp over time.
- Group 3: Wounds treated with Wj-MSCs injected at the edge (Fig. 3.4 (D))
  - A total number of $1x10^6$ human Wj-MSCs at passage 4 in 100 µl PBS were injected into the dermis in all the four directions around the wound edge, with a 25G, 0.1-cc syringe. It was important to ensure that the cell solution was injected into the dermis, but not into the subcutaneous layer of the skin.
- Group 4: Wounds treated with silk fibroin patches cellularized with Wj-MSCs (Fig. 3.4 (E))
  - Sterile electrospun silk fibroin patches 10-mm diameter were seeded with $5x10^4$ Wj-MSCs at passage 4 for four days. On the day of surgery, the cellularized scaffolds (hWj-MSCs-SF) were placed over the wound beds on the back of SKH1 mice, and few drops of a silk fibroin hydrogel 0.7 % were left to cover them to prevent drying.
- Group 5: Wounds treated with Wj-MSCs injected at the edge along with silk fibroin patches cellularized with MSCs covering the wound site.
  - Same amount of Wj-MSCs ($1x10^6$ cells at passage 4) in 100 µl PBS were injected into the dermis around the wound edge. Also, silk fibroin patches 10-mm diameter cellularized with Wj-MSCs were placed onto the wound bed. Likewise, the silk fibroin hydrogel was left to drop over the wound to avoid drying.

Group 2 was considered as control for the mice that were also treated with SF scaffolds, but now cellularized with mesenchymal stem cells. In short, neither cell transplantation nor cellularized silk fibroin scaffold grafting was carried out in control mice.

Critical Steps:

- All Wj-MSCs were used at passage 4 and didn't exceed the 80% of confluence when transplanted into the wound edge or seeded on the SF scaffold.
- MSCs should be prepared under sterile conditions immediately before transplantation; otherwise they form aggregates in PBS and viability decreases gradually over time (data not shown).
- As mentioned earlier, the onset of an inflammatory exudate in the wound site after the surgical procedure, led to hiding the wound edges thus limiting the assessment of the progression in time of the wound closure.

3.8 Histological and Immunohistochemical Study of Wound Healing

A chronologic histological and immunohistochemical analysis of wound samples from all experimental groups was carried out to determined the changes produced *in situ* after the inclusion of silk fibroin scaffold and/or Wharton's jelly mesenchymal stem cells during the skin regeneration process.

3.8.1 Sample preparation

Preparation of the sample is critical for maintaining cell morphology, tissue architecture and the antigenicity of target epitopes. This requires proper tissue collection, fixation, and sectioning.

3.8.1.1 Fixing

Samples from normal skin, brain, liver, spleen, kidneys, testes, heart, lungs and bone marrow were fixed in 4% neutral buffered formalin (Panreac Química, Barcelona, Spain), for 24 hours at room temperature. Then, samples were sectioned into smaller representative slices, placed in plastic cassettes, and re-fixed in 4% neutral buffered formalin for another 24 hours. Fixative volume should be 10 times that of tissue on a weight per volume (1 ml of formalin per 100 mg of tissue) minimum. It is recommended to keep fixation conditions standard for a particular study to minimize variability.

3.8.1.2 Processing - dehydration, clearing, and embedding

The aim of tissue processing is to remove water from tissues and replace it with a medium that solidifies at room temperature to preserve indefinitely the tissues without degenerative changes, and to allow thin sections to be cut. For light microscopy, the paraffin wax embedding is most frequently used.

Once fixed, samples were rinsed with running tap water to remove any excess of formalin, and then dehydrated through a series of graded ethanol baths. This is followed by a hydrophobic clearing agent (such as Xylene) to remove the alcohol, and finally molten paraffin wax, the infiltration agent that replaces the Xylene. Histowax® (Thermo Corporation, Waltham, MA, USA), a low-temperature melting paraffin (56-58^{o}C), was used as the embedding agent. This paraffin is ideal for immunohistochemical studies because its low-melting temperature assures an optimal preservation of antigen structure.

The samples were processed on a Leica TP1050 (Leica Microsystems, Wetzlar, Germany) tissue processor as follows: 50% ethanol for 1 hour, 70% ethanol for 2 hours, 96% ethanol for 2 hours, absolute ethanol (3 steps of one hour each), Xylene substitute (3 steps of one hour each) and finally inclusion in Histowax® (2 steps of 1 hour each and then 1 steps of 2 hours).

Once finished the processing, the samples were embedded into paraffin blocks by using an embedding workstation (HistoStar^{TM}, Thermo Scientific). Tissues embedded into these blocks can be stored at room temperature for years.

3.8.1.3 Sectioning

Paraffin blocks were sectioned using a Leica RM 2155 (Leica) motorized rotary microtome that operates with Accu-Edge® Disposable Microtome Blades (Sakura, Osaka, Japan). 4 and 5-micrometer-thick sections were made for histopathological and immunohistochemical analysis, respectively. The sections were floated on the surface of a 40^{o}C water bath (Kunz Instruments, Nynashamn, Sweden), and then placed onto the surface of glass microscope slides (Dakocytomation. Barcelona, Spain). Then, the mounted sections are treated with the appropriate stain.

3.8.2 Staining

3.8.2.1 Hematoxylin and Eosin (H&E) Stain

Staining of biological material is used to confer both contrasts to the tissue, as well as highlighting particular features of interest. Hematoxylin and eosin stain is the most commonly used light microscopical stain in histology and histopathology.

Hematoxylin, a basic dye, has a dark blue-purple color and stains acids structures, e.g., nucleic acids in the cell nucleus. Eosin, an acidic dye, is orange-red, and stains basic structures. Thus, the stain shows abundant structural information, with particular functional implications [168].

Protocol:

1. Dewaxed of sections with Xylene substitute (Thermo Scientific™) for 15 min.
2. Rehydration of the sections in ethanol baths in the following order: 100% ethanol 5 min (x2), 96% ethanol for 5 min and 70% ethanol for 5 min.
3. Rinse in tap water for 5 min and then dip the slide into a Coplin jar containing Harris Hematoxylin (Thermo Scientific™) for 5 min. Rinse the slide in tap water for 5 min.
4. Partially dehydration of the sections by immersion in 70% ethanol for 5 min.
5. Stain the slide with eosin alcoholic solution (Thermo Scientific™) for 5 min, and then rinse the slide in water for few seconds.
6. Dehydrate the sections with one step of 96% ethanol (1 min), and two changes of absolute ethanol for 5 min each.
7. Extract the alcohol with two changes of Xylene substitute (Thermo Scientific™) and finally,
8. Add one or two drops of a non-aqueous mounting medium (Neo-Mount™. Merck) onto the sample and cover with a coverslip.

3.8.2.2 Masson-Goldner Trichrome Stain

Masson's trichrome is a three-colour (azophloxine, Orange G, and light green SF) staining protocol used in histology for selectively staining muscle fiber, collagenous fiber, fibrin, and erythrocytes. Most protocols derived from Claude L. Pierre Masson's (1880-1959) original assay have been used for different specific applications, but all are suitable for distinguishing cells from surrounding connective tissue.

Procedure of Masson-Goldner trichrome staining (Merck, Darmstadt, Germany):

1. Deparaffinate the sections, and rehydrate up to 70% alcohol solution.

2. Since Trichrome stainings use acid dyes, nuclei have to be stained with Weigert's iron hematoxylin for 5min. Afterward, wash with running tap water 5 min, and then rinse in 1% acetic acid for 30 sec.

3. Azophloxine solution (10 min) and then rinse in 1% acetic acid for 30 sec.

4. Tungstophosphoric acid Orange G solution 1min and then rinse in 1% acetic acid for 30 sec.

5. Light green SF solution (2min) and next rinse in 1% acetic acid for 30 sec.

6. Dehydration in ascending alcohol series, clearing with xylene, and mounting with Neo-Mount®.

Results: Cell nucleus: dark brown to black / Cytoplasm and muscle: brick red / Connective tissue and acidic mucous substance: green / Erythrocytes: bright orange.

Under light microscopy, the sections were observed using an Axio A-10 (Carl Zeiss) microscope, then photographed with an AxioCam ICc 3 digital camera, and at last the images were processed with the Axio Vision 4.8 digital image processing software.

3.8.2.3 Immunohistochemical Staining

Immunohistochemistry (IHC) is a biological method for demonstrating the presence and location of specific antigens or cellular components in tissue sections. Developed from the antigen-antibody binding reaction, it enables the observation of processes in the context of intact tissue. Immunohistochemical staining is accomplished with antibodies that recognize the target protein. Since antibodies are highly specific, the antibody will bind only to the protein of interest in the tissue section. The antibody-antigen interaction is then visualized using either chromogenic detection, in which an enzyme conjugated to the antibody cleaves a substrate to produce a colored precipitate at the location of the protein. In this study, we used an indirect-Avidin-Biotin Complex (ABC) immunohistochemistry method.

The steps of the IHC staining protocol are as follows:

1. Dewaxing of the tissue sections with Xylene substitute (Thermo Scientific™) for 15 min and rehydration through a series of degraded ethanol baths.

2. Rinse the sections in tap water for 5 min.

3. Demasking antigen procedure.

   (a) As formalin fixation induces cross-linking between proteins that can affect the immunological features of the antigens, a demasking antigen procedure was performed. Thus, the sections were immersed in a high Ph demasking antigen solution (Dako) and heated to 98^{o}C for 30 min in a demasking antigen chamber (Dako Pascal®, Dako).

4. Once the demasking procedure was finished, the sections were washed three times in Tris-Buffered-Saline solution (TBS, 0.05M; pH 7.6) for 5 min.

5. Block endogenous peroxidase activity with a 1.5% hydrogen peroxide (Merck) solution in methanol (J.T. Baker) for 30 min.

6. Wash in TBS (3 steps 5 min each) and next, incubate in normal serum (diluted 1:100 in TBS) in a humid chamber at 30°C for 20 min.

7. Incubate with the primary antibody (diluted in TBS) in a humid chamber at 30°C for 1 hour and then, wash in TBS (three steps 5 min each).

8. Incubate with a biotinylated secondary antibody, diluted 1:250 in TBS, in a humid chamber at 30°C for 20 min.

9. Wash in TBS (three steps 5 min each) and next, incubate with the Avidin-Biotin-Peroxidase Complex (Vector Laboratories. Burlingame, CA, USA), diluted in TBS, in a humid chamber at 30°C for 20 min.

10. Wash in TBS (3 steps 5 min each) and subsequently, reveal the immunostaining by incubating in 0.05% 3-3'diaminobenzidine (DAB) tetrahydrochloride solution (Sigma) and 0.03% hydrogen peroxide solution in TBS (pH: 7.6) for 5 min.

11. Wash in running tap water for 5 min and then counterstain with hematoxylin for 3 min, to provide contrast that helps the primary stain stand out.

12. Wash in water for 5 min, dehydrated through graded ethanol baths, and then clear with xylene.

13. Finally, mount the sample in Neo-Mount (Merck) and view the staining under the microscope.

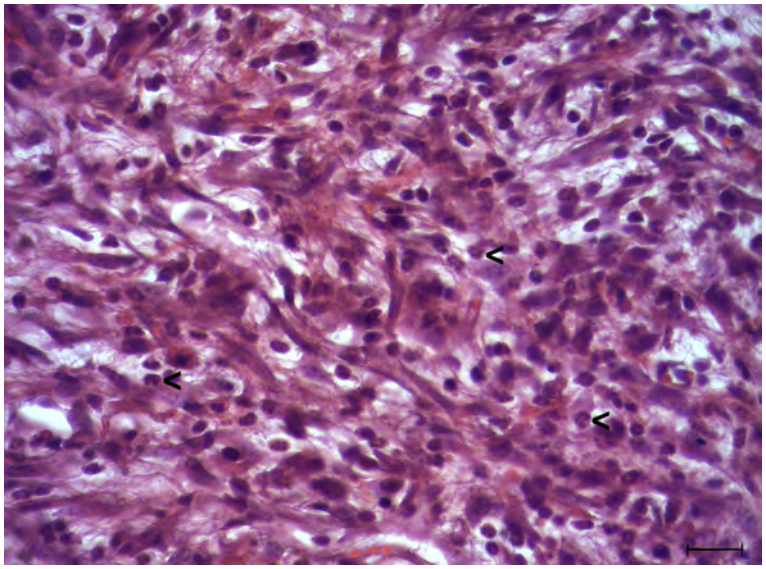

Figure 3.5: **Visual identification of polymorphonuclear neutrophils (<) in mouse skin tissue sections by using H&E staining.** Scale bar 20μm.

Immunohistochemical Studies of Excisional Wounds

- **Measurements of Leucocyte Infiltration**

The number of infiltrating polymorphonuclear neutrophils (PMN) (Figure. 3.5), macrophages, and lymphocytes within the wound beds at all post wound time points were counted in 15-20 randomly chosen visual fields (at high power fields X400) of the sections stained with H&E solution, or with anti-F4/80 and anti-CD3 antibodies, respectively. Half of the fields were selected from each edge of the wound bed, and the remaining fields were from the middle of the wound bed. All measurements were repeated twice and were carried out under double-blind conditions.

Rat anti-F4/80 antibody [clon CI:A3-1] recognises the mouse F4/80 antigen, a 160kD glycoprotein expressed by murine macrophages (see Figure 3.6). Expression of F4/80 is heterogeneous and is reported to vary during macrophage maturation and activation. The F4/80 antigen is expressed on a wide range of macrophage populations including Kupffer cells, microglial cells, epidermal Langerhans cells, and also peri-epithelial macrophages associated with simple epithelia throughout the gastrointestinal, respiratory, and male and female reproductive tract as well as the brain ependyma [169].

Rabbit anti-human CD3 antibody recognizes the intracytoplasmatic portion of the CD3 antigen expressed by T cells. The CD3 is a multimeric protein complex composed of four distinct polypeptide chains (ε, γ, δ, ζ) that assemble and function as three pairs of dimers (εγ, εδ, ζζ). The CD3 complex associates non-covalently with a molecule known as the T-cell receptor to generate an activation signal in T

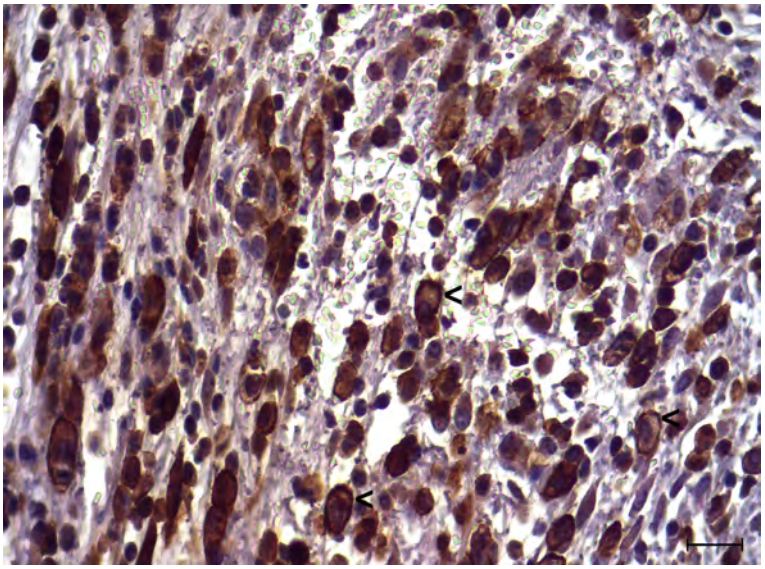

Figure 3.6: **Immunohistochemical expression of F4/80 antigen in mouse skin tissue.** Scale bar 20μm.

lymphocytes. CD3 antigen is first expressed in the cytoplasm of prothymocytes, i.e., the progenitor cells from which T-cells arise in the thymus, in the first stages of lymphocyte development. In cortical thymocytes, the antigen is mostly present in the cytoplasm, but then it appears on the T cell surface at the medullary thymocyte stage [170]. The high specificity, combined with the presence of CD3 at all stages of T-cell development, makes it a useful immunohistochemical marker for T-cells in tissue sections (see Figure 3.7).

- **Assessment of Angiogenesis by Expression of CD31 in Wound Sites**

Angiogenesis was assessed by immunostaining for the platelet endothelial cell adhesion molecule (PECAM-1), also known as cluster of differentiation 31 (CD31) that recognizes a 100kDA glycoprotein in endothelial cells and 130kD in platelets. In the present study vascular areas, defined as CD31-positive ones, were measured in the wound beds at all post wound time points and were expressed as the percentage of the entire wound bed areas. All measurements were performed without a prior knowledge of the experimental procedures. The extent of microvessel formation during the healing process was determined through a qualitative scale as depicted in Table 4.2 which correlates with the images in Figure 3.8 [Normal skin, Grade I (+), Grade II (++), and Grade III (+++)].

- **Expression of Alpha-Smooth Muscle Actin during Wound Healing**

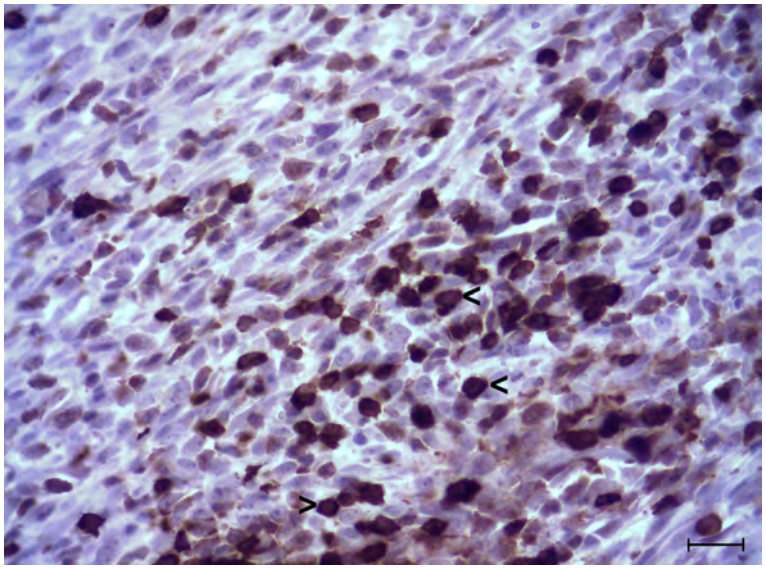

Figure 3.7: **Immunohistochemical expression of CD3 antigen in mouse skin tissue.** Scale bar 20μm.

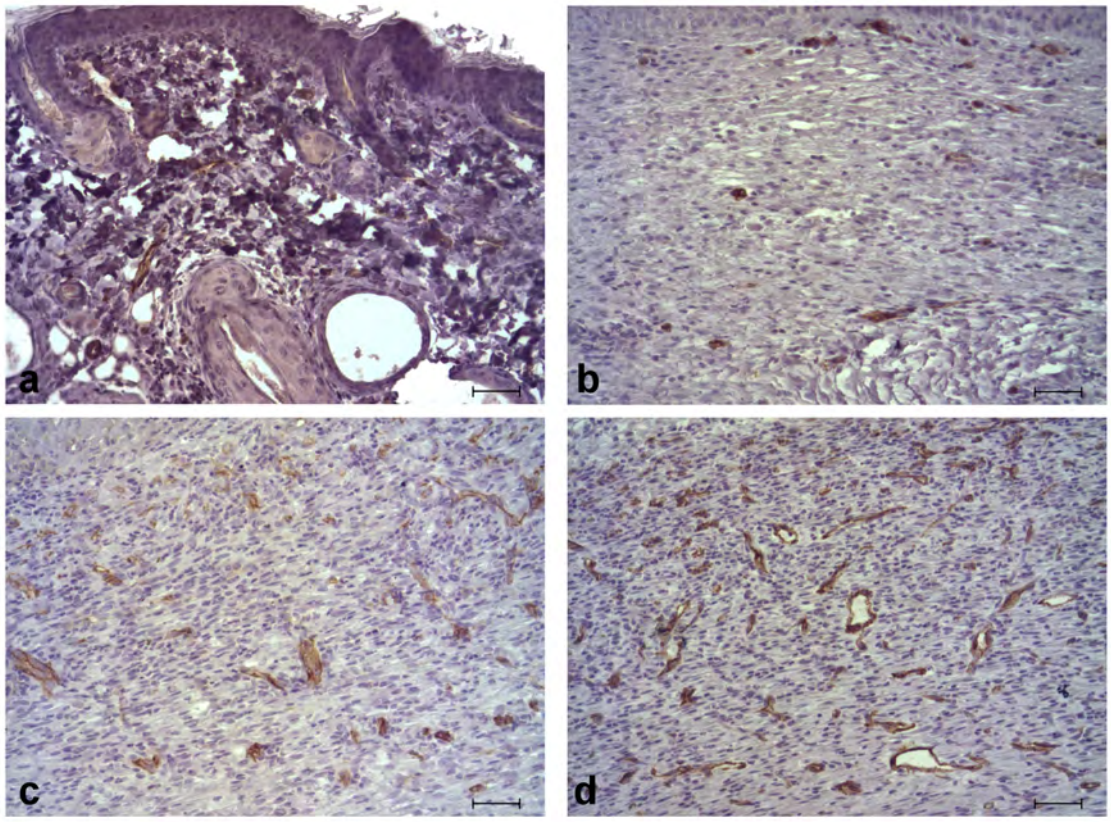

Figure 3.8: **Representative images of CD31 expression in skin sections, according with the qualitative scale depicted in Table 4.2.** (a) Normal Skin (b) + Grade I (c) ++ Grade II (d) +++ Grade III. Scale bar 50μm.

Rabbit monoclonal [E184] to alpha smooth muscle Actin is a specific marker for the single isoform of alpha-smooth muscle actin (α-SMA), the 42 kD weight actin isoform that predominates within vascular smooth-muscle cells. Actin is a globular structural protein that polymerizes in a helical fashion to form an actin filament. Actin filaments provide mechanical support for the cell, determine the cell shape, enable cell movements [171]. During the development of granulation tissue in the inflammatory phase of wound healing process, fibroblasts are activated and express α-SMA up turning thus into myofibroblasts. These myofibroblastic cells synthesize and deposit a large amount of extracellular component proteins. Also, these cells exhibit contractile properties, due to the expression of α-SMA in microfilaments bundles or stress fibers, playing a significant role in the contraction and maturation of the granulation tissue [172]. The immunohistochemical expression of cytoplasmatic α-SMA in myofibroblasts was assessed through a qualitative scale as shown in Table 4.3 which correlates with the images in Figure 3.9 [$<$ 10% (-), 10-25% (+), 26-50% (++), and $>$50% (+++) α-SMA expression].

- **Expression of mesenchymal stem cell marker CD-90 on wound sites**

The Rabbit monoclonal (EPR3133) antibody specifically binds to human CD90, which is also known as Thy-1. CD90 is a 25-35 kDa glycophosphatidylinositol-anchored membrane glycoprotein of the Ig superfamily that can be used as a marker for a variety of stem cells. Immunohistochemical staining using of a pellet composed of mesenchymal cells from Wharton's jelly served as positive control for the different experimental groups (see Figure 4.27 (132)).

Finally, Table 3.1 summarizes the antibodies used for immunohistochemical analysis of skin wound sections.

Marker	Origin	Isotype	Supplier	Cellular Location	Specificity	Dilution
F4/80	Rat	Monoclonal (CI:A3-1)	AbdSerotec	Membrane	Macrophages	1/100
CD3	Rabbit	Polyclonal	DAKO	Membrane	T Lymphocytes	1/500
CD31	Rabbit	Polyclonal	Abcam	Membrane	Endothelium	1/100
α Actin	Rabbit	Monoclonal (E184)	Abcam	Cytoplasm	Myofibroblasts	1/500
CD90	Rabbit	Monoclonal (EPR3133)	Abcam	Membrane	Stem Cells	1/50

Table 3.1: **Antibodies used for immunohistochemical analysis of skin wound sections.** Antigen retrieval at high pH, 97^{o}C. Incubation time: overnight.

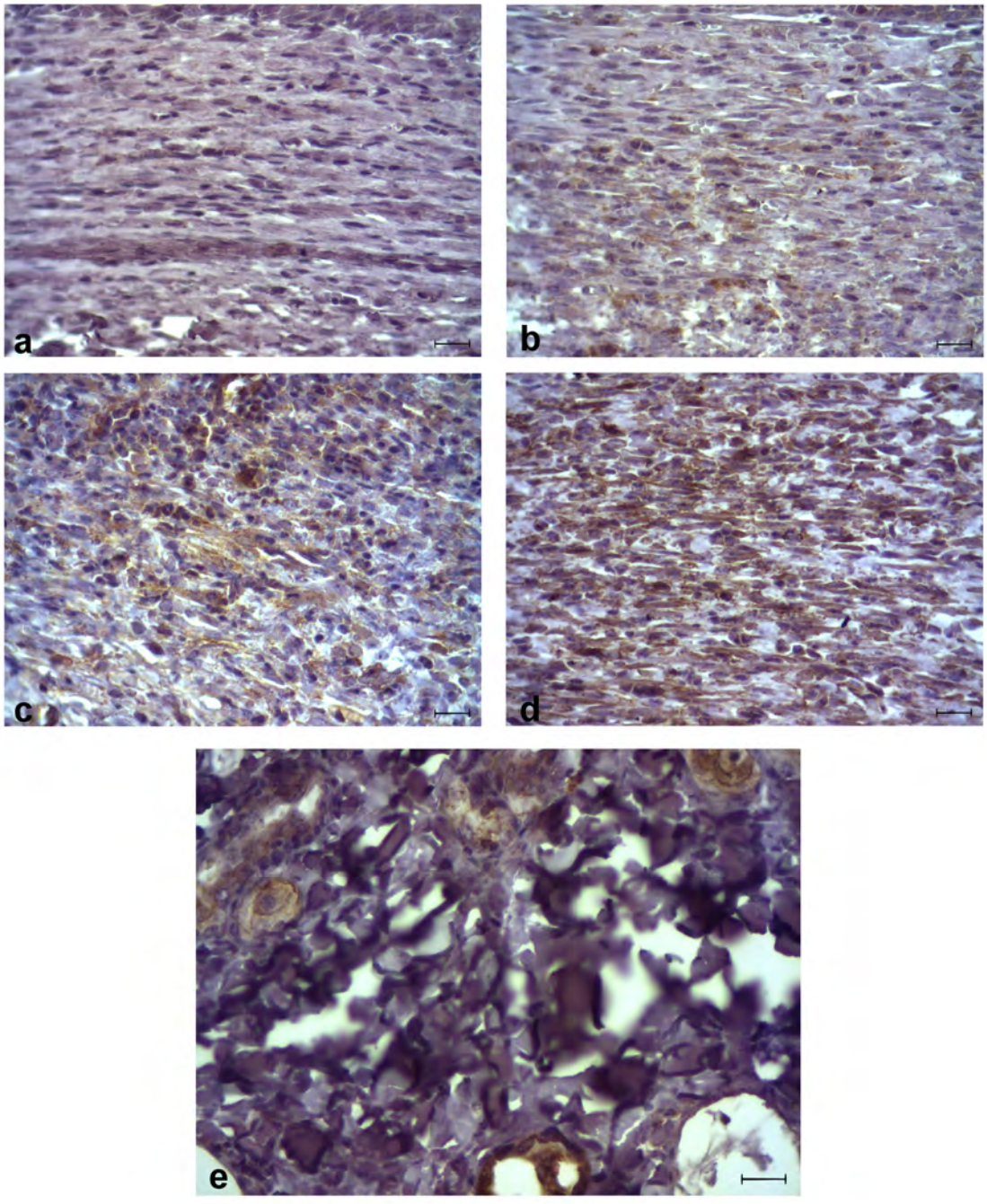

Figure 3.9: **Representative images of α-SMA expression in skin sections, according with the qualitative scale depicted in Table 4.3.** (a) < 10% (-) / (b) 10-25% (+) / (c) 26-50% (++) / (d) >50% (+++) α-SMA expression. (e) Immunohistochemistry (paraffin-embedded normal skin section) - alpha smooth muscle Actin antibody [E184] (ab32575). Scale bar 50μm.

Statistics

All statistics were performed using GraphPad Prism software package (version 6, CA. USA). Results are presented as mean ± standard deviation. To test for statistical significance, a Mann-Whitney test or one-way ANOVA was used. Results were considered to be significant if the p-value was equal to or less than 0.05.

Chapter 4

RESULTS

In vitro Study of the Wharton's Jelly Mesenchymal Stem Cells

4.1 Characterization of human Wharton's jelly mesenchymal stem cells

4.1.1 Morphology of the Mesenchymal Stem Cells derived from human Umbilical Cord Wharton's jelly

As seen in Figure 4.1, mesenchymal stem cells derived from the Wharton's jelly of the human umbilical cord displayed a fibroblastic, spindle-shaped morphology comparable to that of unrestricted somatic stromal cells (USSCs), cord blood mesenchymal stem cells (CB-MSCs), and bone marrow-derived MSCs.

4.1.2 Proliferation Kinetics of Bone Marrow and Wharton's Jelly Mesenchymal Stem Cells

4.1.2.1 Cumulative Population Doubling Level (PD) and Population Doubling Time (PDT)

The proliferation and growth efficiency of Wj-MSCs and BM-MSCs were determined by the total cumulative population doubling level, and the population doubling time using the formulas described in the Materials and Methods chapter (3.4.2). Both cell populations demonstrated differences in their growth dynamics being as the mesenchymal stem cells from the umbilical cord displayed an increased proliferative capacity compared to bone marrow counterparts.

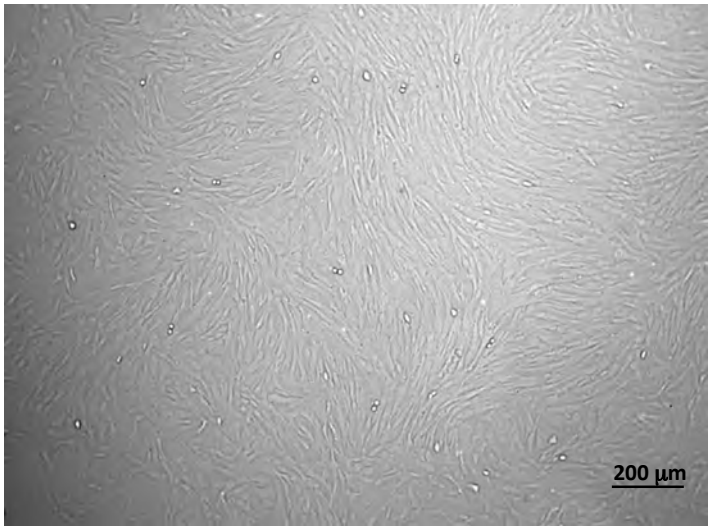

Figure 4.1: **Phase contrast micrograph of human Wj-MSCs at passage 4.** Scale bar: 200 µm.

Figure 4.2 represents the proliferation dynamics of the bone marrow and Wharton's jelly-derived mesenchymal stem cell populations during prolonged *in vitro* subcultivation. The mean cell yield is the one that derived from the serial proliferation of the MSCs following the subculture protocol described in 3.4.2.1. This was significantly higher for Wj-MSCs compared to BM-MScs (1.9-fold, **= $p<0.01$) and related to a relatively constant number of about 3.7 PD per passage (represented by the linearity of the graph showed in Figure 4.2(A)) accumulating to a total of 37 PD (vs 21 PD for BM-MSCs) in the 58-days culture period (ten passages).

Also, the population doubling time of BM-MSCs and Wj-MSCs was calculated from passage 1 to passage 10. There was considerable differences in PDT between BM-MSCs and Wj-MSCs in every single passage. Wj-MSCs had significantly shorter PDT compared to BM-MSCs (P1= 32,46±1,70 vs. 51,01±0 h; P2= 27,80±2,92 vs. 51,02±1,98 h; P3= 27,25±3,19 vs. 46,60±7,30 h; P4= 25,14±1,61 vs. 52,35±0,14 h; P5= 28,73±2,48 vs. 54,08±1,13 h; P6= 29,46±2,49 vs. 54,79±5,59 h; P7= 31,78±4,98 vs. 60,61±0,73 h; P8= 32,67±3,73 vs. 58,47±9,36 h; P9=39,23±5,05 vs. 60,20±21,92 h; and P10= 38,92±4,96 vs. 74,36 ±23,83 h. (P1→P8, ***=$p<0.001$; P9, *=$p<0.05$; P10, **=$p<0.01$) (Figure 4.2(B)). Wj-MSCs grew consistently until passage 10 in contrast to BM-MSCs that showed signs of growth slowdown from passage 9 (*= $p<0,05$).

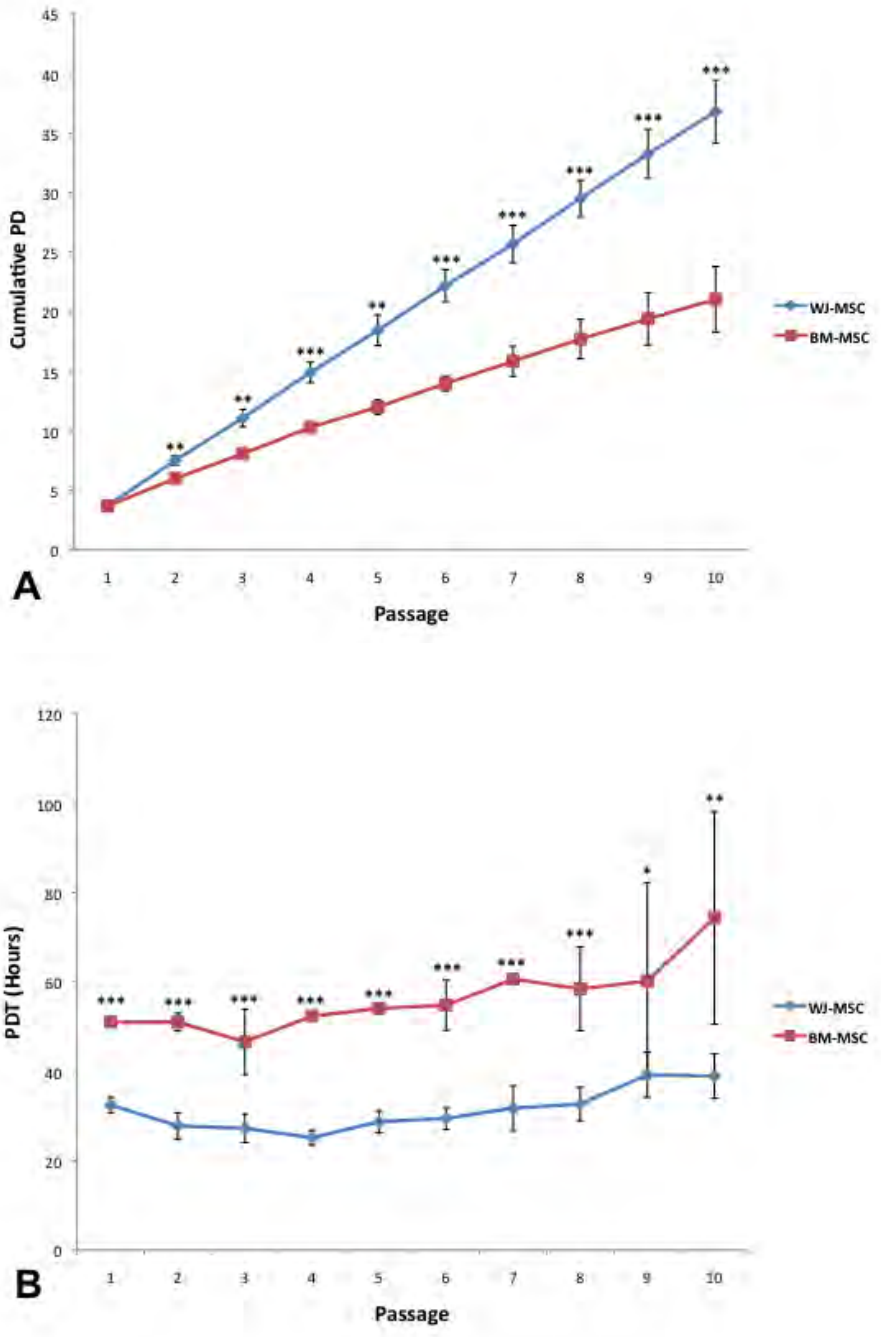

Figure 4.2: **Proliferation kinetics of Wj-MSCs and BM-MSCs over extended *in vitro* propagation.** (A) number of cumulative population doubling level (PD) as a function of time in culture. (B) cell population doubling times -PDT- (hours) at respective passages. Abbreviations: PD: population doubling level; PDT: population doubling time; Wj-MSCs: Wharton's jelly mesenchymal stem cells; BM-MSCs: bone marrow mesenchymal stem cells. Statistically significant differences using one-way ANOVA, * = $p < 0.05$, ** = $p < 0.01$, *** = $p < 0.001$.

4.1.2.2 MTT assay

Figure 4.3 depicts the proliferation rates of Wharton's jelly and bone marrow-derived MSCs at passage fourth after being cultured at a density of 5000 cells/cm^2 in 96-well plates for a week. Both mesenchymal stem cell sources displayed approximately the same proliferation rate during the first 24 hours of culture. However, Wj-MSCs began to proliferate considerably faster than BM-MSCs from the second day of culture onward being these differences statistically significant (* = $p< 0.05$, ** = $p< 0.01$, *** = $p< 0.001$). In all cases, the proliferation rate of Wj-MSCs was higher than that observed for BM-MSCs, reaching a maximum peak after a week of culture (***= $p<0.001$). These results confirmed the previous findings obtained when calculated the PD and PDT in the proliferation kinetics assays using WJ and BM-MSCs over prolonged passaging.

4.1.3 *In vitro* Multilineage Differentiation Capacity

BM-MSCs obtained from 23 different donors and Wj-MSCs derived from 18 different umbilical cords were subjected to differentiation induction protocols (as previously described) to evaluate their stem cell multipotency. While most BM-MSCs samples showed the ability to differentiate into adipocytes, osteoblasts, and chondroblasts, over 75% of the Wj-MSCs samples (14 out of 18) failed to generate adipocytes, and over 85% of the Wj-MSCs samples (16 out of 18) failed to form osteoblasts (Figure 4.4). On the other hand, cartilage was formed by half of the Wj-MSCs samples (9 out of 18). Scoring system of the level of differentiation of Wj-MSCs or BM-MSCs into adipogenic, osteogenic and chondrogenic lineages is shown in Figure 4.5. These results suggest that Wj-MSCs are limited with respect to their capacity to differentiate into mature mesodermal cell lines when compared to BM-MSCs.

4.1.4 Immunomodulatory Properties of Wharton's Jelly Mesenchymal Stem Cells

- **Wharton's jelly mesenchymal stem cells suppress T cell proliferation after stimulation with anti-CD3/CD28 beads**

Experiments in Figure 4.6 show the immunomodulatory effects of hWj-MSCs on the proliferative response of anti-CD3/CD28-stimulated T cells and compared with the effects mediated by hBM-MSCs. The anti-CD3/CD28-stimulated T cells proliferation was decreased when the ratio of hWj-MSCs present in the same culture was

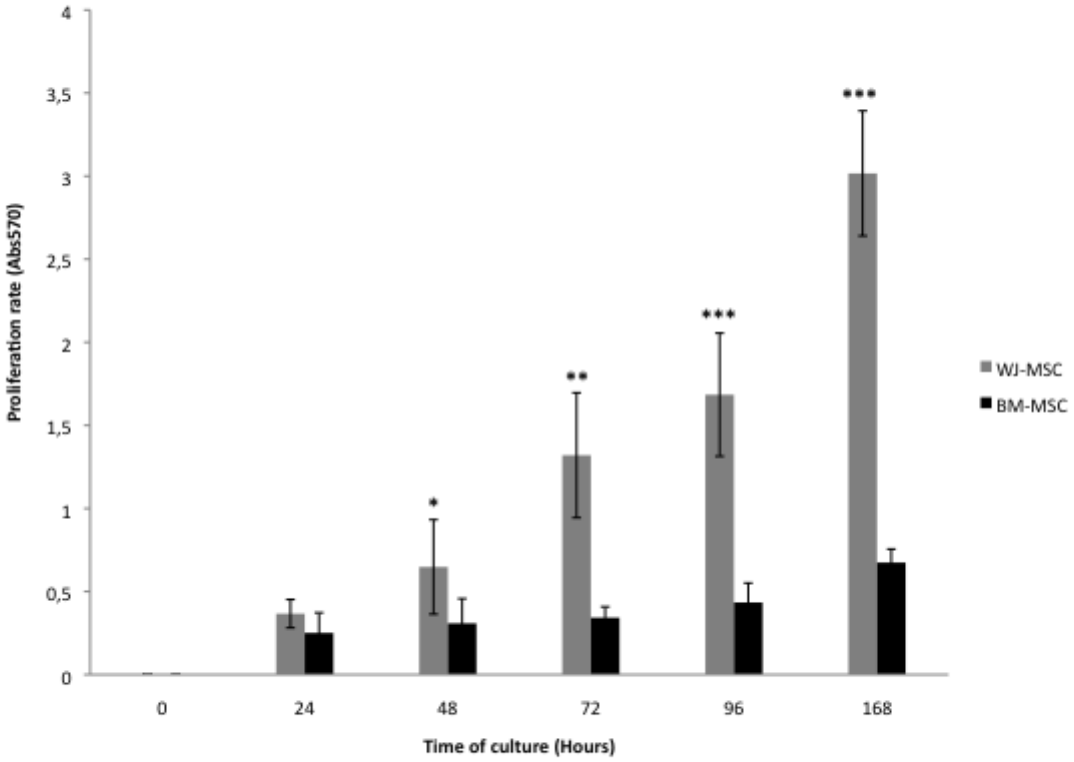

Figure 4.3: **Proliferation rate of Wharton's jelly and bone marrow-derived mesenchymal stem cells as determined by the MTT Cell Proliferation Assay.** Mesenchymal stem cells from both sources were seeded at a density of 5000 cells/cm^2 in 96-well plates and cultured for a week. Abbreviations: Wj-MSCs: Wharton's jelly mesenchymal stem cells; BM-MSCs: bone marrow mesenchymal stem cells. All values are presented as the mean ± SD. Proliferation rate was significantly increased, * = $p< 0.05$, ** = $p< 0.01$, *** = $p< 0.001$, according to one-way ANOVA.

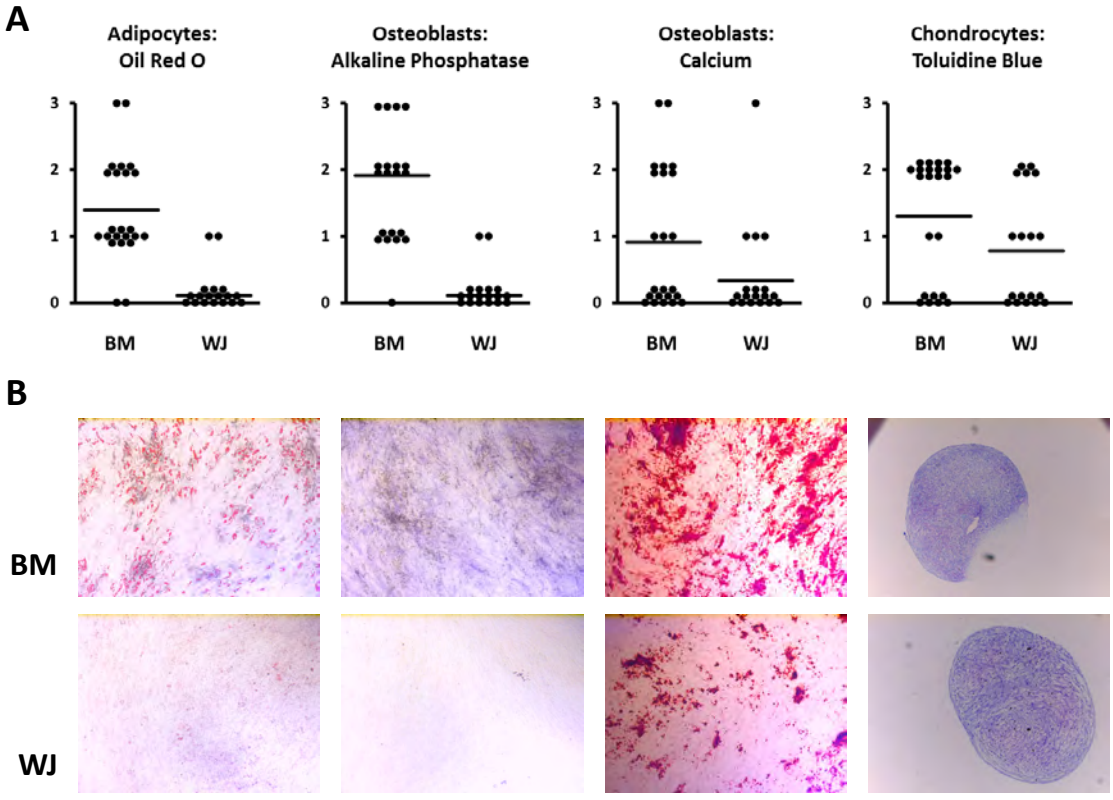

Figure 4.4: **(A)** Capacity of Wharton's jelly mesenchymal stem cells to differentiate into adipocytes (Oil Red O staining), osteoblasts (NBT/BCIP and Alizarin Red staining), and chondrocytes (Toluidine blue staining). Degree of differentiation was assessed using the following scoring system: 0= no differentiated cells, 1= $<$ 20% differentiated cells, 2= $<$ 60% differentiated cells, 3= $>$ 60% differentiated cells. **(B)** Representative pictures of differentiation cultures after incubation with different cell-specific stains.

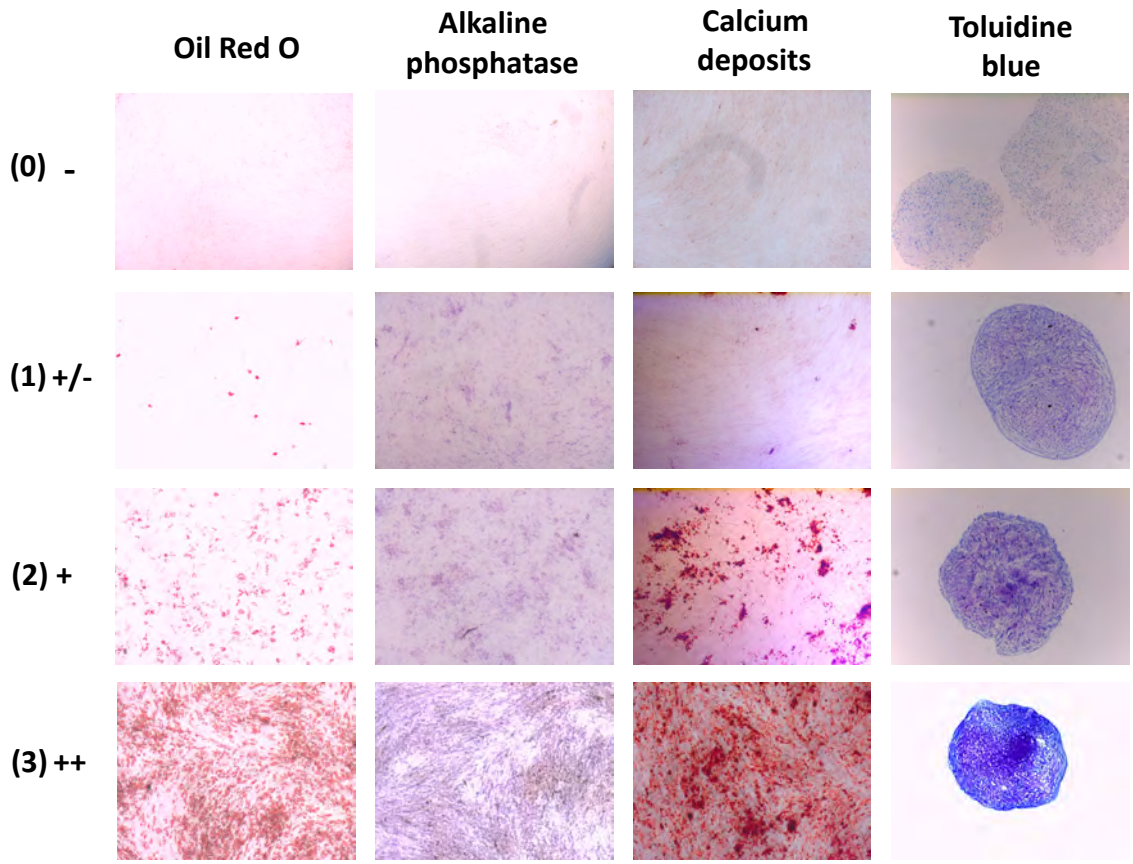

Figure 4.5: **Scoring system of the level of differentiation of Wj-MSCs and BM-MSCs into adipocytes, osteoblasts, and chondroblasts.** The level of staining was assessed for all different samples after specific differentiation cultures and compared to reference stains to determine the final percentage of differentiation, i.e., 0(+) = no differentiated cells, 1(+/-) = < 20% differentiated cells, 2(+) = < 60% differentiated cells, 3(++) = > 60% differentiated cells.

increased. Figure 4.6 also shows that the dose-response effect mediated by hWj-MSCs was the same as that mediated by hBM-MSCs (***= $p<0.001$ for all ratios of MSC:T cells compared to anti-CD3/CD28-stimulated T cells alone). Interestingly, the inhibition of proliferation mediated by hBM-MSCs was slightly lower than that observed for hWj-MSCs at ratios 1:100, 1:33 or 1:10, although not statistically significant. However, hBM-MSCs-mediated inhibition of proliferation was significantly lower than that achieved for hWj-MSCs at ratio 1:1 (BM-MSC 57±5% vs. Wj-MSC 32±3%, ##: $p<0.01$). Moreover, hWj-MSCs did not induce any proliferative response of allogeneic T cells in the absence of anti-CD3/CD28 stimulation, whereas anti-CD3/CD28-activated T cells were used as positive control.

- **Wharton's jelly mesenchymal stem cells suppress T cell proliferation after allogeneic mDCs stimulation**

Irradiated mDCs (as stimulators) were co-cultured with responder allogeneic T cells in the presence of increasing numbers of hWj-MSCs to investigate the immunomodulatory effects of these MSCs on activated T cell proliferation. After five days of co-culture, the proliferation of responder T cells was measured. As observed in Figure 4.7, a significant hWj-MSCs-mediated dose-dependent inhibitory effect on T cell proliferation was observed when compared to proliferation achieved on mDCs/T cells co-cultures in the absence of hWj-MSCs. At the lowest ratio Wj-MSCs: effector T cells (1:100) T cell proliferation was significantly reduced compared to the control co-culture in the absence of MSCs (11,3 % reduction, * = $p<0.05$). Nevertheless, the addition of a higher number of MSCs to the co-culture led to a more marked inhibition of T cell proliferation, ranging from 43,6% (ratio 1:25) to 95,5% (ratio 1:1) (***= $p<0.001$).

- **Wharton's jelly mesenchymal stem cells downmodulate the *in vitro* production of inflammatory cytokines**

To identify the soluble factors that could be involved in the immunosuppressive effects mediated by hWj-MSCs, the production of the pro-inflammatory cytokine IFN-γ released during the culture of T cells stimulated by allogeneic mDCs in the presence of MSCs was investigated. As shown in Figure 4.8, the secretion of IFN-γ was significantly inhibited by hWj-MSCs in a dose-dependent manner. Proportions of at least 1:100 (MSC: effector T cells) in the culture had a significant effect on the production of IFN-γ compared to basal levels produced in the absence of MSCs (reduction of 10,69%, *= $p<0.05$). Furthermore, ratios above 1:25 also significantly decreased the levels of IFN-γ in supernatants from MLC (1:25 = reduction of 35,10%;

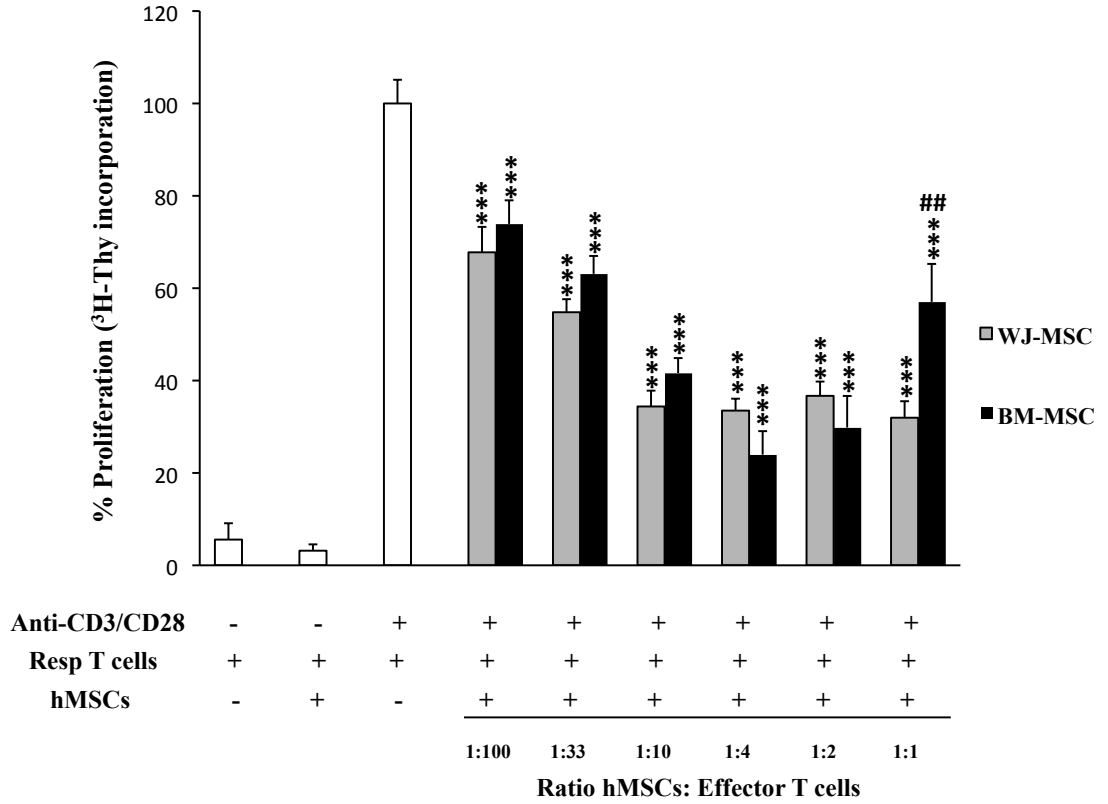

Figure 4.6: **Effect of Wj and BM-MSCs on *in vitro* immunological responses: the capacity of BM or Wj-MSCs to inhibit the proliferation of peripheral blood T cells stimulated with anti-CD3/CD28 beads.** BM or Wj-MSCs were cultured with $1x10^5$ MNCs in different ratios and stimulated with CD3/CD28 beads for five days. After, the proliferation of the T cells was measured by thymidine incorporation and compared to control without MSCs. The MSCs from both sources significantly inhibited the proliferation of the T cells in a dose-dependent manner (***= $p<0.001$ for all ratios according to one-way ANOVA). The proliferation of T cells in the presence of BM-MSCs was significantly higher than that obtained using Wj-MSCs at the same ratio (##= $p<0.01$). All data are presented as mean ± SD. Abbreviations: hMSCs: human mesenchymal stem cells. Wj-MSC: Wharton's jelly mesenchymal stem cells. BM-MSC: bone marrow mesenchymal stem cells.

1:10 = reduction of 48,58%; 1:5 = reduction of 59,06%, and 1:1 = reduction of 71,85%; ***= $p<0.001$ for all ratios).

These results showed that MSCs downmodulate the production of pro-inflammatory cytokines such as IFN-γ by activated T lymphocytes.

- **Immunosuppressive effect of Wharton's jelly mesenchymal stem cells on T-lymphocyte proliferation in response to allogeneic mDCs stimulation is mediated by TGF-β**

Several soluble factors have been associated with the immunomodulation capacity on T-lymphocyte activation and proliferation by MSCs, such as transforming growth factor-β (TGF-β). TGF-β was quantified by Human TGF-β1 Instant ELISA (eBioscience) in the supernatants of co-cultures of T cells and allogeneic mDCs in the absence or presence of Wj-MSCs at differents ratios (hWj-MSCs: effector T cells). As shown in Figure 4.9, the co-culture of stimulator mDCs and responder T cells in the presence of hWj-MSCs significantly increased the secretion of TGF-β in a dose-dependent manner (1:100= 1.32-fold increase, *= $p<0.05$; 1:25= 2.06-fold increase, **= $p<0.01$; 1:10= 3.62-fold increase, ***= $p<0.001$; 1:5= 4.28-fold increase, ***= $p<0.001$, and 1:1= 4.62-fold increase, ***= $p<0.001$), compared to basal levels determined in the absence of MSCs. The maximum level of TGF-β was achieved at 1:1 ratio.

- **PGE_2 is an *in vitro* mediator of the Wharton's jelly mesenchymal stem cells immunosuppressive effects on T lymphocyte proliferation in response to allogeneic mDCs stimulation**

PGE_2 was investigated as one of the mediators responsible for the inhibitory effects of MSCs on the proliferation of activated T lymphocytes. PGE_2 was quantified by PARAMETER^{TM} PGE_2 Assay (R&D Systems) in the supernatants of MLC in the absence or presence of Wj-MSCs at differents ratios (hWj-MSCs: effector T cells). As shown in Figure 4.10, the co-culture of stimulator mDCs and responder T cells in the presence of hWj-MSCs at ratios higher than 1:25 significantly increased the secretion of PGE_2 (1:25= 2.47-fold increase; 1:10= 5.39-fold increase; 1:5= 7.12-fold increase; and 1:1= 12.5-fold increase. ***= $p<0.001$ for all ratios), compared to basal levels determined in the absence of MSCs. No significant differences were observed when MSCs were scarcely present in the MLC (53,33±10,40 pg/ml; ratio 1:100).

- **Inhibition of allogeneic T cell proliferation *in vitro* mediated by indoleamine 2,3-dioxygenase (IDO)**

IDO is also known to have a key role in the T cell immunosuppression mediated by MSC. Therefore, it was quantified by Human indoleamine 2, 3-dioxygenase (IDO) ELISA Kit (Cusabio Biotech) in the supernatants of MLC in the absence or presence of Wj-MSCs at differents ratios (hWj-MSCs: effector T cells). As shown in Figure 4.11, the co-culture of stimulator mDCs and responder T cells in the presence of hWj-MSCs at ratios higher than 1:25 significantly increased the secretion of IDO (1:25= 7.52-fold increase, **= $p< 0.01$; 1:10= 17.52-fold increase, ***= $p< 0.001$; 1:5= 31.14-fold increase, ***= $p< 0.001$; and 1:1= 35.08-fold increase, ***= $p<0.001$), compared to basal levels determined in the absence of MSCs. No significant differences were observed when MSCs were present in the MLC at 1:100 ratio.

- **PGE_2, TGF-β, and IDO play a major role mediating the immunosuppressive effects of Wj-MSCs on T lymphocyte proliferation after allogeneic mDCs stimulation**

To investigate that the anti-inflammatory factors TGF-β, PGE_2 and IDO secreted by hWj-MSCs accounted for the inhibition of T cell proliferation after allogeneic mDCs stimulation, it was carried out additional MLCs experiments in the presence of different specific inhibitors of the biosynthesis or signaling of these factors such as SB-431542, indomethacin (IDM) or 1-methyl-tryptophan (1-MT), respectively (Figure 4.12). T cell proliferation after allogeneic mDCs stimulation was measured in the absence or presence of hWj-MSCs. The same proportion of hWj-MSCs and effector T cells (ratio 1:1) was used in this experimental assay because of the maximum inhibitory effect obtained for this condition in previous experiments (Figure 4.7).

Importantly, the addition of SB-431542, IDM, and 1-MT in the MLCs in the absence of hWj-MSCs did not affect the maximum proliferative capacity of effector T cells, neither the basal proliferation of stimulator mDCs, responder T cells or hWJ-MSCs alone.

The proliferation of mDCs-stimulated T cells significantly decreased when hWj-MSCs were present in the MLC and in the absence of any inhibitor (control) (93,91% reduction). However, the addition of the inhibitors SB-431542, IDM, or 1-MT significantly recovered the proliferative response of mDCs-stimulated T cells compared to the control condition (***= $p<0.001$), although still remained significantly lower than in absence of hWj-MSCs (Δ= $p<0.05$, ΔΔ= $p<0.01$, ΔΔΔ= $p<0.001$).

Strikingly, the simultaneous treatment with the three inhibitors together recovered almost entirely the proliferation rate of mDCs-stimulated T cells, suggesting

that PGE_2, TGF-β, and IDO play a major role mediating the immunosuppressive effects of hWj-MSCs on T lymphocytes proliferation after allogeneic stimulation. Even so, it is not discarded the possibility that some other anti-inflammatory factors released by hWj-MSCs had a minor role in the suppression of T cell proliferation.

On the whole, the co-culture of stimulator mDCs and responder T cells in the presence of hWj-MSCs at 1:1 ratio increased the production of TGF-β (Figure 4.9), PGE_2 (Figure 4.10), and IDO (Figure 4.11) compared to MLCs without MSCs. According to these results, the T cell proliferation rescue mediated by SB-431542, IDM, and 1-MT was correlated to the increase in the levels of the respective anti-inflammatory cytokines TGF-β, PGE_2, and IDO in the co-cultures.

4.2 Electrospun Silk Fibroin Scaffolds

4.2.1 Characterization of Physical and Mechanical Properties of Electrospun Silk Fibroin Scaffolds

4.2.1.1 Scanning Electron Microscopy (SEM)

The SEM pictures of the SF meshes produced were used to visualize the topography and appearance of fibers generated by electrospinning. As can be observed in Figure 4.13, the fibers produced from regenerated silk fibroin solutions were cylindrical and uniform throughout their lengths. In relation to the diameter of electrospun fibers obtained, the average value was 2417±547 nm. No significant differences were found between replicates of the study (Kruskal-Wallis, $p>0.05$), which shows a consistent production method.

4.2.1.2 Mechanical Properties of Electrospun Silk Fibroin Scaffolds

Average values of Young's modulus (MPa) (51.8±8.5), the elongation at break (%) (4.4±1.1), and the ultimate strength (MPa) (1.4±0.5) were calculated using stress-elongation curves (Figure 4.14) generated from tensile tests. There were no significant differences in the mechanical properties between the three replicates tested for each experimental condition (ANOVA, $p>0.05$).

Based on the morphology and mechanics of the scaffold, it was suggested that the electrospun nanofibrous structure would be suitable as a skin substitute.

4.3 Electrospun Silk Fibroin Scaffolds Cellularized with Wharton's Jelly Mesenchymal Stem Cells

4.3.1 Scanning Electron Microscopy Micrographs Analysis

Following an incubation period of four days in the culture medium, silk fibroin scaffolds maintained their integrity and three-dimensional structure after seeding with Wj-MSCs. Cell morphology and the interaction between MSCs and silk fibroin nanofibers were analyzed *in vitro* by scanning electron microscopy (SEM) to evaluate the efficacy of cellularization of the scaffolds. The Wj-MSCs displayed a characteristic spindle-shaped morphology and stretched across the nanofibrous scaffold during their proliferation (Figure 4.15).

The MSCs adhered and spread on the surface of the silk fibroin fiber network and migrated through the pores and grew under layers of the fiber network. Also, these cells interacted and integrated well with the surrounding fibers. Cells grew in the direction of fiber orientation, forming a three-dimensional and multicellular network according to the architecture of the scaffold.

Analysis of the images revealed that Wj-MSCs seeded at intermediate densities formed a continuous monolayer on the silk fibroin scaffold but leaving some spaces available for further growth and avoiding an early confluence. For this reason, it was decided to use silk fibroin scaffolds seeded with Wj-MSCs at a density of $5x10^4$ cells/cm^2 for further transplantation in the mouse wound healing model.

4.3.2 Immunophenotype by Flow Cytometry

In order to confirm the mesenchymal phenotype of isolated hWj-MSC and to determine possible phenotypic changes after their culture on the silk fibroin scaffolds, flow cytometry studies were carried out. These analyzes showed that the MSC surface markers CD73, CD90 and CD105 were expressed to levels greater than 99,5%, whereas expression of the hematopoietic markers CD14, CD20, CD34, and CD45, the MHC-class II HLA-DR, or the costimulatory molecules CD80 and CD86 were less than 5% (Figure 4.16, upper panels). Hence, the cell surface antigen profile denotes the MSCs isolated from the Wharton's jelly of the umbilical cord as belonging to a population of non-hematopoietic, non-endothelial, but mesenchyme-derived adult stem cells. Moreover, flow cytometry analysis revealed that hWj-MSCs cultured on silk fibroin patches for four days maintained their mesenchymal phenotypic profile (Figure 4.16, bottom panels).

4.3.3 Cytotoxicity of Fibroin-based Scaffolds. Apoptosis Analysis

The fundamental principle of tissue engineering in wound healing involves the use of an appropriate cell source and a biocompatible scaffold to produce a construct that structurally and functionally could mimic the skin. Thus, for evaluating the possible toxicity and the biocompatibility of fibroin-based scaffolds, apoptosis analysis of the Wj-MSCs was carried out using the Annexin-V kit (BD Pharmingen, CA, USA). Wj-MSCs were seeded on plastic culture plates (control) or silk fibroin patches and cultured for 1, 3, 5, 7, and 10 days. After, the cells were stained with Annexin-V and 7-AAD and analyzed by flow cytometry.

As seen in Figure 4.17, human Wj-MSCs cultured or not on SF scaffolds displayed a slight initial cell death (94,47±0,19 % viable cells). The percentage of viable cells in the control group decreased significantly after one day of culture (*= $p<0.05$) but recovered soon after three days, reaching and maintaining initial values throughout the assay. On the other hand, Wj-MSCs seeded on silk fibroin patches (Wj-MSCs-SF) displayed a significant decrease in viability over the first three days (70,52±4,65 % viable cells at day 3, **= $p<0.01$) and then increased progressively to values above 80% from day five onward. Even though the percentage of living cells in Wj-MSCs-SF group was significantly lower than the control group during the first five days of culture (#= $p<0.05$, ###= $p<0.001$), no differences between them were detected in later days. Thus, a silk fibroin-based biomaterial could be considered as a promising biocompatible scaffold since it may preserve hWj-MSCs proliferation, viability, and function.

In vivo Study of Wound Healing by Wharton's Jelly Mesenchymal Stem Cells

4.4 Clinical and Paraclinical Observations in mice during Wound Healing

All mice were continuously monitored from the day of surgery until sacrifice. Neither spontaneous mortality occurred in the course of the study, nor it was displayed any pathological condition. At the date of surgery, all mice weighed 27–28 g and maintained their body weight and spontaneous behavior throughout the study. Besides, no significant macroscopic differences were observed between experimental groups

during the necropsy at the end of the study.

Complete blood count (CBC) and serum biochemistry analysis were performed on blood samples taken from the abdominal aorta of the mouse the day of sacrifice. Significant differences in some biochemical parameters were found between the experimental groups Wj-MSCs-SF and Wj-MSCs-Edge+SF and the control group. However, none of these values were outside the normal laboratory reference ranges (Figure 4.1, bold numbers).

4.5 Histological and Immunohistochemical Study of Wound Healing

4.5.1 Hematoxylin and Eosin (H&E) Stain (Figures 4.18 to 4.21)

Normal Skin (photos 11, 22, 38 and 54)

Normal skin has a thin stratified squamous epithelium (i.e., the epidermis), composed of proliferating basal and differentiated suprabasal keratinocytes. The dermis is tightly connected to the epidermis by a basement membrane and is structurally divided into two areas: a superficial area adjacent to the epidermis, called the papillary region, and a deep thicker area known as the reticular region. The reticular region lies deep in the papillary region and is usually much thicker. It is composed of dense irregular connective tissue and receives its name from the dense concentration of collagenous, elastic, and reticular fibers that weave throughout it. Also located within the reticular region are the roots of the hair, sebaceous glands, and blood vessels. However, SKH1 hairless mice lose most of their hair shafts after the first hair cycle at three weeks after birth and majority of hair follicles form cysts.

Group A: wounds covered with Linitul®

A well-formed fibrin mesh was observed at 48 hours (photo 1), in which was evident the presence of an acute inflammatory infiltrate composed mainly of polymorphonuclear (PMN) neutrophils and macrophages (photo 12). At week 1 after wounding, the fibrin mesh started to organize, and a well-formed granulation tissue could then be appreciated (photo 2). In this granulation tissue, both edema and an acute inflammatory infiltrate were still present (photo 13), together with a well-established vascular tissue that was particularly abundant in the area next to the muscular layer. At this point, no signs of epithelialization were observed.

In contrast, at week 2, the epithelialization was completed (photo 3), although it was still immature (given the fact of the presence of intercellular edema of the *stratum spinosum* of the epidermal sheet in several areas). There was still some edema, but the most important finding was the organization of the granulation tissue (photo 14), mainly composed of fibroblasts, inflammatory component (PMN, lymphocytes and macrophages), and numerous blood vessels distributed throughout the thickness of the dermis.

At week 3 after wounding, the epithelial layer was completed, with higher thickness than that at week 2 (photo 4). At this point, the organization of the dermal layer was completed, being composed mainly of fibroblasts, well organized connective tissue, and scarce blood vessels (photo 15). Inflammatory cells (PMN and macrophages mostly), forming clusters as microabscesses, remained in certain areas of the dermis.

Finally, one month after injury, the process of scar formation was completed (photo 5), with an hyperplastic epidermal layer and a dermal layer mainly composed of fibroblasts interspersed within a well-organized connective tissue, with scarce blood vessels in it (photo 16). Thus, a mature scar was indeed configured.

Compared with normal skin (photos 11 and 22), which is composed mainly of a dense irregular connective tissue with its appendages (hair follicles and sebaceous glands), the pattern of organization of the dermis in the group of animals treated with Linitul® was completely different, i.e., with a dense regular connective tissue pattern (causing loss of the elastic and mobile properties), typically observed in scars, and loss of all skin appendages.

Group B: wounds covered with Silk Fibroin (SF) Scaffolds

At 48 hours, the silk fibroin scaffold could be appreciated onto the surface of the wound site (photo 6), and also the presence of an acute inflammatory infiltrate (photo 17), mainly composed of PMNs and macrophages. At this point, the fibrin layer was smaller than that observed in the Linitul®-treated animals.

The main differences started appearing at 1 week after wounding. At this time, the epithelial layer could not be observed (photo 7), and an abundant inflammatory infiltrate (mainly composed of PMNs neutrophils and macrophages) was detected, either in SF scaffolds and the dermal layer (photo 18), suggesting an immunogenic inflammatory reaction against the SF scaffold, a feature not described in the literature [112]. Immature granulation tissue was also observed, and ingrowing vessels, infiltrating either dermis and scaffold could be observed, features consistent with the biocompatibility and biodegradability properties of the SF as a biomaterial. Below

the scaffold, there was a larger cellular component compared with Linitul®-treated animals at this time, mainly composed of fibroblasts, acute inflammatory cells, and blood vessels.

At week 2, **t**he SF scaffold had been partially reabsorbed, but still covered the wound surface (photo 8). The epithelial layer was still not completed, and the granulation tissue of the dermal layer, which resembles that found in the group treated with Linitul® at week 1 (photo 19), was composed of an abundant cellular infiltrate (fibroblasts, PMNs, lymphocytes, and macrophages) and blood vessels, with apparently less amount of connective tissue.

At week 3, the epithelialization was completed, with a hyperplastic epithelial layer (photo 9). The dermal layer, which resembles that found in the group treated with Linitul® at week 2, had fewer collagen formation, with the presence of abundant dermal blood vessels (photo 20).

Finally, at week 4 after wounding, a hyperplastic epithelial layer was completed (photo 10). The dermis had similar histologic features that those observed at week 3 in the group of mice treated with Linitul® and was mainly composed of well-formed dense connective tissue with a regular configuration (photo 21). Blood vessels interspersed with collagen fibers and some resorption areas (microabscesses) could also be observed. At this point, the thickness of the dermal layer was apparently lower than that observed in mice treated with Linitul®.

Group C: wounds with hWj-MSCs injected at the edge

At 48 hours, a fibrin mesh covering the wound surface was observed (photo 23), in similarity to that found in the Linitul®-treated group, but in this instance a dense cellular infiltrate could be appreciated (photo 39). This infiltrate was composed of acute inflammatory cells (PMN neutrophils and macrophages), and spindle-shaped cells.

At week 1 after wounding, although the epithelial layer was still not completed (photo 24), the migrating front was quite advanced, with keratin pearls located below the epithelial layer. The dermal layer was composed of a well-developed and highly-cellularized granulation tissue (photo 40), with blood vessels interspersed with spindle-shaped cells and an acute inflammatory infiltrate (mainly consisting of PMNs and macrophages).

At week 2, the epithelial layer was completed, although it was still immature (photo 25). The dermal layer was structurally similar to that observed in SF-treated mice at week 2, in which a dense connective tissue, high blood vessels density, and mixed inflammatory infiltrate (composed of lymphocytes, PMNs, and macrophages)

were present. These features, which were similar to those observed in the group B at this stage, suggested that the addition of both SF scaffold or MSCs injected at the edge of the wounds induced a delay in the regular wound healing process (observed in the Linitul®-treated group).

At week 3, the epithelial layer was completed, although it was still immature and hyperplastic (photos 26 and 42). The dermal layer was composed of a dense regular connective tissue, with fibroblasts interspersed with collagen fibers (photo 42), and blood vessels.

At week 4 after wounding, the wound healing was completed, with a well conformed and hyperplastic epithelial layer, with a dermal configuration similar to those described in the Linitul®-treated group at this stage. As similar to groups A and B, no skin adnexal structures were evidenced.

Group D: wounds covered with silk fibroin patches cellularized with hWj-MSCs

At 48 hours, the SF scaffold could be easily recognized (photo 28), but in contrast to group B, it was much higher cellularized (presumably due to the MSCs seeded onto the scaffold before transplantation). As similar to other groups described before, the presence of an acute inflammatory infiltrate was also observed (photo 44).

At week 1, as similar to group B, the epithelialization was not completed. Besides, the SF scaffold was infiltrated by an acute inflammatory infiltrate (photo 29), and there was a discrete edema in the transition between the SF scaffold and the dermal granulation tissue. The dermal layer was structurally similar to those observed in group C at this stage, although higher cellularity of the granulation tissue was observed. This granulation tissue was mostly composed of a large number of blood vessels, spindle-shaped cells, and a mixed inflammatory infiltrate consisting of PMNs, macrophages and lymphocytes (photo 45).

Unlike what happens in group C, the epithelial layer was not completed at week 2 post-surgery, in where the SF scaffold was still being reabsorbed (photo 30). At the dermal layer, the granulation tissue was still being organized, with a small amount of dense connective tissue (photo 46), and a dense cellular infiltrate composed of fibroblasts, PMNs, lymphocytes, and macrophages, with a dense network of blood vessels.

Similar to group C, at week 3 after wounding, the epidermal layer was completed, but it was still immature (intercellular edema at the *stratum spinosum*) (photos 31 and 47). The dermis was composed of dense regular connective tissue, which was highly infiltrated by fibroblasts, blood vessels, and mixed inflammatory infiltrate

(photo 47).

Finally, at 1 month, the epidermal layer was completed, and surprisingly, was not hyperplastic. The dermal layer, which was less thick than that in groups A, B, and C, was similar in composition, i.e., dense regular connective tissue with blood vessels and fibroblasts interspersed with collagen fibers. As analogous to the previous groups, not adnexal structures were observed at any stage.

Group E: wounds with silk fibroin patches cellularized with hWj-MSCs over the wound bed combined with hWj-MSCs injected at the edge

The histopathologic analysis of this group at 48 hours (photo 33) revealed a similar spectrum to that described for group C. A higher cellular infiltrate in comparison to groups B and D was observed (photo 49) at this time. As seen in these groups, the epithelialization process had not been completed, and the SF scaffold was being reabsorbed (photo 34). The dermal layer was analogous to that described in group D but, in contrast, the number of spindle-shaped cells was apparently higher (photo 50).

At week 2, the epithelialization process was still not completed due to the reabsorption process of the SF scaffold (photo 35). The granulation tissue of the dermal layer was still being organized and consisted of small amount of collagen fibers, and a dense cellular infiltrate interspersed with numerous blood vessels (photo 51).

At week 3, the epithelialization process was completed and being this slightly hyperplastic (photo 36). The dermal layer was well organized and consisted of a dense regular connective tissue, with fibroblasts and inflammatory cells in it (mainly lymphocytes, PMNs, and macrophages, occasionally forming microabscesses). In contrast to the other groups, several adnexal structures (fully functional hair follicles, and sebaceous glands), could be evidenced in some animals at this time (photo 52). In some cases, a mild inflammatory infiltrate could be observed surrounding these annexes.

At week 4, a completed and hyperplastic epithelial layer could be evidenced (photo 37). The dermis was well developed, with some areas of irregular dense connective tissue, fibroblasts, and blood vessels (photo 53). Surprisingly, the adnexal structures observed at week 3 were disappeared, although atrophic hair follicles could still be observed.

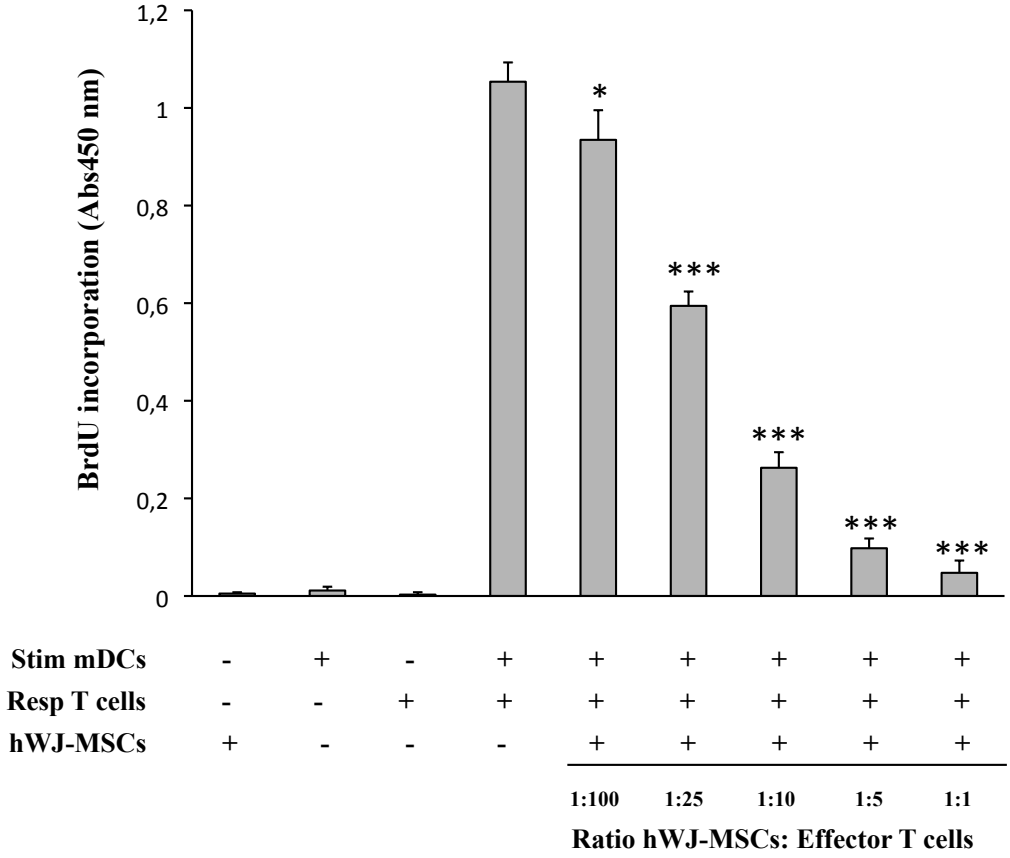

Figure 4.7: **Wharton's jelly mesenchymal stem cells suppress T cell proliferation after stimulation with allogeneic mDCs.** Responder T cell proliferation was significantly inhibited in a dose-dependent manner when Wj-MSCs were added to mixed lymphocyte cultures (MLCs) at different ratios. Results are shown as mean ± SD of three independent experiments performed in triplicate. Proliferation of T cells was significantly inhibited, * = $p<0.05$, ** = $p<0.01$, *** = $p<0.001$, according to one-way ANOVA. Abbreviations: Stim mDCs: stimulator mature myeloid dendritic cells, Resp T cells: responder T cells, hWj-MSCs: human Wharton's jelly mesenchymal stem cells.

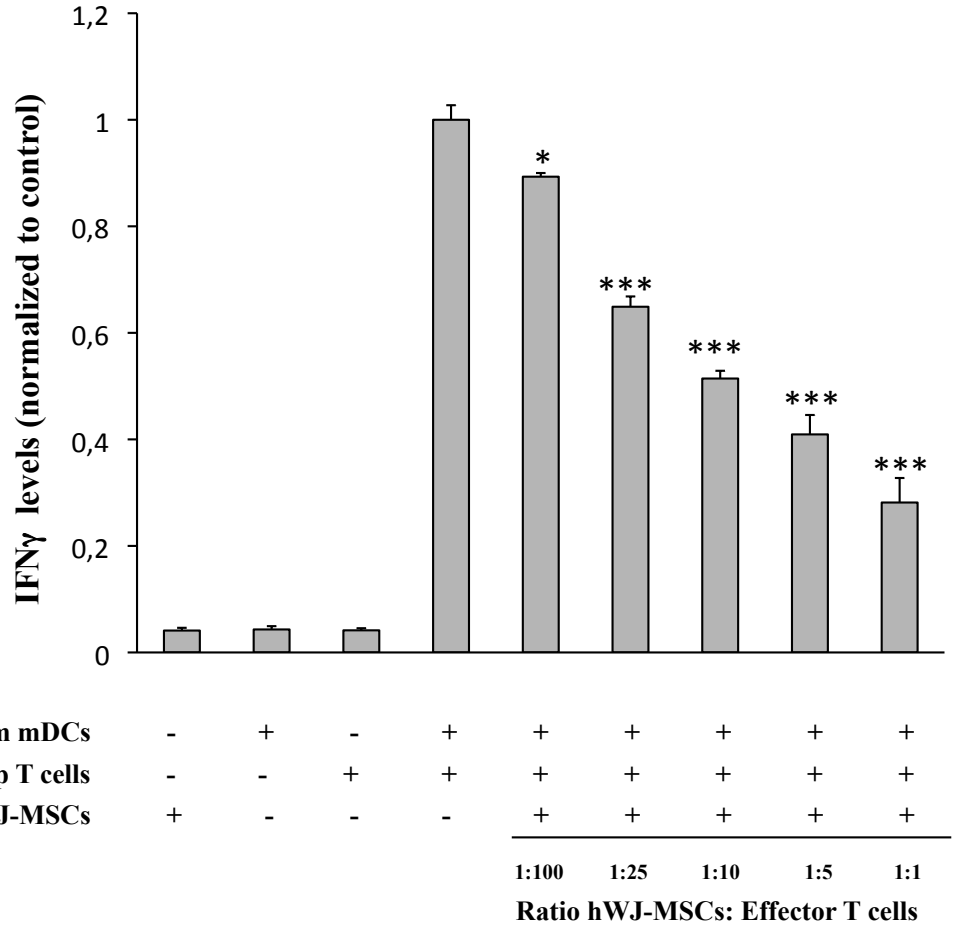

Figure 4.8: **Inhibitory effect of Wharton's jelly mesenchymal stem cells on the production of IFN-γ cytokine secreted by mDCs-activated T lymphocytes.** Analysis of the production of IFN-γ in supernatants from mixed lymphocyte cultures in the absence and the presence of hWj-MSCs added at several ratios (i.e., hWJ-MSCs: effector T cells 1:100, 1:25, 1:10, 1:5, and 1:1). IFN-γ levels were normalized to concentrations of IFN-γ detected in co-cultures without mesenchymal stem cells (mDCs + T cells). Results are shown as mean ± SD of three independent experiments performed in triplicate. Level of IFN-γ was significantly decreased, * = $p<0.05$, ** = $p<0.01$, *** = $p<0.001$, according to one-way ANOVA. Abbreviations: IFN-γ: interferon gamma, Stim mDCs: stimulator mature myeloid dendritic cells, Resp T cells: responders T cells, hWj-MSCs: human Wharton's jelly mesenchymal stem cells.

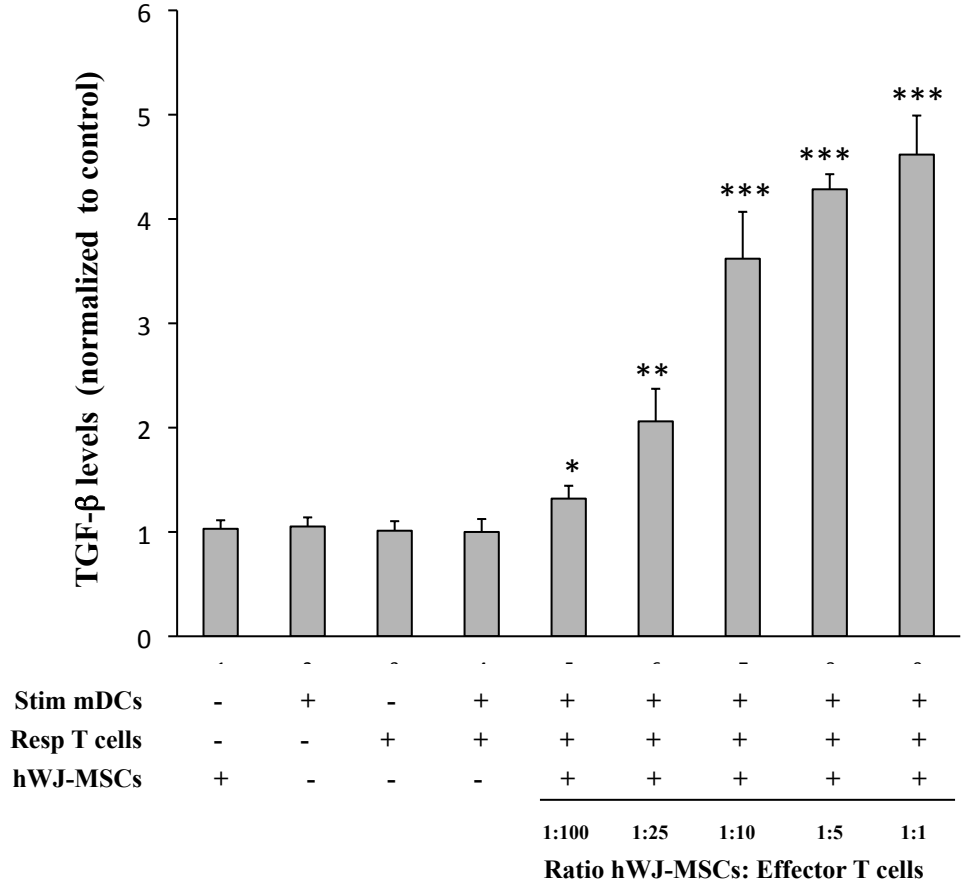

Figure 4.9: **Immunosuppressive effect of Wharton's jelly mesenchymal stem cells on T-lymphocyte proliferation in response to allogeneic mDCs stimulation is mediated by TGF-β.** TGF-β levels assayed by enzyme-linked immunoabsorbent assay (ELISA) in the supernatants of MLC in the absence or presence of Wj-MSCs at differents ratios (hWj-MSCs: effector T cells 1:100, 1:25, 1:10, 1:5, and 1:1) were measured. TGF-β levels were normalized to concentrations of TGF-β in co-cultures without mesenchymal stem cells (mDCs + T cells). Results are shown as mean ± SD of three independent experiments performed in triplicate. Level of TGF-β was significantly augmented, * = $p<0.05$, ** = $p<0.01$, *** = $p<0.001$, according to one-way ANOVA. Abbreviations: TGF-β: transforming growth factor beta, Stim mDCs: stimulator mature myeloid dendritic cells, Resp T cells: responder T cells, hWj-MSCs: human Wharton's jelly mesenchymal stem cells.

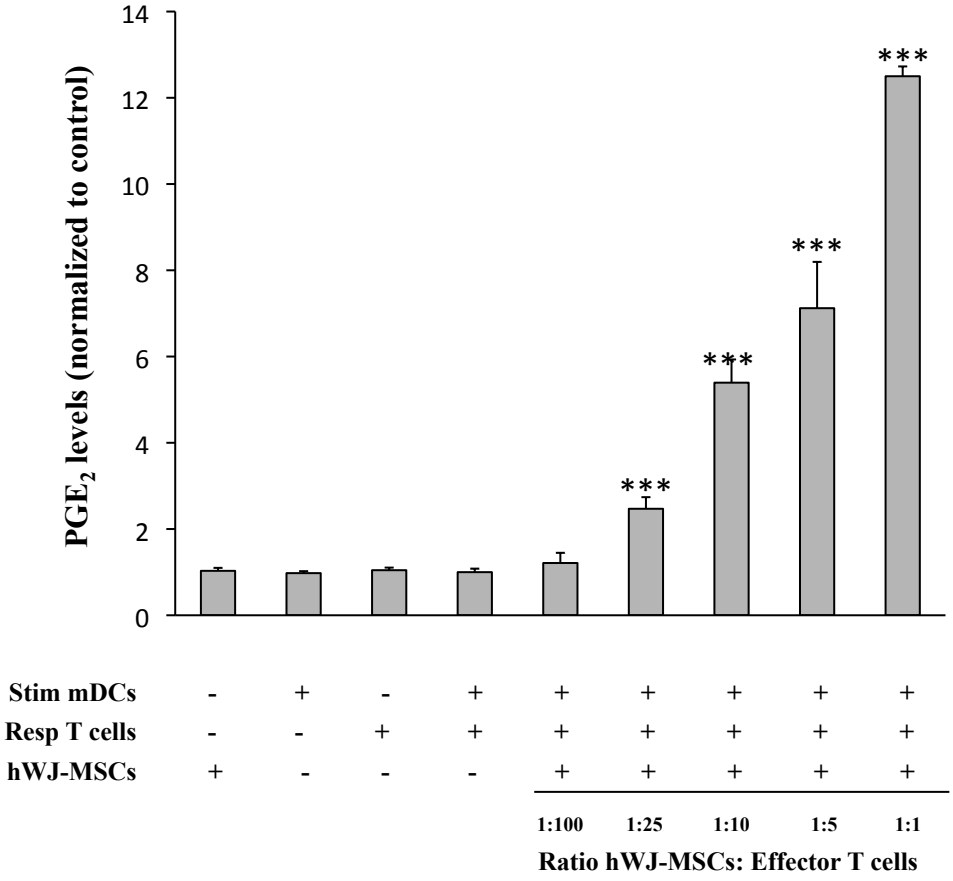

Figure 4.10: **PGE_2 is an *in vitro* mediator of the Wharton's jelly mesenchymal stem cells immunosuppressive effects on T lymphocyte proliferation in response to allogeneic mDCs stimulation.** PGE_2 levels assayed by enzyme-linked immunoabsorbent assay (ELISA) in the supernatants of MLC in the absence or presence of Wj-MSCs at differents ratios (hWj-MSCs: effector T cells 1:100, 1:25, 1:10, 1:5, and 1:1) were measured. PGE_2 levels were normalized to concentrations of PGE_2 in co-cultures without mesenchymal stem cells (mDCs + T cells). Results are shown as mean ± SD of three independent experiments performed in triplicate. Level of PGE_2 was significantly augmented, ***= $p<0.001$, according to one-way ANOVA. Abbreviations: PGE_2: prostaglandin E_2, Stim mDCs: stimulator mature myeloid dendritic cells, Resp T cells: responder T cells, hWj-MSCs: human Wharton's jelly mesenchymal stem cells.

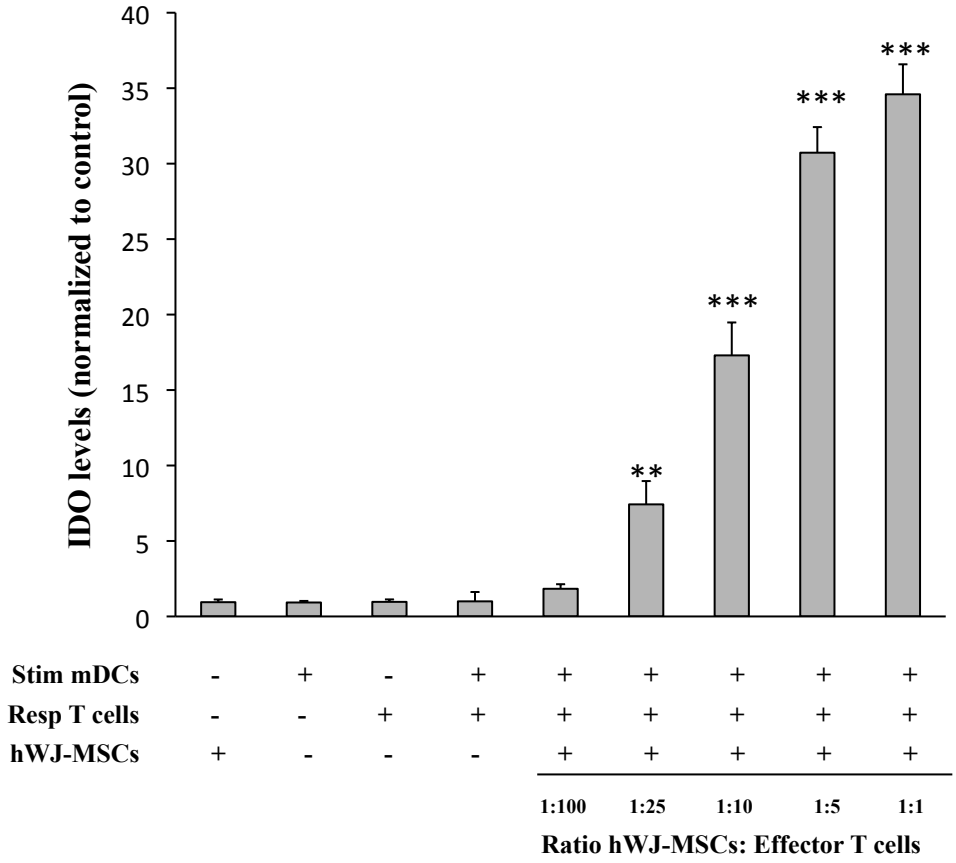

Figure 4.11: **Inhibition of allogeneic T cell proliferation *in vitro* mediated by indoleamine 2,3-dioxygenase (IDO)**. IDO levels assayed by enzyme-linked immunoabsorbent assay (ELISA) in the supernatants of MLC in the absence or presence of Wj-MSCs at differents ratios (hWj-MSCs: effector T cells 1:100, 1:25, 1:10, 1:5, and 1:1) were measured. IDO levels were normalized to concentrations of IDO in co-cultures without mesenchymal stem cells (mDCs + T cells). Results are shown as mean ± SD of three independent experiments performed in triplicate. Level of IDO was significantly increased, **= $p<0.01$, ***= $p<0.001$, according to one-way ANOVA. Abbreviations: IDO: indoleamine 2,3-dioxygenase, Stim mDCs: stimulator mature myeloid dendritic cells, Resp T cells: responder T cells, hWj-MSCs: human Wharton's jelly mesenchymal stem cells.

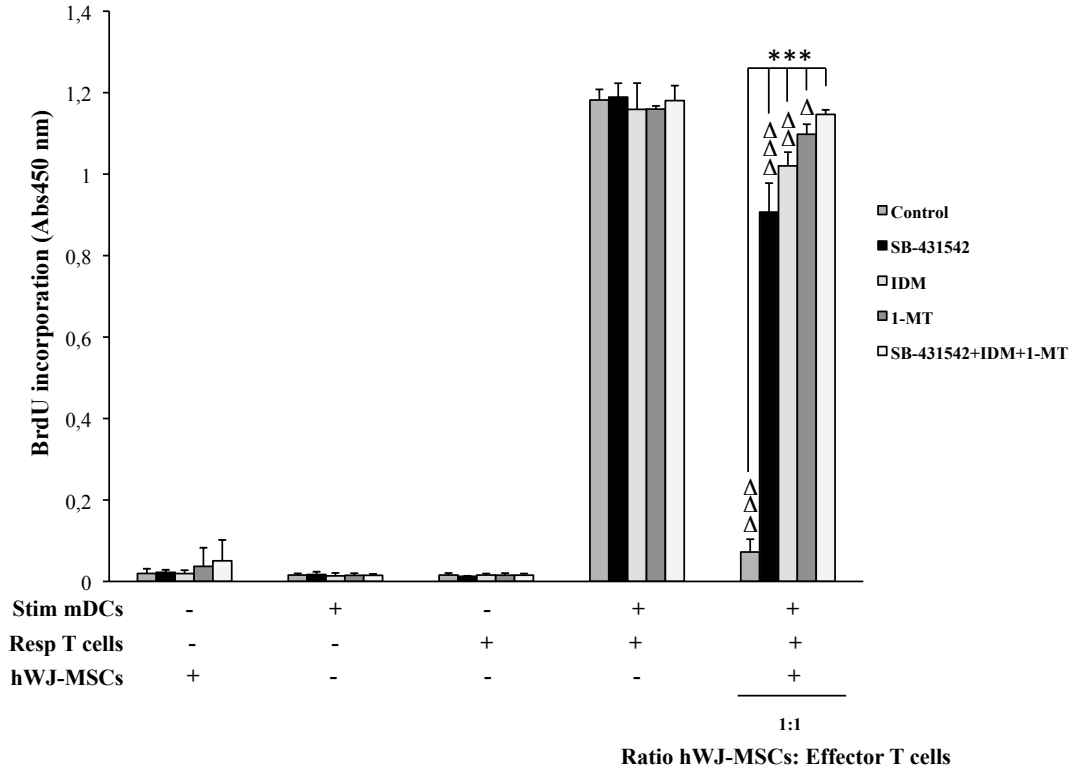

Figure 4.12: **PGE2, TGF-β, and IDO play a major role mediating the immunosuppressive effects of Wj-MSCs on T lymphocyte proliferation after allogeneic mDCs stimulation** Responder T cell proliferation was significantly inhibited when hWj-MSCs at a ratio 1:1 were added to the MLCs in the absence (control) or presence of SB-431542, IDM or 1-MT (Δ= $p<0.05$, $\Delta\Delta$= $p<0.01$, $\Delta\Delta\Delta$= $p<0.001$), according to one-way ANOVA. Also, the proliferation rate of mDCs-stimulated T cells was significantly recovered (***= $p<0.001$). Results are shown as mean ± SD of three independent experiments performed in triplicate. Abbreviations: Stim mDCs: stimulator mature myeloid dendritic cells, Resp T cells: responder T cells, hWj-MSCs: human Wharton's jelly mesenchymal stem cells, SB-431542: TGF-β inhibitor, IDM: indomethacin (PGE_2 inhibitor), 1-MT: 1-methyl-tryptophan (IDO inhibitor).

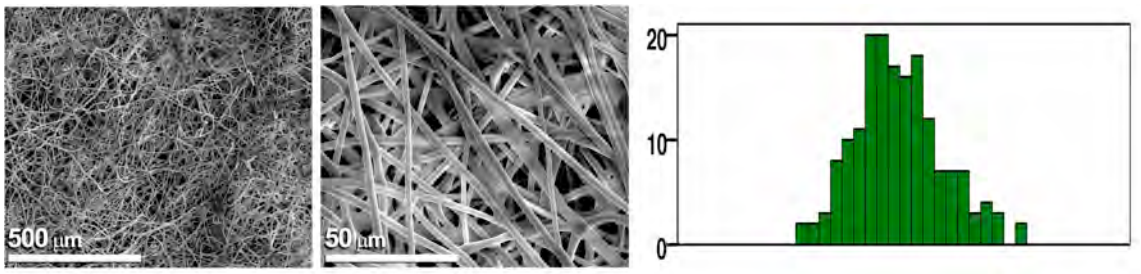

Figure 4.13: **SEM micrographs and histogram of fiber diameters of electrospun SF mats produced with 19% regenerated silk fibroin solutions** [173].

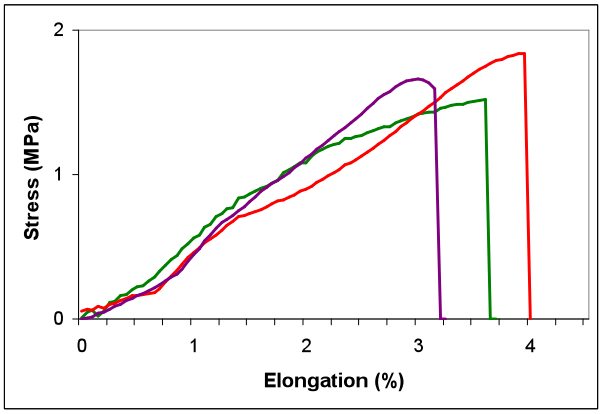

Figure 4.14: **Examples of stress-elongation curves of SF electrospun mats produced from 19% regenerated silk fibroin solutions** [173].

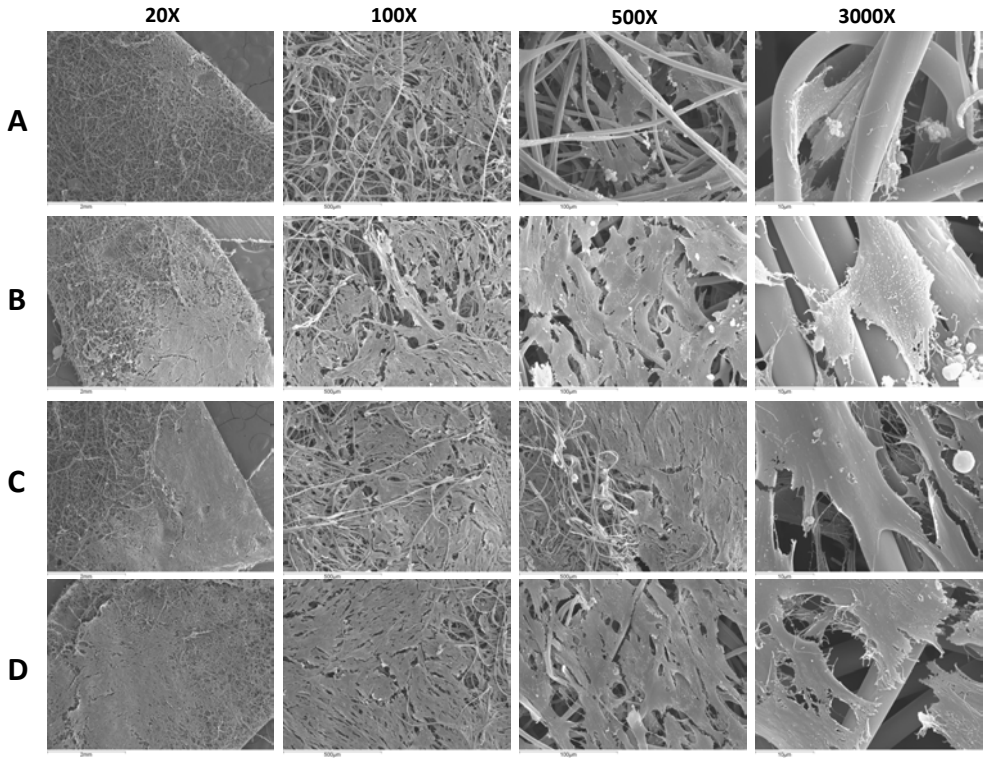

Figure 4.15: **Scanning electron microscopy micrographs of hWj-MSCs growing on electrospun silk fibroin scaffold at different cell densities.** Silk fibroin patches were seeded at a density of $3x10^4$cells/cm^2 (A) , $4x10^4$cells/cm^2 (B), $5x10^4$cells/cm^2 (C) , and $6x10^4$cells/cm^2 (D), and culture for four days. Images at a magnification of 20X, 100X, 500X, and 1000X are shown.

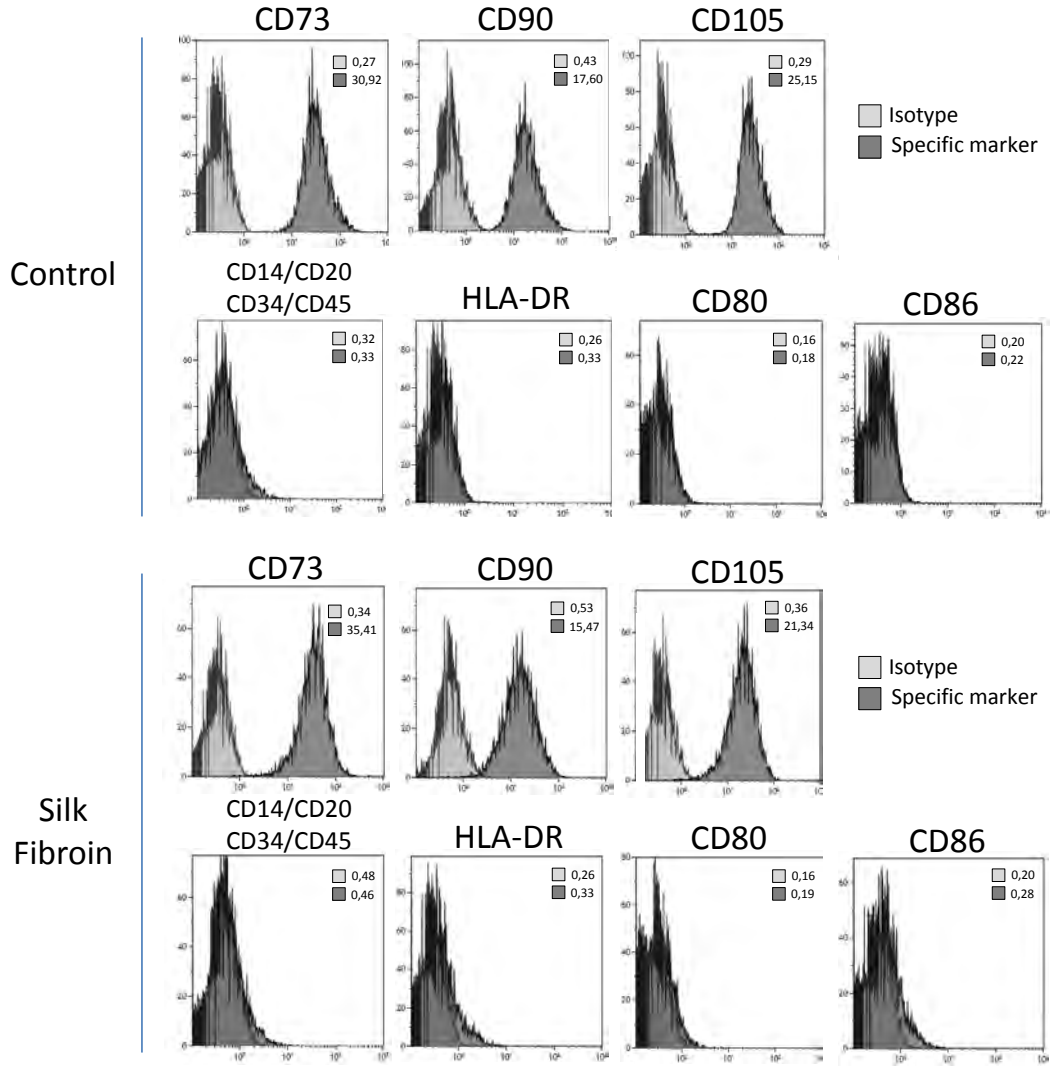

Figure 4.16: **Immunophenotype analysis of hWj-MSCs by flow cytometry.** Wj-MSCs were seeded at a density of $5x10^4$cells/cm^2 on plastic culture plates (control) (upper panels) or silk fibroin patches (bottom panels) for four days. After, cells were detached, washed and labeled with fluorescence-conjugated specific antibodies for the indicated markers or their control isotypes. Insert numbers represent mean fluorescence intensity values from viable cells. Histograms show representative flow cytometry results obtained from three independent experiments.

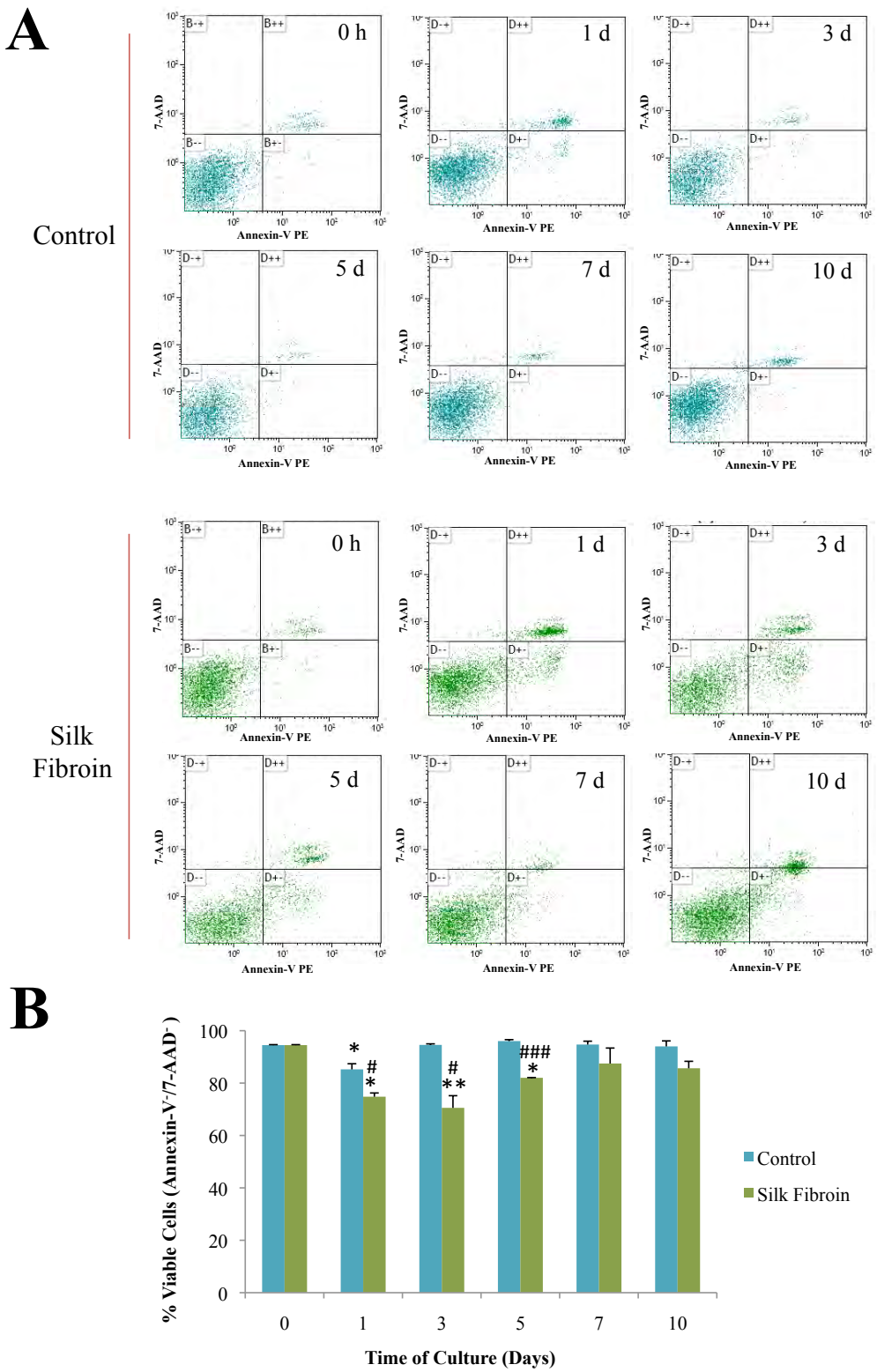

Figure 4.17: **Viability of hWJ-MSCs cultured on electrospun silk fibroin scaffolds for different times.** (A) Percentages of Annexin-V-/7-AAD- cells were analyzed by flow cytometry. (B) Percentage of viable cells significantly decreased compared to values obtained at time 0 (*= $p<0.05$, **= $p<0.01$), according to one-way ANOVA. Also, percentages of viable cells significantly decreased after culture on silk fibroin patches compared to the control group at each time point (#: $p<0.05$, ###= $p<0.001$). Results are shown as mean ± SD of three independent experiments performed in triplicate.

	Control		Wj-MSCs-Edge		Wj-MSCs-SF		Wj-MSCs-Edge+SF	
	Mean	**SD**	**Mean**	**SD**	**Mean**	**SD**	**Mean**	**SD**
Weight$_0$(1)	27,59	1,85	27,35	2,84	28,47	1,36	27,81	2,27
Weight$_f$ (1)	27,79	2,48	27,50	1,67	27,34	1,64	27,11	1,77
WBC (2)	5,75	1,52	6,16	2,02	5,52	1,07	**8,32**	**2,14**
NEU (2)	1,49	0,88	1,89	1,38	1,63	0,70	**3,05**	**1,52**
LYM (2)	4,03	1,07	4,01	1,16	3,61	0,88	4,80	1,39
MONO (2)	0,09	0,08	0,12	0,16	0,12	0,06	**0,26**	**0,21**
EOS (2)	0,01	0,01	0,01	0,01	0,00	0,01	0,01	0,01
BASO (2)	0,14	0,09	0,18	0,11	0,17	0,07	0,20	0,13
RBC (3)	8,77	0,69	9,02	0,52	8,79	0,46	8,76	0,43
HGB (4)	13,56	1,14	14,28	2,76	13,87	0,83	13,31	0,88
HCT (5)	43,98	3,49	45,39	2,35	44,79	2,83	43,85	2,08
MCV (6)	50,15	0,73	50,37	0,54	**50,94**	**0,88**	50,06	0,53
MCH (7)	15,50	1,20	15,82	2,81	15,77	0,36	15,25	0,95
MCHC (4)	34,80	1,42	35,41	1,79	35,47	1,02	**33,88**	**0,60**
PLT (2)	38,43	1,49	39,08	1,88	39,19	1,06	**37,29**	**0,54**
MPV (6)	42,06	1,56	42,75	1,97	42,90	1,11	40,69	0,49
GLUCOSE (8)	285,30	72,33	240,10	34,08	218,30	34,34	**233,20**	**33,58**
UREA (8)	37,35	7,96	40,00	5,73	39,50	6,90	39,92	6,60
T. PROTEIN (4)	4,08	0,73	4,36	0,24	4,41	0,18	4,40	0,22
ALBUMIN (4)	2,69	0,55	2,82	0,27	2,99	0,22	2,80	0,34
BILIRRUBIN (8)	0,06	0,02	0,07	0,02	0,07	0,02	0,06	0,02
SODIUM (9)	140,50	22,58	147,20	4,76	146,10	3,01	143,40	2,18
POTASSIUM (9)	21,59	5,99	22,58	4,08	22,98	3,67	23,22	5,28
CHLORINE (9)	100,70	16,91	103,20	4,13	103,60	2,50	**101,70**	**2,10**
TRIG (8)	83,82	38,38	107,00	55,79	80,43	19,31	84,77	39,46
CHOL (8)	77,87	16,50	87,67	7,52	82,93	10,00	85,69	10,09
GOT (10)	65,24	18,72	74,36	26,51	68,71	14,12	70,69	24,67
GPT (10)	30,89	13,72	31,60	11,46	33,07	6,91	31,69	14,75

Table 4.1: **Complete blood count and serum biochemistry analysis** of blood samples. Experimental groups: **Controls** (wounds covered with Linitul®or Silk Fibroin patches), **Wj-MSCs-Edge** (wounds with hWj-MSCs injected at the edge), **Wj-MSCs-SF** (wounds covered with silk fibroin patches cellularized with hWj-MSCs), and **Wj-MSCs-Edge+SF** (wounds with silk fibroin patches cellularized with hWj-MSCs over the wound bed and hWj-MSCs injected at the edge). **Abbreviations: Weight$_0$**(initial weight, day of surgery), **Weight$_f$**(final weight, day of sacrifice), **WBC**(white blood cells), **NEU**(neutrophils), **LYM**(lymphocytes), **MONO**(monocytes), **EOS**(eosinophils), **BASO**(basophils), **RBC**(red blood cell count), **HGB**(hemoglobin), **HCT**(hematocrit), **MCV**(mean corpuscular volume), **MCH**(mean corpuscular hemoglobin), **MCHC**(mean corpuscular hemoglobin concentration), **PLT**(platelets), **MPV**(mean platelet volume), **TRIG** (triglycerides), **CHOL** (cholesterol), **GOT**(glutamic oxaloacetic transaminase), **GPT**(glutamate-pyruvate transaminase). Units: (1) g; (2) 10e3/uL; (3) 10e6/uL; (4) g/dL; (5) %; (6) fL; (7) pg; (8) mg/dL; (9) mEq/dL; (10) U/L.

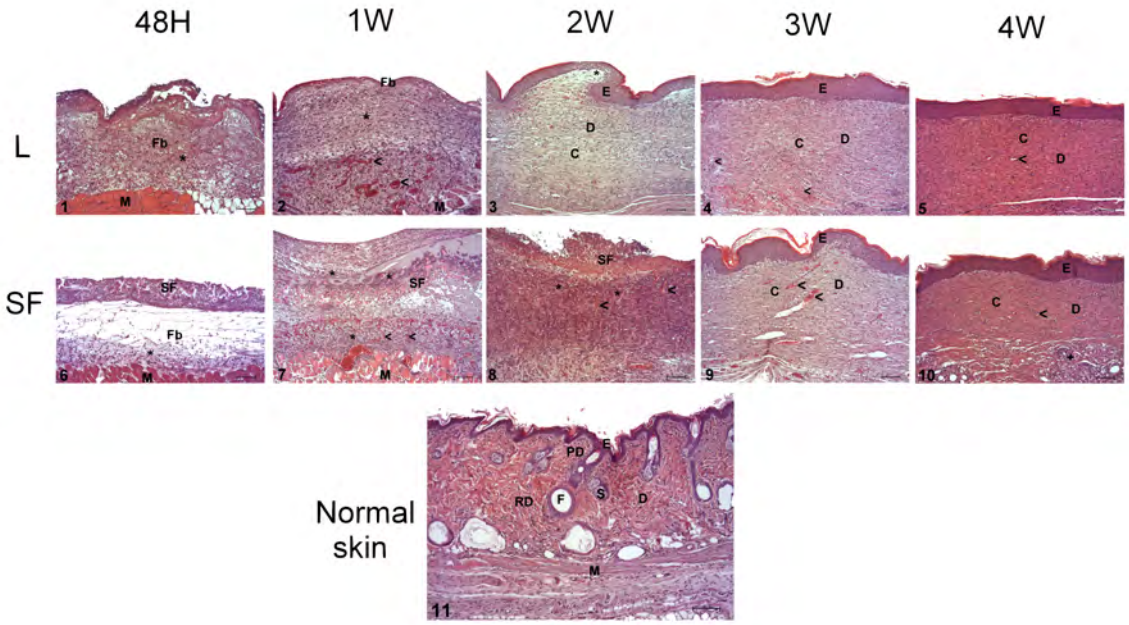

Figure 4.18: **Hematoxylin and Eosin (H&E) Stains**. Control Groups: **L** (wounds covered with Linitul®) and **SF** (wounds covered with Silk Fibroin scaffolds). **Fb**: fibrin, *: inflammatory infiltrate and edema, > : blood vessels, **E**: epidermis, **M**: muscular layer, **D**: dermis, **C**: collagen, **SF**: silk fibroin scaffold, **PD**: papillary dermis, **RD**: reticular dermis, **Sb**: sebaceous gland, **F**: hair follicle. Scale bar: 100μm.

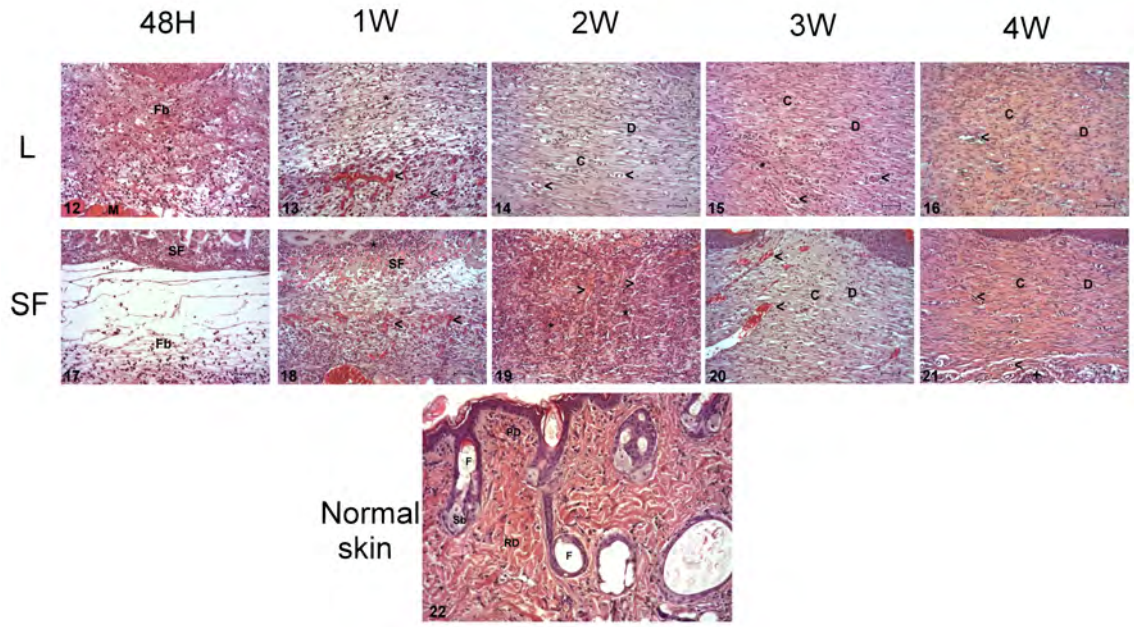

Figure 4.19: **Hematoxylin and Eosin (H&E) Stains**. Control Groups: **L** (wounds covered with Linitul®) and **SF** (wounds covered with Silk Fibroin scaffolds). **Fb**: fibrin, *: inflammatory infiltrate and edema, > : blood vessels, **E**: epidermis, **M**: muscular layer, **D**: dermis, **C**: collagen, **SF**: silk fibroin scaffold, **PD**: papillary dermis, **RD**: reticular dermis, **Sb**: sebaceous gland, **F**: hair follicle. Scale bar: 50µm.

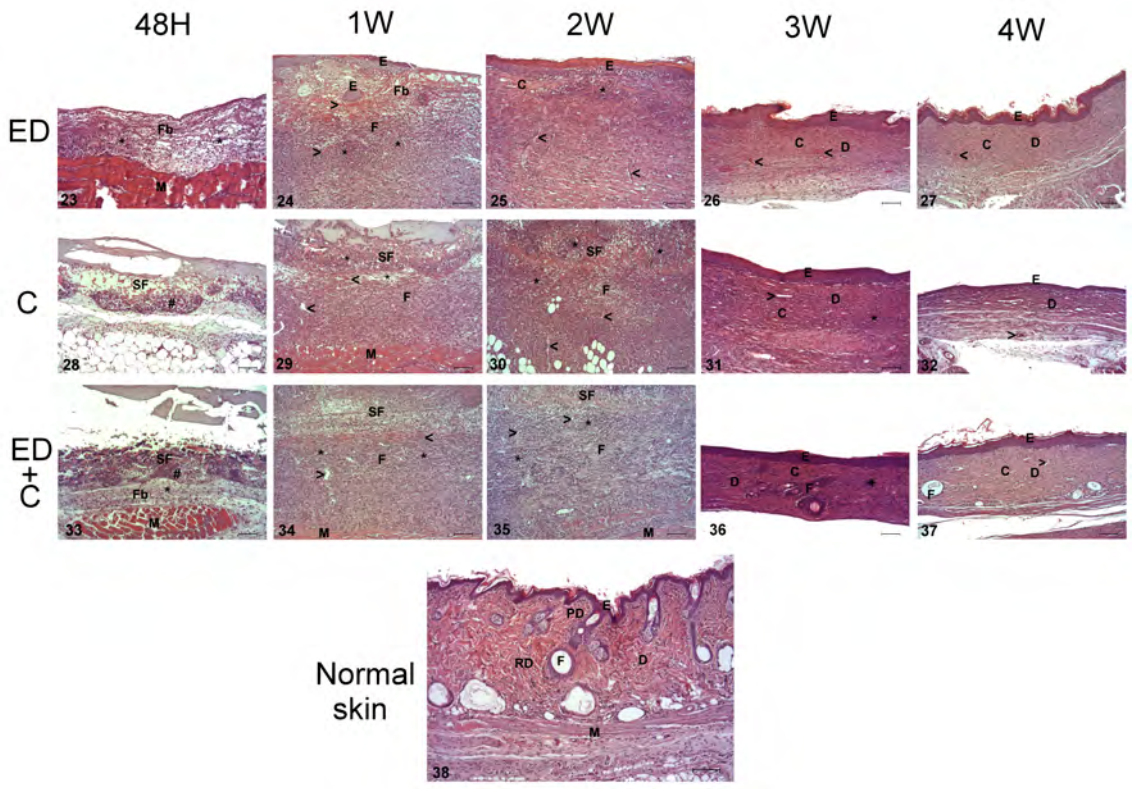

Figure 4.20: **Hematoxylin and Eosin (H&E) Stains.** Treated Groups: **ED** (wounds with hWj-MSCs injected at the edge), **C** (wounds covered with silk fibroin patches cellularized with hWj-MSCs), and **ED+C** (wounds with silk fibroin patches cellularized with hWj-MSCs over the wound bed and hWj-MSCs injected at the edge). **Fb**: fibrin, ***** : inflammatory infiltrate and edema, $>$: blood vessels, **E**: epidermis, **M**: muscular layer, **D**: dermis, **C**: collagen, **SF**: silk fibroin scaffold, **PD**: papillary dermis, **RD**: reticular dermis, **Sb**: sebaceous gland, **F**: hair follicle. Scale bar: 100μm.

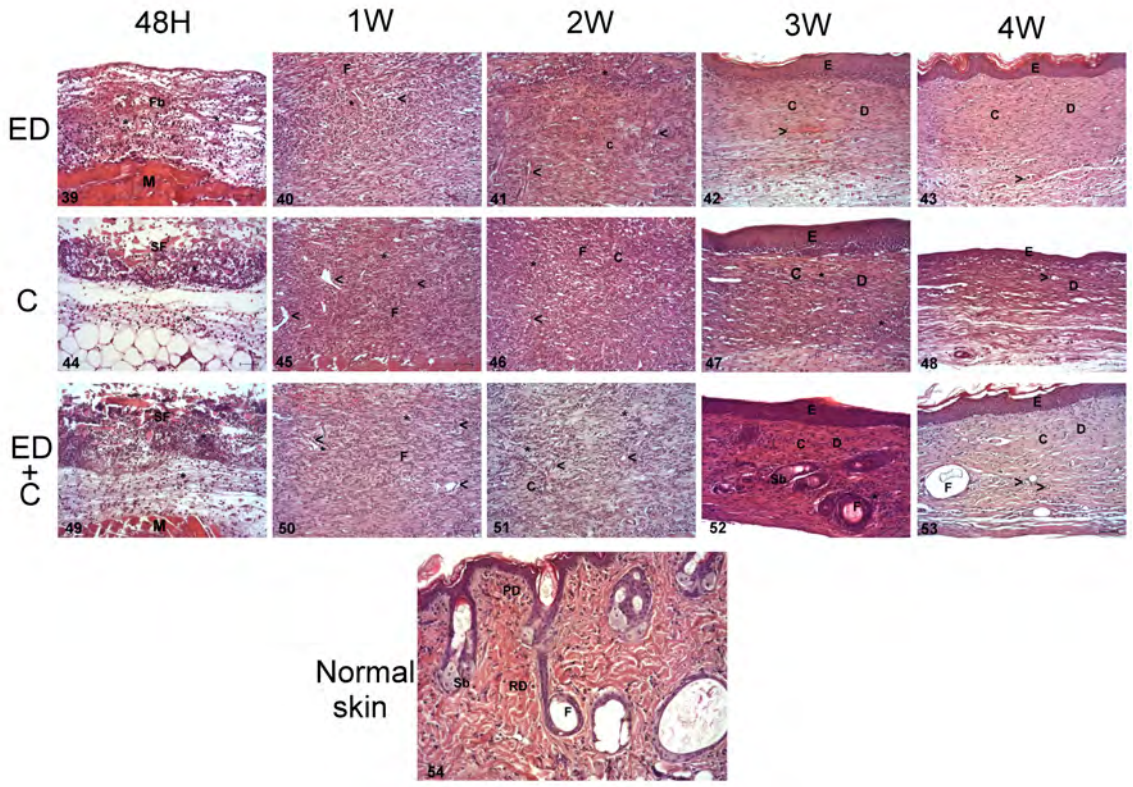

Figure 4.21: **Hematoxylin and Eosin (H&E) Stains.** Treated Groups: **ED** (wounds with hWj-MSCs injected at the edge), **C** (wounds covered with silk fibroin patches cellularized with hWj-MSCs), and **ED+C** (wounds with silk fibroin patches cellularized with hWj-MSCs over the wound bed and hWj-MSCs injected at the edge). **Fb**: fibrin, ***** : inflammatory infiltrate and edema, $>$: blood vessels, **E**: epidermis, **M**: muscular layer, **D**: dermis, **C**: collagen, **SF**: silk fibroin scaffold, **PD**: papillary dermis, **RD**: reticular dermis, **Sb**: sebaceous gland, **F**: hair follicle. Scale bar: 50μm.

4.5.2 Masson-Goldner trichrome Stain (Figures 4.22 to 4.25)

Normal Skin (photos 65, 76, 92, and 108)

Reticular dermis in normal skin consists of a dense and not shaped connective tissue. Degenerated hair follicles are present along the dermal layer in the skin of SKH1 mice. Note the organization of collagen fibers at the dermis (photo 108), with a dense irregular connective tissue configuration.

Group A: wounds covered with Linitul®

A dense fibrin mesh with abundant inflammatory infiltrate comprised the scab observed at 48 hours (photos 55 and 66). One week after wounding, some edema and fibroblast proliferation, with discrete collagen synthesis (photos 56 and 67), associated with profuse neovascularization were present in the area next to the muscle sheet.

At week 2, there were still some areas of reabsorption and inflammatory infiltrate in the dermal layer (photo 57). Collagen synthesis was much more prominent, and fibers were disposed following the same direction. Thus, the dermis consisted of an immature, dense and regular connective tissue (photo 68).

At week 3, the dense connective tissue forming the dermis was now well structured (photo 58), and newly formed blood vessel were prompt to bleed because of the weakness of the vascular walls. There were some remaining areas of edema and inflammatory infiltrate (photo 69).

Hyperplasia of the epithelial sheet with the consequent increase of thickness was evident one month after wounding (photo 59). At this time point, the dermis was formed by a well-structured, dense, and regular connective tissue, as seen in a standard scar with not skin appendages in there (photo 70).

Group B: wounds covered with Silk Fibroin (SF) Scaffolds

At 48 hours, there was no evidence of collagen synthesis into the dermal layer yet (photos 60 and 71). At week 1, the amount of collagen in the connective tissue present in the dermal sheet was less compared to the group treated with Linitul® (photos 61 and 72). Newly formed blood vessels grew from the muscle sheet upward.

At week 2, there were areas of SF scaffold reabsorption with lots of cells around it (photo 62). It was noticeable a large number of blood vessels, running from the bottom upward, that penetrated the SF scaffold. There were fewer collagen fibers forming the granulation tissue compared to the group treated with Linitul® (photo 73). On the whole, it was an unresolved granulation tissue.

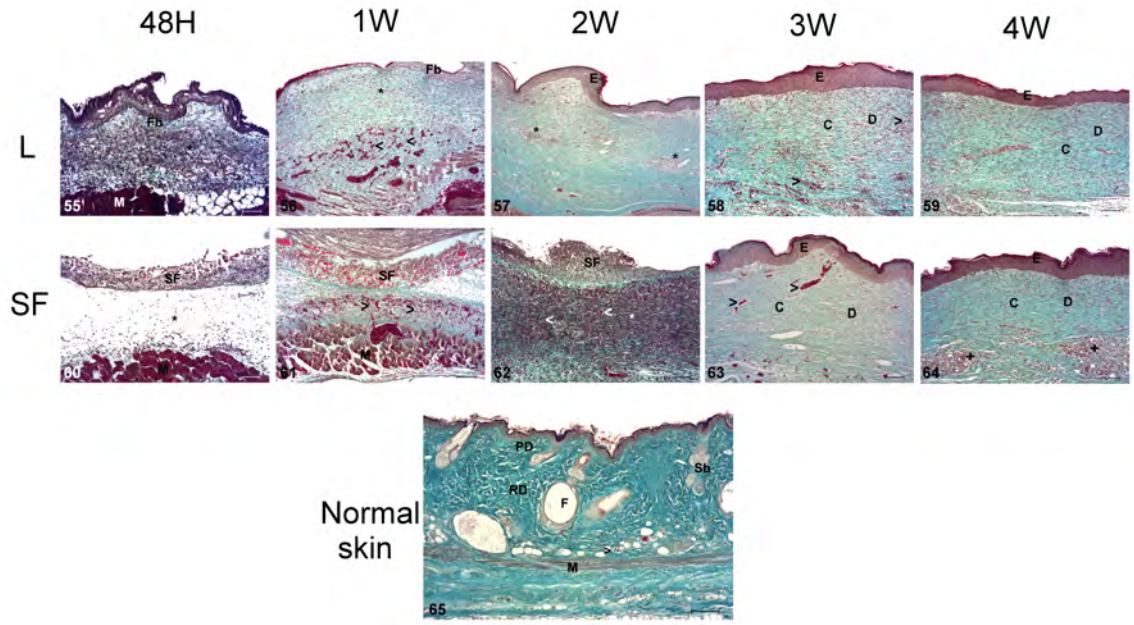

Figure 4.22: **Masson-Goldner trichrome Stains**. Control Groups: **L** (wounds covered with Linitul®) and **SF** (wounds covered with Silk Fibroin scaffolds). **Fb**: fibrin, *: inflammatory infiltrate and edema, > : blood vessels, **E**: epidermis, **M**: muscular layer, **D**: dermis, **C**: collagen, **SF**: silk fibroin scaffold, **PD**: papillary dermis, **RD**: reticular dermis, **Sb**: sebaceous gland, **F**: hair follicle. Scale bar: 100μm.

Noteworthy changes occurred from week 2 to week 3 in the skin of mice treated with SF scaffold. At this time point, there was less amount of collagen fibers, which were still disorganized, in comparison to Linitul®-treated animals (photo 63). Thus, the dermal layer was mostly composed of an immature dense connective tissue with blood vessels interspersed between collagen fibers (photo 74).

At week 4, the histological structure of the skin was quite similar to that from the group treated with Linitul® (photo 64). The hyperplastic epithelial sheet was completed, and the dermal layer still possessed some areas of reabsorption and inflammatory infiltrate (photo 75). A dense, regular, and mature connective tissue built the new scar tissue with no skin appendages in it.

Group C: wounds with hWj-MSCs injected at the edge

At 48 hours (photo 77), there were numerous cells interspersed within fibrin (photo 93). At week 1, epithelialization was in progress and some "pearl-like" regions result-

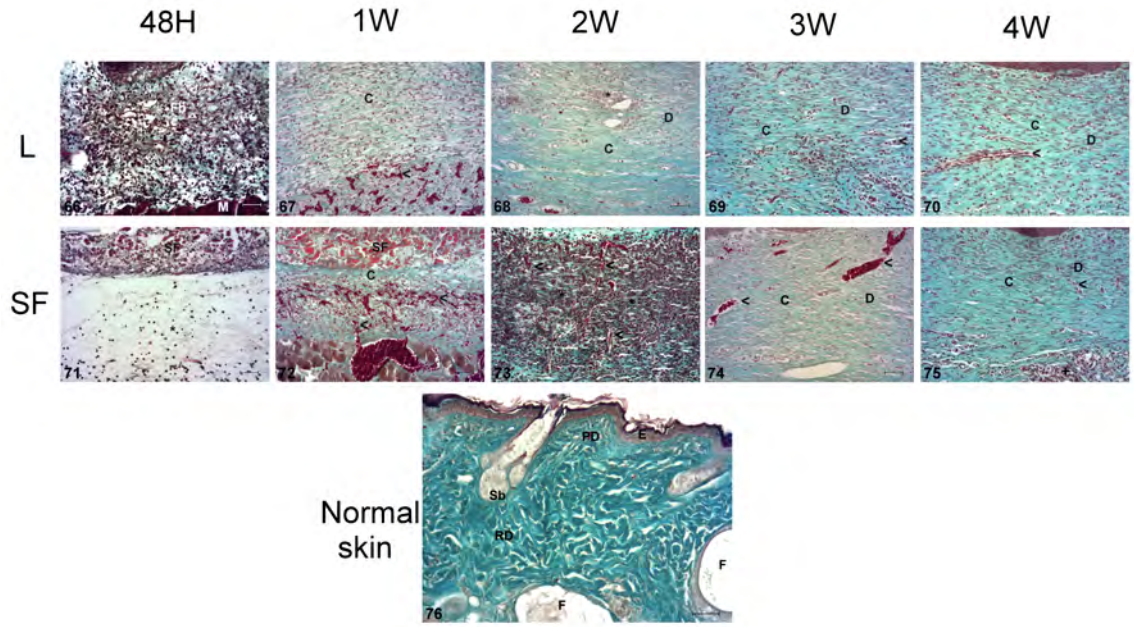

Figure 4.23: **Masson-Goldner trichrome Stains**. Control Groups: **L** (wounds covered with Linitul®) and **SF** (wounds covered with Silk Fibroin scaffolds). **Fb**: fibrin, *: inflammatory infiltrate and edema, > : blood vessels, **E**: epidermis, **M**: muscular layer, **D**: dermis, **C**: collagen, **SF**: silk fibroin scaffold, **PD**: papillary dermis, **RD**: reticular dermis, **Sb**: sebaceous gland, **F**: hair follicle. Scale bar: 50μm.

ing from clustering of epithelial cells were displayed in areas close to the epithelial sheet (photo 78). Many spindle-shaped cells intermingled with some areas of inflammatory infiltrate made up most of the dermis. Additionally, scarce collagen fibers and newly formed blood vessels gave rise to a net that provided support to the cells (photo 94).

At week 2, epithelization was complete but still immature (photo 79). Dermis comprised two roughly divided areas (photo 95). The outer area near the epithelium consisted of a granulation tissue with a huge amount of cells (i.e., inflammatory cells and spindle-shaped cells), a higher amount of blood vessels compared to the control group treated with Linitul®, and few collagen fibers. A dense connective tissue formed the deepest dermal layer, what it was previously formed by a more disorganized collagen matrix. These findings were consistent with those observed both in Linitul® and SF-treated groups.

At week 3, the connective tissue on both the surface and the deep area of the dermal sheet was much more organized (photo 80). Hence, the dermis was formed by a dense and regular connective tissue, with areas of neovascularization on it. The thickness of the epithelial layer apparently was less than control groups, and some areas of inflammatory infiltrate were still present in the dermis. Skin appendages were absent (photo 96).

At week 4, the collagen fibers forming the dermal layer followed a regular pattern (photo 81). No skin appendages were present in the newly formed tissue (photo 97).

Group D: wounds covered with silk fibroin patches cellularized with hWj-MSCs

At 48 hours, only the SF scaffold along with many cells were visualized (photo 82), occupying the wound site. As expected, there was still no collagen synthesis (photo 98).

At week 1, there was less production of collagen fibers compared to the previous group (photo 83), and many branched blood vessels were immersed in the connective tissue matrix that configures the dermis (photo 99). SF scaffolds coupled with the hWj-MSCs seemed to exert a synergistic control on the production of collagen.

At week 2, the amount and configuration of collagen (photo 84) differed from that observed in group A. In this case, collagen fibers were disposed interspersed within blood vessels, resembling an irregular dense connective tissue (photo 100).

Epithelialization was completed, at week 3 post-wounding (photo 85). Some areas of inflammatory infiltrate were still present in the dermis. The amount of connective tissue was less in the area near the epithelium, and in the deep dermis

the collagen fibers began to arrange to form a more organized and regular structure (photo 101).

One month after the injury occurs, the dermis was finally formed (photo 86) by a dense and regular connective tissue whose thickness was much smaller than all the groups described above (photo 102).

Group E: wounds with silk fibroin patches cellularized with hWj-MSCs over the wound bed and hWj-MSCs injected at the edge

At 48 hours, SF scaffold along with much more cells, compared to previous groups, covered the wound site (photo 87). As in other groups, collagen had not been produced yet in the wound site (photo 103).

At week 1, SF scaffold and the consequent foreign body reaction with large numbers of inflammatory cells and some edema were present in the external region of the dermis (photo 88). On the other hand, a higher synthesis of connective tissue, and randomly arranged blood vessels (neovascularization), with many spindle-shaped cells around filled the internal region of the dermal sheet (photo 104). From the structural point of view, the image at one week manifested the histological findings of the other two treated groups.

At week 2, collagen fibers in the dermis were randomly disposed following the tortuous path of the newly formed blood vessels which provided it with a non-shaped connective tissue (photos 89 and 105). Nonetheless, the connective tissue found in the deep dermis tended to organize into a banding pattern as seen in the previous group.

Noteworthy changes occurred between the second and third week in this experimental group (photo 90). The dermis was made up of a dense and organized connective tissue with a regular configuration, whose thickness was smaller than the other groups. Most importantly, the presence of skin appendages along the entire new tissue was what made it different from other experimental groups (photo 106).

At week 4, the collagen tended to organize into a pattern resembling the dense irregular connective tissue of the reticular dermis in normal skin (photo 91). The most relevant finding was the presence of degenerating skin appendages as observed in the normal skin of SKH1 mice (photo 107). The thickness of the dermis was apparently less than control group treated with Linitul®.

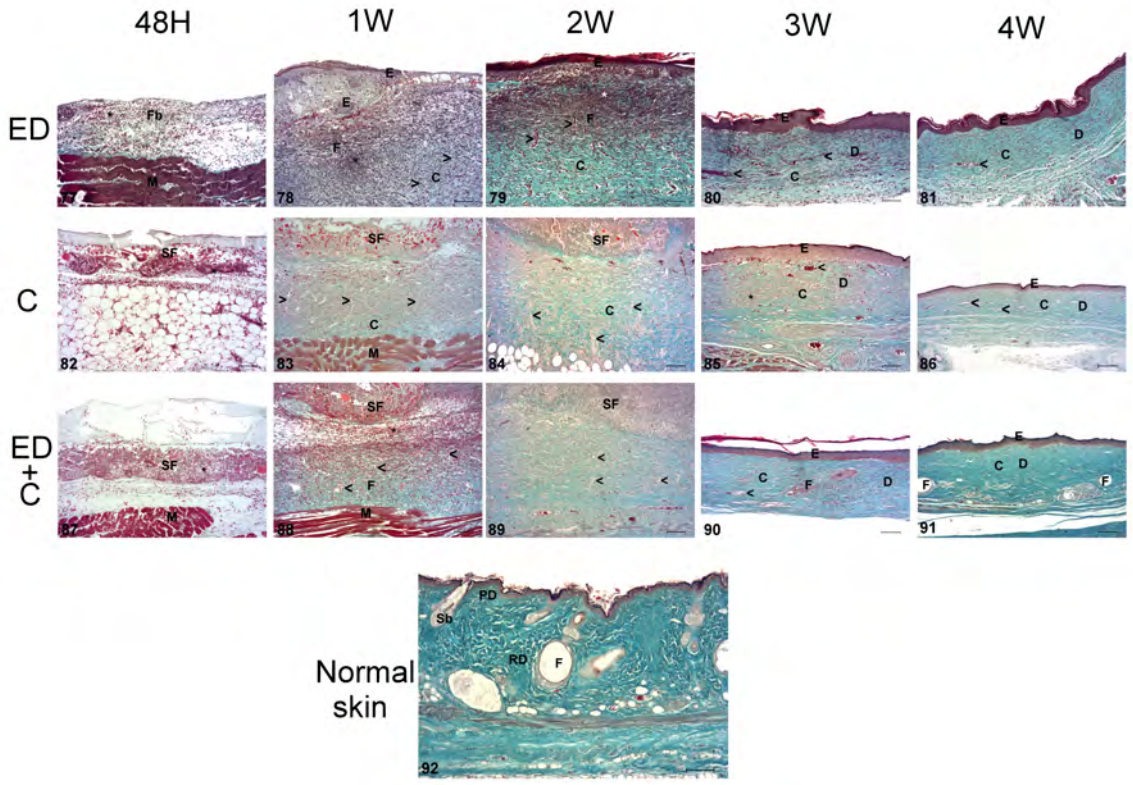

Figure 4.24: **Masson-Goldner trichrome Stains**. Treated Groups: **ED** (wounds with hWj-MSCs injected at the edge), **C** (wounds covered with silk fibroin patches cellularized with hWj-MSCs), and **ED+C** (wounds with silk fibroin patches cellularized with hWj-MSCs over the wound bed and hWj-MSCs injected at the edge). **Fb**: fibrin, *: inflammatory infiltrate and edema, > : blood vessels, **E**: epidermis, **M**: muscular layer, **D**: dermis, **C**: collagen, **SF**: silk fibroin scaffold, **PD**: papillary dermis, **RD**: reticular dermis, **Sb**: sebaceous gland, **F**: hair follicle. Scale bar: 100μm.

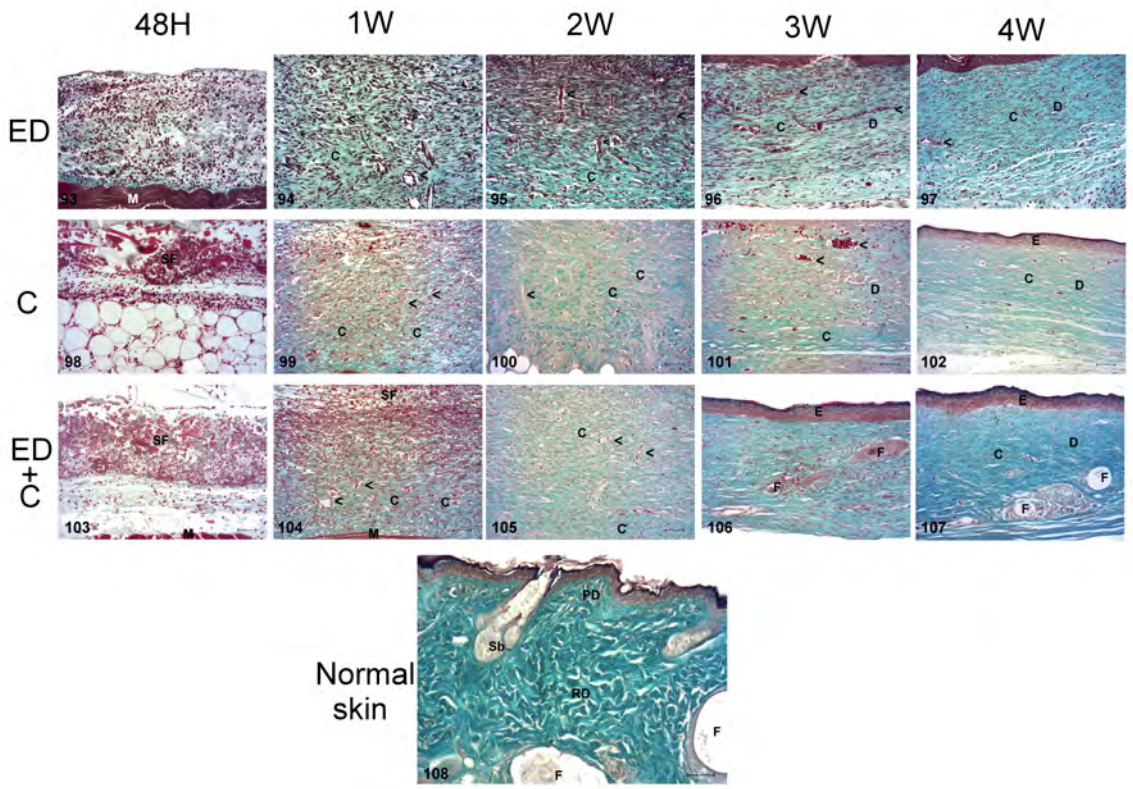

Figure 4.25: **Masson-Goldner trichrome Stains**. Treated Groups: **ED** (wounds with hWj-MSCs injected at the edge), **C** (wounds covered with silk fibroin patches cellularized with hWj-MSCs), and **ED+C** (wounds with silk fibroin patches cellularized with hWj-MSCs over the wound bed and hWj-MSCs injected at the edge). **Fb**: fibrin, *: inflammatory infiltrate and edema, $>$: blood vessels, **E**: epidermis, **M**: muscular layer, **D**: dermis, **C**: collagen, **SF**: silk fibroin scaffold, **PD**: papillary dermis, **RD**: reticular dermis, **Sb**: sebaceous gland, **F**: hair follicle. Scale bar: 50μm.

4.5.3 Measurements of Leucocyte Infiltration

4.5.3.1 Polymorphonuclear neutrophils

As seen in Fig. 4.26 (a-c), wounds treated with Linitul® exhibited an early rise (at 48 hours) and a subsequent progressive decrease in the number of neutrophils as normally occurs during the healing process of skin wounds.

In the group of wounds treated with SF scaffolds a significant increase in neutrophils was observed within two weeks of implanting the biomaterial, and then they abruptly decreased the third week reaching values close to those of the control group (Fig. 4.26 (a-c)).

The number of neutrophils in the group of wounds treated with MSCs injected at the edge (Fig. 4.26 (a)) was significantly lower during the first week when compared to the Linitul®group. However, it remained constant until the second week, when started decreasing to significantly fewer counts compared to the control group. It is noteworthy that after two weeks following injury the number of neutrophils was significantly lower compared to wounds treated with the SF scaffold, and not considerably higher (no significant differences) than the group treated with Linitul®.

The behaviour followed by neutrophils during the first two weeks of healing in the group of mice treated only with cellularized SF scaffolds (Fig. 4.26 (b)) or with the biomaterial together with Wj-MSCs injected at the wound edges (Fig. 4.26 (c)) was quite similar to that described above. That is, neutrophils rose over the first week, and then they kept constant until the second week when they started descending to lower levels than controls. The presence of mesenchymal stem cells in all cases were associated with a lower inflammatory response, expressed by less amount of neutrophils in the wound tissue, than the foreign body reaction induced by the biomaterial itself.

4.5.3.2 Macrophages infiltration at the wound site (Figure 4.26 (e-h))

As seen in Figure 4.26 (e-g), maximum values of macrophages were reached a week post-injury in the control group treated with Linitul® like in those treated with the SF scaffold, being significantly lower in the latter. However, in the group treated with Linitul®, the number of macrophages gradually descended from the first week, following a dynamic similar to that outlined by the wounds treated with the scaffold (no significant differences were seen between them from the second week onwards).

Importantly, wounds treated with MSCs injected at the wound edges (Fig. 4.26 (e)) also showed the highest counts of macrophages during the first two weeks, although later they descended to significantly lower levels than the control groups. It

is striking that combining stem cells with the biomaterial caused a limited influx of macrophages into the wound site, especially the first two weeks. This immunomodulatory effect was observed throughout the entire healing process and was expressed by the significantly lower counts of macrophages in groups treated with hWJ-MSCs-SF and hWJ-MSCs-SF + Edge (fig. 4.26 (f-h)) in comparison to those treated with Linitul® or the biomaterial alone.

4.5.3.3 CD3 T Lymphocytes (Figure 4.26 (i-l))

It is well known that lymphocytes normally migrate to the wound site in large numbers four to 7 days following injury. After reaching a peak at two weeks, they begin to decline slightly over the next few weeks, as observed in the control group treated with Linitul®. The same trend was seen in the beds of wounds covered by the SF scaffold, being the number of lymphocytes significantly higher at all times from the first week, compared to the Linitul® group (fig. 4.26 (i-k)).

The influx of lymphocytes into the wounds was higher during the first two weeks in all groups treated with MSCs, i.e., both injected into the wound edge (Fig. 4.26 (i)) as those seeded onto the transplanted scaffolds (Fig. 4.26 (j, k)), compared to the control group treated with Linitul®. However, two weeks after injury, the number of lymphocytes turned importantly lower in the group treated only with MSCs or remained at slightly higher counts when combining biomaterials with MSCs, although not significant (Fig. 4.26 (l)).

4.5.4 Assessment of Angiogenesis by Expression of CD31 In Wound Sites

As seen in Table 4.2 (A), during normal healing conditions (Linitul®) a moderate expression (grade II) of CD31 into the newly formed granulation tissue was observed during the first two weeks, and then it decreased gradually to come practically negative one month after wounding.

Maximum CD31 expression (grade III) was reached the initial 2 weeks of healing in wounds that underwent either treatment with SF scaffolds or the stem cell-based therapy, separately or in combination. The group of wounds that were covered only with the SF scaffolds adopted during the last two weeks the same level of CD31 expression than wounds from the control group (Table 4.2 (B)). On the contrary, angiogenesis remained at moderate and constant levels in all experimental groups receiving treatment with Wj-MSCs (Table 4.2 (C-E)). It is striking that the group of wounds treated with Wj-MSCs at the edge + Wj-MSCs/SF scaffolds had the

highest expression of CD31 throughout the healing process, thus reflecting robust angiogenic processes at the wound site in this particular experimental group (Table 4.2 (E)).

EXPERIMENTAL GROUPS	48 H	1 W	2 W	3 W	4 W
(A) LINITUL®	-	++	++	+	-
(B) SF SCAFFOLD	-	+++	+++	+	-
(C) WJ-MSCs EDGE	-	+++	+++	++	++
(D) WJ-MSCs-SF	-	+++	+++	++	++
(E) WJ-MSCs-SF + EDGE	-	+++	+++	++/+++	++

Table 4.2: **Qualitative scale for immunohistochemical analysis of CD31 expression in wound sections.** Experimental groups: (A) wounds covered with Linitul®; (B) wounds covered with silk fibroin scaffolds; (C) Wharton's jelly mesenchymal stem cells injected at the wound edge; (D) wounds covered with silk fibroin scaffolds cellularized with Wharton's jelly mesenchymal stem cells (E) wounds treated with Wharton's jelly mesenchymal stem cells injected at the wound edge and cellularized silk fibroin scaffolds onto the wound bed. Scale for CD31 expression: - no expression, +: Grade I / ++: Grade II / +++: Grade III.

4.5.5 Expression of Alpha-Smooth Muscle Actin during Wound Healing

Table 4.3 comprises the immunohistochemical analysis of alpha-smooth muscle actin expression (α-SMA), as the most reliable marker of the myofibroblastic phenotype, in wound sections of the different experimental groups. Skin healing process in the control group (Linitul®) showed a moderate expression of α-SMA (26-50%) during the first week following injury. Then, it diminished forth the second and third week of healing (10-25%) until having an expression less than 10% at one-month post wounding (Table 4.3 (A)).

In the group of mice treated with SF scaffolds, a huge amount of myofibroblasts was present at the wound site during the first two weeks of healing since the expression of α-SMA was much higher in this group in comparison to that treated with Linitul®. However, the number of myofibroblasts dropped steeply after the second week to follow the same trend as the control group (Table 4.3 (B)).

Wounds treated with Wj-MSCs injected at the edge also showed high expression of α-SMA (>50%) one week after the injury occurs but unlike the SF-scaffold group the number of myofibroblasts was much lower on day 14. Then, it returned to the normal level as did preceding groups (Table 4.3 (C)).

Both Wj-MSCs-SF and Wj-MSCs-SF+Edge groups had the same expression pat-

tern of α-SMA throughout the wound healing stages. It resembled the one observed with the control group, i.e., moderate expression of myofibroblast marker (26-50%) the first week and then a gradually decrease from the second week onward (Table 4.3 (D-E)).

In brief, the highest influx of myofibroblasts into the granulation tissue at the wound site was observed during the first two weeks following injury in the group of wounds only treated with SF scaffolds (group B) or with the mesenchymal stem cells injected at the edge of the wound (group C). On the contrary, the expression of α-SMA marker was importantly less in the group of wounds treated simultaneously with both therapeutic agents (groups D and E).

EXPERIMENTAL GROUPS	48 H	1 W	2 W	3 W	4 W
(A) LINITUL®	-	++	+	+	-
(B) SF SCAFFOLD	-	+++	+++	+	-
(C) WJ-MSCs EDGE	-	+++	++	+	-
(D) WJ-MSCs-SF	-	++	+	+/-	-
(E) WJ-MSCs-SF + EDGE	-	++	+	+/-	-

Table 4.3: **Qualitative scale for immunohistochemical analysis of alpha-smooth muscle actin expression in wound sections.** Experimental groups: (A) wounds covered with Linitul®; (B) wounds covered with silk fibroin scaffolds; (C) Wharton's jelly mesenchymal stem cells injected at the wound edge; (D) wounds covered with silk fibroin scaffolds cellularized with Wharton's jelly mesenchymal stem cells (E) wounds treated with Wharton's jelly mesenchymal stem cells injected at the wound edge and cellularized silk fibroin scaffolds onto the wound bed. Scale for alpha-smooth muscle actin expression: - (<10%) / + (10-25%) / ++ (26-50%) / +++ (>50%).

4.5.6 Expression of the Mesenchymal Stem Cell Marker CD90 on Wound Sites (Figures 4.27 to 4.29)

As mentioned above, a rabbit monoclonal antibody (clone EPR3133) that specifically binds to human CD90 protein was used as a marker to identify human mesenchymal stem cells. The specificity of the anti-CD90 antibody was previously demonstrated by the intense membrane staining of the human Wharton's jelly mesenchymal stem cells that made up the pellet that served as positive control (Fig. 4.27 (118) and Fig. 4.28 (132)).

Contrary to what was observed in the positive control, CD90 immunohistochemical staining was absent on normal mouse skin (Fig. 4.27 (117) and Fig. 4.28 (131)) and also in the wound sites of mice treated with Linitul® (Fig. 4.27 (109-112)) or

with the SF-scaffolds (Fig. 4.27 (113-116)) over the different time points. Thus, it suggests that the anti-CD90 antibody did not bind to any CD90 positive cell in the normal mouse tissues or wounds that did not receive human mesenchymal stem cell therapy.

On the other hand, a clear and abundant positivity to CD90 protein was immunohistochemically evidenced into the wound sites of mice treated with human Wj-MSCs applied either by injection into the wound edge or by covering the wound bed with cellularized SF scaffolds (Fig. 4.28). Numerous spindle-shaped cells positive for CD90 were immersed in the granulation tissue of wounds from mice treated with human MSCs during the first two weeks following the injury (Fig. 4.28 (119-120, 123-124, 127-128)). The immunostaining was clearly negative from the second week, so seemingly transplanted mesenchymal stem cells "faded" from the tissue (Fig. 4.28 (121-122, 125-126, 129-130)).

Figure 4.29 shows the expression at week 2 of the mesenchymal stem cell marker CD90 in wounds from mice treated with silk fibroin patches cellularized with hWj-MSCs over the wound bed, and hWj-MSCs injected at the edge. CD90 positive cells were appreciated forming the migrating epithelial front, but also making up small clusters of about 8-10 cells nearby the newly formed epithelium (Figure 4.29 (135-136)). These cells share the same round-cuboid shape resembling epithelial cells. Nonetheless, many other CD90-positive cells maintained the typical mesenchymal shape in deeper areas of granulation tissue as depicted in Figure 4.29 (133-134).

4.5.7 Histopathological Examination of Distant Organs and Analysis of Tumor Formation after Transplantation of Wj-MSCs

In vivo toxicity and biodistribution of Wj-MSCs was evaluated in SKH1 mice to rule out ectopic tissue formation and tumorigenesis. Lungs, heart, liver, spleen, kidneys, testis, brain and bone marrow were examined by hematoxylin and eosin stain (Figure 4.30).

A mild associated acute interstitial inflammatory infiltrate in lung tissue, and an increased number of alveolar macrophages were observed until the second week after the wound occurs in some mice treated with MSC-seeded SF scaffolds (depicted in Figure 4.31 (a-b)). Same findings were identified over the four weeks following injury in some of the mice given both therapies, i.e., cells injected into the wound edge and cellularized SF scaffolds covering the wound bed.

As seen in Figure 4.31 (c-d), scarce hepatic microabscesses were occasionally

evidenced until two weeks following injury, in mice treated with MSCs injected at the edge, and in those whose wounds were covered with cellularized SF scaffolds. This liver involvement lasted until the fourth week of healing in mice receiving combined treatment.

Hyperplasia of the splenic white pulp was observed in all experimental groups until the third week after surgery. This affection was still present until the fourth week in mice treated simultaneously with MSCs injected at the wound edge, and MSC-seeded SF scaffolds (Figure 4.31 (e-f)).

Histopathological examination of all the excised organs at different time points did not reveal tumor formation in any experimental group. After human Wj-MSCs injections or biomaterial-assisted mesenchymal stem cell therapy, transplanted stem cells did not seem to have anarchical proliferation, form teratomas or undergo spontaneous malignant transformation.

Besides, analysis of biodistribution of transplanted Wj-MSCs by immunohistochemistry using an anti-CD90 antibody showed no presence of MSCs in any examined organs.

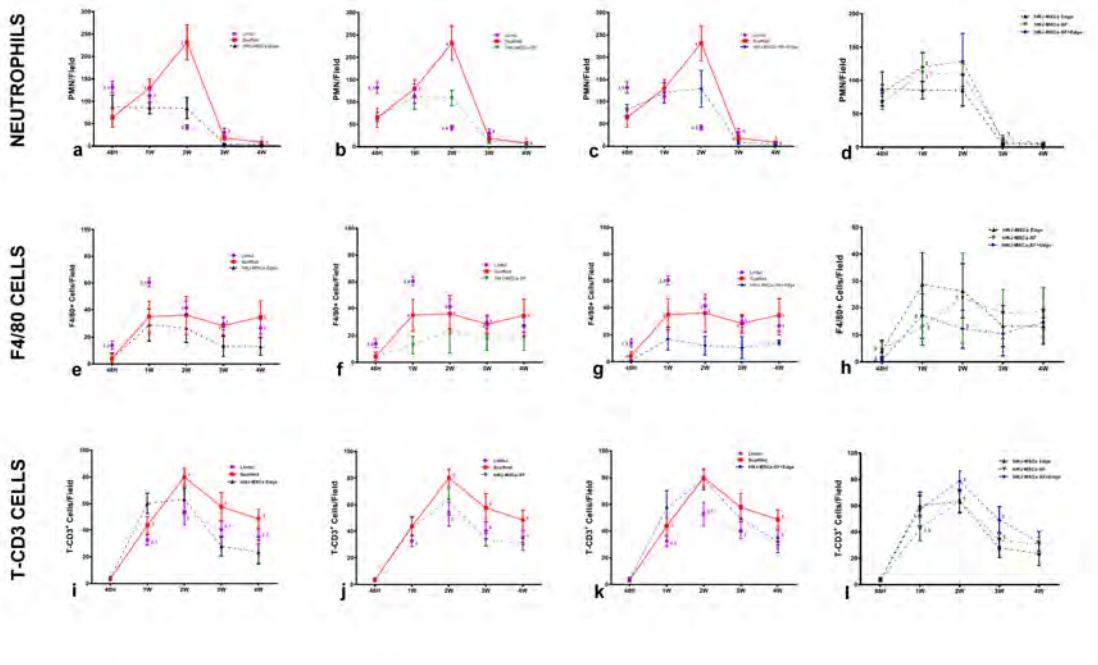

Figure 4.26: **Influx of inflammatory cells into wounded tissues: polymorphonuclear neutrophils (a-d), macrophages (e-h), and lymphocytes (i-l).** Experimental groups: wounds covered with Linitul® (purple line); wounds covered with silk fibroin scaffolds (red line); Wharton's jelly mesenchymal stem cells injected at the wound edge (hWJ-MSCs Edge) (black line); wounds covered with silk fibroin scaffolds cellularized with Wharton's jelly mesenchymal stem cells (hWJ-MSCs-SF) (green line); and wounds treated with Wharton's jelly mesenchymal stem cells injected at the wound edge and cellularized silk fibroin scaffolds onto the wound bed (hWJ-MSCs-SF + Edge) (blue line). Statistically significant differences ($p<0.05$) compared to Linitul® (value 1); Scaffold (value 2); hWJ-MSCs Edge (value 3); hWJ-MSCs-SF (value 4), and hWJ-MSCs-SF + Edge (value 5), according to one-way ANOVA.

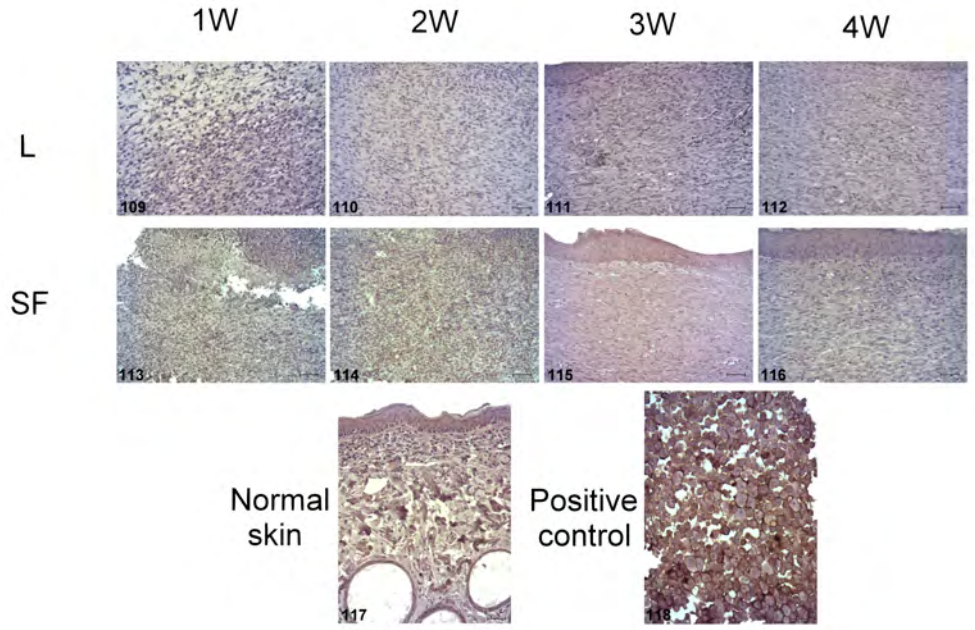

Figure 4.27: **Expression of mesenchymal stem cell marker CD90 on dermal wounds.** Experimental Groups: **L** (wounds covered with Linitul®) and **SF** (wounds covered with Silk Fibroin scaffolds). Immunostaining with the anti-CD90 antibody of a pellet made of Wj-MSCs served as positive control (117)**.** Scale bar: 50μm.

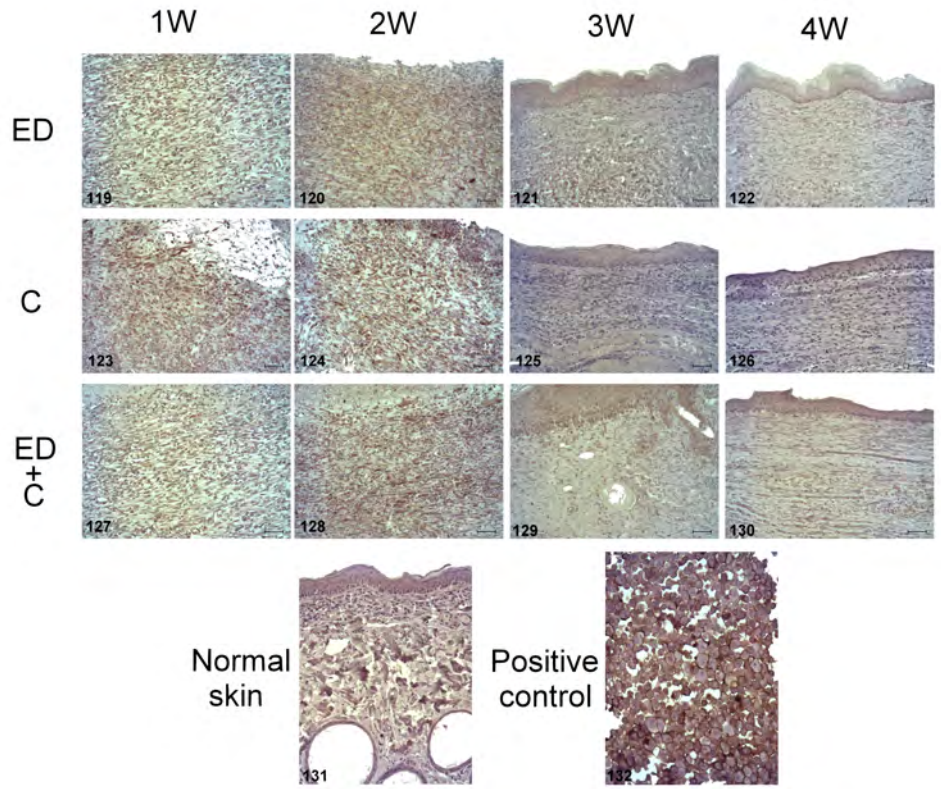

Figure 4.28: **Expression of mesenchymal stem cell marker CD90 on dermal wounds.** Experimental Groups: **ED** (wounds with hWj-MSCs injected at the edge), **C** (wounds covered with silk fibroin patches cellularized with hWj-MSCs), and **ED+C** (wounds with silk fibroin patches cellularized with hWj-MSCs over the wound bed and hWj-MSCs injected at the edge). Scale bar: 50μm.

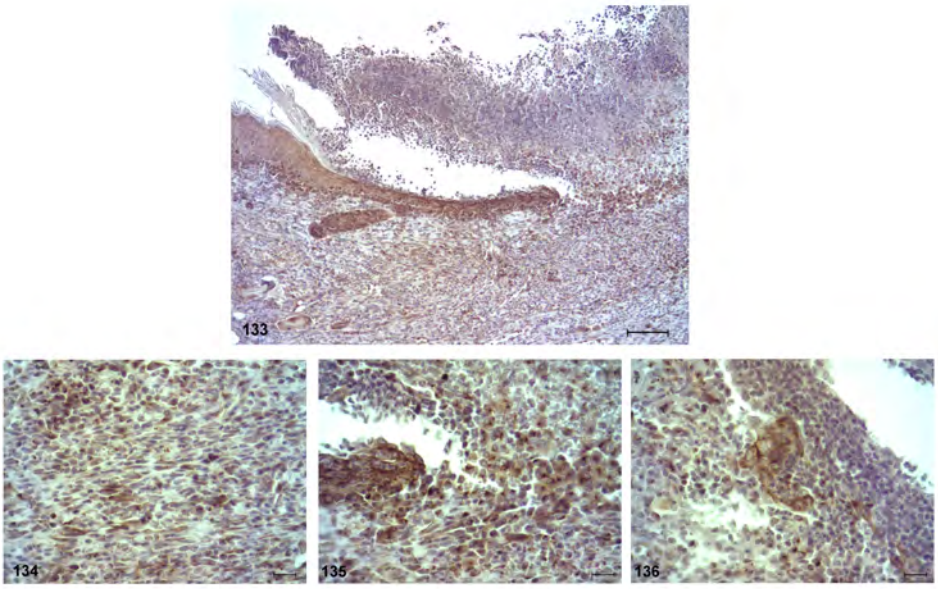

Figure 4.29: **Expression at two weeks of mesenchymal stem cell marker CD90** at the migrating epithelial front in wounds from mice treated with silk fibroin patches cellularized with hWj-MSCs and mesenchymal stem cells injected at the edge. Scale bar: 100μm (image 133) and 20μm (images 134-136).

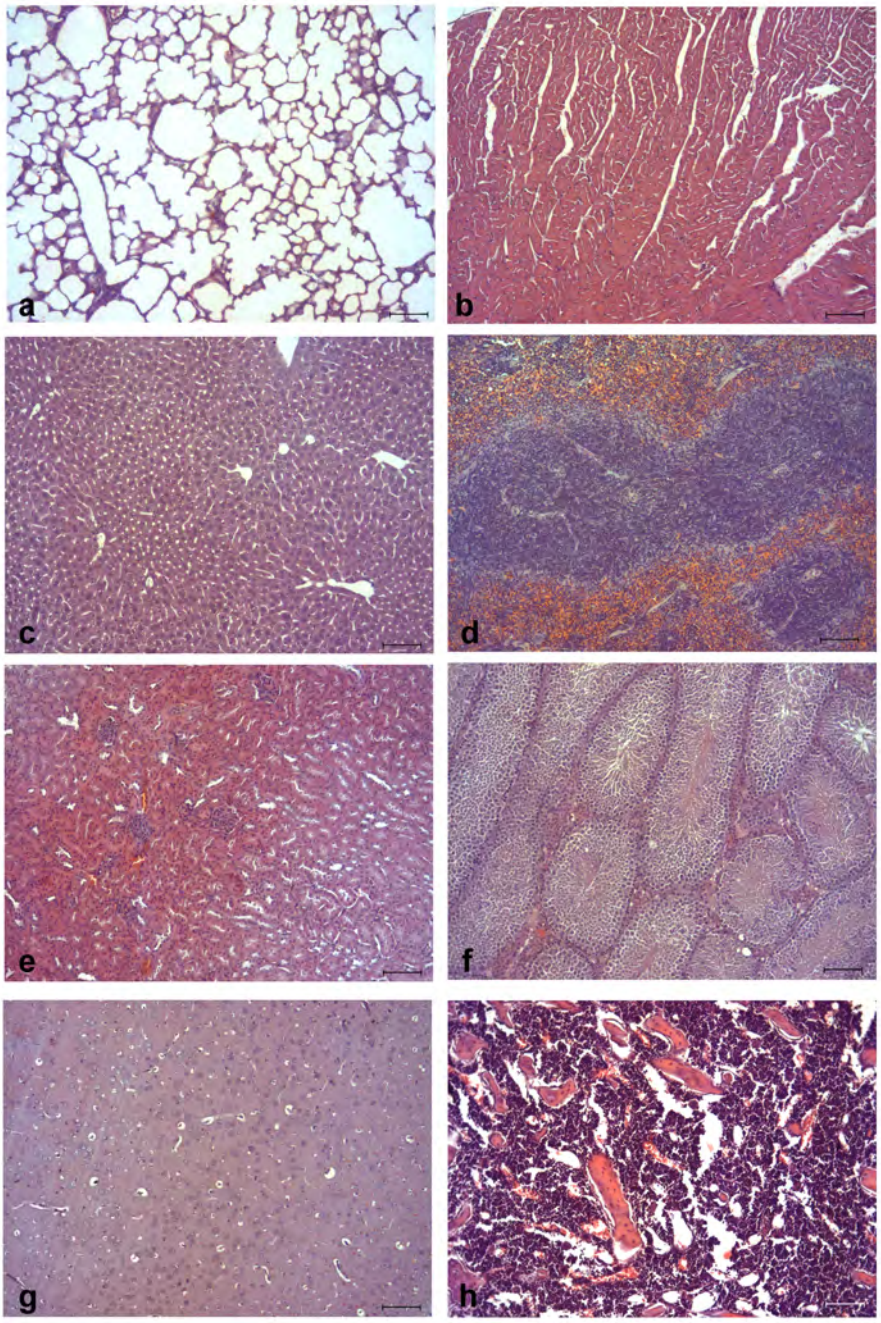

Figure 4.30: **H&E staining for standard histological examination of (a) lungs, (b) heart, (c) liver, (d) spleen, (e) kidneys, (f) testis, (g) brain and (h) bone marrow.** Scale bar: 50μm.

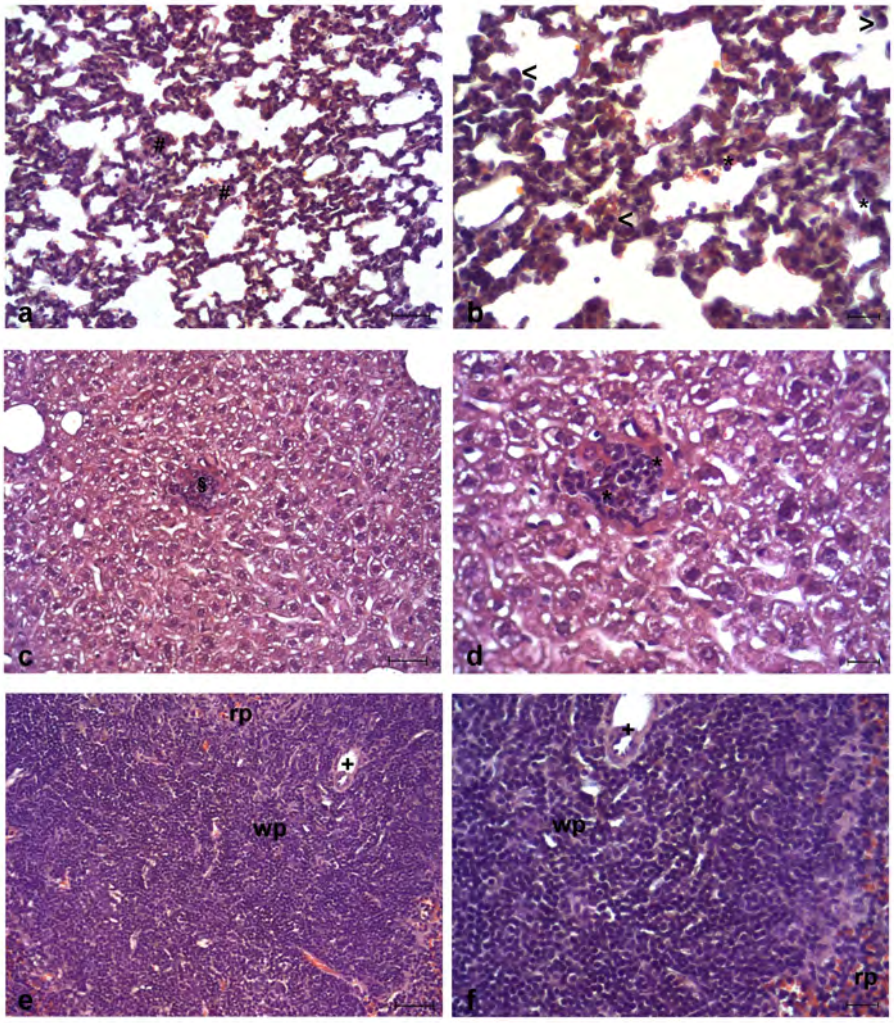

Figure 4.31: **Histopathological findings in lung (a-b), liver (c-d), and spleen (e-f) sections stained by H&E.** (a, b) Interstitial inflammatory infiltrate (#), and alveolar macrophages (<) in lung tissue. (c, d) Image of a liver microabscess (§), with polymorphonuclear cells in it (*). (e, f) Hyperplasia of the splenic white pulp (+ splenic arteriole). Abbreviations: wp: white pulp; rp: red pulp. Left panel - 20X magnification. Right panel 40X magnification.

Chapter 5

DISCUSSION

In this study, we have first standardized the protocol for the isolation and characterization of mesenchymal stem cells derived from the Wharton's jelly of the human umbilical cord. Further, these MSCs along with the combination of silk fibroin scaffolds were used to test their wound healing properties by creating skin wounds in an experimental murine model.

MSCs can be isolated from several compartments of the umbilical cord, i.e., from umbilical cord blood, umbilical vein subendothelium, and the Wharton's jelly. Within Wharton's jelly, MSCs have been isolated from three relatively indistinct regions: the perivascular zone, the intervascular zone, and the subamnion [174]. This discussion is aimed to the MSCs isolated from the Wharton's jelly of the human umbilical cord.

MSCs from Wharton's jelly can be isolated using either enzymatic digestion (e.g., collagenase, hyaluronidase) or mechanical dissection of the umbilical cord (i.e., explant method). We compared both methods of isolation proving the explant method to be more suitable because of its ease and speed of completion. Thus, Wj-MSCs were isolated from explants and then expanded following the *in vitro* culturing protocols of the LUMC and the Jon J van Rood Center for Transfusion Medicine Research (Leiden-The Netherlands).

Cells isolated from the Wharton's jelly of the umbilical cord exhibited a fibroblastic morphology, as shown by mesenchymal stem cells from other sources, and after a lag phase of 10 days, they grew and became confluent layers of adherent cells. At passage fourth, Wj-MSCs cultures displayed MSC surface markers uniformly positive for CD90, CD105, CD73 with no detectable presence of hematopoietic cells suggesting that they belonged to the MSC family.

Although several authors claim that Wj-MSCs can differentiate into adipocytes, chondrocytes, and osteoblasts, we found that these cells are limited in their ability

to differentiate into mature mesodermal cell lines. These findings are supported by a recently published paper by the group of Kögler [175], who also looked at the transcriptome for lineage-specific gene expression in differentiated cells. Likewise, others authors found that Wj-MSCs differ from BM-MSCs because of their poor capacity to differentiate into adipocytes [60, 176, 177].

One of the most important factors for successful cellular therapy using MSC is the amount of cells available for transplantation to provide a therapeutic effect. The cells from cultures in their first passages are preferred for cellular therapy. Therefore, a larger number of MSCs in early passages is required from a single source and single donor [178].

The proliferation analysis performed in this study revealed that mesenchymal stem cells from the umbilical cord were highly proliferative whereas the growth potential of BM-MSCs cultured in the same conditions was significantly lower. Such proliferation characteristics did not change even after ten passages, unlike BM-MSCs that increased the PDT from passage nine. This feature is thought to reflect the relatively primitive nature of cells derived from the umbilical cord compared to adult BM-MSCs [174]. Besides, Wj-MSCs were easily accessible since a high number of cells could be isolated from close to 100% of the umbilical cords processed in our facilities with no donor site morbidity.

As highlighted earlier, an accumulating number of publications show that fetal stem cells present some advantages, e.g., ease expandability, differentiation ability, and immunomodulatory capacity, that renders these cells an excellent alternative for regenerative medical applications in comparison to adult mesenchymal stem cells [61].

In addition to pluripotency, MSCs are known to be immunoprivileged as well as they have immunosuppressive effects involving various mechanisms, resulting in evading the allogeneic host immunosurveillance system. Hence, neither autologous nor allogeneic MSCs induce immunoreactivity in the host on local transplantation or systemic administration [99, 179]. Thus, these cells represent an important therapeutic tool for regenerative medicine and tissue engineering [180].

In wound healing process, inflammation is a very important phenomenon because include induction of inflammatory factors and accumulation of various inflammatory cells that start tissue regeneration by replenishment of cells and extracellular components [181]. MSCs have the ability to modulate both innate and adaptive immune response by complex interactions with T cells, B cells, NK cells, dendritic cells, macrophages, neutrophils and Toll-like receptors (TLRs).

Wj-MSCs were shown to have significant immune modulatory effects on the pro-

liferative response of peripheral T cells subjected to CD3/CD28-beads stimulation as compared with the effects mediated by BM-MSCs. The CD3/CD28 beads-mediated proliferation of T cells decreased when the proportion of Wj-MSCs in the culture was increased. The same dose-response effect mediated by hWj-MSCs was seen on MLCs after allogeneic mDCs stimulation. In all experiments, maximal inhibition was achieved when MSCs and MNCs were co-culture at a 1:1 ratio. It is unlikely that the reduction in lymphocyte proliferation was caused by the exhaustion of the culture media or cell crowding in the wells. The culture medium in MLCs including MSCs was normal in color and were used as control cultures. Also, Trypan Blue staining showed >95% cell viability of both MSCs and lymphocytes at the time of harvest.

When we studied the effects of MSCs on lymphocyte proliferation in MLC, it was evident that Wj-MSCs were immunosuppressive and inhibited T-cell proliferation. Ennis et al. also found these cells to be non-immunogenic since a single injection of MHC-mismatched unactivated umbilical cord tissue-derived cells did not induce a detectable immune response. However, when injected into an inflamed region, repeatedly injected in the same area or stimulated with IFN-γ before injection, these cells were immunogenic [182]. The finding that MSCs induced inhibition of MLCs and T cells has clinical implications since allogeneic stem cell transplantation could modulate the immune response during stem cell-based regenerative therapy.

Several studies have shown that fetal MSCs significantly express a higher level of immunomodulatory factors (e.g., TGF-β1, IDO, PGE2) in comparison to adult bone marrow-derived MSCs [61]. This fact matches well with what we found after performing the *in vitro* characterization of the immunological properties of the Wj-MSCs.

Regarding the *in vitro* immunoregulatory properties of Wj-MSCs, our data are also consistent with previous studies showing that these MSCs (a) do not induce proliferation of allogeneic T cells, (b) suppress the proliferation of T cells induced either by CD3/CD28 beads or allogeneic mDCs cells, (c) secrete soluble factors that mimic the immunosuppressive effects associated with the co-culture of the MSCs with the T cells (i.e., TGF-β, IDO, and PGE2), and (d) inhibit the production of pro-inflammatory cytokines (e.g., IFN-γ) of T cells stimulated by allogeneic stimuli.

Wound healing is a complex process involving coordinated interaction between cells, growth factors, and extracellular proteins. Several reports on different animal models and clinical trials indicate that MSCs may play a beneficial role in augmenting the wound healing process. Thus, an excisional wound splinting model in SKH1 mice were used herein to study the therapeutic effect of human Wj-MSCs in wound

healing. We found that splinting prevented skin contraction, and consequently minimizing the variations caused by it which finally led uniform wound closure. Also, this model allowed wounds to heal through granulation and re-epithelialization, as previously reported [134]. This model allowed the study of the mechanisms underlying wound healing and provided means to modulate the wound milieu with exogenous factors to enhance wound healing. In this study, Wj-MSCs were implanted into the wound bed in an electrospun silk fibroin scaffold and/or injected into the dermis of the surrounding skin.

SKH1 mice were divided into five groups based on the type of treatment. The first two groups have been classified as control groups, of which one group was treated with Linitul® and the other one with silk fibroin scaffolds without MSCs. In the third group, only Wj-MSCs were injected in the wound edge, the fourth group consisted of grafting of Wj-MSCs seeded on the silk fibroin scaffolds over the wound site, and the last group was treated with MSCs injected in the edge together with the cellularized SF scaffold onto the wound.

In cell-based regenerative medicine applications, choice of cell delivery vehicle is an important consideration. The delivery of cells to cutaneous wounds presents a unique and specific set of challenges. Although systemic delivery is an attractive option, the engraftment efficiency can be difficult to predict without improved methods to ensure that the cells will home to the site of injury [140].

On the other hand, the injection of a suspension of cells may be the simplest method, but this may not be the optimum method to deliver cells to a cutaneous wound. First of all, direct injection into the wound may be difficult in long-standing leg ulcers that have a thick layer of dense scar tissue. To solve this issue and to also provide a more receptive environment for administered cells, debridement of the wound site is often performed before the delivery of cells. The debridement removes any scar tissue, fibrin, and necrotic tissue and also achieves bleeding from the wound bed. This bleeding aims to tackle the second issue; most chronic wounds are ischemic in nature. They exhibit poor blood flow and present a hostile environment for any cells. It is theorized that, by inducing bleeding, this may be enough to mitigate the hostile environment for long enough for the administered cells to take hold and stimulate a healing cascade. These limitations led to the development of alternative approach with the aim of reducing costs or increase efficacy [6].

It is important to know that the choice of biomimetic scaffold plays a pivotal role in driving appropriate tissue regeneration *in vivo*. Since the extracellular matrix plays a key role in guiding various biological processes, electrospun nanofibrous scaffolds could provide a three-dimensional structure that mimic the *in vivo* stem cell

niche providing cues for stem cells attachment, growth, migration and differentiation into host cells. Furthermore, nanoscaffolds can be designed to biodegrade at required times allowing the stem cells to complete healing until wound closure [106].

MSCs have been incorporated into three-dimensional scaffolds as a mean to improve skin substitutes that are used to repair full-thickness wounds resulting from trauma or burns [183]. We have used electrospun silk fibroin as a scaffold for culturing Wj-MSCs before transplantation since it is a clinically relevant method to deliver cells to dermal wounds. In addition, SF is a substrate that acts as a provisional matrix through which cells migrate, during wound healing process, to populate the wound site.

In this study, cells seeded on silk fibroin scaffolds were found to have appropriate interactions with their environment based on the following observations. First, the cells maintained a spindle-shaped morphology, suggesting that cells function biologically within this structure. Also, Wj-MSCs cultured on SF scaffolds did not show any change in the cell surface marker expression profile or viability when compared to cells cultured on plastic culture plates. Second, the cells adhered to the fibers and stretched across the nanofibrous substrates during proliferation. Third, these cells crosslinked the nanofibers and integrated with the surrounding fibers to form a three-dimensional cellular network. Therefore, the electrospun SF scaffolds cellularized with Wj-MSCs were found to be suitable as a skin substitute since the architecture of the structure is similar to that of natural extracellular matrix found in normal skin. Besides, this artificial "dermal layer" proved to adhere to and integrate well with the wound. Hence, we considered SF scaffold as the ideal MSC-delivering biomaterial because of its ability to retain MSC potential and long-term survival within a hostile microenvironment.

Yoshikawa et al. cultured human BM-MSCs and then placed them in artificial dermis made of collagen sponge that was later implanted subcutaneously into the dorsal wound of a nude mouse. Furthermore, BM-MSCs suspension was injected subcutaneously around the wound without the artificial dermis. Macroscopic findings showed that the artificial dermis without cultured BM-MSCs was flattened within two weeks after implantation. When BM-MSCs were injected without artificial dermis, marked tissue regeneration was not observed macroscopically. In contrast, when the artificial dermis was implanted with cultured BM-MSCs, the artificial dermis was not flattened at two weeks after graft placement, and its thickness was maintained macroscopically. Concerning histologic findings, only the artificial dermis containing the cultured cells showed any improvement in repair with increased vascularity, fat, and matrix deposition compared to the other groups. The next step

following the study in mice was to treat 20 patients with chronic wounds using cultured autologous BM-MSCs/artificial dermis composite grafts. The wounds mostly healed in 18 of the 20 patients; the remaining two patients died of causes unrelated to transplantation. Thus, autologous BM-MSCs transplantation was shown to be therapeutically effective in all patients [104]. This study was the first to suggest that the use of scaffold for administering the MSCs to the wound may be more beneficial than just injecting the cells around the wound site. Hence, the delivery of cells is an important and often neglected aspect of any therapeutic approach.

Recent studies have used new and innovative cell delivery systems that maximize the efficacy of MSC therapy for nonhealing cutaneous wounds. Tam et al. evaluated the use of a wound dressing patch made up of an aloe vera-polycaprolactone nanoscaffold impregnated with hWj-MSCs or its conditioned medium (CM) for enhanced healing of excisional and diabetic wounds *in vitro* and *in vivo*. They previously reported that hWj-MSCs or its conditioned medium alone without a scaffold enhanced healing of excisional and diabetic wounds [184]. Histological examination of wound biopsies in groups treated with hWj-MSCs or its CM on days 7 and 14 showed the formation of stratified squamous epithelium, increased numbers of sebaceous glands and hair follicles and greater cellularity and vasculature compared to controls. Immunohistochemistry of excisional and diabetic murine wound biopsies showed the presence of human keratinocyte markers such as cytokeratin, involucrin, and filaggrin. Moreover, the gene expression profiles showed the upregulation of ICAM-1, TIMP-1, and VEGF-A compared to controls favoring cell adhesion, increased angiogenesis and epithelialization during wound healing. Finally, high concentrations of proteins comprising the ECM, i.e., fibronectin that provides fibroblast migration, and collagen and elastin that give tissue strength and resiliency, were produced, suggesting their contribution to the wound healing process [106].

Sabapathy et al. have shown that combinational therapy of Wj-MSCs and decellularized amniotic membrane scaffold had the best regeneration according to the histomorphologic Singer's classification to quantify cutaneous scars after burns. The results also showed that the Wj-MSCs labeled with fluorescence probes were tracked successfully *in vivo* for around 10 days. Furthermore, the analysis of the biomechanical properties of the regenerated skin tissue demonstrated that biomechanical property of the Wj-MSCs/scaffold was better compared to other groups including Wj-MSCs injected tissue [61]. The enhanced efficiency of wound healing in the two treatment groups (hWj-MSC-SF and hWj-MSCs-SF+Edge) of the present study may be attributed to the synergistic effect of the stem cells and nanoscaffolds, where the nanoscaffold provided the stem cell niches and porosity for the Wj- MSCs to attach,

differentiate and allow its secretions to penetrate into the wound beds.

The wound healing potential of Wj-MSCs was assessed by classical histopathological staining techniques (i.e., H-E, and Masson's trichrome staining) and immunohistopathological examination of the skin at different time points after performing the wound. After analyzing all skin samples, significant differences regarding wound healing can be found between the experimental groups. The groups of mice treated with hWj-MSCs injected at the wound edge or SF scaffolds cellularized with hWj-MSCs (hWj-MSC-SF), or both treatments healed better compared to controls (i.e., wounds treated with Linitul® or SF scaffold without MSCs).

Best quality of scarring regarding mobility and aesthetic appearance could be attributed to the group of wounds treated with the hWj-MSC/SF scaffold at one month since the epithelial sheet and the dermis were apparently thinner compared to other groups. Nevertheless, wounds treated with both hWj-MSC/SF scaffold and hWj-MSCs injected at the wound edge had more histological similarities with normal skin. As mentioned earlier, the newly formed dermis of these mice was made of a dense and irregular connective tissue whose collagen fibers were disposed in a disorganized fashion that resembled the mesh-like pattern seen in the dermis of the normal skin. Also, the transitory presence of skin appendages such as hair follicles in the dermis after three weeks of injuring makes it structurally comparable to the normal skin even when at one month only degenerating appendages were present.

The histological study of regenerated wound tissue three weeks post-injury demonstrated the striking presence of skin appendages such as hair follicles into the dermal layer of the skin in mice receiving the combined treatment. Some considerations should be taken into account when analyzing the origin of the hair follicles in the Wj-MSC-SF+Edge group. First, the presence of hair follicles could be related to some effect exerted by the MSCs during wound healing since appendages were not present in the control groups. That means that Linitul® and SF scaffolds are not able on their own to stimulate the emergence of skin appendages.

The theory of transdifferentiation of hWj-MSCs into skin appendages (here into hair follicles) is not discarded at all considering that MSCs can differentiate into any cell type under certain conditions. It is hard to think that the hair was of murine origin since SKH1 mice lose their hair during growth and then manifest rudimentary hair follicles most of which form cysts. On the other hand, the size of the hair did no correspond to the normal dimensions of the appendage in mouse skin. As shown in Figure 4.21 (52), the hair follicle was very large compared to the size of the other structures that make up the skin and also it was located in the area of skin that had been newly regenerated.

Regarding the speed of healing, wounds treated with SF scaffolds alone or in combination with hWj-MSCs showed a delay in the formation of the epithelial sheet of the skin during the first two weeks of healing. Moreover, the SF scaffold may slow the process of granulation tissue maturation. On the contrary, wounds treated with Linitul® and those treated with hWj-MSCs injected at the wound edges had completely re-epithelialized after two weeks of injuring, and the granulation tissue in the dermis was formed by a mature, dense, and regular connective tissue. Maturation of the granulation tissue was completed at three weeks in all cases, except for the control group treated with Linitul®, in which the healing process was faster and ended earlier. Nevertheless, the wound healing process in this group of mice finished with the formation of scar tissue that was thick and possessed structural characteristics that made it less mobile and aesthetics with respect to the other groups.

Healing by connective tissue starts with the formation of granulation tissue. It consists of new capillaries (neovascularization) in an edematous environment of fibroblasts, myofibroblasts, mononuclear inflammatory cells, macrophages, neutrophils, and cellular debris. Collagen fibers are aligned following the course of fibrin and the newly formed blood vessels so that the more dispersed the vessels are greater disorganization/destructuration will have the connective tissue. Then, the maturation of granulation tissue will replace the damaged area with a scar.

The presence of the SF scaffold and the continuous inflammatory infiltrate, generated with the intention to remove it from the wound site, promotes the formation of new blood vessels which could delay the reorganization of connective tissue during the healing process. This phenomenon was particularly evident in the group treated with SF scaffolds before three weeks post-wounding. Thus, the group of wounds treated with hWj-MSCs injected at the edge lack of any scaffold covering the wound bed and, therefore, had the added advantage of prompt formation of the epithelial sheet. However, the wound healing process in the group of wounds treated with the cellularized SF scaffold ended with the formation of a very thin dermal layer whose collagen fibers arranged more loosely giving the scar tissue less stiffness and more resemblance to normal skin.

Although several reports have proved some efficacy for MSCs, it is still controversial whether MSCs can contribute significantly to regenerate damaged tissue via tissue-specific transdifferentiation. This may be explained, at least in part, by the poor viability of the transplanted cells. Furthermore, a suitable microenvironment to promote specific transdifferentiation might be strictly provided, so that MSCs local application without additional treatment failed to form a biologically complete

tissue. Physiological accumulation of enough MSCs might induce further cell type differentiation, resulting in the better functional organization of the wounded tissue [181].

In our case, accumulation of MSCs, predominantly delivered by applying cellularized SF scaffolds to the specific tissue might be one of the efficient strategies for tissue regeneration. Wounding stimulated the engraftment of Wj-MSCs to the skin and induced them to incorporate into and differentiate into skin structures. Other explanations of the effect of Wj-MSCs application might be due to the release of soluble factors that regulate inflammation and angiogenesis. Fong et al. have postulated that the introduction of soluble bioactive molecules into wounds via the hWj-MSC-conditioned medium and secretion of the same molecules by the engrafted hWj-MSCs creates a niche for the recruitment of native skin MSCs and progenitor cells to the wound site to facilitate healing [184].

In the present study, the Wj-MSCs-SF and Wj-MSCs-SF+Edge groups displayed noticeable better wound healing compared to controls suggesting that direct and indirect mechanisms of wound healing may taking place by directed differentiation of Wj-MSCs into keratinocytes and indirectly by the release of important bioactive molecules that initiate and facilitate the host response to tissue repair.

Several animal transplantation studies have shown that MSCs can differentiate into cells of the residing tissue, repair tissue damaged by trauma or disease, and partially restore its normal function. During the proliferative phase of wound healing process, native MSCs are recruited to differentiate into new keratinocytes [185].

The potential of MSCs to differentiate into skin tissue cells has been extensively described [130, 186, 187, 181], albeit there are many issues still to be addressed with respect to the use of these cells for skin regeneration, not least of which are the concerns that adnexal structures are generally not found in the reconstituted epithelium. Even though, the work of Sasaki et al. indicated the possibility of trans-germ line differentiation of MSCs in this regard. Sasaki's research group injected BM-MSCs, derived from GFP transgenic mice, into the tail vein of back skin-injured mice and showed that MSCs had the capacity to differentiate into multiple skin cell types including keratinocytes, endothelial cells, pericytes, and monocytes [181].

Several studies have also shown that human umbilical cord MSCs could enhance the healing of mice skin defect wounds and that the implanted MSCs could differentiate into keratinocytes when administered locally into the wound beds [188]. Similar results have been observed in a murine excisional injury model, in which mouse BM-MSCs accelerated wound closure by increasing re-epithelialization, cellularity and by differentiating directly into epithelial cells expressing keratin, a keratinocyte-

specific protein. In addition, wounds treated with MSCs appeared to have increased numbers of skin appendages and formed glandular structures, suggesting a direct contribution of BM-MSCs to cutaneous regeneration [130].

In turn, Ma et al. showed that allogeneic BM-MSCs seeded onto a nanofiber matrix and applied to full-thickness excisional wounds in rats significantly increased the rate of wound closure. Besides, BM-MSCs (labeled with fluorescent quantum dots) were found to colocate with the expression of the epithelial cells-specific markers keratin 10 and filaggrin after wound closure, which suggested that BM-MSCs had undergone epidermal differentiation at the early and intermediate differentiation stages [189].

In this study, immunostaining for CD90 on human MSCs showed that cells from the Wharton's jelly of the umbilical cord were engrafted into the newly formed tissue and closely associated with other cells in the wound. While the SF scaffold could ensure better survival of MSCs into the wound site, $CD90^{+}$ cells were present at the wound site until the second week after the injury occurred, and then no hWj-MSCs were visualized in any of the groups. These cells appeared to acquire an epithelial-like phenotype, i.e., they shared the same round-cuboid shape typically displayed by epithelial cells, and unexpectedly were localized forming the migrating epithelial front. However, many $CD90^{+}$ cells kept their spindle-shaped morphology, in deeper areas of granulation tissue, suggesting that these cells may not only transdifferentiate into specialized skin cells but also participate in the healing process through other inherent stemness mechanisms. Strikingly, hWj-MSCs incorporated into skin appendages in the wound of mice treated with hWj-MSCs-SF+Edge at day fourteen. Thus, our results indicate that Wj-MSCs can contribute to cutaneous structures.

The repair functions of MSC are thought to involve the secretion of factors such as vascular endothelial growth factor (VEGF) or fibroblast growth factor (FGF) which could help prevent apoptosis, promote angiogenesis, assist in matrix reorganization, and increase the recruitment of circulating MSC [190]. One substantial benefit of including MSCs into three-dimensional tissue-engineered constructs is to promote angiogenesis throughout the scaffold, which allows for the transport of nutrients and reparative cell types that can remodel the scaffold [140].

Our data suggest that promotion of angiogenesis is one of the mechanisms by which Wj-MSCs enhanced wound healing in SKH1 mice. This fact was corroborated by the higher expression of CD31 marker observed in wounds that underwent stem cell-based therapy in comparison with the control group treated with Linitul®. Similarly, the use of silk fibroin scaffold onto the wound bed also promoted angiogenesis during the first two weeks of healing. This effect was maintained throughout the

healing process only when MSCs were associated with the scaffold.

Certainly, the increased vascularity of the Wj-MSCs-treated wounds, compared to controls, corroborates the findings of many researchers who have reported the angiogenic effects of human MSCs. However, equally important is the impact generated by the SF scaffolds in the wound site on the proliferation and migration of blood vessels within the biomaterial and the newly formed granulation tissue.

Ichioka et al. used a skinfold chamber of original design which visualized microcirculation following wound creation on the dorsal skin of the mouse to establish an *in vivo* experimental model to estimate angiogenesis. They used collagen matrix impregnated with murine bone marrow MSCs for the promotion of wound healing. Wounds treated with BM-MSCs showed an increased rate in the functional capillary density when compared to controls on days 3, 5 and 7 after the creation of the wound. This fact led the group to test this application in a patient with a chronic leg ulcer that was unhealed for over a year despite conventional therapy. BM-MSCs were obtained from her iliac crest, and a collagen matrix (TERDERMIS) was impregnated with the autologous MSCs suspension and applied to the debrided surface. Two weeks later well vascularised healthy granulation tissue had developed, and split-thickness skin was grafted onto it to close completely the wound. The patient remained free of complications for 1.5 years since treatment [191].

Another alternative method of delivering MSCs was described by Falanga et al. in an attempt to facilitate the translation of a cell-based wound healing therapy into clinical practice. They cultured autologous BM-MSCs and applied them up to four times to full-thickness wounds using a fibrin polymer spray system with a double-barreled syringe. This biologic wound dressing was sufficient to stimulate complete closure in diabetic mice, whereas controls remained in a chronic, non-healing state. Furthermore, tracking of green fluorescent protein $(GFP)^+$ MSC in mouse wounds showed GFP^+ blood vessels, suggesting that the applied cells may persist as well as act to stimulate the wound repair process through angiogenesis [101].

Similarly, Egaña et al. combined the use of a bioartificial collagen scaffold and a defined human mesenchymal cell line termed V54/2 in order to improve vascularization during dermal regeneration. The mesenchymal cells seeded in the scaffold were able to survive, proliferate, and secrete significant amounts of vascular endothelial growth factor (VEGF) and basic fibroblast growth factor (bFGF) during 2 weeks *in vitro*. Afterward, scaffolds with or without cells were transplanted into nude mice full skin defect model to induce dermal regeneration. After 2 weeks of transplantation, scaffolds seeded with V54/2 cells showed more vascularization during the dermal regeneration process than controls suggesting that combined use of MSCs

and bioartificial scaffolds may induce therapeutic angiogenesis during the scaffold-based dermal regeneration process [192].

Lee et al. observed an improvement in vascularity in patients with critical limb ischemia who had been treated with intramuscular injections of autologous adipose tissue MSCs (AT-MSCs). Clinical improvement occurred in 66.7% of patients together with a decrease in pain rating scales and claudication walking distance. Digital subtraction angiography before and six months after AT-MSCs implantation showed the formation of numerous vascular collateral networks across affected arteries. They had previously demonstrated that the proangiogenic action of adipose tissue-derived cells in hindlimb ischemia model of nude mice is mostly resulted from AT-MSC-derived paracrine factors including angiogenic and antiapoptotic factors, although a small fraction of transplanted cells is differentiated into endothelial cells [193].

Zebardast et al. harvested an MSC population from human umbilical cord perivascular tissue and then delivered these cells in a fibrin vehicle into skin defects in immune-compromised mice. Compared to fibrin-only controls, the introduction of human umbilical cord perivascular cells (hUCPVCs) within fibrin sealant provided a decrease in contraction of the wound, an increase in matrix deposition and wound strength, and rapid re-epithelialization of the wounds. They postulate that hUCPVCs may play both a structural role -maintaining the dermis, preventing wound collapse- and a paracrine role; eliciting increased vascularization and epithelial overgrowth [194].

Wu et al. studied the effect of BM-MSCs in wound healing by using an excisional wound splinting model. They found that injection around the wound and application to the wound bed of allogeneic BM-MSCs significantly enhanced wound healing in normal and diabetic mice compared with that of allogeneic neonatal dermal fibroblasts or vehicle control medium. BM-MSCs-treated wounds exhibited accelerated wound closure with increased angiogenesis. Immunohistological staining of tissue sections for the endothelial marker CD31 showed increased vasculature and capillarity density in BM-MSC-treated wounds at 7 and 14 days compared with vehicle medium-or fibroblasts-treated wounds. They also showed that BM-MSCs conditioned medium promoted endothelial cell tube formation and consequently proposed that MSCs could enhance angiogenesis through a paracrine effect. Real-time polymerase chain reaction and Western blot analysis revealed high levels of vascular endothelial growth factor and angiopoietin-1 and significantly greater amounts of the proteins in BM-MSC-treated wounds [130].

Li et al. demonstrated that bone-marrow-derived MSCs contribute to wound

healing of skin appendages. They co-cultured BrdU-labeled adult human BM-MSCs with heat-shocked confluent adult human-derived sweat gland cells (SGCs) *in vitro* and later intravenously injected into full-thickness skin wounds in rats. Immunoenzymatic double-staining showed that BrdU-labeled MSCs were incorporated into SGC layers, and some BrdU-labeled human MSCs were also positive for the SGC markers, CK19 and CEA. The *in vivo* results revealed $BrdU^+$ MSCs into skin structures, such as blood vessels, hair follicles, sebaceous glands, and dermis in full-thickness wounds. After wound healing, some labeled MSCs returned to the bone marrow, whereas other were retained in the dermis [187].

The key cellular mediator of fibrosis is the myofibroblast, which when activated serves as the primary collagen-producing cell. Myofibroblasts are generated from a variety of sources including resident mesenchymal cells, epithelial and endothelial cells in processes termed epithelial/endothelial-mesenchymal (EMT/EndMT) transition, as well as from circulating fibroblast-like cells called fibrocytes that are derived from bone-marrow stem cells. Activated fibroblasts transform into α-SMA-expressing myofibroblasts as they migrate along the fibrin lattice into the wound. Following activation, the myofibroblasts promote wound contraction, the process in which the edges of the wound migrate towards the center. The reversal of experimental tissue fibrosis *in vivo* has been highly correlated with a decreasing expression of profibrotic mediators type I collagen and α-SMA [195].

In our study, the α-SMA expression was examined by immunohistochemical staining to determine whether Wj-MSCs have an influence on the expression of this protein. Immunohistochemical staining of α-SMA was strongly detected during the first two weeks of healing in wound areas of the control group treated only with the SF-scaffold and the group treated with MSCs injected around the wound margins. It is striking that MSCs transplanted by applying cellularized SF patches onto the wound bed resulted in a scarce arrangement of the collagen, similar to normal skin collagen distribution. Besides, α-SMA-positive cells in this group were less detectable by day 14 after wounding. By contrast, when applied separately Wj-MSCs or silk fibroin scaffolds, increased α-SMA-positive cell expression was seen at day 14. Therefore, Wj-MSCs appear to promote the production of an ECM that more closely resembles uninjured dermal tissue.

Similarly, Huang et al. found that wounds treated with MSCs delivered by microspheres had reduced the thickness of collagen fibrils that were well-organized in a basket-weave pattern after 14 days. Also, the expression of type I collagen and α-SMA was downregulated in MSCs treatment groups and significantly decreased in wounds with MSCs delivered by microspheres. Besides, their results suggested that

MSCs could exert the suppressive effect on the inflammatory cytokine-induced excess proliferation of fibroblasts by releasing growth factors that reduce scar formation in the skin such as HGF and TGF-β3 [196].

The influx of neutrophils and macrophages during the inflammatory phase after damage to tissues is important for both clearing the wound from invading microbes but also for producing wound growth factors and cytokines signals that are important for the repair process. Martin et al. reported wound healing studies in PU.1 null mouse, which is genetically incapable of setting up the normal inflammatory response due to lack of macrophages and functioning neutrophils. They showed that PU.1 null mice were able to heal skin wounds with similar time course to wild-type siblings. Moreover, PU.1 null wounds had a more mature, repaired keratinocyte epidermal layer, overlaying a fairly well-organized wound connective tissue (with not apparent inflammatory cells or apoptotic cell corpses) that is quite similar to that present in the adjacent unwounded dermis. Besides, it was shown by transmission electron microscopy that cell and matrix debris were engulfed and removed by stand-in fibroblast phagocytes in PU.1 null wounds, which was also associated with an enhanced angiogenic response. The absence of inflammatory cells was also responsible for the modified profile of growth factor and cytokine signals present at the wound site, which was associated with scarce matrix deposition and scar contracture post-repair. These data strongly suggested that the inflammatory response not is entirely necessary for efficient tissue repair and might be causal of fibrosis at sites of adult healing [197].

We also studied whether the immunoregulatory properties that characterized Wj-MSCs *in vitro* had a biological effect on the experimental murine model of wound healing. Local modulation of the cellular inflammatory response, demonstrated by a low number of PMN and macrophages, at the wound site of mice treated with Wj-MSCs might be a beneficial therapeutic strategy for management of tissue repair since it is associated with reduced scar formation and the replacement of damaged tissue with equally functional skin. This study corroborated previous findings that xenograft MSCs elicit little immunogenicity from their host [99, 198], and indicate that MSCs are immunoprivileged during cutaneous wound healing.

Shumakov et al. showed that the transplantation of autologous and allogeneic bone marrow mesenchymal stem cells on the surface of deep burn wounds in rats decreases inflammatory cell infiltration into the wound and accelerates the formation of new vessels and granulation tissue in comparison with burn wounds without cell transplantation. The regeneration process was most active after the transplantation of autologous cells, which was confirmed by a more rapid decrease in burn

surface area. Wound healing after transplantation of BM-MSCs was associated with the long functioning of transplanted cells, as was shown that transplanted cells remained viable on the surface and in the depth of regenerating wounds throughout the observation period [199].

Neutrophils are not often found in normal skin, but they are quickly recruited in high numbers within 24-48 hours following injury. They are the first circulating inflammatory cell to move to the site of the wound, probably due to their function of defense against infections. The immune reaction to an implant begins with an acute response to the injury and innate recognition of foreign materials, with the subsequent chronic immune response involving specific recognition of antigens (e.g., transplanted cells) by the adaptive immune response, which can eventually lead to rejection of the implant.

Biomaterials aim to create a local environment to promote tissue growth; however, both the injury incurred during the implantation process and the host inflammatory response to the implanted material can negatively impact this local environment. This response can lead to the repair of the injury site through repopulation with granulation tissue that can result in fibrosis while regeneration by local progenitor cells can produce fully functional tissue. An immune response immediately follows tissue injury, which can have a large impact on whether the wound is merely repaired or regenerated [200].

Normally, the epithelial sheet is completed formed two weeks after the wound occurs, as demonstrated by the H&E and Masson-Goldner trichrome Stains of wound tissues in mice treated with Linitul®. When the silk fibroin scaffold was present in the wound bed, re-epithelialization was delayed about a week, and granulation tissue maturation took longer to be reached. Therefore, the enhanced and prolonged innate immune response of the body against the biomaterial would justify the temporary presence of greater number of polymorphonuclear neutrophils in the wound tissue. Once the Wj-MSCs are transplanted to the wound site either associated with the scaffold or injected at the wound edge, the immune response against them is importantly diminished. A quick resolution (two weeks) to this chronic cellular presence at the tissue-material interface is often compatible with implant acceptance while persistence of a large immune cell presence often indicates infection and/or rejection of the implant [200].

An understanding of the foreign body reaction is important as it may impact the biocompatibility (safety) of the implanted biomaterial and may significantly impact short- and long-term tissue responses with tissue-engineered constructs containing proteins, cells, and other biological components for use in tissue engineering and

regenerative medicine [201].

Macrophages appear at the site of injury within 48-96 hours in response to chemoattractants such as TGF-β, which is produced primarily by platelets. In our study, the number of macrophages in wounds treated with SF scaffold remained lower in comparison to control wounds treated with Linitul®. The huge difference observed between both groups was probably due to the easy degradation by macrophages of silk fibroin fibers forming the scaffold compared to the fibrin mesh that is shaped during the normal healing process. As shown in Fig. 4.26 (e-h), macrophages were still present in the wound tissue one month after wounding. Thereby, it is important that macrophages be kept until the healing process has ended since they are necessary for the reorganization of the granulation tissue.

Once again, the combination of Wj-MSCs with the SF-scaffold limited importantly the influx of macrophages to the wound site in comparison with the control groups. This effect could be due to the immunomodulatory effect referred to MSCs and previously demonstrated here by *in vitro* assays. On the whole, it is evident that the MSCs exert an immunomodulatory role over the cellular components of innate immunity response generated during the inflammatory phase of wound healing. This regulating action over the immune system seems not to involve adaptative T cell-mediated immunity, as demonstrated by the noteworthy existence of T-CD3 cells during the first two weeks of healing. In any case, further investigation is needed to elucidate the interactions between Wj-MSCs and the various immune and wound healing cell types that are present in the wound bed, as these studies would be useful to optimize the timing and dosage of MSC delivery to the wound for maximal efficacy.

Histopathological examination of distant organs of mice receiving MSCs therapy revealed certain affections such as acute interstitial inflammatory infiltrates in lungs, scarce hepatic microabscesses, and hyperplasia of the white pulp in the spleen. Nevertheless, they were not common for all mice and were negative for CD90 immunoexpression. In addition, no clinical or paraclinical manifestations were seen throughout the healing process and human Wj-MSCs transplanted into the wound bed did not experience abnormal proliferation or formed teratomas and/or tumors.

Finally, analysis of biodistribution of transplanted Wj-MSCs did not show the presence of the cells in any examined organs. Thus, xenotransplant of human Wharton's jelly MSCs in SKH1 mice proved to be safe and effective for the treatment of skin wounds.

On the whole, the data suggested that the combined treatment of MSCs injected at the wound edge along with cellularized SF scaffolds covering the wound site

exhibited better wound healing capabilities compared to both single treatments and control groups. Therefore, Wj-MSCs delivered in an SF scaffold onto the wound bed contributed to the generation of a high-quality, well-vascularized granulation tissue, enhanced re-epithelialization of the wound, and attenuated the formation of fibrotic scar tissue. In conclusion, we propose al least two possibilities by which Wj-MSCs may improve wound healing. First, Wj-MSCs have the capacity to secrete a variety of growth factors and cytokines either constitutively or upon stimulation, which are relevant to tissue repair and regeneration. The production of these soluble mediators by Wj-MSCs could complement endogenously produced growth factors and cytokines that regulate cellular processes such as chemotaxis, cell proliferation, cell signaling, extracellular matrix formation and angiogenesis in the wound. The second possibility relates to the extraordinary plasticity and the ability of MSCs to differentiate into a variety of cell types and integrate into tissues as described by McFarlin et al. [202].

Thus, Wj-MSCs may facilitate wound healing by trans-differentiating into keratinocytes or glandular cells. Although our data showed localization of topically administered Wj-MSCs to the wound, they did not directly addressed whether local growth factor production and integration of Wj-MSCs into wound tissue were part of the mechanisms by which these cells improve wound healing. Therefore, more rigorous investigations are needed to substantiate the role of growth factor production and differentiation of Wj-MSCs into cellular components of the wounds. Nowadays, Wharton's jelly MSCs are being commercially collected and stored for preclinical works. We expect that the combination of human Wj-MSCs and SF scaffolds could be considered as improved therapy to accelerate skin wound healing especially refractory, common therapy-resistant skin ulcers.

Chapter 6

CONCLUSIONS

1. The explant method proved to be an efficient method for the isolation of mesenchymal stem cells from the Wharton's jelly of the human umbilical cord.

2. Human Wharton's jelly mesenchymal stem cells have greater growth potential than bone marrow mesenchymal stem cells and possess a limited capacity to differentiate into mature mesodermal cell lines.

3. Wharton's jelly MSCs have reduced immunogenicity, did not express costimulatory molecules, and express cytokines that may modulate immune function. The immunosuppressive effects on T lymphocytes proliferation induced by allogeneic mDCs or CD3/CD28 beads stimulation are mediated by the secretion of the anti-inflammatory factors TGF-β, PGE2 and IDO and by inhibiting the production of the pro-inflammatory cytokine IFN-γ. Together, these results suggest that human Wj-MSCs could be immuno-tolerated after their allogeneic transplantation.

4. Electrospun silk fibroin scaffolds are suitable from both the morphological (fiber size and porosity)/structural (stability), and biological (cytocompatibility) point of view to be used as tissue engineering matrices in tissue regeneration of skin.

5. The excisional wound splinting model created in SKH1 mice allowed to study the mechanisms underlying wound healing after the implantation of cellularized silk fibroin patches or the injection of Wj-MSCs into the wound edges. This SKH1 mice skin injury model suggests that combination of electrospun silk fibroin scaffolds along with Wj-MSCs can be efficiently used to treat the skin injury.

6. Wharton's jelly mesenchymal stem cells combined with silk fibroin scaffolds in the wound bed contributed to the generation of a high-quality, well-vascularized granulation tissue, enhanced re-epithelialization of the wound, and attenuated the formation of fibrotic scar tissue. Wj-MSCs could transdifferentiate into epidermal cells, keratinocytes, and microvascular endothelium, therefore they seem to promote the production of an ECM that more closely resembles uninjured dermal tissue.

7. Wharton's jelly from the human umbilical cord may be an adequate source for obtaining mesenchymal stem cells for wound healing given its several advantages and together with the synergistic benefits of a nanoscaffold they make ideal combinations as wound dressings for slow healing and hard-to-heal chronic wounds.

Chapter 7

ABSTRACT

Introduction: The skin is the largest organ in the human body and forms a self-renewing and self-repairing interface between the body and the environment. Cutaneous wounds are the result of disrupted skin integrity [1]. Wound healing is a dynamic, interactive biological process involving soluble mediators, blood cells, extracellular matrix proteins, and parenchymal cells. The purpose of wound healing is to repair the skin to prevent infection and to restore the tissue integrity and function.

Wound healing consists of three distinct and overlapping phases: inflammation, cell proliferation (neoangiogenesis, granulation, and re-epithelialization), and a remodeling phase (extracellular matrix remodeling). Standard treatment of chronic wounds is commonly addressed to modify controllable causative factors, but so far no ideal therapy is available to treat troublesome chronic wounds. Mesenchymal stem cells are emerging as a promising candidate for cell-based therapy for the treatment of chronic wounds because of their enormous potential for enhancing tissue repair and regeneration following injury.

Bone marrow MSCs are usually considered as a gold standard and the most investigated mesenchymal stem cell source. However, the use of MSCs obtained from bone marrow exposes the donor to a painful and invasive procedure, leading to the use of non-invasive and ethically non-problematic sources. Thus, MSCs obtained from ethically approved sources that otherwise would be discarded in hospitals are also used in studies, considering their multiple properties [56].

From the different available sources of MSCs, the umbilical cord represents a cost-effective, productive, feasible, accepted, and non-invasive method to isolate MSCs, and is considered advantageous compared with bone marrow and adipose-derived MSCs for some researchers [141].

Mesenchymal stem cells have immune avoidance mechanisms that reduce im-

munogenicity that is necessary to avoid the acute rejection response by the host following xenogeneic transplantation. Hypoimmunogenicity of MSCs confers a critical advantage in their use for cell therapy. Furthermore, MSC immunomodulation takes place over a multistage process involving (1) MSC responsiveness to inflammation and possible migration to the site of tissue injury, (2) licensing or activation of MSCs, (3) promotion of pathogen clearance if required and (4) modulation of inflammation [77].

The rapidly developing fields of stem cell biology and skin tissue engineering have created translational opportunities for the development of novel stem cell-based wound healing therapies that show promising results in preclinical and clinical trials for the treatment of chronic wounds.

Both topical and systemic MSCs delivery methods have been shown to be effective for wound healing. While systemic delivery of MSCs has been shown to deposit cells at the injury site, cell engraftment and survival, have been limited. This has led to the majority of studies looking at novel cell delivery systems to enhance wound healing [55].

Several different biosynthetic scaffolds have been used alone or in combination with cells to treat wounds. Among the various scaffolds employed, silk fibroin cellularized with MSCs from different sources has been shown to be effective in repairing experimental wounds of the skin [145].

Electrospun silk fibroin scaffolds have two distinctive characteristics that make them very appropriate for tissue engineering. First, the morphology and architecture of the electrospun structure is similar to those of some natural extracellular matrix (ECM) in the skin that are composed of randomly oriented collagens of nanometer-scale diameters. Second, the scaffold structure changes dynamically over time, as the polymer nanofibers degrade allowing the seeded cells to proliferate and produce their own ECM [118].

Given their mesenchymal phenotype and easy isolation, we hypothesized that human Wj-MSCs may constitute an alternative source of cells for dermal wound healing as they avoid the inherent sourcing limitations displayed by human BMMSCs. In this study, we pretended to investigate the behavior of Wj-MSCs both *in vitro* and *in vivo* when cultivated on electrospun silk fibroin scaffolds and implanted in immunocompetent mice. Thus, the purpose of the present study was to determine whether Wj-MSCs delivered in silk fibroin scaffolds into skin defects in SKH1 mice would contribute to dermal wound healing.

Objectives

General: Standardize the protocol for the isolation and characterization of

human Wharton's jelly mesenchymal stem cells and investigate its therapeutic effect on cutaneous wound healing process in mice.

Specific:

1. To standardize the explant method for the isolation of mesenchymal stem cells from the Wharton's jelly of the human umbilical cord.

2. To characterize the Wharton's jelly mesenchymal stem cells regarding its differentiation capacity, immunophenotype, proliferation kinetics, and immunomodulatory properties.

3. To test the ability of a three-dimensional nanofibrous scaffold fabricated by electrospinning of silk fibroin to support the growing and spreading of human Wharton's jelly MSCs and its use in wound healing.

4. To assess the effect of Wharton's jelly mesenchymal stem cells in cutaneous regeneration by using the excisional wound splinting model in SKH1 mice.

5. To perform an histological and immunohistochemical study of the wound healing process in the transplanted mice, regarding inflammation, re-epithelialization, granulation tissue formation, angiogenesis and remodeling of the wound. Furthermore, to test the safety and biodistribution of the locally implanted human Wj-MSCs in the murine model of wound healing.

Methodology: In this study, we have first standardized the protocol for the isolation and characterization of MSCs derived from the Wharton's jelly of the human umbilical cord. Further, these MSCs along with the combination of silk fibroin scaffolds were used to test their wound healing properties by creating skin wounds in an experimental murine model.

Human umbilical cords were collected after obtaining informed consent from patients undergoing full-term pregnancy elective caesarean section. Wj-MSCs were isolated from explants and then expanded following the standard *in vitro* culturing protocols.

For the characterization of Wj-MSCs, differentiation analysis was carried out to demonstrate that these cells possess mesodermal plasticity under *in vitro* conditions. In addition, proliferation kinetics of Wharton's jelly was stimated by determining the population doubling levels and population doubling time, and compared to that displayed by BM-MSCs. Also, MTT assay was performed to determine the metabolic activity of the MSCs.

MSCs from the Wharton's jelly of the umbilical cord were compared to bone marrow-derived MSCs regarding the T-cell proliferation inhibition potential after

stimulation with allogeneic mDCs or CD3/CD28 coated beads. Besides, cytokines released by the MSCs were quantified in the supernatants of MLCs.

Silk fibroin scaffolds were made by the Department of Biotechnology (IMIDA) by following the protocol previously described by Aznar-Cervantes et al. [162]. Analysis of expression of MSC surface markers by flow cytometry and cell viability analysis were performed to discard possible cytotoxic effects of silk fibroin scaffolds on Wj-MSCs.

Two groups of seventy-five mice each group were divided into five different subgroups (n=15), based on the type of treatment applied, i.e., Group 1: wounds covered by Linitul®; Group 2: wounds covered by silk fibroin scaffolds; Group 3: wounds treated with Wj-MSCs injected at the edge (Wj-MSCs Edge); Group 4: wounds treated with silk fibroin patches cellularized with Wj-MSCs (Wj-MSCs-SF); and Group 5: wounds treated with Wj-MSCs injected at the edge along with silk fibroin patches cellularized with MSCs covering the wound site (Wj-MSCs-SF + Edge). Every subgroup underwent the sacrifice of three mice at different times, i.e., 48 hours, 7 days, 14 days, 21, and 28 days.

A chronologic histological and immunohistochemical analysis of wound samples from all experimental groups was carried out to determine the changes produced *in situ* after the inclusion of silk fibroin scaffold and/or Wharton's jelly MSCs during the skin regeneration process.

Results: Cells isolated from the Wharton's jelly of the umbilical cord exhibited a fibroblastic morphology and displayed MSC surface markers uniformly positive for CD90, CD105, CD73 with no detectable presence of hematopoietic cells markers, suggesting that they belonged to the MSC family. Moreover, Wj-MSCs were limited with respect to their ability to differentiate into adipocytes, chondrocytes, and osteoblasts.

The proliferation analysis performed in this study revealed that MSCs from the umbilical cord were highly proliferative whereas the growth potential of BM-MSCs was significantly lower. Such proliferation characteristics did not change even after ten passages, unlike BM-MSCs that increased the PDT from passage nine.

Wharton's jelly MSCs suppressed T cell proliferation after stimulation with anti-CD3/CD28 coated beads and allogeneic mDCs. This effect was dose-dependent, and maximal inhibition was achieved when mononuclear cells and MSCs were cultured in a 1:1 ratio. Wharton's jelly MSCs downmodulated the *in vitro* production of the pro-inflammatory cytokine IFN-γ by activated T lymphocytes. This immunosuppressive effect was also mediated by the production of the anti-inflammatory cytokines TGF-β, IDO, and PGE2. MLCs experiments in the presence of different specific inhibitors

of the biosynthesis or signaling of these anti-inflammatory factors such as SB-431542, indomethacin (IDM) or 1-methyl-tryptophan (1-MT), respectively, recovered almost entirely the proliferation rate of mDCs-stimulated T cells.

Wj-MSCs seeded on silk fibroin scaffolds maintained a spindle-shaped morphology and did not show any change in the cell surface marker expression profile. Therefore, the electrospun SF scaffold cellularized with Wj-MSCs were found to be suitable as a skin substitute. Treatment of skin injury of SKH1 mice model demonstrated that combination of Wj-MSCs and silk fibroin scaffold exhibited significantly better wound-healing capabilities, and contributed to the generation of a high-quality, well-vascularized granulation tissue, enhanced re-epithelialization of the wound and reduced the formation of fibrotic scar tissue, ending in a better aesthetic appearance of regenerated skin compared to Wj-MSCs alone.

Analysis of biodistribution of transplanted Wj-MSCs did not show the presence of cells in any examined organs, and besides these cells did not experience abnormal proliferation or formed teratomas and/or tumors.

Conclusions: The explant method proved to be an efficient method for the isolation of MSCs from the Wharton's jelly of the human umbilical cord.

Human Wharton's jelly MSCs have greater growth potential than bone marrow MSCs and possess a limited capacity to differentiate into mature mesodermal cell lines.

Wharton's jelly MSCs have reduced immunogenicity, did not express costimulatory molecules, and express cytokines that may modulate immune function. The immunosuppressive effects on T lymphocytes proliferation induced by allogeneic mDCs or CD3/CD28 beads stimulation are mediated by the secretion of the anti-inflammatory factors TGF-β, PGE2 and IDO and by inhibiting the production of the pro-inflammatory cytokine IFN-γ. Together, these results suggest that human Wj-MSCs could be immunotolerated after their allogeneic transplantation.

Electrospun silk fibroin scaffolds are suitable from both the morphological (fiber size and porosity)/structural (stability), and biological (cytocompatibility) point of view to be used as tissue engineering matrices in tissue regeneration of skin.

The excisional wound splinting model created in SKH1 mice allowed to study the mechanisms underlying wound healing after the implantation of cellularized silk fibroin patches or the injection of Wj-MSCs into the wound edges. This SKH1 mice skin injury model suggests that combination of electrospun silk fibroin scaffolds along with Wj-MSCs can be efficiently used to treat the skin injury.

Wharton's jelly MSCs combined with silk fibroin scaffolds in the wound bed contributed to the generation of a high-quality, well-vascularized granulation tissue,

enhanced re-epithelialization of the wound, and attenuated the formation of fibrotic scar tissue. Wj-MSCs could transdifferentiate into epidermal cells, keratinocytes, and microvascular endothelium, therefore they seem to promote the production of an ECM that more closely resembles uninjured dermal tissue.

Wharton's jelly from the human umbilical cord may be an adequate source for obtaining MSCs for wound healing given its several advantages and together with the synergistic benefits of a nanoscaffold they make ideal combinations as wound dressings for slow healing and hard-to-heal chronic wounds.

Chapter 8

RESUMEN

Introducción: La piel es el órgano más extenso del cuerpo humano y forma una interfase entre el cuerpo y el medio ambiente, que se autorenueva y regenera [1]. Las heridas cutáneas son producto de la ruptura de la integridad de la piel. La cicatrización de heridas es un proceso biológico dinámico que implica mediadores solubles, células sanguíneas, proteínas de la matriz extracelular y células del parenquima. La finalidad del proceso de cicatrización de heridas es reparar la piel para evitar la aparición de infecciones y restaurar la integridad y función del tejido.

El proceso de cicatrización consiste en tres fases distintas que se solapan entre sí: inflamación, proliferación celular (neoangiogénesis, formación de tejido de granulación y re-epitelización) y una fase de remodelado (remodelado de la matriz extracelular). El tratamiento estándar de las heridas crónicas está dirigido a modificar los factores que originan las mismas, sin embargo no existe un tratamiento ideal para tratar heridas crónicas de difícil cicatrización. Las células mesenquimales (MSCs) están emergiendo como fuertes candidatas para ser usadas como terapia celular en el tratamiento de heridas crónicas, dado su enorme potencial para mejorar la reparación y regeneración de los tejidos posterior a una lesión.

Las MSCs de la médula ósea (BM-MSCs) son consideradas el modelo de referencia y siguen siendo las células más investigadas hasta el momento. Sin embargo, el uso de MSCs obtenidas de la médula ósea requiere la realización de un proceso invasivo que resulta doloroso e implica riesgos para el donante, lo que ha conllevado al uso de otras fuentes de MSCs que no están relacionadas con procesos invasivos ni generan problemas de carácter ético para su obtención [56].

De las diferentes fuentes disponibles de MSCs, el cordón umbilical representa una fuente rentable, productiva, viable, aceptada, y no invasiva para aislar MSCs, y algunos investigadores consideran que tiene ventajas en comparación con MSCs provenientes de la médula ósea y del tejido adiposo [141].

Las MSCs tienen mecanismos de evasión inmune que reducen su inmunogenicidad evitando así la respuesta de rechazo agudo por el huésped después del trasplante xenogénico. La baja inmunogenicidad de las MSCs les confiere una ventaja importante en su uso para terapia celular. Además, la inmunomodulación que presentan las MSCs es un proceso que tiene lugar a través de múltiples etapas que implican: (1) la capacidad de respuesta de las MSCs a la inflamación y posible migración al sitio de la lesión tisular, (2) la activación de las MSCs, (3) promoción de eliminación de agente patógeno cuando es necesario, y (4) modulación de la inflamación [77].

El rápido desarrollo de los campos de la biología de las células madre y de ingenería tisular han creado una oportunidad en la medicina traslacional para el desarrollo de nuevas terapias para la cicatrización de heridas basadas en la utilización de células madre mostrando resultados prometedores en ensayos preclínicos y clínicos para el tratamiento de heridas crónicas.

Tanto los métodos de aplicación tópica como sistémica de MSCs han demostrado ser efectivos para la cicatrización de heridas. Aunque la aplicación sistémica de MSCs ha demostrado ser capaz de llevar las células hasta el lugar de la lesión, el injerto y la supervivencia de las células es limitada. Esto ha conllevado a la búsqueda de nuevos sistemas de administración de células para mejorar la cicatrización de heridas [55].

En la actualidad se han utilizado diferentes constructos biosintéticos, ya sean sólos o combinados con células, para el tratamiento de heridas. Entre los diversos constructos empleados, la fibroína de la seda celularizada con MSCs de diferentes fuentes ha demostrado ser eficaz en la curación de heridas experimentales de la piel [145].

Los constructos electrohilados de fibroína de la seda tienen dos características distintivas que los hacen muy adecuados para su utilización en ingeniería tisular. En primer lugar, la morfología y la arquitectura de la estructura electrohilada es similar a la observada en la matriz extracelular de la piel, la cual se compone de nanofibras de colágeno orientadas al azar. En segundo lugar, la estructura del constructo cambia dinámicamente con el tiempo, ya que las nanofibras del polímero se degradan permitiendo que las células sembradas proliferen y produzcan su propia matriz extracelular [118].

Dado su fenotipo mesenquimal y su facilidad de aislamiento, nuestra hipótesis es que las MSCs de la gelatina de Wharton del cordón umbilical humano (Wj-MSCs) pueden constituir una fuente alternativa de células para ser utilizadas en la cicatrización de heridas dado el hecho de que su uso no conlleva las limitaciones inherentes a las MSCs derivadas de la médula ósea. En este estudio pretendemos

investigar el comportamiento de las Wj-MSCs tanto *in vitro* como *in vivo* tras ser sembradas en un constructo electrohilado compuesto de fibroína de la seda y posteriormente implantado en ratones inmunocompetentes. Por lo tanto, el propósito del presente estudio fue determinar si las Wj-MSCs aplicadas mediante constructos de fibroína de seda en heridas creadas en el dorso de ratones SKH1 contribuyen a mejorar la cicatrización de la lesión.

Objetivo general: Estandarizar el protocolo de aislamiento y caracterización de las MSCs de la gelatina de Wharton del cordón umbilical humano e investigar su efecto terapéutico en el proceso de cicatrización de heridas en un modelo murino.

Objetivos específicos:

- Estandarizar el método de explante para aislamiento de las Wj-MSCs y posteriormente realizar la caracterización de las mismas en cuanto a su capacidad de diferenciación, inmunofenotipo, cinética de proliferación, así como el estudio de sus propiedades inmunomoduladoras.

- Estudiar la capacidad del constructo fabricado mediante electrohilado de fibroína de la seda para mantener el crecimiento y extensión de las Wj-MSCs y su uso para la cicatrización de heridas.

- Determinar el efecto de las Wj-MSCs en la regeneración cutánea usando para ello un modelo murino de heridas, realizando posteriormente un estudio histológico e inmunohistoquímico del proceso de cicatrización. Finalmente, estudiar la seguridad y biodistribución de las MSCs en los ratones transplantados.

Metodología: En este estudio inicialmente hemos puesto a punto el protocolo para el aislamiento y caracterización de las MSCs derivadas de la gelatina de Wharton del cordón umbilical humano. Posteriormente, estas MSCs en combinación con un constructo fabricado a partir de la fibroína de la seda fueron utilizados para probar sus propiedades terapéuticas en un modelo murino experimental de heridas.

Los cordones umbilicales de origen humano fueron recolectados luego de la obtención del consentimiento informado de pacientes con embarazo a término que iban a ser sometidas a cesárea. Las Wj-MSCs fueron aisladas mediante el método de explante y posteriormente fueron expandidas siguiendo los protocolos estándar de cultivo *in vitro*.

Para realizar la caracterización de las Wj-MSCs, se llevó a cabo un análisis de la capacidad de diferenciación de estas células para demostrar que tienen plasticidad mesodérmica bajo ciertas condiciones *in vitro*. Además, se analizó la cinética de proliferación mediante la determinación del número y tiempo de duplicación de la

población celular y se comparó con la mostrada por las MSCs de la médula ósea. Por otra parte, también se realizaron ensayos de MTT para determinar la actividad metabólica de ambas fuentes de MSCs.

Las MSCs mesenquimales derivadas del cordón umbilical fueron comparadas con las aisladas de la médula ósea en cuanto al potencial para inhibir la proliferación de linfocitos T tras ser estimulados con esferas conjugadas con anticuerpos anti-CD3/CD28, así como con células dendríticas maduras (mDCs) alógenicas. También se cuantificó mediante ELISA la producción de citokinas pro-inflamatorias y anti-inflamatorias en los sobrenadantes de los cultivos mixtos de linfocitos.

Los constructos de fibroína de seda fueron fabricados en el departamento de Biotecnología del Instituto Murciano de Investigación y Desarrollo Agrario y Alimentario (Murcia, España) siguiendo el protocolo descrito previamente por Aznar-Cervantes y colaboradores [163]. Además, se realizó mediante citometría de flujo el análisis de la expresión de marcadores de superficie mesenquimales y un estudio de viabilidad celular para descartar posibles efectos citotóxicos del constructo de fibroína de seda sobre las MSCs de la gelatina de Wharton.

Los experimentos *in vivo* fueron realizados en dos grupos de setenta y cinco ratones cada uno que a su vez fueron divididos en cinco subgrupos diferentes (n = 15), dependiendo del tipo de tratamiento aplicado sobre la herida. Es decir, el grupo 1, estuvo compuesto por los ratones cuyas heridas fueron cubiertas con Linitul®; en el Grupo 2 , las heridas fueron cubiertas por los constructos de fibroína de seda; en el Grupo 3, las heridas fueron tratadas con Wj-MSCs inyectadas en el borde de la herida (Wj-MSC Edge); en el Grupo 4, las heridas fueron tratadas con parches de fibroína de seda celularizados con Wj-MSCs (Wj-MSC-SF); y finalmente el Grupo 5, cuyas heridas fueron tratadas con Wj-MSC inyectadas en el borde junto con parches de fibroína de seda celularizados con MSCs que cubrían la zona de la herida (Wj-MSC-SF + Edge). Tres ratones de cada subgrupo fueron sacrificados a distintos tiempos, es decir, a las 48 horas, 7 días, 14 días, 21 y 28 días sucesivos a la realización de la herida. Posteriormente se llevaron a cabo análisis histológicos e inmunohistoquímicos de las muestras de las heridas de todos los grupos experimentales a lo largo del tiempo para determinar los cambios producidos *in situ* después de la inclusión del constructo de fibroína de seda y/o de MSCs de la gelatina de Wharton durante el proceso de regeneración de la piel.

Resultados: Las MSCs aisladas de la gelatina de Wharton del cordón umbilical mostraron una morfología fibroblástica, y presentaron en su superficie la expresión de marcadores mesenquimales que fueron positivos de manera uniforme para CD90, CD105, CD73, y sin presencia detectable de marcadores de células hematopoyéticas,

lo que sugirió que estas células eran de origen mesenquimal. Por otra parte, las Wj-MSCs mostraron una capacidad limitada para diferenciarse hacia adipocitos, condrocitos, y osteoblastos.

El análisis de la proliferación realizado en este estudio reveló que las MSCs procedentes del cordón umbilical fueron altamente proliferativas mientras que el potencial de crecimiento de las BM-MSCs fue significativamente menor. Tales características de proliferación no cambiaron incluso después de realizar diez pases, a diferencia de las BM-MSCs que aumentaron el tiempo de duplicación de la población a partir del pase 9.

Las MSCs de la gelatina de Wharton inhibieron de forma significativa la proliferación de células T tras ser estimuladas con esferas anti-CD3/CD28, así como con células dendríticas maduras alogénicas. Este efecto fue dosis-dependiente, consiguiéndose la inhibición máxima cuando las células mononucleadas y las MSCs se cultivaron en una proporción de 1: 1. Las MSCs de la gelatina de Wharton disminuyeron la producción *in vitro* de la citoquina pro-inflamatoria IFN-γ por los linfocitos T activados. Este efecto inmunosupresor también estuvo mediado por la producción de los factores anti-inflamatorios TGF-β, IDO, y PGE2. Los experimentos con cultivos mixtos de linfocitos en presencia de diferentes inhibidores específicos de la biosíntesis o la señalización de estos factores anti-inflamatorios tales como SB-431542, indometacina (IDM), o 1-metil-triptófano (1-MT) respectivamente, recuperaron casi en su totalidad el nivel de proliferación de las células T estimuladas con células dendríticas maduras.

Las Wj-MSCs sembradas sobre constructos de fibroína de seda mantuvieron una morfología fibroblástica y no mostraron ningún cambio en el perfil de expresión de marcadores de superficie celular. Por lo tanto, los constructos electrohilados de fibroína de seda celularizados con Wj-MSCs resultaron ser adecuados como un sustituto de la piel. El tratamiento de las heridas de la piel en ratones SKH1 demostró que la combinación de Wj-MSCs y el constructo de fibroína de la seda mejoró significativamente la capacidad de cicatrización de heridas, y contribuyó a la generación de un tejido de granulación bien vascularizado y de alta calidad, al aumento de la re-epitelización de las heridas y a la reducción de la formación de tejido cicatrizal, culminando en la formación de una piel regenerada con mejor aspecto estético en comparación con los animales tratados sólo con Wj-MSCs o los grupos controles.

El análisis de la biodistribución de las Wj-MSCs trasplantadas no mostró la presencia de células en ninguno de los órganos examinados tras el sacrifico de los ratones. Además, estas células no experimentaron proliferación anormal ni formaron

teratomas y/o tumores.

Conclusiones:

- El método de explante demostró ser un método eficaz para el aislamiento de MSCs de la gelatina de Wharton del cordón umbilical humano.
- Las MSCs de la gelatina de Wharton tienen mayor potencial de crecimiento que las células madre mesenquimales de la médula ósea y poseen una capacidad limitada para diferenciarse en líneas celulares mesodérmicas maduras.
- Las MSCs de la gelatina de Wharton del cordón umbilical humano son poco inmunogénicas, no expresan moléculas coestimuladoras, y expresan citoquinas que pueden modular la función inmune. Los efectos inmunosupresores sobre la proliferación de linfocitos T inducidos por mDCs alogénicas o esferas anti-CD3/CD28 están mediados por la secreción de los factores anti-inflamatorios TGF-β, PGE2 y IDO y la inhibición de la producción de la citoquina pro-inflamatoria IFN-γ. En conjunto, estos resultados sugieren que las Wj-MSCs podrían ser inmunotoleradas después de su trasplante alogénico.
- Los constructos electrohilados de fibroína de seda son adecuados tanto desde el punto de vista morfológico (tamaño de la fibra y porosidad) / estructural (estabilidad), y biológico (citocompatibilidad) para ser utilizado como matrices de ingeniería tisular en la regeneración de la piel.
- El modelo murino de herida creado en ratones SKH1 permitió estudiar los mecanismos subyacentes a la curación de heridas después de la implantación de los parches de fibroína de seda celularizados o la inyección de Wj-MSCs en los bordes de la herida. Este modelo sugiere que la combinación de constructos electrohilados de fibroína de seda junto con Wj-MSCs puede ser utilizada eficientemente para el tratamiento de lesiones de la piel.
- La combinación de MSCs de la gelatina de Wharton con los constructos de fibroína de seda contribuyó a la generación de un tejido de granulación de alta calidad, y escasa formación de tejido cicatrizal. Las Wj-MSCs podrían transdiferenciarse hacia células epidérmicas, queratinocitos, y endotelio microvascular, y por lo tanto, parecen promover la producción de una matriz extracelular que se asemeja bastante al tejido dérmico no lesionado.
- La gelatina de Wharton del cordón umbilical humano puede ser una fuente adecuada para la obtención de MSCs para ser utilizadas en la cicatrización de heridas debido a sus diversas ventajas y junto con los beneficios sinérgicos de

un constructo pudieran conformar una combinación ideal como apósitos para heridas crónicas de lenta y difícil curación.

Bibliography

[1] Adam Singer and Richard Clark. Cutaneous wound healing. *The New England Journal of Medicine*, 341(10):738–746, 1999.

[2] P Martin. Wound healing-aiming for perfect skin regeneration. *Science*, 276(5309):75–81, 1997.

[3] E Fuchs and S Raghavan. Getting under the skin of epidermal morphogenesis. *Nature Reviews Genetics*, 3(3):199–209, 2002.

[4] BL Seal, TC Otero, and A Panitch. Polymeric biomaterials for tissue and organ regeneration. *Materials Science and Engineering: R: Reports*, 34(4):147 – 230, 2001.

[5] E Contassot, HD Beer, and LE French. Interleukin-1, inflammasomes, autoinflammation and the skin. *Swiss Medical Weekly.142:w13590*, 2012.

[6] GT Kirby, SJ Mills, AJ Cowin, and LE Smith. Stem cells for cutaneous wound healing. *BioMed Research International*, 2015:285869, 2015.

[7] GC Gurtner, S Werner, Y Barrandon, and MT Longaker. Wound repair and regeneration. *Nature*, 453(7193):314–321, 2008.

[8] P Coutinho, C Qiu, S Frank, K Tamber, and D Becker. Dynamic changes in connexin expression correlate with key events in the wound healing process. *Cell Biology International*, 27(7):525–541, 2003.

[9] TA Springer. Traffic signals on endothelium for lymphocyte recirculation and leukocyte emigration. *Annual Review of Physiology*, 57(1):827–872, 1995.

[10] R Mori, KT Power, CM Wang, P Martin, and DL Becker. Acute downregulation of connexin43 at wound sites leads to a reduced inflammatory response, enhanced keratinocyte proliferation and wound fibroblast migration. *Journal of Cell Science*, 119(24):5193–5203, 2006.

[11] S Schreml, RM Szeimies, L Prantl, and M Landthaler. Wound healing in the 21st century. *Journal of the American Academy of Dermatology*, 63(5):866–881, 2010.

[12] V Falanga. Wound healing and its impairment in the diabetic foot. *Lancet*, 366(9498):1736–43, 2005.

[13] S Barrientos, O Stojadinovic, MS Golinko, H Brem, and M Tomic-Canic. PERSPECTIVE ARTICLE: growth factors and cytokines in wound healing. *Wound Repair and Regeneration*, 16(5):585–601, 2008.

[14] GL Brown, L Curtsinger, JR Brightwell, DM Ackerman, GR Tobin, HC Polk, C George-Nascimento, P Valenzuela, and GS Schultz. Enhancement of epidermal regeneration by biosynthetic epidermal growth factor. *The Journal of Experimental Medicine*, 163(5):1319–1324, 1986.

[15] Y Li, J Fan, M Chen, W Li, and DT Woodley. Transforming growth Factor-Alpha: a major human serum factor that promotes human keratinocyte migration. *Journal of Investigative Dermatology*, 126(9):2096–2105, 2006.

[16] I Kim, JE Mogford, JD Chao, and TA Mustoe. Wound epithelialization deficits in the transforming growth factor-alpha knockout mouse. *Wound Repair and Regeneration*, 9(5):386–390, 2001.

[17] Gerhard Raab and Michael Klagsbrun. Heparin-binding EGF-like growth factor. *Biochimica et Biophysica Acta*, 1333:F179–99, 1997.

[18] Y Shirakata, R Kimura, D Nanba, R Iwamoto, S Tokumaru, C Morimoto, K Yokota, M Nakamura, K Sayama, E Mekada, S Higashiyama, and K Hashimoto. Heparin-binding EGF-like growth factor accelerates keratinocyte migration and skin wound healing. *Journal of Cell Science*, 118(11):2363–2370, 2005.

[19] N Itoh and DM Ornitz. Fibroblast growth factors: from molecular evolution to roles in development, metabolism and disease. *Journal of Biochemistry*, 149(2):121–130, 2011.

[20] SP Bennett, GD Griffiths, AM Schor, GP Leese, and SL Schor. Growth factors in the treatment of diabetic foot ulcers. *British Journal of Surgery*, 90(2):133–146, 2003.

[21] MA Seeger and AS Paller. The roles of growth factors in keratinocyte migration. *Advances in Wound Care*, 4(4):213–224, 2015.

[22] J Niu, Z Chang, B Peng, Q Xia, W Lu, P Huang, MS Tsao, and PJ Chiao. Keratinocyte growth Factor/Fibroblast growth factor-7-regulated cell migration and invasion through activation of NF-kappaB transcription factors. *Journal of Biological Chemistry*, 282(9):6001–6011, 2007.

[23] J Reibman, S Meixler, TC , Lee, LI Gold, BN Cronstein, KA Haines, SL Kolasinski, and G Weissmann. Transforming growth factor beta 1, a potent chemoattractant for human neutrophils, bypasses classic signal-transduction pathways. *Proceedings of the National Academy of Sciences*, 88(15):6805–6809, 1991.

[24] R Montesano and L Orci. Transforming growth factor beta stimulates collagen-matrix contraction by fibroblasts: implications for wound healing. *Proceedings of the National Academy of Sciences*, 85(13):4894–4897, 1988.

[25] Teerin Meckmongkol, Robert Harmon, Paula McKeown-Longo, and Livingston Van De Water. The fibronectin synergy site modulates TGF-beta-dependent fibroblast contraction. *Biochemical and biophysical research communications*, 360(4):709–714, 2007.

[26] K Riedel, F Riedel, UR Goessler, G Germann, and M Sauerbier. TGF-beta antisense therapy increases angiogenic potential in human keratinocytes in vitro. *Archives of Medical Research*, 38(1):45–51, 2007.

[27] JJ Hsuan. Transforming growth factor beta. *British Medical Bulletin*, 45(2):425–37, 1989.

[28] LA White, TI Mitchell, and CE Brinckerhoff. Transforming growth factor beta inhibitory element in the rabbit matrix metalloproteinase-1 (collagenase-1) gene functions as a repressor of constitutive transcription. *Biochimica et Biophysica Acta (BBA) - Gene Structure and Expression*, 1490(3):259–68, 2000.

[29] M Uutela, M Wirzenius, K Paavonen, I Rajantie, Y He, T Karpanen, M Lohela, H Wiig, P Salven, K Pajusola, U Eriksson, and K Alitalo. PDGF-D induces macrophage recruitment, increased interstitial pressure, and blood vessel maturation during angiogenesis. *Blood*, 104(10):3198–3204, 2004.

[30] P Lindahl, BR Johansson, P Leveen, and C Betsholtz. Pericyte loss and microaneurysm formation in PDGF-B-deficient mice. *Science*, 277(5323):242–245, 1997.

[31] H Brem and J Folkman. Angiogenesis and basic fibroblast growth factor during wound healing. In: Friedlander, GE.; Lane, JM., editors. Bone Formation and Repair. Rosemont: American Academy of Orthopedic Surgeons. pages 213–22, 1994.

[32] S Frank, G Hubner, G Breier, MT Longaker, DG Greenhalgh, and S Werner. Regulation of vascular endothelial growth factor expression in cultured keratinocytes. implications for normal and impaired wound healing. *Journal of Biological Chemistry*, 270(21):12607–12613, 1995.

[33] IA Silver. The measurement of oxygen tension in healing tissue. *Progress in Respiratory Research*, 3:124–35, 1969.

[34] M Detmar, LF Brown, B Berse, RW Jackman, BM Elicker, HF Dvorak, and KP Claffey. Hypoxia regulates the expression of vascular permeability factor/vascular endothelial growth factor (vpf/vegf) and its receptors in human skin. *Journal of Investigative Dermatology*, 108:263–8, 1997.

[35] Philip Bao, Arber Kodra, Marjana Tomic-Canic, Michael S Golinko, H Paul Ehrlich, and Harold Brem. The role of vascular endothelial growth factor in wound healing. *Journal of Surgical Research*, 153(2):347–358, 2009.

[36] Y Fang, J Shen, M Yao, KW Beagley, BD Hambly, and S Bao. Granulocyte-macrophage colony-stimulating factor enhances wound healing in diabetes via upregulation of proinflammatory cytokines. *British Journal of Dermatology*, 162(3):478–486, 2010.

[37] A Yonem, B Cakir, S Guler, O Azal, and A Corakci. Effects of granulocyte-colony stimulating factor in the treatment of diabetic foot infection. *Diabetes, Obesity and Metabolism*, 3(5):332–7, 2001.

[38] F Bussolino, JM Wang, P Defilippi, F Turrini, F Sanavio, CJ Edgell, M Aglietta, P Arese, and A Mantovani. Granulocyte- and granulocyte-macrophage-colony stimulating factors induce human endothelial cells to migrate and proliferate. *Nature*, 337(6206):471–473, 1989.

[39] CA Dinarello. Immunological and inflammatory functions of the interleukin-1 family. *Annual Review of Immunology*, 27(1):519–550, 2009.

[40] AA Thomay, JM Daley, E Sabo, PJ Worth, LJ Shelton, MW Harty, JS Reichner, and JE Albina. Disruption of interleukin-1 signaling improves the quality of wound healing. *The American Journal of Pathology*, 174(6):2129–36, 2009.

[41] ZQ Lin, T Kondo, Y Ishida, T Takayasu, and N Mukaida. Essential involvement of IL-6 in the skin wound-healing process as evidenced by delayed wound healing in IL-6-deficient mice. *Journal of Leukocyte Biology*, 73(6):713–721, 2003.

[42] GS Ashcroft, MJ Jeong, JJ Ashworth, M Hardman, W Jin, N Moutsopoulos, T Wild, N McCartney-Francis, D Sim, G McGrady, XY Song, and SM Wahl. Tumor necrosis factor-alpha is a therapeutic target for impaired cutaneous wound healing. *Wound Repair and Regeneration*, 20(1):38–49, 2012.

[43] DT Graves and Y Jiang. Chemokines, a family of chemotactic cytokines. *Critical Reviews in Oral Biology and Medicine*, 6(2):109–18, 1995.

[44] SL Deshmane, S Kremlev, S Amini, and BE Sawaya. Monocyte chemoattractant protein-1 (MCP-1): an overview. *Journal of Interferon and Cytokine Research*, 29(6):313–26, 2009.

[45] C Wetzler, H Kampfer, B Stallmeyer, J Pfeilschifter, and S Frank. Large and sustained induction of chemokines during impaired wound healing in the genetically diabetic mouse: prolonged persistence of neutrophils and macrophages during the late phase of repair. *Journal of Investigative Dermatology*, 115(2):245–53, 2000.

[46] QE Low, IA Drugea, LA Duffner, DG Quinn, DN Cook, BJ Rollins, EJ Kovacs, and LA DiPietro. Wound healing in MIP-1alpha(-/-) and MCP-1(-/-) mice. *The American journal of pathology*, 159(2):457–463, 2001.

[47] E Engelhardt, A Toksoy, M Goebeler, S Debus, EB Brocker, and R Gillitzer. Chemokines IL-8, GRO alpha, MCP-1, IP-10, and Mig are sequentially and differentially expressed during phase-specific infiltration of leukocyte subsets in human wound healing. *The American journal of pathology*, 153(6):1849–1860, 1998.

[48] Rita E Mirza and Timothy J Koh. Contributions of cell subsets to cytokine production during normal and impaired wound healing. *Cytokine*, 71(2):409–412, 2015.

[49] TA Beyer, U Auf dem Keller, S Braun, M Schafer, and S Werner. Roles and mechanisms of action of the Nrf2 transcription factor in skin morphogenesis, wound repair and skin cancer. *Cell Death & Differentiation*, 14(7):1250–1254, 2007.

[50] S Braun, C Hanselmann, MG Gassmann, U auf dem Keller, C Born-Berclaz, K Chan, YW Kan, and S Werner. Nrf2 transcription factor, a novel target of keratinocyte growth factor action which regulates gene expression and inflammation in the healing skin wound. *Molecular and Cellular Biology*, 22(15):5492–5505, 2002.

[51] A Kumin, M Schafer, N Epp, P Bugnon, C Born-Berclaz, A Oxenius, A Klippel, W Bloch, and S Werner. Peroxiredoxin 6 is required for blood vessel integrity in wounded skin. *The Journal of Cell Biology*, 179(4):747–760, 2007.

[52] A Nauta, GC Gurtner, and MT Longaker. Wound healing and regenerative strategies. *Oral Diseases*, 17(6):541–549, 2011.

[53] S Guo and LA Dipietro. Factors affecting wound healing. *Journal of Dental Research*, 89(3):219–229, 2010.

[54] Osman Koese and Ahmad Waseem. Keloids and hypertrophic scars: are they two different sides of the same coin? *Dermatologic Surgery*, 34(3):336–346, 2008.

[55] M Isakson, C de Blacam, D Whelan, A McArdle, and A.J.P Clover. Mesenchymal stem cells and cutaneous wound healing: Current evidence and future potential. *Stem Cells International*, 2015, 2015.

[56] R Haddad and F Saldanha-Araujo. Mechanisms of T-Cell immunosuppression by mesenchymal stromal cells: What do we know so far? *BioMed Research International*, 2014, 2014.

[57] M Owen and AJ Friedenstein. Stromal stem cells: marrow-derived osteogenic precursors. *Ciba Foundation symposium*, 136:42–60, 1988.

[58] Hassan Abdulrazzak, Dafni Moschidou, Gemma Jones, and Pascale V Guillot. Biological characteristics of stem cells from foetal, cord blood and extraembryonic tissues. *Journal of the Royal Society, Interface / the Royal Society*, 7 Suppl 6:S689–S706, 2010.

[59] M Dominici, K Le Blanc, I Mueller, I Slaper-Cortenbach, Fc Marini, Ds Krause, Rj Deans, A Keating, Dj j Prockop, and Em Horwitz. Minimal criteria for defining multipotent mesenchymal stromal cells. the international society for cellular therapy position statement. *Cytotherapy*, 8(4):315–317, 2006.

[60] Akiva J. Marcus and Dale Woodbury. Fetal stem cells from extra-embryonic tissues: do not discard. *Journal of Cellular and Molecular Medicine*, 12(3):730–742, 2008.

[61] V Sabapathy, B Sundaram, P Mankuzhy, and S Kumar. Human Wharton's jelly mesenchymal stem cells plasticity augments scar-free skin wound healing with hair growth. *PloS one*, 9(4), 2014.

[62] KD Mc Elreavey, AI Irvine, KT Ennis, and WH McLean. Isolation, culture and characterisation of fibroblast-like cells derived from the wharton's jelly portion of human umbilical cord. *Biochem Soc Trans*, 19(1):29S, 1991.

[63] Kathy E Mitchell, Mark L Weiss, Brianna M Mitchell, Phillip Martin, Duane Davis, Lois Morales, Bryan Helwig, Mark Beerenstrauch, Abou-Easa, Khalil, Tammi Hildreth, Deryl Troyer, and Satish Medicetty. Matrix cells from wharton's jelly form neurons and glia. *Stem Cells*, 21(1):50–60, 2003.

[64] Mark L. Weiss, Satish Medicetty, Amber R. Bledsoe, Raja Shekar Rachakatla, Michael Choi, Shosh Merchav, Yongquan Luo, Mahendra S. Rao, Gopalrao Velagaleti, and Deryl Troyer. Human umbilical cord matrix stem cells: Preliminary characterization and effect of transplantation in a rodent model of parkinson's disease. *STEM CELLS*, 2006.

[65] YuâShow Fu, YunâChih Cheng, MaanâYuh Anya Lin, Henrich Cheng, PeiâMing Chu, ShihâChich Chou, YangâHsin Shih, MiauâHwa Ko, and MinâShan Sung. Conversion of human umbilical cord mesenchymal stem cells in wharton's jelly to dopaminergic neurons in vitro: Potential therapeutic application for parkinsonism. *STEM CELLS*, 2006.

[66] Y Kuroda, M Kitada, S Wakao, and M Dezawa. Mesenchymal stem cells and umbilical cord as sources for schwann cell differentiation: their potential in peripheral nerve repair. *The Open Tissue Engineering and Regenerative Medicine Journal*, 4:54–63, 2011.

[67] Kai Wu, Bin Zhou, Cun Yu, Bin Cui, Shi Lu, Zhong Han, and Ying Liu. Therapeutic potential of human umbilical cord derived stem cells in a rat myocardial infarction model. *The Annals of thoracic surgery*, 83(4):1491–1498, 2007.

[68] Tao Du, Xiangyu Zou, Jun Cheng, Shuai Wu, Liang Zhong, Guanqun Ju, Jiang Zhu, Guohua Liu, Yingjian Zhu, and Shujie Xia. Human wharton's

jelly-derived mesenchymal stromal cells reduce renal fibrosis through induction of native and foreign hepatocyte growth factor synthesis in injured tubular epithelial cells. *Stem cell research and therapy*, 4(3), 2013.

[69] Yuben Moodley, Daniel Atienza, Ursula Manuelpillai, Chrishan S Samuel, Jorge Tchongue, Sivakami Ilancheran, Richard Boyd, and Alan Trounson. Human umbilical cord mesenchymal stem cells reduce fibrosis of bleomycin-induced lung injury. *The American journal of pathology*, 175(1):303–313, 2009.

[70] Melania Lo Iacono, Rita Anzalone, Simona Corrao, Mario Giuffre, Antonino Di Stefano, Pantaleo Giannuzzi, Francesco Cappello, Felicia Farina, and Giampiero La Rocca. Perinatal and wharton's Jelly-Derived mesenchymal stem cells in cartilage regenerative medicine and tissue engineering strategies. *The Open Tissue Engineering and Regenerative Medicine Journal*, 4:72–81.

[71] M Tamura, A Kawabata, and N Ohta. Wharton's jelly stem cells as agents for cancer therapy. *The Open Tissue Engineering and Regenerative Medicine Journal*, 4:39–47, 2011.

[72] RD Lund, S Wang, B Lu, S Girman, and T Holmes. Cells isolated from umbilical cord tissue rescue photoreceptors and visual functions in a rodent model of retinal disease. *Stem Cells*, 25:602–611, 2007.

[73] Sachiko Jomura, Marc Uy, Kathy Mitchell, Renee Dallasen, Claudia J Bode, and Yan Xu. Potential treatment of cerebral global ischemia with oct-4+ umbilical cord matrix cells. *Stem Cells*, 25(1):98–106, 2007.

[74] C Zhou, B Yang, Y Tian, H Jiao, W Zheng, J Wang, and F Guan. Immunomodulatory effect of human umbilical cord Wharton's jelly-derived mesenchymal stem cells on lymphocytes. *Cellular Immunology*, 272(1):33–38, 2011.

[75] M Di Nicola, C Carlo-Stella, M Magni, M Milanesi, PD Longoni, P Matteucci, S Grisanti, and AM Gianni. Human bone marrow stromal cells suppress t-lymphocyte proliferation induced by cellular or nonspecific mitogenic stimuli. *Blood*, 99(10):3838–3843, 2002.

[76] MK Majumdar, M Keane-Moore, D Buyaner, WB Hardy, MA Moorman, KR McIntosh, and JD Mosca. Characterization and functionality of cell surface molecules on human mesenchymal stem cells. *Journal of Biomedical Science*, 10(2):228–241, 2003.

[77] Karen English. Mechanisms of mesenchymal stromal cell immunomodulation. *Immunology and Cell Biology*, 91(1):19–26, 2012.

[78] M Krampera, L Cosmi, R Angeli, A Pasini, F Liotta, A Andreini, V Santarlasci, B Mazzinghi, G Pizzolo, F Vinante, P Romagnani, E Maggi, S Romagnani, and F Annunziato. Role for interferon-gamma in the immunomodulatory activity of human bone marrow mesenchymal stem cells. *Stem Cells*, 24(2):386–398, 2006.

[79] D Polchert, J Sobinsky, G Douglas, M Kidd, A Moadsiri, E Reina, K Genrich, S Mehrotra, S Setty, B Smith, and A Bartholomew. Ifn-gamma activation of mesenchymal stem cells for treatment and prevention of graft versus host disease. *European Journal of Immunology*, 38(6):1745–1755, 2008.

[80] G Ren, L Zhang, X Zhao, G Xu, Y Zhang, AI Roberts, RC Zhao, and Y Shi. Mesenchymal stem Cell-Mediated immunosuppression occurs via concerted action of chemokines and nitric oxide. *Cell Stem Cell*, 2(2):141–150, 2008.

[81] R Waterman, SL Tomchuck, SL Henkle, and AM Betancourt. A new mesenchymal stem cell (MSC) paradigm: Polarization into a Pro-Inflammatory MSC1 or an immunosuppressive MSC2 phenotype. *PLoS ONE*, 5(4), 2010.

[82] G Ren, X Zhao, L Zhang, J Zhang, A L'Huillier, W Ling, AI Roberts, AD Le, S Shi, C Shao, and Y Shi. Inflammatory Cytokine-Induced intercellular adhesion molecule-1 and vascular cell adhesion molecule-1 in mesenchymal stem cells are critical for immunosuppression. *The Journal of Immunology*, 184(5):2321–2328, 2010.

[83] A Sica and A Mantovani. Macrophage plasticity and polarization: in vivo veritas. *Journal of Clinical Investigation*, 122(3):787–795, 2012.

[84] JH Ylöstalo, TJ Bartosh, K Coble, and DJ Prockop. Human mesenchymal stem/stromal cells cultured as spheroids are self-activated to produce prostaglandin e2 that directs stimulated macrophages into an anti-inflammatory phenotype. *STEM CELLS*, 30(10):2283–2296, 2012.

[85] CA Opitz, UM Litzenburger, C Lutz, TV Lanz, I Tritschler, A Köppel, E Tolosa, M Hoberg, J Anderl, WK Aicher, M Weller, W Wick, and M Platten. Toll-like receptor engagement enhances the immunosuppressive properties of human bone marrow-derived mesenchymal stem cells by inducing indoleamine-2,3-dioxygenase-1 via interferon-beta and protein kinase R. *Stem Cells*, 27(4):909–919, 2009.

[86] W Ge, J Jiang, J Arp, W Liu, B Garcia, and H Wang. Regulatory t-cell generation and kidney allograft tolerance induced by mesenchymal stem cells associated with indoleamine 2,3-dioxygenase expression. *Transplantation*, 90(12):1312–1320, 2010.

[87] RH Lee, AA Pulin, MJ Seo, DJ Kota, J Ylostalo, BL Larson, L Semprun-Prieto, P Delafontaine, and DJ Prockop. Intravenous hMSCs improve myocardial infarction in mice because cells embolized in lung are activated to secrete the anti-inflammatory protein TSG-6. *Cell Stem Cell*, 5(1):54–63, 2009.

[88] GW Roddy, JY Oh, RH Lee, TJ Bartosh, J Ylostalo, K Coble, RH Rosa, and DJ Prockop. Action at a distance: Systemically administered adult stem/progenitor cells (mscs) reduce inflammatory damage to the cornea without engraftment and primarily by secretion of tnf alpha stimulated gene/protein 6. *STEM CELLS*, 29(10):1572–1579, 2011.

[89] H Choi, RH Lee, N Bazhanov, JY Oh, and DJ Prockop. Anti-inflammatory protein tsg-6 secreted by activated mscs attenuates zymosan-induced mouse peritonitis by decreasing tlr2/nf-?b signaling in resident macrophages. *Blood*, 118(2):330–338, 2011.

[90] SG Harris, J Padilla, L Koumas, D Ray, and RP Phipps. Prostaglandins as modulators of immunity. *Trends in Immunology*, 23(3):144–150, 2002.

[91] L Zhou, MM Chong, and DR Littman. Plasticity of CD4+ t cell lineage differentiation. *Immunity*, 30(5):646–655, 2009.

[92] S Ghannam, J Pène, G Moquet-Torcy, G Torcy-Moquet, C Jorgensen, and H Yssel. Mesenchymal stem cells inhibit human th17 cell differentiation and function and induce a t regulatory cell phenotype. *The Journal of Immunology*, 185(1):302–312, 2010.

[93] K English, FP Barry, and BP Mahon. Murine mesenchymal stem cells suppress dendritic cell migration, maturation and antigen presentation. *Immunology Letters*, 115(1):50–58, 2008.

[94] X Liu, X Qu, Y Chen, L Liao, K Cheng, C Shao, M Zenke, A Keating, and RC Zhao. Mesenchymal Stem/Stromal cells induce the generation of novel IL-10-Dependent regulatory dendritic cells by SOCS3 activation. *The Journal of Immunology*, 189(3):1182–1192, 2012.

[95] M Di Ianni, B Del Papa, M De Ioanni, L Moretti, E Bonifacio, D Cecchini, P Sportoletti, F Falzetti, and A Tabilio. Mesenchymal cells recruit and regulate t regulatory cells. *Experimental hematology*, 36(3):309–318, 2008.

[96] K English, JM Ryan, L Tobin, MJ Murphy, FP Barry, and BP Mahon. Cell contact, prostaglandin E2 and transforming growth factor beta 1 play non-redundant roles in human mesenchymal stem cell induction of CD4+CD25(High)forkhead box P3+ regulatory T cells. *Clinical & Experimental Immunology*, 156(1):149–160, 2009.

[97] K Nemeth, A Keane-Myers, JM. Brown, DD Metcalfe, JD Gorham, VG Bundoc, MG Hodges, I Jelinek, S Madala, S Karpati, and E Mezey. Bone marrow stromal cells use tgf-beta to suppress allergic responses in a mouse model of ragweed-induced asthma. 107(12):5652–5657, 2010.

[98] W Ge, J Jiang, ML Baroja, J Arp, R Zassoko, W Liu, A Bartholomew, B Garcia, and H Wang. Infusion of mesenchymal stem cells and rapamycin synergize to attenuate alloimmune responses and promote cardiac allograft tolerance. *American Journal of Transplantation*, 9(8):1760–1772, 2009.

[99] E Mansilla, GH Marin, F Sturla, HE Drago, MA Gil, E Salas, MC Gardiner, G Piccinelli, S Bossi, E Salas, L Petrelli, G Iorio, CA Ramos, and C Soratti. Human mesenchymal stem cells are tolerized by mice and improve skin and spinal cord injuries. *Transplantation Proceedings*, 37(1):292 – 294, 2005.

[100] EV Badiavas and V Falanga. Treatment of chronic wounds with bone marrow-derived cells. *Archives of Dermatology*, 139(4):510–516, 2003.

[101] V Falanga, S Iwamoto, M Chartier, T Yufit, J Butmarc, N Kouttab, D Shrayer, and P Carson. Autologous bone marrow-derived cultured mesenchymal stem cells delivered in a fibrin spray accelerate healing in murine and human cutaneous wounds. *Tissue Engineering*, 13(6):1299–1312, 2007.

[102] NR Dash, SN Dash, P Routray, S Mohapatra, and PC Mohapatra. Targeting nonhealing ulcers of lower extremity in human through autologous bone Marrow-Derived mesenchymal stem cells. *Rejuvenation Research*, 12(5):359–366, 2009.

[103] D Lu, B Chen, Z Liang, W Deng, Y Jiang, S Li, J Xu, Q Wu, Z Zhang, B Xie, and S Chen. Comparison of bone marrow mesenchymal stem cells with bone marrow-derived mononuclear cells for treatment of diabetic critical limb

ischemia and foot ulcer: a double-blind, randomized, controlled trial. *Diabetes research and clinical practice*, 92(1):26–36, 2011.

[104] T Yoshikawa, H Mitsuno, I Nonaka, Y Sen, K Kawanishi, Y Inada, Y Takakura, K Okuchi, and A Nonomura. Wound therapy by marrow mesenchymal cell transplantation. *Plastic and reconstructive surgery*, 121(3):860–877, 2008.

[105] Yajing Zhang, Haojie Hao, Jiejie Liu, Xiaobing Fu, and Weidong Han. Repair and regeneration of skin injury by transplanting microparticles mixed with wharton's jelly and MSCs from the human umbilical cord. *The international journal of lower extremity wounds*, 11(4):264–270, 2012.

[106] Kimberley Tam, Suganya Cheyyatraviendran, Jayarama Venugopal, Arijit Biswas, Mahesh Choolani, Seeram Ramakrishna, Ariff Bongso, and Chui-Yee Y Fong. A nanoscaffold impregnated with human wharton's jelly stem cells or its secretions improves healing of wounds. *Journal of cellular biochemistry*, 115(4):794–803, 2014.

[107] J Vojtassák, L Danisovic, M Kubes, D Bakos, L Jarábek, M Ulicná, and M Blasco. Autologous biograft and mesenchymal stem cells in treatment of the diabetic foot. *Neuroendocrinology Letters*, 27(suppl 2):134–137, 2006.

[108] Charu Vepari and David L. Kaplanl. Silk as a biomaterial. *Progress in Polymer Science*, 32(8-9), 2007.

[109] Cong-Zhao Zhou, Fabrice Confalonieri, Nadine Medina, Yvan Zivanovic, Catherine Esnault, Tie Yang, Michel Jacquet, Joel Janin, Michel Duguet, Roland Perasso, and Zhen-Gang Li. Fine organization of bombyx mori fibroin heavy chain gene. *Nucleic Acids Research*, 28(12):2413–2419, 2000.

[110] Tanaka Kazunori, Inoue Satoshi, and Mizuno Shigeki. Hydrophobic interaction of P25, containing Asn-linked oligosaccharide chains, with the H-L complex of silk fibroin produced by bombyx mori. *Insect Biochemistry and Molecular Biology*, 29(3):269–276, 1999.

[111] Satoshi Inoue, Kazunori Tanaka, Fumio Arisaka, Sumiko Kimura, Kohei Ohtomo, and Shigeki Mizuno. Silk fibroin of Bombyx mori is secreted, assembling a high molecular mass elementary unit consisting of H-chain, L-chain, and P25, with a 6: 6: 1 molar ratio. *Journal of Biological Chemistry*, 275(51):40517–40528, 2000.

[112] L Meinel and DL Kaplan. Silk constructs for delivery of musculoskeletal therapeutics. *Advanced Drug Delivery Reviews*, 64:1111–1122, 2012.

[113] CZ Zhou, F Confalonieri, M Jacquet, R Perasso, ZG Li, and J Janin. Silk fibroin: structural implications of a remarkable amino acid sequence. *Proteins*, 44(2):119–122, 2001.

[114] Rockwood Danielle, Preda Rucsanda, Yucel Tuna, Wang Xiaoqin, Lovett Michael, and Kaplan David. Materials fabrication from bombyx mori silk fibroin. *Nature Protocols*, 6(10):1612–1631, 2011.

[115] Fiorenzo G Omenetto and David L Kaplan. New opportunities for an ancient material. *Science*, 329:528–531, 2010.

[116] A Murphy and DL Kaplan. Biomedical applications of chemically-modified silk fibroin. *Journal of Materials Chemistry*, 19(36):6443–6450, 2009.

[117] X Zhang, MR Reagan, and DL Kaplan. Electrospun silk biomaterial scaffolds for regenerative medicine. *Advanced Drug Delivery Reviews*, 61(12):988–1006, 2009.

[118] WJ Li, CT Laurencin, EJ Caterson, RS Tuan, and FK Ko. Electrospun nanofibrous structure: a novel scaffold for tissue engineering. *J Biomed Mater Res.*, 60(4):613–21, 2002.

[119] Darrell Reneker and Iksoo Chun. Nanometre diameter fibres of polymer, produced by electrospinning. *Nanotechnology*, 7:216–223, 1996.

[120] Y.K Luu, K Kim, B.S Hsiao, B Chu, and M Hadjiargyrou. Development of a nanostructured DNA delivery scaffold via electrospinning of PLGA and PLA-PEG block copolymers. *Journal of Controlled Release*, 89(2):341–353, 2003.

[121] WJ Li, R Tuli, X Huang, P Laquerriere, and RS Tuan. Multilineage differentiation of human mesenchymal stem cells in a three-dimensional nanofibrous scaffold. *Biomaterials*, 26(25):5158–5166, 2005.

[122] EJ Chong, TT Phan, IJ Lim, YZ Zhang, BH Bay, S Ramakrishna, and CT Lim. Evaluation of electrospun PCL/gelatin nanofibrous scaffold for wound healing and layered dermal reconstitution. *Acta biomaterialia*, 3(3):321–330, 2007.

[123] I Tocco, B Zavan, F Bassetto, and V Vindigni. Nanotechnology-Based therapies for skin wound regeneration. *Journal of Nanomaterials*, 2012, 2012.

[124] M Vert, SM Li, G Spenlehauer, and P Guerin. Bioresorbability and biocompatibility of aliphatic polyesters. *Journal of Materials Science: Materials in Medicine*, 3:432–446, 1992.

[125] Kundu Banani, Rajkhowa Rangam, Kundu Subhas C, and Wang Xungai. Silk fibroin biomaterials for tissue regenerations. *Advanced Drug Delivery Reviews*, 65(4):457–470, 2013.

[126] Y Wang, DD Rudym, A Walsh, L Abrahamsen, HJ Kim, HS Kim, and DL Kirker-Head, C andKaplan. In vivo degradation of three-dimensional silk fibroin scaffolds. *Biomaterials*, 29(24-25):3415–3428, 2008.

[127] R Murugan and S Ramakrishna. Nano-featured scaffolds for tissue engineering: a review of spinning methodologies. *Tissue Engineering*, 12(3):435–447, 2006.

[128] BM Min, G Lee, SH Kim, YS Nam, TS Lee, and WH Park. Electrospinning of silk fibroin nanofibers and its effect on the adhesion and spreading of normal human keratinocytes and fibroblasts in vitro. *Biomaterials*, 25(7-8):1289–1297, 2004.

[129] BM Min, L Jeong, YS Nam, JM Kim, JY Kim, and WH Park. Formation of silk fibroin matrices with different texture and its cellular response to normal human keratinocytes. *International Journal of Biological Macromolecules*, 34(5):223–230, 2004.

[130] Yaojiong Wu, Liwen Chen, Paul G Scott, and Edward E Tredget. Mesenchymal stem cells enhance wound healing through differentiation and angiogenesis. *Stem cells*, 25(10):2648–2659, 2007.

[131] Liwen Chen, Edward E. Tredget, Philip Y. G. Wu, and Yaojiong Wu. Paracrine factors of mesenchymal stem cells recruit macrophages and endothelial lineage cells and enhance wound healing. *PLoS ONE*, 3(4), 2008.

[132] JM Davidson. Animal models for wound repair. *Archives of dermatological research*, 290 Suppl:S1–11, 1998.

[133] F Benavides, TM Oberyszyn, and AM van Buskirk. The hairless mouse in skin research. *Journal of Dermatological Science*, 53:10–18, 2009.

[134] Robert D Galiano, Joseph Michaels, Michael Dobryansky, Jamie P Levine, and Geoffrey Gurtner. Quantitative and reproducible murine model of excisional wound healing. *Wound Repair and Regeneration*, 12(4):485–492, 2004.

[135] Xusheng Wang, Jianfeng Ge, Edward E Tredget, and Yaojiong Wu. The mouse excisional wound splinting model, including applications for stem cell transplantation. *Nature protocols*, 8(2):302–309, 2013.

[136] Liwen Chen, Edward E. Tredget, Chenxiong Liu, and Yaojiong Wu. Analysis of allogenicity of mesenchymal stem cells in engraftment and wound healing in mice. *PLoS ONE*, 4(9), 2009.

[137] CJ Caspersen, GD Thomas, LA Boseman, GL Beckles, and AL Albright. Aging, diabetes, and the public health system in the united states. *American journal of public health*, 102(8):1482–1497, 2012.

[138] S Liu, M Yuan, K Hou, L Zhang, X Zheng, B Zhao, X Sui, W Xu, S Lu, and Q Guo. Immune characterization of mesenchymal stem cells in human umbilical cord Wharton's jelly and derived cartilage cells. *Cellular immunology*, 278(1-2):35–44, 2012.

[139] Kiarash Khosrotehrani. Mesenchymal stem cell therapy in skin: why and what for? *Experimental Dermatology*, 22(5):307–310, 2013.

[140] Jackson Wesley, Nesti Leon, and Tuan Rocky. Concise Review: Clinical translation of wound healing therapies based on mesenchymal stem cells. *Stem Cells Translational Medicine*, 1(1):44–50, 2012.

[141] SE Hanson, ML Bentz, and P Hematti. Mesenchymal stem cell therapy for nonhealing cutaneous wounds. *Plastic and Reconstructive Surgery*, 125(2):510–516, 2010.

[142] JM Sorrell and Arnold I Caplan. Topical delivery of mesenchymal stem cells and their function in wounds. *Stem cell research & therapy*, 1(4):30, 2010.

[143] WY Huang, CL Yeh, JH Lin, JS Yang, TH Ko, and YH Lin. Development of fibroblast culture in three-dimensional activated carbon fiber-based scaffold for wound healing. *Journal of Materials Science: Materials in Medicine*, 23(6):1465–1478, 2012.

[144] D Sundaramurthi, KS Vasanthan, P Kuppan, UM Krishnan, and S Sethuraman. Electrospun nanostructured chitosan-poly (vinyl alcohol) scaffolds: a

biomimetic extracellular matrix as dermal substitute. *Biomedical Materials*, 7(4), 2012.

[145] G Guan, L Bai, B Zuo, M Li, Z Wu, Y Li, and L Wang. Promoted dermis healing from full-thickness skin defect by porous silk fibroin scaffolds (PSFSs). *Bio-Medical Materials and Engineering*, 20(5):295–308, 2010.

[146] S Kanokpanont, S Damrongsakkul, J Ratanavaraporn, and P Aramwit. An innovative bi-layered wound dressing made of silk and gelatin for accelerated wound healing. *International Journal of Pharmaceutics*, 436(1-2):141–153, 2012.

[147] Kiran Seshareddy, Deryl Troyer, and Mark L Weiss. Method to isolate mesenchymal-like cells from wharton's jelly of umbilical cord. *Methods in cell biology*, 86:101–119, 2008.

[148] C De Bruyn, M Najar, G Raicevic, N Meuleman, K Pieters, B Stamatopoulos, A Delforge, D Bron, and L Lagneaux. A rapid, simple, and reproducible method for the isolation of mesenchymal stromal cells from Wharton's jelly without enzymatic treatment. *Stem Cells and Development*, 20(3):547–557, 2011.

[149] Jorge Perez-Galarza, Francoise Carlotti, Martijn Rabelink, Steve Cramer, Rob Hoeben, Willem Fibbe, and Melissa van Pel. Optimizing reporter constructs for in-vivo bioluminescence imaging of interferon gamma stimulated mesenchymal stromal cells. *Experimental Hematology*, 42(9):793–803, 2014.

[150] M Duijvestein, ME Wildenberg, MM Welling, S Hennink, I Molendijk, VL van Zuylen, T Bosse, AC Vos, ES de Jonge-Muller, H Roelofs, L van der Weerd, HW Verspaget, WE Fibbe, AA te Velde, GR van den Brink, and DW Hommes. Pretreatment with interferon gamma enhances the therapeutic activity of mesenchymal stromal cells in animal models of colitis. *Stem Cells*, 29(10):1549–1558, 2011.

[151] H Zhu, ZK Guo, XX Jiang, H Li, XY Wang, HY Yao, Y Zhang, , and N Mao. A protocol for isolation and culture of mesenchymal stem cells from mouse compact bone. *Nature Protocols*, 5(3):550–560, 2010.

[152] F Langenbach and J Handschel. Effects of dexamethasone, ascorbic acid and beta-glycerophosphate on the osteogenic differentiation of stem cells *in vitro*. *Stem Cell Research and Therapy*, 4(5), 2013.

[153] L Janderová, M McNeil, AN Murrell, RL Mynatt, and SR Smith. Human mesenchymal stem cells as an in vitro model for human adipogenesis. *Obesity Research*, 11(1):65–74, 2003.

[154] ML Elks and VC Manganiello. A role for soluble cAMP phosphodiesterases in differentiation of 3T3-L1 adipocytes. *Journal of Cellular Physiology*, 124(2):191–198, 1985.

[155] M Styner, B Sen, Z Xie, N Case, and J Rubin. Indomethacin promotes adipogenesis of mesenchymal stem cells through a cyclooxygenase independent mechanism. *Journal of Cellular Biochemistry*, 111(4):1042–1050, 2010.

[156] HA Awad, YD Halvorsen, JM Gimble, and F Guilak. Effects of transforming growth factor beta1 and dexamethasone on the growth and chondrogenic differentiation of adipose-derived stromal cells. *Tissue Engineering*, 9(6):1301–12, 2003.

[157] G Sridharan and A Shankar. Toluidine blue: A review of its chemistry and clinical utility. *Journal of Oral and Maxillofacial Pathology*, 16(2):251–255, 2012.

[158] J van Meerloo, GJ Kaspers, and J Cloos. Cell sensitivity assays: the MTT assay. *Methods Mol Biol*, 731:237–45, 2011.

[159] LL Cavanagh, RJ Saal, KL Grimmett, and R Thomas. Proliferation in monocyte-derived dendritic cell cultures is caused by progenitor cells capable of myeloid differentiation. *Blood*, 92(5):1598–607, 1998.

[160] Jin Hu, Ola Winqvist, Flores-Morales, Amilcar, Ann-Charlotte Wikstrom, and Gunnar Norstedt. SOCS2 influences LPS induced human monocyte-derived dendritic cell maturation. *PloS one*, 4(9), 2009.

[161] GJ Inman, FJ Nicolás, JF Callahan, JD Harling, LM Gaster, AD Reith, NJ Laping, and CS Hill. SB-431542 is a potent and specific inhibitor of transforming growth factor-beta superfamily type I activin receptor-like kinase (alk) receptors ALK4, ALK5, and ALK7. *Molecular Pharmacology*, 62(1):65–74, 2002.

[162] A Trickett and YL Kwan. T cell stimulation and expansion using anti-CD3/CD28 beads. *Journal of Immunological Methods*, 275(1-2):251–5, 2003.

[163] Salvador Aznar-Cervantes, MI Roca, JG Martinez, Luis Meseguer-Olmo, JL Cenis, JM Moraleda, and TF Otero. Fabrication of conductive electrospun silk fibroin scaffolds by coating with polypyrrole for biomedical applications. *Bioelectrochemistry*, 85:36–43, 2012.

[164] EM Horwitz, K Le Blanc, M Dominici, I Mueller, I Slaper-Cortenbach, FC Marini, RJ Deans, DS Krause, and A Keating. Clarification of the nomenclature for MSC: the international society for cellular therapy position statement. *Cytotherapy*, 7(5):393–395, 2005.

[165] G Koopman, CP Reutelingsperger, GA Kuijten, RM Keehnen, ST Pals, and MH van Oers. Annexin V for flow cytometric detection of phosphatidylserine expression on B cells undergoing apoptosis. *Blood*, 84(5):1415–1420, 1994.

[166] SJ Martin, CP Reutelingsperger, AJ McGahon, JA Rader, RC van Schie, DM LaFace, and DR Green. Early redistribution of plasma membrane phosphatidylserine is a general feature of apoptosis regardless of the initiating stimulus: inhibition by overexpression of Bcl-2 and Abl. *The Journal of experimental medicine*, 182(5):1545–1556, 1995.

[167] AM Collaco and ME Geusz. Monitoring immediate-early gene expression through firefly luciferase imaging of HRS/J hairless mice. *BMC Physiol*, 3(8), 2003.

[168] AH Fischer, KA Jacobson, J Rose, and R Zeller. Hematoxylin and eosin staining of tissue and cell sections. *CSH protocols*, 2008(6), 2008.

[169] DA Hume, VH Perry, and S Gordon. The mononuclear phagocyte system of the mouse defined by immunohistochemical localisation of antigen f4/80: macrophages associated with epithelia. *Anatomical Record*, 210(3):503–12, 1984.

[170] HR Rodewald and HJ Fehling. Molecular and cellular events in early thymocyte development. *Advances in Immunology*, 69:1–112, 1998.

[171] Shen Cherng, Young Jenny, and Hongbao Ma. Alpha-smooth muscle actin (α-SMA). *The Journal of American Science*, 4(4):7–9, 2008.

[172] B Hinz, G Celetta, JJ Tomasek, G Gabbiani, and C Chaponnier. Alpha-Smooth muscle actin expression upregulates fibroblast contractile activity. *Molecular Biology of the Cell*, 12(9):2730–2741, 2001.

[173] SD Aznar-Cervantes, AA Lozano-Pérez, M García, G Víllora, D Vicente-Cervantes, and JL Cenis. Importance of refrigeration time in the electrospinning of silk fibroin aqueous solutions. *Journal of Materials Science*, 50(14):4879–4887, 2015.

[174] DL Troyer and ML Weiss. Wharton's jelly-derived cells are a primitive stromal cell population. *Stem Cells*, 26(3):591–599, 2008.

[175] J Bosch, AP Houben, TF Radke, D Stapelkamp, E Bünemann, P Balan, A Buchheiser, S Liedtke, and G Kögler. Distinct differentiation potential of "MSC" derived from cord blood and umbilical cord: are cord-derived cells true mesenchymal stromal cells? *Stem Cells and Development*, 21(11):1977–1988, 2012.

[176] LL Lu, YJ Liu, SG Yang, QJ Zhao, X Wang, W Gong, ZB Han, ZS Xu, YX Lu, D Liu, ZZ Chen, and ZC Han. Isolation and characterization of human umbilical cord mesenchymal stem cells with hematopoiesis-supportive function and other potentials. *Haematologica*, 91(8):1017–26, 2006.

[177] S Karahuseyinoglu, O Cinar, E Kilic, F Kara, CG Akay, DO Demiralp, A Tukun, D Uckan, and A Can. Biology of stem cells in human umbilical cord stroma: in situ and in vitro surveys. *Stem Cells*, 25(2):319–331, 2007.

[178] JH Yoon, EY Roh, S Shin, NH Jung, EY Song, JY Chang, BJ Kim, and HW Jeon. Comparison of Explant-Derived and enzymatic Digestion-Derived MSCs and the growth factors from Wharton's jelly. *BioMed Research International*, 2013, 2013.

[179] H Liu, DM Kemeny, BC Heng, HW Ouyang, AJ Melendez, and T Cao. The immunogenicity and immunomodulatory function of osteogenic cells differentiated from mesenchymal stem cells. *The Journal of Immunology*, 176(5):2864–2871, 2006.

[180] S Bajada, I Mazakova, JB Richardson, and N Ashammakhi. Updates on stem cells and their applications in regenerative medicine. *Journal of tissue engineering and regenerative medicine*, 2(4):169–183, 2008.

[181] M Sasaki, R Abe, Y Fujita, S Ando, D Inokuma, and H Shimizu. Mesenchymal stem cells are recruited into wounded skin and contribute to wound repair by transdifferentiation into multiple skin cell type. *The Journal of Immunology*, 180(4):2581–2587, 2008.

[182] PS Cho, DJ Messina, EL Hirsh, N Chi, SN Goldman, DP Lo, IR Harris, SH Popma, DH Sachs, and CA Huang. Immunogenicity of umbilical cord tissue derived cells. *Blood*, 111(1):430–8, 2008.

[183] E Mansilla, R Spretz, G Larsen, H Drago, F Sturla, GH Marin, G Roque, K Martire, V Diaz, S Bossi, C Gardiner, R Lamonega, N Lauzada, J Cordone, JC Raimondi, JM Tau, NR Biasi, JE Marini, AN Patel, TE Ichim, N Riordan, and A Maceira. Outstanding survival and regeneration process by the use of intelligent acellular dermal matrices and mesenchymal stem cells in a burn pig model. *Transplantation Proceedings*, 42(10):4275–4278, 2010.

[184] CY Fong, K Tam, S Cheyyatraivendran, SU Gan, K Gauthaman, A Armugam, K Jeyaseelan, M Choolani, A Biswas, and Bongso. Human wharton's jelly stem cells and its conditioned medium enhance healing of excisional and diabetic wounds. *Journal of Cellular Biochemistry*, 115(2):290–302, 2014.

[185] S Maxson, EA Lopez, D Yoo, A Danilkovitch-Miagkova, and MA Leroux. Concise review: role of mesenchymal stem cells in wound repair. *Stem Cells Translational Medicine*, 1(2):142–149, 2012.

[186] EV Badiavas, M Abedi, J Butmarc, V Falanga, and P Quesenberry. Participation of bone marrow derived cells in cutaneous wound healing. *Journal of cellular physiology*, 196(2):245–250, 2003.

[187] H Li, X Fu, Y Ouyang, C Cai, J Wang, and T Sun. Adult bone-marrow-derived mesenchymal stem cells contribute to wound healing of skin appendages. *Cell and Tissue Research*, 326(3):725–736, 2006.

[188] G Luo, W Cheng, W He, X Wang, J Tan, M Fitzgerald, X Li, and J Wu. Promotion of cutaneous wound healing by local application of mesenchymal stem cells derived from human umbilical cord blood. *Wound Repair and Regeneration*, 18(5):506–513, 2010.

[189] K Ma, S Liao, L He, J Lu, S Ramakrishna, and CK Chan. Effects of nanofiber/stem cell composite on wound healing in acute full-thickness skin wounds. *Tissue Engineering Part A*, 17(9-10):1413–1424, 2011.

[190] AI Caplan and JE Dennis. Mesenchymal stem cells as trophic mediators. *Journal of cellular biochemistry*, 98(5):1076–1084, 2006.

[191] S Ichioka, S Kouraba, N Sekiya, N Ohura, and T Nakatsuka. Bone marrow-impregnated collagen matrix for wound healing: experimental evaluation in a

microcirculatory model of angiogenesis, and clinical experience. *British Journal of Plastic Surgery*, 58(8):1124–1130, 2005.

[192] JT Egaña, FA Fierro, S Krüger, M Bornhäuser, R Huss, S Lavandero, and HG Machens. Use of human mesenchymal cells to improve vascularization in a mouse model for scaffold-based dermal regeneration. *Tissue engineering. Part A*, 15(5):1191–1200, 2009.

[193] HC Lee, SG An, HW Lee, JS Park, KS Cha, TJ Hong, JH Park, SY Lee, SP Kim, YD Kim, SW Chung, YC Bae, YB Shin, JI Kim, and JS Jung. Safety and effect of adipose tissue-derived stem cell implantation in patients with critical limb ischemia: a pilot study. *Circulation Journal*, 76(7):1750–1760, 2012.

[194] Nazlee Zebardast, David Lickorish, and John E Davies. Human umbilical cord perivascular cells (hucpvc): A mesenchymal cell source for dermal wound healing. *Organogenesis*, 6(4):197–203, 2010.

[195] TA Wynn. Cellular and molecular mechanisms of fibrosis. *The Journal of Pathology*, 214(2):199–210, 2008.

[196] S Huang, Y Wu, D Gao, and X Fu. Paracrine action of mesenchymal stromal cells delivered by microspheres contributes to cutaneous wound healing and prevents scar formation in mice. *Cytotherapy*, 17(7):922–931, 2015.

[197] P Martin, D D'Souza, J Martin, R Grose, L Cooper, R Maki, and SR McKercher. Wound healing in the PU.1 null Mouse-Tissue repair is not dependent on inflammatory cells. *Current Biology*, 13(13):1122–8, 2003.

[198] JM Ryan, FP Barry, JM Murphy, and BP Mahon. Mesenchymal stem cells avoid allogeneic rejection. *Journal of Inflammation*, 2(1):8, 2005.

[199] VI Shumakov, NA Onishchenko, MF Rasulov, ME Krasheninnikov, and VA Zaidenov. Mesenchymal bone marrow stem cells more effectively stimulate regeneration of deep burn wounds than embryonic fibroblasts. *Bulletin of Experimental Biology and Medicine*, 136(2):192–195, 2003.

[200] RM Boehler, JG Graham, and LD Shea. Tissue engineering tools for modulation of the immune response. *Biotechniques*, 51(4):239–40, 242, 244 passim, 2011.

[201] JM Anderson, A Rodriguez, and DT Chang. Foreign body reaction to biomaterials. *Seminars in Immunology*, 20(2):86–100, 2008.

[202] K McFarlin, X Gao, and YB Liu. Bone marrow-derived mesenchymal stromal cells accelerate wound healing in the rat. *Wound Repair and Regeneration*, 14(4):471–8, 2006.

DOCUMENTO DE INFORMACIÓN AL DONANTE (v.3)

UTILIZACIÓN DE DATOS CLÍNICOS Y MATERIAL BIOLÓGICO EXCEDENTE DEL PROCESO ASISTENCIAL PARA INVESTIGACIÓN BIOMÉDICA Y SU CONSERVACIÓN EN UN BIOBANCO.

En el ***Hospital Clínico Universitario Virgen de la Arrixaca***, igual que en la mayoría de hospitales, además de la asistencia a los pacientes, se realiza investigación biomédica. La finalidad de esta investigación es progresar en el conocimiento de las enfermedades y en su prevención, diagnóstico, pronóstico y tratamiento. Esta investigación biomédica requiere recoger datos clínicos y muestras biológicas de pacientes y donantes sanos para analizarlos y obtener conclusiones con el objetivo de conocer mejor las enfermedades y avanzar su diagnóstico y/o tratamiento.

Las muestras y datos clínicos obtenidos para el diagnóstico o control de las enfermedades, una vez utilizadas con esta finalidad, resultan también útiles y necesarias para la investigación. De hecho, muchos de los avances científicos obtenidos en los últimos años en medicina son fruto de este tipo de estudios

Solicitamos su autorización para incorporar al *Biobanc-Mur Nodo Área I* del hospital el material biológico sobrante de las pruebas que, como parte del actual proceso asistencial, se le han realizado o se le van a realizar en este centro, con el fin de que puedan ser utilizadas en investigación biomédica.

Siguiendo lo establecido por la Ley 14/2007, de Investigación Biomédica, la Ley Orgánica 15/1999, de Protección de Datos Personales, y sus normas de desarrollo, le solicitamos que lea detenidamente este documento de información y el consentimiento informado que se le adjunta al final para su firma, si está de acuerdo en participar en esta propuesta

¿Qué es un biobanco?: *Institución para favorecer la investigación y la salud.*

Un biobanco es una institución, regulada por leyes específicas, que facilita la investigación biomédica, es decir, aquella dirigida a promover la salud de las personas.

Las muestras incluidas en un biobanco pueden ser cedidas para investigación en Medicina, siempre bajo la supervisión de un comité científico y otro de ética. Las muestras se cederán generalmente sin información personal asociada, aunque a veces podrá ser necesario el acceso a la historia clínica o al resultado de otras pruebas para completar la investigación.

La investigación biomédica es, hoy en día, un fenómeno global por lo que ocasionalmente estas muestras podrán ser cedidas a grupos de investigación fuera de España, siempre que se cumplan los requisitos de la legislación española y lo aprueben los correspondientes comités.

Muestras biológicas e información asociada: *En ningún caso se le practicarán más pruebas de las imprescindibles para su adecuada atención médica.*

Se guardará y dispondrá del material biológico sobrante que se le extraiga durante el proceso asistencial (muestras de sangre, líquidos biológicos y/o tejidos), sin que este hecho le cause molestias adicionales. La donación de muestras excedentes de este proceso asistencial no impedirá que usted o su familia puedan usarlas, cuando sea necesario por motivos de salud, siempre que estén disponibles. Las muestras y la información asociada a las mismas se custodiarán y/o guardarán en el Biobanco ***Biobanc-Mur Nodo Área I*** del ***Hospital Clínico Universitario Virgen de la Arrixaca*** hasta su extinción. Este Biobanco forma parte como nodo de la Red Temática de Investigación Cooperativa (RETIC) de Biobancos del Instituto de Salud Carlos III con la referencia ***RD09/0076/00065***, y está en proceso de Registro con el desarrollo de la normativa regional de Biobancos que aplica la normativa nacional.

Este biobanco acoge colecciones organizadas de muestras biológicas e información asociada en las condiciones y garantías de calidad y seguridad que exige la legislación anteriormente referida y los códigos de conducta aprobados por los Comités de Ética. Dichas muestras y su información asociada quedan disponibles para aquellos investigadores que lo soliciten al biobanco.

Cualquier estudio de investigación para el que se solicite la utilización de estos datos o muestras deberá disponer siempre de la aprobación del Comité de Ética de la Investigación (CEI) competente, que velará para que los investigadores desarrollen sus estudios siguiendo siempre las más estrictas normas éticas y legales. Además, el comité científico del biobanco garantizará que los proyectos sean de excelencia científica.

A partir de las muestras donadas, en los casos en que la investigación lo requiera, se realizarán estudios genéticos, y a partir de ellos se puede obtener información acerca de su salud y la de sus familiares. Siempre se actuará velando por la protección de esta información (ver apartado de protección de datos y confidencialidad).

Por este consentimiento, los responsables del Biobanco del Hospital podrán consultar su historial clínico, solamente en el caso de que ello sea imprescindible para la realización del proyecto para el que se soliciten las muestras y previa autorización por parte del Comité de Ética correspondiente.

En caso de ser necesaria alguna muestra adicional, la institución sanitaria se podría poner en contacto con usted para solicitarle nuevamente su colaboración. En este caso se le informará de los motivos y se le solicitará de nuevo su consentimiento.

Protección de datos y confidencialidad*: Las muestras se conservarán codificadas.*

Los datos personales que se recojan serán obtenidos, tratados y almacenados cumpliendo en todo momento el deber de secreto, de acuerdo con la legislación vigente en materia de protección de datos de carácter personal.

La identificación de las muestras biológicas del Biobanco será sometida a un proceso de codificación. A cada muestra se le asigna un código de identificación, que será el utilizado por los investigadores. Únicamente el personal autorizado por el biobanco podrá relacionar su identidad con los citados códigos. Mediante este proceso los investigadores que soliciten muestras al biobanco no podrán conocer ningún dato que revele su identidad. Asimismo, aunque los resultados obtenidos de la investigación realizada con sus muestras se publiquen en revistas científicas, su identidad no será facilitada. En aquellos estudios en los que no se prevean resultados potencialmente útiles para su salud, y de acuerdo con el correspondiente Comité de Ética, las muestras y datos podrán ser anonimizadas, es decir, no habrá ninguna posibilidad de volver a asociar la muestra con su identidad.

Sus muestras y los datos clínicos asociados a las mismas, pasarán a formar parte del fichero del Biobanco, inscrito en la Agencia de Protección de datos.

Responsable del fichero : Fundación para la Formación e Investigación Sanitarias de la Región de Murcia.
Dirección Postal: Calle Luis Fontes Pagan, 9-1, 30003 Murcia

Usted podrá ejercer sus derechos de acceso, rectificación, cancelación y objeción, así como obtener información sobre el uso de sus muestras y datos asociados, dirigiéndose a:

Fundación para la Formación e Investigación Sanitarias de la Región de Murcia
Responsable del nodo Calle Luis Fontes Pagan, 9-1, 30003 Murcia
Tel.: 968359757 E-mail: juanp.serna@carm.es

Carácter altruista de la donación. ***La cesión de muestras biológicas que usted realiza al Biobanco del Hospital Clínico Universitario Virgen de la Arrixaca es gratuita.***

La donación tiene por disposición legal carácter altruista, por lo que usted no obtendrá ni ahora ni en el futuro ningún beneficio económico por la misma, ni tendrá derechos sobre posibles beneficios comerciales de los descubrimientos que puedan conseguirse como resultado de la investigación biomédica. Sin embargo, los conocimientos obtenidos gracias a los estudios llevados a cabo a partir de su muestra y de muchas otras pueden ayudar al avance médico y, por ello, a otras personas.

Participación voluntaria. ***Su negativa NO repercutirá en su asistencia médica, presente o futura***

Su participación es totalmente voluntaria. Si firma el consentimiento informado, confirmará que desea participar. Puede negarse a participar o retirar su consentimiento en cualquier momento posterior a la firma sin tener que explicar los motivos y esto no repercutirá negativamente en su asistencia médica, presente o futura.

Revocación del consentimiento*: si usted decide firmar este consentimiento, podrá también cancelarlo libremente***.**

Si en un futuro usted quisiera anular su consentimiento, sus muestras biológicas serían destruidas y los datos asociados a las mismas serían retirados del biobanco. También podría solicitar la anonimización de las muestras, en cuyo caso se eliminaría la relación entre sus datos personales (que revelan su identidad) y sus muestras biológicas y datos clínicos asociados. Los efectos de esta cancelación o anonimización no se podrían extender a la investigación que ya se hubiera llevado a cabo.

Si deseara anular su consentimiento, deberá solicitarlo por escrito al Director del Biobanco, en la dirección anteriormente indicada.

Información sobre los resultados de la investigación: ***se le proporcionará información si usted desea recibirla***

En el caso de que usted lo solicite expresamente, el Biobanco podrá proporcionarle información acerca de cuáles son las investigaciones en que se han utilizado sus muestras y de los resultados globales de dichas investigaciones, salvo en el caso de cancelación o anonimización.

Los métodos utilizados en investigación Biomédica suelen ser diferentes de los aprobados para la práctica clínica, por lo que no deben de ser considerados con valor clínico para usted. Sin embargo, en el caso que estas investigaciones proporcionen datos que pudieran ser clínica o genéticamente relevantes para usted e interesar a su salud o a la de su familia, le serán comunicados si así lo estima oportuno. Asimismo, podría darse el caso de obtenerse información relevante para su familia, le corresponderá a usted decidir si quiere o no comunicárselo. Si Ud. quiere que se le comunique dicha información relevante debe consignarlo en la casilla que aparece al final de este documento.

Si usted no desea recibir esta información, tenga en cuenta que la ley establece que, cuando la información obtenida sea necesaria para evitar un grave perjuicio para la salud de sus familiares biológicos, un Comité de expertos estudiará el caso y deberá decidir si es conveniente informar a los afectados o a sus representantes legales.

Por favor, pregunte al personal sanitario que le ha comunicado esta información sobre cualquier duda que pueda tener, ahora o en el futuro, en relación con este consentimiento. Asimismo, puede comentar sus dudas con su médico, quien le pondrá en contacto con el personal sanitario autorizado.

Le agradecemos su desinteresada colaboración con el avance de la ciencia y la medicina. De esta forma está usted colaborando a vencer las enfermedades y ayudar a multitud de enfermos actuales y futuros.

CONSENTIMIENTO INFORMADO

UTILIZACIÓN DE DATOS CLÍNICOS Y MATERIAL BIOLÓGICO EXCEDENTE DEL PROCESO ASISTENCIAL PARA INVESTIGACIÓN BIOMÉDICA Y SU CONSERVACIÓN EN UN BIOBANCO

Nombre y Apellidos (donante)……. Etiqueta Identificativa Paciente Edad: Sexo: DNI:…….	Persona del centro que informa …… DNI:…….

Si ha comprendido la información que se le ha proporcionado, ha resuelto cualquier duda que pudiese tener y decide colaborar con *Biobanc-Mur Nodo Área I* en los términos antes explicados, por favor, lea y firme a continuación esta hoja

El abajo firmante autoriza al ***Hospital Clínico Universitario Virgen de la Arrixaca*** a que el material biológico sobrante de las pruebas que se le han realizado o se le van a realizar como parte del actual proceso asistencial sean incorporadas en el *Biobanco* ***Biobanc-Mur Nodo Área I***, y que sea cedido desde el mismo con la finalidad de llevar a cabo proyectos de investigación biomédica, siempre que éstos cuenten con la obligada aprobación del Comité de Ética de Investigación competente. Esta autorización la concede tras haber sido informado verbalmente y haber leído la información adjunta.

Confirmo que:

1. Autoriza al ***Hospital Clínico Universitario Virgen de la Arrixaca*** a que el material biológico sobrante de las pruebas que se le han realizado o se le van a realizar como parte del actual proceso asistencial sean incorporadas en el ***Biobanc-Mur Nodo Área I***, y que sea cedido desde el mismo con la finalidad de llevar a cabo proyectos de investigación biomédica, siempre que éstos cuenten con la obligada aprobación del Comité de Ética de Investigación competente. Esta autorización la concede tras haber sido informado verbalmente y haber leído la información adjunta.

☐SI ☐NO

2. Desea que se le comunique la información derivada de la investigación que realmente sea relevante y aplicable para su salud o la de su familia ☐SI ☐NO Teléfono o E-mail de contacto…….

3. Autoriza a ser contactado en el caso de necesitar más información o muestras biológicas adicionales

☐SI ☐NO Teléfono o E-mail de contacto: …….

4. He expresado mi deseo de que se respeten las siguientes excepciones respecto al objetivo y métodos de las investigaciones:

……
……
……

DONANTE	PERSONA QUE INFORMA
Firma	**Firma**

En....., a….. de…….. de.....

CONSENTIMIENTO INFORMADO ANTE TESTIGOS

UTILIZACIÓN DE DATOS CLÍNICOS Y MATERIAL BIOLÓGICO EXCEDENTE DEL PROCESO ASISTENCIAL PARA INVESTIGACIÓN BIOMÉDICA Y SU CONSERVACIÓN EN UN BIOBANCO.

Nombre y Apellidos (donante)……. Etiqueta Identificativa Paciente Edad: Sexo: DNI:……	Persona del centro que informa …… DNI:……

Nombre y apellidos del testigo que firma..... DNI……

Relación con el donante:……

Si ha comprendido la información que se le ha proporcionado, ha resuelto cualquier duda que pudiese tener y decide colaborar con *Biobanc-Mur Nodo Área I* en los términos antes explicados, por favor, lea y firme a continuación esta hoja

El abajo firmante confirma que el donante:

1. Autoriza al ***Hospital Clínico Universitario Virgen de la Arrixaca*** a que el material biológico sobrante de las pruebas que se le han realizado o se le van a realizar como parte del actual proceso asistencial sean incorporadas en el ***Biobanc-Mur Nodo Área I***, y que sea cedido desde el mismo con la finalidad de llevar a cabo proyectos de investigación biomédica, siempre que éstos cuenten con la obligada aprobación del Comité de Ética de Investigación competente. Esta autorización la concede tras haber sido informado verbalmente y haber leído la información adjunta.

☐SI ☐NO

2. Desea que se le comunique la información derivada de la investigación que realmente sea relevante y aplicable para su salud o la de su familia ☐SI ☐NO Teléfono o E-mail de contacto……

3. Autoriza a ser contactado en el caso de necesitar más información o muestras biológicas adicionales

☐SI ☐NO Teléfono o E-mail de contacto: ……

4. He expresado mi deseo de que se respeten las siguientes excepciones respecto al objetivo y métodos de las investigaciones:

……

……

……

5. Me autoriza a firmar en su nombre.

TESTIGO	**PERSONA QUE INFORMA**
Firma	**Firma**

En....., a….. de…….. de.....

CONSENTIMIENTO INFORMADO PARA MENORES

UTILIZACIÓN DE DATOS CLÍNICOS Y MATERIAL BIOLÓGICO EXCEDENTE DEL PROCESO ASISTENCIAL PARA INVESTIGACIÓN BIOMÉDICA Y SU CONSERVACIÓN EN UN BIOBANCO.

Nombre y Apellidos (donante)……. Etiqueta Identificativa Paciente Edad: Sexo: DNI:…….	Persona del centro que informa …….. DNI:…….

Nombre y apellidos del tutor legal que firma..... DNI……

Relación con el donante:……

Si ha comprendido la información que se le ha proporcionado, ha resuelto cualquier duda que pudiese tener y decide colaborar con *Biobanc-Mur Nodo Área I* en los términos antes explicados, por favor, lea y firme a continuación esta hoja

El abajo firmante autoriza al ***Hospital Clínico Universitario Virgen de la Arrixaca*** a que el material biológico sobrante de las pruebas que se le han realizado o se le van a realizar como parte del actual proceso asistencial sean incorporadas en el *Biobanco* ***Biobanc-Mur Nodo Área I***, y que sea cedido desde el mismo con la finalidad de llevar a cabo proyectos de investigación biomédica, siempre que éstos cuenten con la obligada aprobación del Comité de Ética de Investigación competente. Esta autorización la concede tras haber sido informado verbalmente y haber leído la información adjunta.

El abajo firmante confirma que:

1. Se me ha informado que, llegada la mayoría de edad de mi representado, este tendrá derecho a revocar o modificar este consentimiento, para lo cual deberá estar debidamente informado. En caso de que no ejerza dicho derecho, se considerará que el actual documento de consentimiento informado sigue vigente.
☐SI ☐NO

2. Desea que se le comunique la información derivada de la investigación que realmente sea relevante y aplicable para su salud o la de su familia ☐SI ☐NO Teléfono o E-mail de contacto…….

3. Autoriza a ser contactado en el caso de necesitar más información o muestras biológicas adicionales
☐SI ☐NO Teléfono o E-mail de contacto: …….

4. He expresado mi deseo de que se respeten las siguientes excepciones respecto al objetivo y métodos de las investigaciones:
……
……
……

5. Me autoriza a firmar en su nombre.

TUTOR	ASENTIMIENTO DEL MENOR CAPACITADO	PERSONA QUE INFORMA
Firma	**Firma**	**Firma**

En....., a….. de…….. de.....

REVOCACIÓN DEL CONSENTIMIENTO

UTILIZACIÓN DE DATOS CLÍNICOS Y MATERIAL BIOLÓGICO EXCEDENTE DEL PROCESO ASISTENCIAL PARA INVESTIGACIÓN BIOMÉDICA Y SU CONSERVACIÓN EN UN BIOBANCO.

POR EL DONANTE:

Yo, D./Dña. ..... con DNI …….. anulo el consentimiento prestado en fecha..... de.....de 20..... y no deseo proseguir la donación voluntaria al biobanco ***Biobanc-Mur Nodo Área I***, que doy por finalizada al día de hoy.

☐ SOLICITO ELIMINACIÓN SOLO DE LA MUESTRA.

☐ SOLICITO ELIMINACIÓN SOLO DE MIS DATOS PERSONALES.

La muestra quedará anonimizada irreversiblemente y podrá ser utilizada en proyectos de investigación.

☐ SOLICITO ELIMINACIÓN TOTAL DE MIS DATOS Y MUESTRAS.

Fdo.:

En.....a.....de.....de 20……

POR EL TUTOR/REPRESENTANTE LEGAL DEL DONANTE:

Yo, D./Dña. ..... con DNI ……., Como representante legal de D/Dña.……., con DNI……., anulo el consentimiento prestado en fecha.....de.....de 20.....y no deseo proseguir la donación voluntaria al biobanco ***Biobanc-Mur Nodo Área I*** , que doy por finalizada al día de hoy.

☐ SOLICITO ELIMINACIÓN SOLO DE LA MUESTRA.

☐ SOLICITO ELIMINACIÓN SOLO LOS DATOS PERSONALES.

La muestra quedará anonimizada irreversiblemente y podrá ser utilizada en proyectos de investigación.

☐ SOLICITO ELIMINACIÓN TOTAL DE MIS DATOS Y MUESTRAS.

Fdo.:

En.....a.....de.....de 20……

UMBILICAL CORD DATA SHEET

Patient ID:

Age:

Patient Medical Record number:

Umbilical Cord record number:

Date of Cesarean:

Time of Umbilical Cord collection:

Time of Umbilical Cord processing:

General Appearance:

Thickness:	Thin:	Medium:	Thick:
Blood Clots:	Few:	Moderate:	Plenty:
Wharton's jelly:	Scarce:	Moderate:	Plenty:

Initial Weight: **Final Weight:**

Lenght:

Mycobacterial Testing with BacT/ALERT® Systems:

Explant Procedure: Number of plates:

Date/Time: